



University of Kentucky
UKnowledge

Theses and Dissertations--Chemical and
Materials Engineering

Chemical and Materials Engineering

2011

DYNAMIC RELAXATION PROPERTIES OF AROMATIC POLYIMIDES AND POLYMER NANOCOMPOSITES

Anthony C. Comer

University of Kentucky, anthony.comer@uky.edu

[Right click to open a feedback form in a new tab to let us know how this document benefits you.](#)

Recommended Citation

Comer, Anthony C., "DYNAMIC RELAXATION PROPERTIES OF AROMATIC POLYIMIDES AND POLYMER NANOCOMPOSITES" (2011). *Theses and Dissertations--Chemical and Materials Engineering*. 1.
https://uknowledge.uky.edu/cme_etds/1

This Doctoral Dissertation is brought to you for free and open access by the Chemical and Materials Engineering at UKnowledge. It has been accepted for inclusion in Theses and Dissertations--Chemical and Materials Engineering by an authorized administrator of UKnowledge. For more information, please contact UKnowledge@lsv.uky.edu.

STUDENT AGREEMENT:

I represent that my thesis or dissertation and abstract are my original work. Proper attribution has been given to all outside sources. I understand that I am solely responsible for obtaining any needed copyright permissions. I have obtained and attached hereto needed written permission statements(s) from the owner(s) of each third-party copyrighted matter to be included in my work, allowing electronic distribution (if such use is not permitted by the fair use doctrine).

I hereby grant to The University of Kentucky and its agents the non-exclusive license to archive and make accessible my work in whole or in part in all forms of media, now or hereafter known. I agree that the document mentioned above may be made available immediately for worldwide access unless a preapproved embargo applies.

I retain all other ownership rights to the copyright of my work. I also retain the right to use in future works (such as articles or books) all or part of my work. I understand that I am free to register the copyright to my work.

REVIEW, APPROVAL AND ACCEPTANCE

The document mentioned above has been reviewed and accepted by the student's advisor, on behalf of the advisory committee, and by the Director of Graduate Studies (DGS), on behalf of the program; we verify that this is the final, approved version of the student's dissertation including all changes required by the advisory committee. The undersigned agree to abide by the statements above.

Anthony C. Comer, Student

Dr. Douglass S. Kalika, Major Professor

Dr. Stephen E. Rankin, Director of Graduate Studies

ABSTRACT OF DISSERTATION

Anthony C. Comer

The Graduate School
University of Kentucky

2011

DYNAMIC RELAXATION PROPERTIES OF AROMATIC POLYIMIDES AND
POLYMER NANOCOMPOSITES

ABSTRACT OF DISSERTATION

A dissertation submitted in partial fulfillment of the
requirements for the degree of Doctor of Philosophy in the
College of Engineering
at the University of Kentucky

By

Anthony C. Comer

Lexington, Kentucky

Director: Dr. Douglass S. Kalika, Professor of Chemical Engineering

Lexington, Kentucky

2011

Copyright © Anthony C. Comer 2011

ABSTRACT OF DISSERTATION

DYNAMIC RELAXATION PROPERTIES OF AROMATIC POLYIMIDES AND POLYMER NANOCOMPOSITES

The dynamic relaxation characteristics of Matrimid[®] (BTDA-DAPI) polyimide and several functionalized aromatic polyimides have been investigated using dynamic mechanical and dielectric methods. The functionalized polyimides were thermally rearranged to generate polybenzoxazole membranes with controlled free volume characteristics. All polyimides have application in membrane separations and exhibit three motional processes with increasing temperature: two sub-glass relaxations (γ and β transitions), and the glass-rubber (α) transition. For Matrimid, the low-temperature γ transition is purely non-cooperative, while the β sub-glass transition shows a more cooperative character as assessed via the Starkweather method. For the thermally rearranged polyimides, the γ transition is a function of the polymer synthesis method, thermal history, and ambient moisture. The β relaxation shows a dual character with increasing thermal rearrangement, the emerging lower-temperature component reflecting motions encompassing a more compact backbone contour. For the glass-rubber (α) transition, dynamic mechanical studies reveal a strong shift in T_α to higher temperatures and a progressive reduction in relaxation intensity with increasing degree of thermal rearrangement.

The dynamic relaxation characteristics of poly(ether imide) and poly(methyl methacrylate) nanocomposites were investigated by dynamic mechanical analysis and dielectric spectroscopy. The nanoparticles used were native and surface-modified fumed silicas. The nanocomposites display a dual glass transition behavior encompassing a bulk polymer glass transition, and a second, higher-temperature transition reflecting relaxation of polymer chain segments constrained owing to their proximity to the particle surface. The position and intensity of the higher-temperature transition varies with particle loading and surface chemistry, and reflects the relative populations of segments constrained or immobilized at the particle-polymer interface. Dielectric measurements, which were used to probe the time-temperature response across the local sub-glass relaxations, indicate no variation in relaxation characteristics with particle loading.

Nanocomposite studies were also conducted on rubbery poly(ethylene oxide) networks crosslinked in the presence of MgO or SiO₂ nanoparticles. The inclusion of nanoparticles led to a systematic increase in rubbery modulus and a modest positive offset in the measured glass transition temperature (T_g) for both systems. The sizeable increases in gas transport with particle loading reported for certain other rubbery nanocomposite systems were not realized in these crosslinked networks.

KEYWORDS: glass transition, membranes, nanocomposites, dynamic mechanical analysis, broadband dielectric spectroscopy

Anthony C. Comer

4/12/2011

DYNAMIC RELAXATION PROPERTIES OF AROMATIC POLYIMIDES AND
POLYMER NANOCOMPOSITES

By
Anthony C. Comer

Dr. Douglass S. Kalika
Director of Dissertation

Dr. Stephen E. Rankin
Director of Graduate Studies

4/12/2011

RULES FOR THE USE OF DISSERTATIONS

Unpublished dissertations submitted for the Doctor's degree and deposited in the University of Kentucky Library are as a rule open for inspection but are to be used only with due regard to the rights of the authors. Bibliographical references may be noted, but quotations or summaries of parts may be published only with the permission of the author, and with the usual scholarly acknowledgements.

Extensive copying or publication of the dissertation in whole or in part also requires the consent of the Dean of the Graduate School of the University of Kentucky.

A library that borrows this dissertation for use by its patrons is expected to secure the signature of each user.

Name

Date

DISSERTATION

Anthony C. Comer

The Graduate School
University of Kentucky
2011

DYNAMIC RELAXATION PROPERTIES OF AROMATIC POLYIMIDES AND
POLYMER NANOCOMPOSITES

DISSERTATION

A dissertation submitted in partial fulfillment of the
requirements for the degree of Doctor of Philosophy in the
College of Engineering
at the University of Kentucky

By

Anthony C. Comer

Lexington, Kentucky

Director: Dr. Douglass S. Kalika, Professor of Chemical Engineering

Lexington, Kentucky

2011

Copyright © Anthony C. Comer 2011

ACKNOWLEDGEMENTS

I want to first acknowledge my advisor, Dr. Douglass S. Kalika, for his time, expertise, and friendship. He has been committed to working with me weekly for the last few years, even daily and on weekends when required. He promotes a standard of excellence in teaching and research which I hope to apply as I move on in my career. Most of all I appreciate his “down to earth” personality which made communicating, learning and relating a pleasant experience.

I want to thank the University of Kentucky Graduate School and the Department of Chemical and Materials Engineering for their financial support. In addition, I want to acknowledge the significant contributions to my research that resulted from the collaboration with Dr. Benny Freeman from the University of Texas at Austin and members of his group (Dr. Claudio Ribeiro and Dr. Brandon Rowe). Also, I wish to acknowledge the contributions of Dr. Sumod Kalakkunnath, Michael Danquah, Dr. Scott Matteucci, Alex Heilman, and Michael Abney to the early stages of this work.

Special thanks go to my wife (Janice), and my three daughters (Dominique, Antoinette and Colette). I know it was a tremendous sacrifice financially and the timing was not ideal. To my wife in particular, I could not have done this without your love and support. As we all look back on these last few years in Lexington, I know that we can now say it was well worth it.

Last but not least, I want to thank the Lord Jesus Christ for orchestrating this significant milestone in my life. My prayer is that I will gratefully render service to mankind that will make the world a better place.

TABLE OF CONTENTS

ACKNOWLEDGEMENTS	iii
LIST OF TABLES	viii
LIST OF FIGURES	ix
Chapter 1: Introduction and Objectives	1
Chapter 2: Background	8
2.1 OVERVIEW	8
2.2 AROMATIC POLYIMIDES	10
2.3 POLYMER NANOCOMPOSITES	13
2.3.1 Glassy Polymer Nanocomposites	13
2.3.2 Rubbery Polymer Nanocomposites	19
Chapter 3: Experimental Methods	36
3.1 MATERIALS	36
3.1.1 Matrimid [®] Polyimide	36
3.1.2 Functionalized Aromatic Polyimides	36
3.1.3 PEI & PMMA Nanocomposites	37
3.1.4 Crosslinked PEO Nanocomposites	38
3.2 DYNAMIC MECHANICAL ANALYSIS (DMA)	39
3.2.1 DMA Theory	39
3.2.2 Time-Temperature Superposition	41
3.2.3 Kohlrausch-Williams-Watts (KWW) Model	41
3.2.4 The DMA Instrument	42
3.2.5 Sample Preparation and Experimental Procedures	43
3.3 BROADBAND DIELECTRIC SPECTROSCOPY (BDS)	43
3.3.1 Dielectric Theory	43
3.3.1.1 Static Measurements	44
3.3.1.2 Dynamic Measurements	45
3.3.2 Dynamic Relaxation Models	46
3.3.3 The BDS Instrument	47
3.3.4 Sample Preparation	48
3.3.5 Experimental Procedures	48
3.4 DENSITY DETERMINATIONS	48
3.5 THERMOGRAVIMETRIC ANALYSIS	49
Chapter 4: Dynamic Relaxation Characteristics of Matrimid [®] Polyimide	63
4.1 INTRODUCTION	63

4.2 EXPERIMENTAL	66
4.2.1 <i>Materials</i>	66
4.2.2 <i>Sample Preparation</i>	66
4.2.3 <i>Dynamic Mechanical Analysis</i>	67
4.2.4 <i>Broadband Dielectric Spectroscopy</i>	67
4.3 RESULTS AND DISCUSSION	67
4.3.1 <i>Relaxation Properties of Matrimid[®] Polyimide</i>	67
4.3.2 <i>Sub-glass Relaxation Processes</i>	68
4.3.3 <i>Glass-rubber Relaxation Process</i>	72
4.4 CONCLUSIONS	75
 Chapter 5: Relaxation Characteristics of Aromatic Polyimides	 91
5.1 INTRODUCTION	91
5.2 EXPERIMENTAL	92
5.2.1 <i>Polymer Synthesis</i>	92
5.2.1.1 <i>API Polymers Prepared via Chemical Imidization</i>	92
5.2.1.2 <i>API Polymers Prepared via Thermal Imidization</i>	92
5.2.2 <i>Dynamic Mechanical Analysis</i>	93
5.2.3 <i>Broadband Dielectric Spectroscopy</i>	93
5.3 RESULTS AND DISCUSSION	94
5.3.1 <i>HAB-6FDA Polyimide</i>	94
5.3.1.1 <i>Thermal Stability</i>	94
5.3.1.2 <i>Dynamic Mechanical Analysis</i>	95
5.3.1.3 <i>Broadband Dielectric Spectroscopy</i>	97
5.3.2 <i>APAF-ODPA Polyimide</i>	98
5.3.2.1 <i>Thermal Stability</i>	98
5.3.2.2 <i>Dynamic Mechanical Analysis</i>	99
5.3.2.3 <i>Broadband Dielectric Spectroscopy</i>	102
5.3.3 <i>APAF-6FDA Polyimide</i>	103
5.3.3.1 <i>Dynamic Mechanical Analysis</i>	103
5.3.3.2 <i>Broadband Dielectric Spectroscopy</i>	105
5.4 INFLUENCE OF AMBIENT MOISTURE ON API SUB-GLASS RELAXATIONS	106
5.5 CONCLUSIONS	107
 Chapter 6: Dynamic Relaxation Characteristics of Polymer Nanocomposites based on Poly (ether imide) and Poly (methyl methacrylate)	 142
6.1 INTRODUCTION	142
6.2 EXPERIMENTAL	144
6.2.1 <i>Materials</i>	144
6.2.2 <i>Sample Preparation</i>	145
6.2.3 <i>Film Density</i>	146
6.2.4 <i>Dynamic Mechanical Analysis</i>	146
6.2.5 <i>Broadband Dielectric Spectroscopy</i>	146

6.3 RESULTS AND DISCUSSION	147
6.3.1 Nanocomposite Density	147
6.3.2 PEI Composites – Dynamic Mechanical Analysis.....	148
6.3.3 PMMA Composites – Dynamic Mechanical Analysis	153
6.3.4 PEI Composites – Dielectric Spectroscopy	154
6.3.5 PMMA Composites – Dielectric Spectroscopy	156
6.4 CONCLUSIONS	157
 Chapter 7: Glass-Transition and Gas-Transport Characteristics of Polymer Nanocomposites Based on Crosslinked Poly(ethylene oxide).....	 180
7.1 INTRODUCTION.....	180
7.2 EXPERIMENTAL	183
7.2.1 Materials	183
7.2.2 Sample Preparation	184
7.2.3 Film Density.....	185
7.2.4 Dynamic Mechanical Analysis.....	185
7.2.5 Broadband Dielectric Spectroscopy	185
7.2.6 Gas Transport Measurements	186
7.3 RESULTS AND DISCUSSION	187
7.3.1 Dynamic Mechanical Analysis.....	187
7.3.2 Broadband Dielectric Spectroscopy	190
7.3.3 Nanocomposite Density	192
7.3.4 Gas Transport	194
7.4 CONCLUSIONS	197
 Chapter 8: Conclusions.....	 216
 Bibliography	 219
 Nomenclature.....	 232
 Abbreviations.....	 236
 Vita	 238

LIST OF TABLES

Table 6.1:	Glass transition temperatures for PEI / nanoparticle composites as a function of particle loading (wt%).....	160
------------	--	-----

LIST OF FIGURES

Figure 2.1:	Typical viscoelastic response curves for an amorphous polymer: (a) storage modulus and (b) loss modulus vs. temperature	22
Figure 2.2:	Frequency dependence of dynamic mechanical relaxation properties: (a) storage modulus and (b) loss modulus vs. temperature	23
Figure 2.3:	Typical Arrhenius plot for sub-glass relaxations	24
Figure 2.4:	Chemical structures for Matrimid [®] and Kapton [®] commercial polyimides.....	25
Figure 2.5:	General thermal rearrangement of an aromatic polyimide	26
Figure 3.1:	Chemical structures for aromatic polyimides prepared via chemical imidization or thermal imidization	50
Figure 3.2:	TR conversion structures (PBO's) for aromatic polyimides prepared via chemical imidization or thermal imidization	51
Figure 3.3:	Chemical structures for poly (ether imide) [PEI] and poly (methyl methacrylate) [PMMA]	54
Figure 3.4:	Surface chemistry of fumed silica nanoparticles: a) TS-530; b) TS-610; c) TS-720	55
Figure 3.5:	Chemical structure for cross-linked poly(ethylene glycol) diacrylate [XLPEGDA]	56
Figure 3.6:	Typical viscoelastic response curves on a frequency basis	57
Figure 3.7:	Storage modulus master curve obtained via time-temperature superposition	58
Figure 3.8:	Test configurations for dynamic mechanical analysis	59
Figure 3.9:	Charge separation in a parallel-plate capacitor	60
Figure 3.10:	Novocontrol “Concept 40” Broadband Dielectric Spectrometer sample cell	61

Figure 4.1:	Storage modulus and loss modulus <i>vs.</i> temperature for Matrimid [®] polyimide	77
Figure 4.2:	Dynamic mechanical loss modulus and dielectric loss <i>vs.</i> temperature for Matrimid [®] polyimide across the sub-glass transition region	78
Figure 4.3:	Loss modulus <i>vs.</i> temperature for Matrimid [®] polyimide: (a) γ transition; (b) β transition	79
Figure 4.4:	Arrhenius plots of $\log(f_{MAX})$ <i>vs.</i> $1000/T$ based on dynamic mechanical and dielectric results: (a) γ transition; (b) β transition.....	80
Figure 4.5:	Dielectric loss <i>vs.</i> frequency for Matrimid [®] polyimide: (a) γ transition; (b) β transition	81
Figure 4.6:	Havriliak-Negami (HN) parameters <i>vs.</i> temperature for γ and β transition regions	82
Figure 4.7:	Apparent activation energy <i>vs.</i> relaxation temperature at 1 Hz based on dynamic mechanical and dielectric results.....	83
Figure 4.8:	Storage modulus and loss modulus <i>vs.</i> temperature for Matrimid [®] polyimide in the vicinity of the glass-rubber (α) relaxation	84
Figure 4.9:	Dynamic mechanical time-temperature master curves	85
Figure 4.10:	Cooperativity plot of $\log(a_T)$ <i>vs.</i> T_α/T based on dynamic mechanical measurements	86
Figure 5.1:	Chemical structures for diamines and dianhydrides	108
Figure 5.2:	Chemical structures for aromatic polyimides prepared via chemical imidization and thermal imidization.....	109
Figure 5.3:	TR conversion structures (PBO's) for aromatic polyimides initially prepared via chemical imidization and thermal imidization	110
Figure 5.4:	HAB-6FDA theoretical weight loss (chemically imidized): acetate degradation and TR conversion	111
Figure 5.5:	Chemically imidized HAB-6FDA exposed to various thermal histories	112

Figure 5.6:	Storage modulus and $\tan \delta$ vs. temperature for chemically imidized HAB-6FDA-TR300	113
Figure 5.7:	Multi-frequency plots of storage modulus and $\tan \delta$ vs. temperature for chemically imidized HAB-6FDA-TR300	114
Figure 5.8:	Arrhenius plot (dynamic mechanical sub-glass transitions) for chemically imidized HAB-6FDA TR series	115
Figure 5.9:	Storage modulus and $\tan \delta$ vs. temperature for chemically imidized HAB-6FDA TR series	116
Figure 5.10:	$\tan \delta$ vs. temperature for chemically imidized HAB-6FDA TR series in the sub-glass region	117
Figure 5.11:	Dielectric properties vs. temperature for chemically imidized HAB-6FDA-TR 300	118
Figure 5.12A:	Dielectric loss vs. frequency for chemically imidized HAB-6FDA; γ transition	119
Figure 5.12B:	Dielectric loss vs. frequency for chemically imidized HAB-6FDA; β transition	120
Figure 5.13:	$\tan \delta$ vs. temperature for chemically imidized HAB-6FDA-TR300	121
Figure 5.14:	Chemically imidized APAF-ODPA exposed to various thermal histories	122
Figure 5.15:	Dynamic mechanical $\tan \delta$ vs. temperature for chemically imidized APAF-ODPA TR series	123
Figure 5.16:	Dynamic mechanical results ($\tan \delta$ vs. temperature) for APAF-ODPA samples synthesized via chemical imidization and exposed to various thermal histories	124
Figure 5.17:	Comparison of dynamic mechanical $\tan \delta$ for APAF-ODPA samples synthesized via chemical and thermal imidization	125
Figure 5.18A:	Dynamic mechanical properties for thermally imidized APAF-ODPA TR series: storage modulus results	126
Figure 5.18B:	Dynamic mechanical properties for thermally imidized APAF-ODPA TR series: $\tan \delta$ results	127

Figure 5.19:	Tan δ vs. temperature for thermally imidized APAF-ODPA TR series in the sub-glass region	128
Figure 5.20:	Storage modulus and tan δ vs. temperature for thermally imidized APAF-ODPA-TR400 at different hold times	129
Figure 5.21:	Storage modulus and tan δ vs. temperature for thermally imidized APAF-ODPA-TR450 at different hold times	130
Figure 5.22:	Dielectric loss vs. temperature for thermally imidized APAF-ODPA TR series	131
Figure 5.23:	Tan δ vs. temperature for thermally imidized APAF-ODPA-TR 350. Dielectric and DMA results	132
Figure 5.24:	Storage modulus and tan δ vs. temperature for chemically imidized APAF-6FDA TR series.....	133
Figure 5.25:	Storage modulus and tan δ vs. temperature for thermally imidized APAF-6FDA TR series.....	134
Figure 5.26:	Tan δ vs. temperature for thermally imidized APAF-6FDA TR series in the sub-glass region	135
Figure 5.27:	Tan δ vs. temperature for thermally imidized APAF-ODPA & APAF-6FDA TR series in sub-glass region	136
Figure 5.28:	Dielectric loss vs. temperature for thermally imidized APAF-6FDA TR series in sub-glass region.....	137
Figure 5.29:	Tan δ vs. temperature for thermally imidized APAF-6FDA-TR 350. Dielectric and DMA results	138
Figure 5.30:	Tan δ vs. temperature for sub-glass relaxations showing effects of moisture.....	139
Figure 5.31:	Tan δ vs. temperature for sub-glass relaxations showing the reversibility of moisture effects	140
Figure 6.1:	Density vs. weight percent filler for PEI nanocomposites.....	161
Figure 6.2:	Dynamic mechanical properties vs. temperature for PEI/TS-610 nanocomposites.....	162
Figure 6.3:	Dynamic mechanical properties vs. temperature for PEI/SiO ₂ nanocomposites. a) storage modulus; b) tan δ	163

Figure 6.4:	Dynamic mechanical properties <i>vs.</i> temperature for PEI nanocomposites with particle loading of 15 wt% SiO ₂ ; TS-530; TS-610; TS-720. a) storage modulus (Pa); b) tan δ	164
Figure 6.5:	Dynamic mechanical tan δ <i>vs.</i> temperature for PEI/TS-610 (30 wt%) nanocomposite	165
Figure 6.6:	Arrhenius plots for PEI/TS-610 nanocomposites based on maxima in dynamic mechanical tan δ	166
Figure 6.7:	Time-temperature master curves for PEI/TS-610 nanocomposites	167
Figure 6.8:	Dynamic mechanical properties <i>vs.</i> temperature for PMMA/TS-610 nanocomposites. a) storage modulus; b) tan δ	168
Figure 6.9:	Dielectric loss <i>vs.</i> temperature for unfilled PEI	169
Figure 6.10:	Dielectric loss <i>vs.</i> frequency for PEI/TS-610 (20 wt%) nanocomposite	170
Figure 6.11:	Dielectric loss <i>vs.</i> frequency for PEI/TS-610 nanocomposites at 260°C (glass-rubber relaxation).....	171
Figure 6.12:	Arrhenius plots for PEI/TS-610 nanocomposites based on maxima in dielectric loss	172
Figure 6.13:	Arrhenius plots for PEI/TS-610 nanocomposites across the glass-rubber relaxation.....	173
Figure 6.14:	Dielectric loss <i>vs.</i> temperature for PMMA/TS-610 nanocomposite.....	174
Figure 6.15:	Arrhenius plots for PMMA/TS-610 nanocomposites based on maxima in dielectric loss	175
Figure 7.1:	Dynamic mechanical properties <i>vs.</i> temperature for PEGDA/MgO nanocomposites. (a) storage modulus; (b) tan δ	199
Figure 7.2:	Dynamic mechanical properties <i>vs.</i> temperature for PEGDA/SiO ₂ nanocomposites. (a) storage modulus; (b) tan δ	200
Figure 7.3:	Dynamic mechanical peak temperature <i>vs.</i> weight percent filler for XLPEGDA nanocomposites; glass-rubber transition	201
Figure 7.4:	Rubbery modulus <i>vs.</i> volume percent filler for XLPEGDA nanocomposites.....	202

Figure 7.5:	Time-temperature master curves for PEGDA/MgO nanocomposites.....	203
Figure 7.6:	Dielectric properties vs. temperature for PEGDA + 30 wt% MgO nanocomposite. (a) dielectric constant; (b) dielectric loss	204
Figure 7.7:	Dielectric constant vs. temperature for PEGDA/MgO nanocomposites at 130 Hz	205
Figure 7.8:	Density vs. weight percent filler for XLPEGDA nanocomposites: (a) PEGDA/MgO; (b) PEGDA/SiO ₂	206
Figure 7.9:	Infinite dilution permeability vs. volume percent filler for PEGDA/MgO nanocomposites at 35°C.....	207
Figure 7.10:	CO ₂ permeability at infinite dilution vs. volume percent filler for PEGDA/MgO nanocomposites at 35°C.....	208
Figure 7.11:	Diffusion coefficients at ~ 4.4 atm upstream pressure vs. volume percent filler for PEGDA/MgO nanocomposites at 35°C	209
Figure 7.12:	Solubility coefficients at ~ 4.4 atm upstream pressure vs. volume percent filler for PEGDA/MgO nanocomposites at 35°C	210

Chapter 1

Introduction and Objectives

The dynamic relaxation response characteristics of polymeric materials provide useful insights as to polymer architecture and local relaxation environment. Motional relaxations in polymers (*i.e.*, the glass-rubber relaxation; sub-glass relaxations) are highly-sensitive to polymer structure and morphology, and often reflect subtle changes in composition or motional constraint that can have significant ramifications for material attributes related to mechanical performance, thermal resistance and membrane transport. In nanocomposites, the inclusion of nanoscale filler and the creation of large amounts of internal surface area may produce dramatic shifts in glass transition temperature, for example, that correlate with the properties of the filler, the quality of the internal interfaces, and the physical confinement imposed by the filler on the responding polymer chains.

In the work presented here, the dynamic relaxation characteristics of two classes of polymeric materials are examined in detail in order to more fully establish how variations in polymer backbone structure, thermal rearrangement, and the presence of fillers influence polymer chain mobility and corresponding bulk properties. Studies of (unfilled) aromatic polyimides focus on their relaxation characteristics as related to repeat unit structure and potential conversion to more rigid, thermally-resistant films with unique free-volume morphologies for use as gas separation membranes. Investigations on polymer nanocomposites encompass both glassy polymers and *in-situ* polymerized rubbery systems, with a goal of determining how the presence of either compatible or

incompatible inorganic fillers can potentially alter segmental polymer response. In both cases, the elucidation of polymer viscoelastic properties provides foundational understanding that can be exploited via strategic materials design to achieve enhanced performance.

Polyimides have been in commercial use for many years and are commonly applied in the electronics industry as an insulating barrier, as well as in gas separation membrane applications [1-3]. Of particular interest is the commercial polyimide based on 3,3'-4,4'-benzophenone tetracarboxylic dianhydride and diaminophenylindane (BTDA-DAPI), *i.e.*, Matrimid®. Matrimid membranes show favorable transport properties, good mechanical strength and chemical stability, but are susceptible to physical aging effects. Physical aging is strongly dependent on the system temperature, which affects both segmental mobility and displacement from equilibrium [4,5]. Molecular motions that persist below the glass transition, related to secondary transitions, allow physical aging to proceed by small localized rearrangements towards equilibrium [6]. By studying these secondary relaxations, the molecular motions responsible for the observed behaviors can be related to moieties in the polymer backbone structure.

Recently, several non-commercial aromatic polyimides interconnected with heterocyclic rings have shown unprecedented chemical resistance and gas transport properties [7]. These aromatic polyimides have an unusual microstructure with cavity size and distribution that can be tuned by combining various functionalized diamines and dianhydrides and converting them to polybenzoxazoles via exposure to high temperature (350°C – 450°C) rearrangement. Investigation of the dynamic relaxation properties of these polymers affords valuable insight as to how molecular structure and thermal history

is related to the resulting transport properties, thereby leading to more effective membrane design.

Another area of interest is the incorporation of nanoparticles in polymer matrices. Nanocomposite technology has progressed rapidly owing to the enhanced properties that can be achieved in polymer nanocomposites over those of the pure polymer [8-10]. Relevant studies in the design of membranes for gas separation have shown increased permeability and selectivity in certain glassy polymer nanocomposite systems upon the introduction of fumed silica nanofiller [11,12]. The presence of the particles can disrupt chain packing and increase overall free volume, and has the potential to introduce alternate transport pathways. The quality of particle-polymer interactions and physical confinement effects can substantially modify polymer chain dynamics, and the local segmental mechanisms responsible for penetrant transport.

Rubbery nanocomposites have also shown enhanced gas transport properties upon inclusion of nanoscale filler. Recently, a series of rubbery copolymer membranes based on crosslinked poly(ethylene oxide) [XLPEO] were investigated for use in CO₂/light gas separations [13,14]. The polymers display high CO₂ permeability and favorable CO₂/light gas selectivity owing to their rubbery character and the presence of polar ether oxygens in the polymer network that interact preferentially with CO₂. Given the commercial potential of these rubbery network polymers for use as CO₂-selective membranes, it is of interest to explore possible enhancements in gas separation performance achieved by direct incorporation of metal oxide nanoparticles (e.g., MgO, SiO₂) in the crosslinked matrix. Here again, elucidation of the dynamic relaxation properties of the resulting nanocomposite networks is useful in determining those

modifications most effective in improving both the mechanical and separation performance of these materials.

The overall goal of the work presented in this dissertation is to investigate the dynamic relaxation properties of aromatic polyimides and polymer nanocomposites using dynamic mechanical analysis and broadband dielectric spectroscopy.

Specific objectives are as follows:

- Characterization of the dynamic relaxation properties of Matrimid® (BTDA-DAPI) polyimide focusing on local sub-glass relaxation processes.
- Characterization of the sub-glass and glass-rubber relaxation processes in thermally-rearranged aromatic polyimides (HAB-6FDA, APAF-ODPA, and APAF-6FDA) as a function of backbone structure and thermal exposure. Assessment as to how the degree of thermal conversion can be monitored directly via dynamic mechanical and dielectric methods.
- Investigation of the influence of silica and modified silica nanoparticles on the static and dynamic properties of poly (ether imide) and poly (methyl methacrylate) nanocomposites; studies include variation of particle loading and surface chemistry as related to bulk morphology.
- Investigation of the influence of MgO and SiO₂ nanoparticles on the static and dynamic properties of crosslinked poly(ethylene glycol) diacrylate networks. Processing parameters include particle loading and influence of dispersion aids, with corresponding measurement of dynamic mechanical and dielectric response properties, as well as pure gas permeation.

Chapter 2 of the dissertation describes the characteristics of dynamic relaxations found in amorphous polymers. It also describes the structure, properties, and areas of application for aromatic polyimides and polymer nanocomposites. The experimental methods used to characterize these materials are discussed in Chapter 3. Aromatic polyimides are described in detail in Chapters 4 and 5: Chapter 4 is devoted to Matrimid[®] polyimide and Chapter 5 to thermally-rearranged aromatic polyimides. Polymer nanocomposite materials are examined in Chapters 6 and 7; specifically, glassy poly(ether imide) and poly(methyl methacrylate) nanocomposites are discussed in Chapter 6 and rubbery crosslinked poly(ethylene glycol) diacrylate nanocomposites are discussed in Chapter 7. Finally, in Chapter 8 the major findings of the dissertation are summarized.

References

- [1] Bryant, R.G. *Polyimides*; John Wiley & Sons: New York, **2002**.
- [2] Tanaka, K.; Okamoto, K.-I., "Structure and Transport Properties of Polyimides as Materials for Gas and Vapor Membrane Separation", In *Materials Science of Membranes for Gas and Vapor Separation*; Yampolskii, Y.; Pinnau, I.; Freeman, B.D., eds.; John Wiley & Sons: New York, **2006**; pp 271-291.
- [3] Kase, Y., "Gas Separation by Polyimide Membranes", In *Advanced Membrane Technology Applications*; Li, N.; Fane, A.G.; Ho, W.S.W.; Matsuura, T., eds.; John Wiley & Sons: New York, **2008**; pp 581-598.
- [4] Huang, Y.; Paul, D.R. "Physical Aging of Thin Glassy Polymer Films Monitored by Gas Permeability", *Polymer* **2004**, *45*, 8377.
- [5] Huang, Y.; Paul, D.R. "Experimental Methods for Tracking Physical Aging of Thin Glassy Polymer Films by Gas Permeation", *Journal of Membrane Science* **2004**, *244*, 167.
- [6] Hutchinson, J.M. "Physical Aging of Polymers", *Progress Polymer Science* **1995**, *20*, 703.
- [7] Park, H.B.; Jung, C.H.; Lee, Y.M.; Hill, A.J.; Pas, S.J.; Mudie, S.T.; Van Wagner, E.; Freeman, B.D.; Cookson, D.J. "Polymers with Cavities Tuned for Fast Selective Transport of Small Molecules and Ions", *Science* **2007**, *318*, 254.
- [8] Mayes, A.M. "Nanocomposites Softer at the Boundary", *Nature Materials* **2005**, *4*, 651.
- [9] Balazs, A.C.; Emrick, T.; Russell, T.P. "Nanoparticle Polymer Composites: Where Two Small Worlds Meet", *Science* **2006**, *314*, 1107.
- [10] Paul, D.R.; Robeson, L.M. "Polymer Nanotechnology: Nanocomposites", *Polymer* **2008**, *49*, 3187.
- [11] Merkel, T.C.; Freeman, B.D.; Spontak, R.J.; He, Z.; Pinnau, I.; Meakin, P.; Hill, A.J. "Ultraparpermeable, Reverse-Selective Nanocomposite Membranes", *Science* **2002**, *296*, 519.
- [12] Merkel, T.C.; He, Z.; Pinnau, I.; Freeman, B.D.; Meakin, P.; Hill, A.J. "Effect of Nanoparticles on Gas Sorption and Transport in Poly(1-trimethylsilyl-1-propyne)", *Macromolecules* **2003**, *36*, 6844.

- [13] Lin, H.; Van Wagner, E.; Freeman, B.D.; Toy, L.G.; Gupta, R.P. "Plasticization-Enhanced Hydrogen Purification Using Polymeric Membranes", *Science* **2006**, *311*, 639.
- [14] Lin, H.; Van Wagner, E.; Raharjo, R.; Freeman, B.D.; Roman, I. "High-Performance Polymer Membranes for Natural-Gas Sweetening", *Advanced Materials* **2006**, *18*, 39.

Chapter 2

Background

2.1 Overview

Dynamic relaxations in polymeric materials are a manifestation of the viscoelastic response of the material to small scale mechanical or electrical perturbations. The glass-rubber (α) relaxation describes the transition from a glassy state with little chain mobility at low temperatures to a higher temperature rubbery entangled state where the polymer chains have sufficient internal energy to undergo longer-range segmental motion. The molecular motions responsible for the α relaxation are cooperative in nature and typically encompass multiple neighboring chains (*i.e.*, intermolecular motion). The sub-glass relaxations (designated β , γ , δ etc.) are primarily non-cooperative in nature and consist of limited-range intramolecular motions in the glassy state associated with rotations or vibrations along the polymer chain, as well as localized motions involving pendant groups. Typical mechanical relaxation curves for an amorphous polymer are shown in **Figure 2.1** where storage and loss moduli are plotted versus temperature. The details of these response curves are a function of polymer backbone structure, intra- and intermolecular forces and physical confinement effects. Intra- and intermolecular forces include van der Waals forces that can encompass both polymer-polymer interactions and polymer-particle interactions (re: composite systems). Physical confinement results from restricted movement owing to bulky substituent groups, spatial alignment, and the presence of fillers.

The dynamic relaxations observed in polymeric materials are time (frequency) dependent. As perturbation frequency increases, it shifts the observed relaxations in storage (E') and loss modulus (E'') to higher temperatures (see **Figure 2.2**). As functions of both time and temperature, these relaxations can be described using the empirical time-temperature superposition (TTS) principle which states that for many polymer response characteristics, time and temperature are interchangeable. Time-temperature superposition is used to extend the range of observed viscoelastic behavior as a function of time at specific temperatures. It avoids the impractical aspects of measuring polymer behavior over long periods of time at a specified temperature by utilizing the fact that at higher temperatures, the polymer will display the same response as would be measured at long observation times [1]. For sub-glass relaxations in polymeric materials, the time-temperature relationship can be described by an Arrhenius equation:

$$\tau_{ave} = A \exp \left[\frac{E_A}{RT} \right] \quad 2.1a$$

$$\tau_{ave} = \frac{1}{2\pi f_{MAX}} \quad 2.1b$$

where τ_{ave} is the average relaxation time, A is a constant of the polymer material, E_A is the apparent activation energy, f_{MAX} is the frequency corresponding to the position of the maximum in the dynamic mechanical or dielectric loss modulus peak, and T is the absolute temperature. An Arrhenius-style plot of $\log(f_{MAX})$ vs $1/T$ (see **Figure 2.3**) leads to a straight-line result, with slope corresponding to E_A/R . The Williams-Landel-Ferry

(WLF) equation is often used to describe the time-temperature relationship for the glass-rubber (α) relaxation [1]:

$$\log \left[\frac{\tau_{ave}}{\tau_{0,ave}} \right] = - \frac{C_1(T - T_0)}{C_2 + T - T_0} \quad 2.2$$

where $\tau_{0,ave}$ is the average relaxation time at reference temperature T_0 , and C_1 and C_2 are constants of the polymer material based on the value of T_0 .

2.2 Aromatic Polyimides

Aromatic polyimides (APIs) are high performance engineering polymers that are used in a wide range of specialty applications, most notably in the electronics industry. They are thermally stable at elevated temperatures (typically above 400°C [2,3]) and display outstanding mechanical properties [3]. They are also insoluble in most common solvents and chemically resistant to acids and caustics [2]. The general chemical structure of polyimides consists of a –OC-NR-CO- repeat unit in the backbone. The structures of two key industrial polyimides are shown in **Figure 2.4**. APIs are synthesized by several methods described in literature [3]. The most common approach consists of a two-step procedure that involves (i) combining a diamine with a dianhydride to form a polyamic acid, followed by (ii) thermal or chemical imidization to form the polyimide.

The dynamic relaxation properties of aromatic polyimides have been studied extensively using dynamic mechanical and dielectric analysis [4-18]; characteristics include relaxation temperature, intensity, and time-temperature relationships. Typical relaxations for polyimides include the glass-rubber (α) relaxation and two sub-glass relaxations (γ , β) as identified by several authors [12,16,18]. For aromatic polyimides, T_γ (1 Hz) is located

in the vicinity of -100°C , while T_{β} is observed in the range 50°C to 150°C . Glass transition temperatures at or above 200°C are common for the aromatic polyimide structures [3]. Studies have been conducted that associate the individual sub-glass relaxations with the diamine and dianhydride moieties, respectively, or with correlated motions that encompass both units [16,18]. Although the sub-glass relaxations are typically associated with local molecular motions, moisture content has been found to be a significant factor as well [18,19]. Dynamic mechanical and dielectric analysis on Kapton polyimides show an increase in the sub-glass $\tan \delta$ peaks (γ , β) as the moisture content of the Kapton increases [20]. The $\tan \delta$ peaks in these materials have also been shown to increase with film thickness [6].

Aromatic polyimides have been identified as viable materials for use as gas separation membranes [21-26]. APIs display some of the highest selectivities measured for gas separations and help to establish the permeability-selectivity performance upper bound [27]. Crosslinked APIs have been identified with CO_2/CH_4 selectivities that exceed those of the leading commercial materials such as cellulose acetate [24]. One of the challenges associated with API membranes in gas separations is their susceptibility to plasticization from CO_2 adsorption and liquid hydrocarbons [24,28]. Plasticization increases the free volume and molecular motions of the polymer matrix which increases permeability; however this also decreases selectivity for all diffusing materials [29]. Several methods have been devised for reducing the effects of plasticization including crosslinking, thermal treating, and polymer blending [23,24,28,30]. Physical aging is another problem that decreases the performance of API membranes in gas separations [31-33], and occurs in the sub-glass region as localized molecular motions facilitate changes in polymer chain

conformation (*i.e.*, towards a minimum energy, equilibrium morphology). This causes a reduction in the free volume of the polymer matrix and hence can significantly reduce permeability [34]. The rate of physical aging is a function of molecular structure, thermal history, and membrane film thickness [35-37].

Recently, a new class of aromatic polyimides with exceptionally high thermal and chemical resistance properties has been identified for use as gas separation membranes under extreme conditions. These materials are based on specifically functionalized polyimide structures designed to render them soluble for membrane casting. The presence of *ortho*-positioned functional groups enhances solubility, and also serves as the basis of thermal rearrangement (TR) at elevated temperature for the production of polybenzoxazoles (PBOs) according to the procedures described by Park *et al.* [38]. The resulting “TR” polyimides (*i.e.*, PBOs) are resistant to plasticization and exhibit significantly higher permeabilities and selectivities (CO_2/CH_4 , O_2/N_2 , H_2/N_2) than the original API materials thereby exceeding the membrane performance upper bound. These enhancements are due to a narrow distribution of free volume elements and unique “hourglass” shaped cavities formed in the thermal rearrangement process. A schematic of the thermal rearrangement chemistry is shown in **Figure 2.5**.

In this study, dynamic mechanical analysis (DMA) and broadband dielectric spectroscopy (BDS) are used to elucidate the sub-glass and glass-rubber relaxation characteristics of functionalized APIs as they relate to their structural details and thermal exposure history; the information obtained through these methods provides insight as to the relative flexibility of the polymers, their local relaxation environment and corresponding free volume, and the influence of thermal rearrangement on segmental

mobility and ultimate membrane performance. The contrasting nature of the dynamic mechanical and dielectric probes can be used to more precisely establish those structural elements encompassed by a given relaxation process.

2.3 Polymer Nanocomposites

2.3.1 Glassy Polymer Nanocomposites

Inclusion of nanofillers in polymers is important because the combined properties that can be achieved are often significantly enhanced over those of the neat polymer, as well as composites based on conventional fillers. Nanofillers are much smaller than traditional micro-fillers. Their size is typically 1-100 nm in dimension. One primary factor that gives nanocomposites their superior properties is the higher aspect ratios of nanofillers relative to micro-fillers. This creates much more surface area between the polymer and the filler, as governed by filler size, shape, and volume fraction [39]. Nanofillers are available in different geometries (*i.e.*, particles, platelets, and carbon nanotubes) and surface chemistries. Researchers have studied particle fillers that include metal oxides such as TiO_2 , Fe_2O_3 , SiO_2 , etc. [40]. Platelets have the advantage over fibers or particles in that they can reinforce a composite biaxially. Examples include organoclays, and nanoceramics [41,42]. Studies show that three times as much glass fiber and four times as much conventional talc can be required to achieve the same mechanical reinforcement that is obtained in nanocomposite materials using montmorillonite platelets as filler [43]. Results from numerical finite-difference modeling, comparing the effects of platelets versus fiber-like particles in nanocomposite systems, show that platelets produced a higher modulus because of their higher aspect

ratio [44]. Other fillers that have gained much attention in recent years because of their tremendous electrical and mechanical properties are carbon nanotubes [45-47].

Nanoparticles must be well-dispersed throughout the polymer matrix in order to fully realize the enhanced properties of the nanocomposite. One of the major challenges facing scientists is to avoid particle agglomeration [48]. Nanoparticles tend to agglomerate because they have a greater affinity for each other rather than the polymer. These agglomerations result in micron-sized behavior and negate the nano-effect. To help minimize agglomeration, researchers have sought to use nanoparticles that are inherently compatible with the polymer, or else to modify the nanoparticles by attaching compatible surface groups [39,48].

Fundamental insight regarding the character of the particle-polymer interface and the quality of the particle dispersion can be obtained by investigating the dynamic relaxation properties of the nanocomposite, and specifically the glass transition. Shifts in the glass transition temperature (T_g) relative to that of the unfilled polymer can potentially reflect specific particle-polymer interactions, as well as physical confinement effects. If there is a strong attraction between the polymer and the particles, T_g may increase [49]. If the particle surface is strongly de-wetting, T_g has been observed to decrease [50]. Competing forces that cancel out one another or balanced attraction forces can leave T_g unchanged. Sample preparation can also affect the T_g values observed [51]. In some cases, dual T_g behavior has been noted. Tsagaropoulos conducted dynamic mechanical studies on poly(vinyl acetate) comparing the effects of no particles, micron-size particles, and nanoparticles [52]. Results for the nanocomposite system showed two loss peaks, one for the bulk polymer and the second T_g about 100°C higher. The second peak was attributed

to constrained polymer at the surface of the filler. This second T_g was not seen with the micron-size particles because the surface area was not large enough to create a significant population of constrained polymer. Similar results were seen with polystyrene, PMMA, and poly(4-vinylpyridine) [52]. Tsagaropoulos went on to look at the effects of polymer molecular weight, particle loading, and heat treatment on this dual T_g behavior [53]. Higher molecular weight polymers showed more distinct loss peaks which were attributed to longer chains having more restricted mobility in the presence of the particles. Interestingly, at high filler loadings, the second loss peak decreased in intensity and shifted to lower temperatures. Tsagaropoulos explained that as particle loading increases, the restricted polymer region increases, causing a second T_g . However, at high loadings, a portion of the restricted polymer becomes immobile, and no longer contributes to the observed high-temperature glass transition. The polymer that remains mobile (and thus contributes to the higher T_g) is a sub-population further removed from the particle surface. This explains the loss peak shifting to lower temperatures, with reduced intensity [53].

Modeling the behavior of well-dispersed nanocomposites is complicated by the fact that real nanocomposites have (i) wide ranges of inter-particle distances and (ii) T_g 's that may be impacted by multiple nanoparticles within the length scale. One simple model consists of a polymer supported between two silica slides. Results from this model have been compared with real nanocomposites based on poly(2-vinyl pyridine) (P2VP) and poly (methyl methacrylate) [PMMA] [54]. Both P2VP and PMMA polymers are attracted to silica because of hydrogen bonding resulting in T_g increases across the length scale where confinement effects are observed. Ash studied the T_g behavior of PMMA

filled with alumina nanoparticles [55]. He observed a drop in T_g with the addition of nanoparticles as compared to the unfilled polymer. Scanning electron microscopy (SEM) analysis showed good dispersion of the nanoparticles but a lack of wetting of the particle surface by the polymer. When micron sized alumina particles were employed there was no significant change in T_g from that of the unfilled polymer. This implies that both surface area and interfacial quality play a significant role in determining the influence of the particles on T_g [50].

The glass transition characteristics observed for polymer thin films can provide useful insights into the relaxation behavior of polymer chains confined in the vicinity of a solid surface (*i.e.*, within a nanocomposite). Consequently, much research is focused in this area [56-68]. In thin films where film thickness is reduced below 150 nm, T_g begins to deviate from that of the bulk polymer. Films can be self-supporting, supported on one side, or sandwiched between two hard surfaces. T_g will vary depending on film thickness and compatibility of the polymer with the surface. Forrest saw reductions in T_g for self-supporting films as film thickness decreased [58,59,61]. For films supported by a substrate, T_g is highly sensitive to the character of the solid surface. Results have shown that T_g decreases when there is little compatibility between the polymer and the substrate. Others have seen increases in T_g that were attributed to greater compatibility or specific interactions [67]. As the polymer film thickness decreases, the T_g shifts are more pronounced. Mundra's work shows that the free surface of the polymer competes with the forces at the polymer-substrate interface, and that the ratio of these surface areas has a significant impact on the shift in T_g [68].

With film thickness establishing the confining dimension, studies have been undertaken to evaluate the relative importance of physical confinement on T_g as compared to specific polymer-surface interactions. For example, Keddie studied the effects of molecular weight for polystyrene thin films on silicon wafers. He found no strong molecular weight dependence [56]. However, later studies by others on free-standing films of polystyrene concluded that there is a significant molecular weight dependence on T_g in the thin film region, and that chain confinement effects are important [60,61]. In molecular dynamics simulations, confinement effects were not necessary to explain polymer-particle dynamics near the interface: predicted T_g shifts were similar to experimental results even though confinement effects were not required. This implies that surface interactions are dominant relative to the physical constraint [62].

Bansal reported a quantitative comparison for variations in T_g as a function of polymer thin film thickness, and interparticle spacing in bulk polymer nanocomposites below the length scale of ~ 150 nm [65]. He studied the effect of SiO_2 filler loadings on the T_g of polystyrene (PS) nanocomposites. It was observed that decreases in T_g with increasing filler content tracked with the results for planar free-standing films. This led to the conclusion that when the particle spacing is on the same scale as film thickness, the T_g response is the same. Further studies using modified (wetting) SiO_2 nanoparticles confirmed these results in comparison to substrate-supported thin films. Different solvents were used in film preparation affecting both particle spacing and degree of agglomeration, but this did not alter the fundamental relationship between thin film thickness and interparticle spacing.

In addition to enhanced mechanical and thermal performance characteristics, improved transport properties have been achieved with certain nanocomposite systems used as selective gas separation membranes. For example, Merkel found that gas permeability and selectivity were enhanced with the addition of fumed silica nanoparticles in high-free volume, glassy poly(4-methyl-2-pentyne) (PMP) [69,70]. The increased permeability was a result of an increase in diffusion and not a significant function of gas solubility. The silica nanoparticles disrupt chain packing resulting in a subtle increase in local free volume, as confirmed by positron annihilation lifetime spectroscopy (PALS). For reverse-selective separations where smaller molecules are retained relative to larger molecules, the presence of the nanoparticles weakens the size-sieving capability of the PMP, leading to an overall improvement in selectivity. Merkel conducted similar studies combining silica nanoparticles with other high free volume glassy polymers and obtained comparable results [71,72].

Takahashi introduced different types of silica into glassy, amorphous polyetherimide (PEI) [73]. As with Merkel, Takahashi generally observed increases in permeability with particle loading, but unlike Merkel selectivity decreased as particle loading increased. Although the silica types were all hydrophobic, the resulting nanocomposites suffered from varying levels of agglomeration and particle void formation at the polymer-particle interface resulting in decreased selectivity from the neat polymer. SEM and transmission electron microscopy (TEM) confirmed the particle distribution. The permeability and selectivity results can be explained by an apparent dual diffusion pathway, with gas molecules moving simultaneously through the voids formed at the polymer-particle interface and the bulk polymer matrix. Takahashi later chemically coupled the silica

particles to the polymer matrix which resulted in better dispersion but did not entirely eliminate void formation [74]. Permeability decreased as particle loading increased while selectivity decreased or remained the same.

The largest increases in permeability with glassy polymer nanocomposites were reported by Matteucci [75]. In these studies, MgO nanoparticles were dispersed in poly(1-trimethylsilyl-1-propyne) (PTMSP). TEM analysis showed that MgO does not disperse throughout the polymer matrix as nano-size particles, but instead forms regions of micron-sized aggregates. Gas permeability increased significantly (17 to 40 times) with particle loading, which was attributed to void formation within the composite. Matteucci also conducted studies with PTMSP using titanium dioxide (TiO₂) nanoparticles which dispersed primarily as single particles (3 nm diameter) at low loadings and as micron-sized aggregates at high loadings [76]. Permeability decreased below that of the unfilled polymer at low loadings, and increased more than 2 to 4 times that of the unfilled polymer at high loadings. Selectivity showed no significant change with particle loading owing to the offsetting effects of solubility increasing and diffusivity decreasing in the presence of the particles.

2.3.2 Rubbery Polymer Nanocomposites

Rubbery polymer nanocomposites are typically comprised of a semi-crystalline or chemically crosslinked polymer matrix in combination with nanoscale filler. Recently, a series of fundamental studies were completed on the dynamic relaxation and gas transport properties of amorphous crosslinked poly(ethylene oxide) networks formulated for the separation of quadrupolar-nonpolar gas pairs (CO₂/H₂ and CO₂/CH₄). The crosslinked

networks were intentionally designed to suppress crystallinity, enhance fractional free volume, and engender maximum solubility of quadrupolar gases such as CO₂ relative to light gases such as H₂ or CH₄. Studies by Lin *et al.* [77] using crosslinked poly (ethylene glycol diacrylate) [XLPEGDA] showed that crosslink density does not adversely affect the gas transport properties of these membranes. XLPEGDA displays favorable gas solubility [78] and diffusion characteristics for CO₂ which account for a combination of both high selectivity and permeability [79-81]. Through strategic modifications to the network structure (for example, via copolymerization with PEO-rich co-monomer), material design strategies were refined for the optimization of membrane separation performance in the crosslinked PEO membranes [82-85]. Detailed investigation of the segmental relaxation properties of these materials helped to establish the underlying relationships between molecular structure and enhanced transport properties [86-90].

In addition to competitive transport properties, viable commercial gas separation membranes must have good mechanical properties that can withstand demanding industrial conditions. The incorporation of nanofiller in crosslinked PEO membranes without a significant reduction in transport properties makes this an attractive option. Initial gas transport studies of nanocomposites based on XLPEGDA have indicated minimal changes in permeability and selectivity at relatively low particle loadings. Patel used silica nanoparticles modified with methacrylate surface groups to permit covalent coupling with the acrylate-terminated polymer chains [91,92]. He later compared PEGDA nanocomposites with poly(propylene glycol diacrylate) [PPGDA] using silica nanoparticles and saw similar results. It was observed that an increase in oligomer

molecular weight corresponded to a systematic increase in permeability and selectivity [93], as influenced by crosslink density.

An alternative approach for the formulation of rubbery nanocomposite membranes is the introduction of nanoscale particles into semi-crystalline polymer rubbers. For example, Matteucci recently explored the incorporation of TiO₂ nanoparticles dispersed in 1,2-polybutadiene (PB), wherein the resulting composite showed increases in CO₂, CH₄, N₂ and H₂ permeability of more than three times the unfilled polymer with no change in selectivity [94]. The permeability enhancement was attributed to an increase in gas solubility owing to the presence of highly sorbing filler. Similar studies were conducted dispersing MgO nanoparticles in PB [95]. Transport measurements showed increases in permeability of more than ten times the unfilled polymer coupled with only a limited decrease in selectivity. However, density determinations and transmission electron microscopy analysis indicated substantial void volume with increased filler loading, with void fraction exceeding 50% at the highest loadings studied. The large enhancements in permeability for this composite system were attributed primarily to transport through the void regions of the membrane.

For the work presented in this dissertation, investigations of both glassy and rubbery polymers filled with nanoparticles of various size, shape, and chemical composition are expected to yield broad insights regarding polymer-particle interaction and physical confinement effects. Through the use of dynamic mechanical and dielectric methods, the molecular motions of these nanocomposites may be correlated with their chemical structure and transport morphology, facilitating new strategies for membrane design and other potential applications.

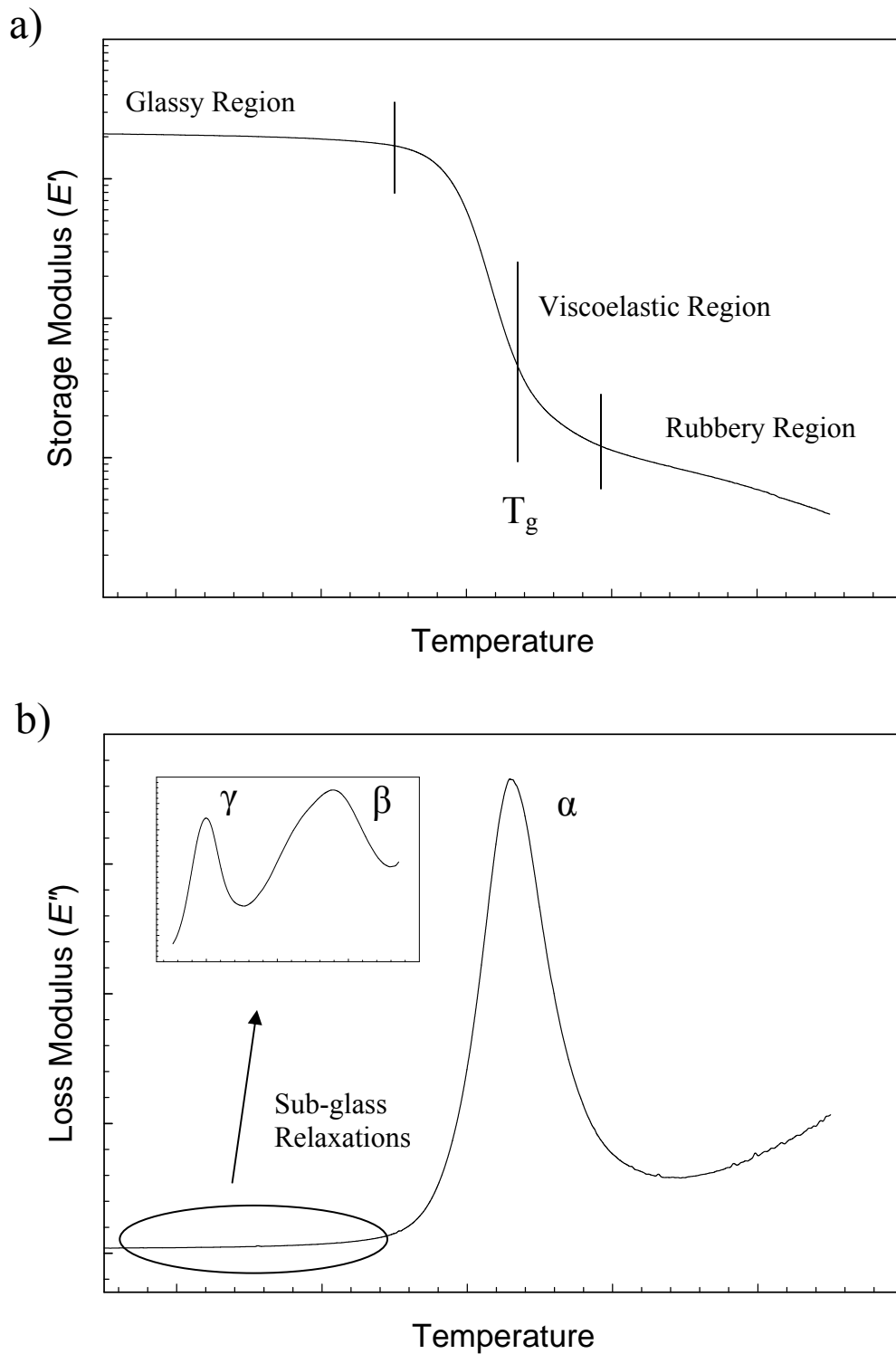


Figure 2.1: Typical viscoelastic response curves for an amorphous polymer: (a) storage modulus (E') and (b) loss modulus (E'') vs. temperature.

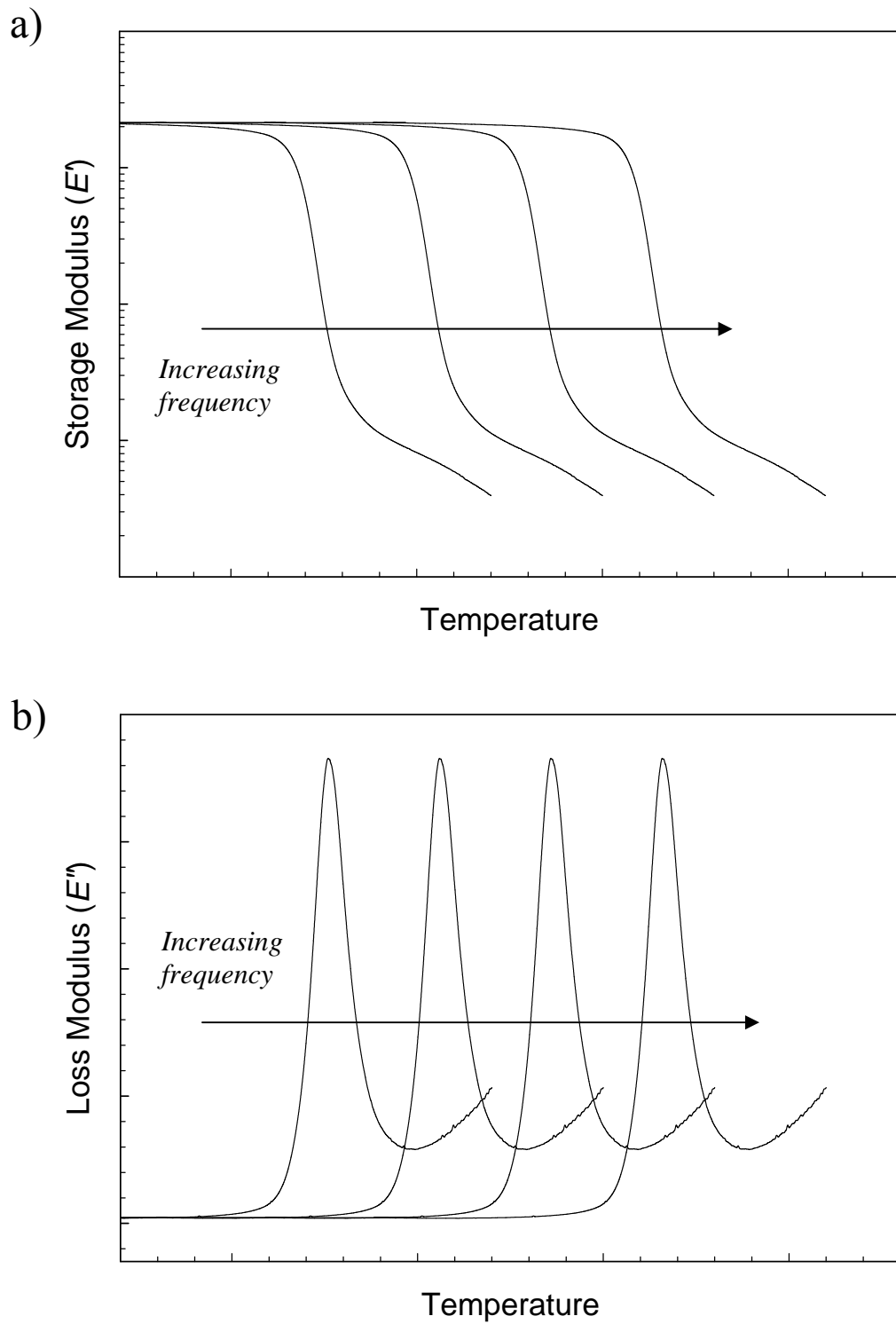


Figure 2.2: Frequency dependence of dynamic mechanical relaxation properties: (a) storage modulus (E') and (b) loss modulus (E'') vs. temperature.

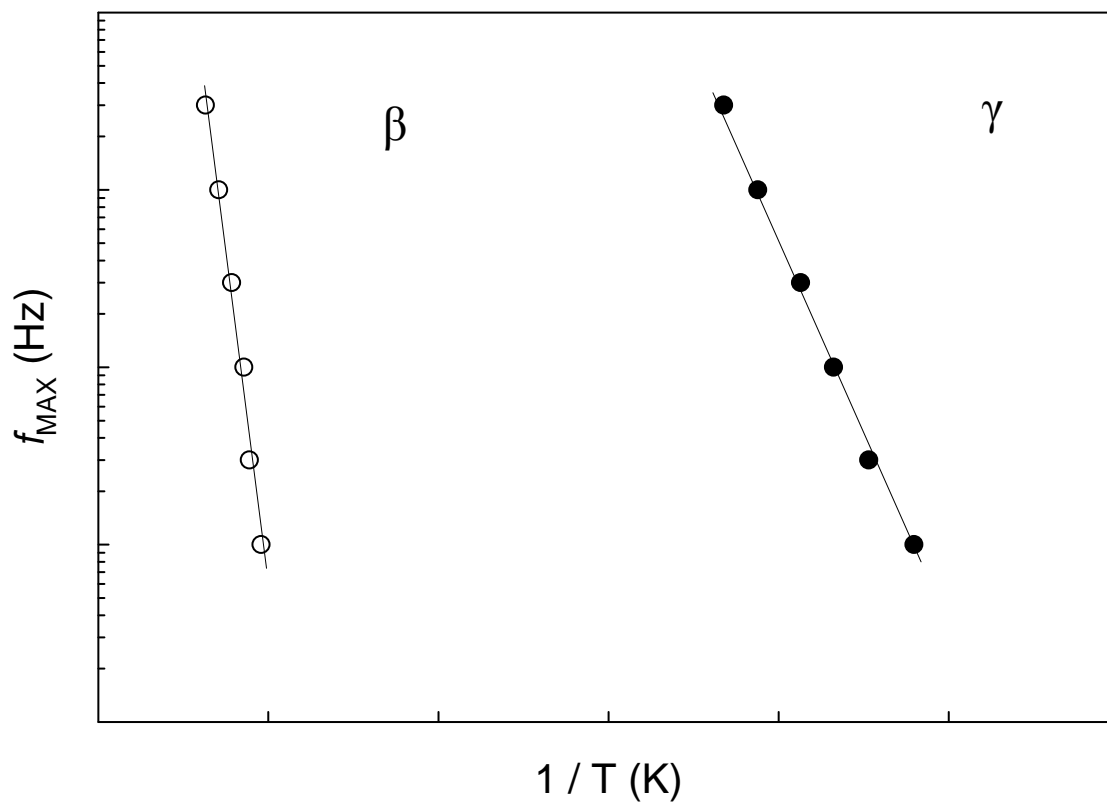
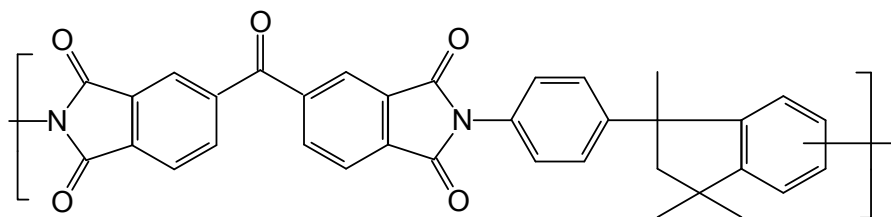
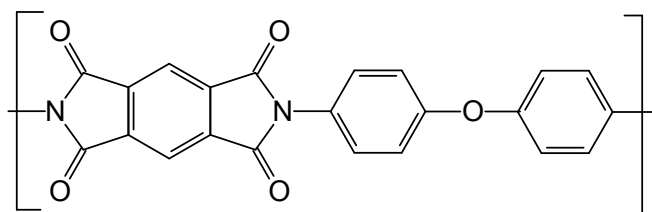


Figure 2.3: Typical Arrhenius plot for sub-glass relaxations.



Matrimid[®]



Kapton[®]

Figure 2.4: Chemical structures for Matrimid[®] and Kapton[®] commercial polyimides.

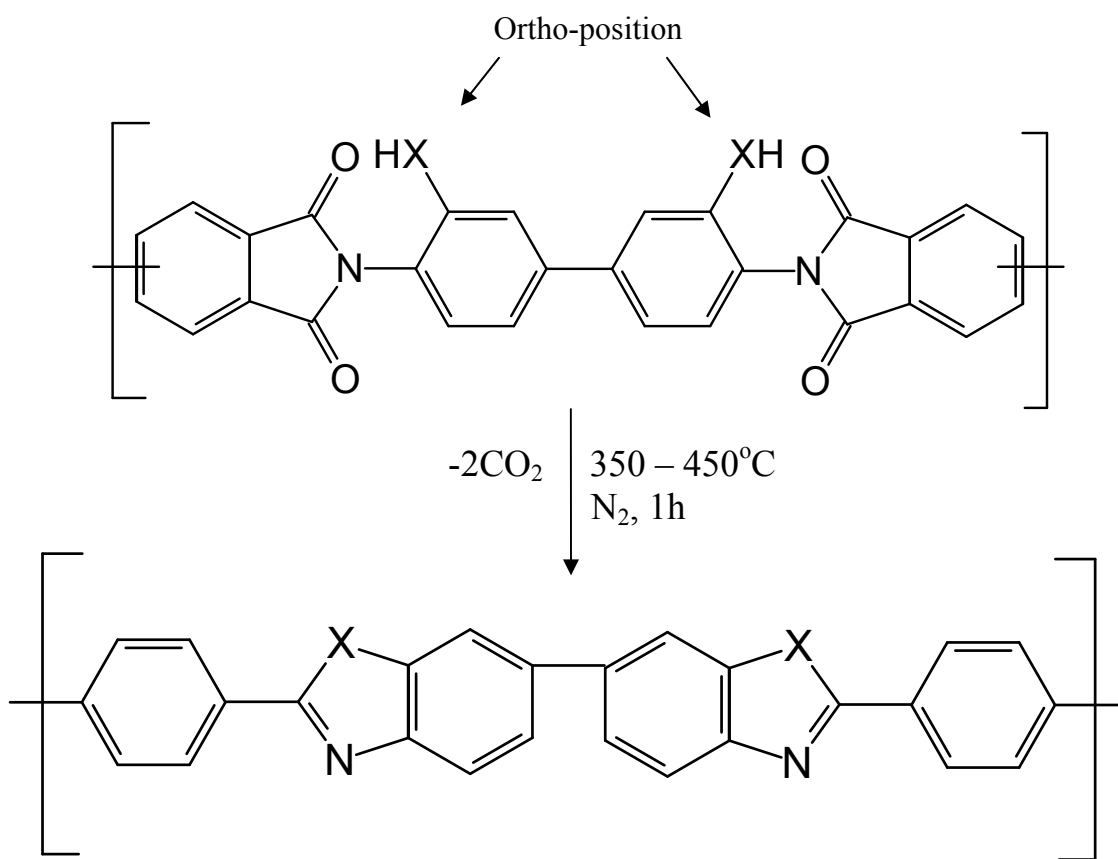


Figure 2.5: General thermal rearrangement of an aromatic polyimide [38].

References

- [1] Ferry, J.D. *Viscoelastic Properties of Polymers*, 3rd edition; John Wiley and Sons: New York, **1980**.
- [2] Sroog, C.E., "Polyimides", In *Encyclopedia of Polymer Science and Technology*, 1st edition; John Wiley & Sons, Inc., **1969**; Vol. 11, pp 247-272.
- [3] Sroog, C.E. "Polyimides", *Progress in Polymer Science* **1991**, *16*, 561.
- [4] Lim, T.; Frosini, V.; Zaleckas, V.; Morrow, D.; Sauer, J.A. "Mechanical Relaxation Phenomena in Polyimide and Poly(2,6-dimethyl-p-phenylene oxide) from 100K to 700K", *Polymer Engineering and Science* **1973**, *13*, 51.
- [5] Perena, J.M. "Dynamic Mechanical Relaxations in Polyimide and Polyamideimide", *Angewandte Makromolekulare Chemie* **1982**, *106*, 61.
- [6] Xu, G.; Gryte, C.C.; Nowick, A.S.; Li, S.Z.; Pak, Y.S.; Greenbaum, S.G. "Dielectric Relaxation and Deuteron NMR of Water in Polyimide Films", *Journal of Applied Physics* **1989**, *66*, 5290.
- [7] Sun, Z.; Dong, L.; Zhuang, Y.; Cao, L.; Ding, M.; Feng, Z. "Beta Relaxation in Polyimides", *Polymer* **1992**, *33*, 4728.
- [8] Arnold, F.E., Jr.; Bruno, K.R.; Shen, D.; Eashoo, M.; Lee, C.J.; Harris, F.W.; Cheng, S.Z.D. "The Origin of β Relaxations in Segmented Rigid-Rod Polyimide and Copolyimide Films", *Polymer Engineering and Science* **1993**, *33*, 1373.
- [9] Coburn, J.C.; Soper, P.D.; Auman, B.C. "Relaxation Behavior of Polyimides Based on 2,2'-Disubstituted Benzidines", *Macromolecules* **1995**, *28*, 3253.
- [10] Cheng, S.Z.D.; Chalmers, T.M.; Gu, Y.; Yoon, Y.; Harris, F.W.; Cheng, J.; Fone, M.; Koenig, J.L. "Relaxation Processes and Molecular Motion in a New Semicrystalline Polyimide", *Macromolecular Chemistry and Physics* **1995**, *196*, 1439.
- [11] Kim, Y.H.; Moon, B.S.; Harris, F.W.; Cheng, S.Z.D. "Polymerization, Structure and Thermal Properties of ODPa-DMB Polyimide Films", *Journal of Thermal Analysis and Calorimetry* **1996**, *46*, 921.
- [12] Habas, J.P.; Peyrelasse, J.; Grenier-Loustalot, M.F. "Rheological Study of a High-Performance Polyimide. Interpretation of the Secondary Mechanical Relaxations of a Nadimide Crosslinked System", *High Performance Polymers* **1996**, *8*, 515.

- [13] Li, S.; Hsu, B.L.; Li, F.; Li, C.Y.; Harris, F.W.; Cheng, S.Z.D. "A Study of Polyimide Thermoplastics Used as Tougheners in Epoxy Resins - Structure, Property and Solubility Relationships", *Thermochimica Acta* **1999**, 340-341, 221.
- [14] Li, F.; Fang, S.; Ge, J.J.; Honigfort, P.S.; Chen, J.C.; Harris, F.W.; Cheng, S.Z.D. "Diamine Architecture Effects on Glass Transitions, Relaxation Processes and Other Material Properties in Organo-Soluble Aromatic Polyimide Films", *Polymer* **1999**, 40, 4571.
- [15] Li, F.; Ge, J.J.; Honigfort, P.S.; Fang, S.; Chen, J.-C.; Harris, F.W.; Cheng, S.Z.D. "Dianhydride Architectural Effects on the Relaxation Behaviors and Thermal and Optical Properties of Organo-Soluble Aromatic Polyimide Films", *Polymer* **1999**, 40, 4987.
- [16] Qu, W.; Ko, T.M.; Vora, R.H.; Chung, T.S. "Effect of Polyimides with Different Ratios of Para- to Meta- Analogous Fluorinated Diamines on Relaxation Process", *Polymer* **2001**, 42, 6393.
- [17] Eichstadt, A.E.; Ward, T.C.; Bagwell, M.D.; Farr, I.V.; Dunson, D.L.; McGrath, J.E. "Synthesis and Characterization of Amorphous Partially Aliphatic Polyimide Copolymers Based on Bisphenol-A Dianhydride", *Macromolecules* **2002**, 35, 7561.
- [18] Bas, C.; Tamagna, C.; Pascal, T.; Alberola, N.D. "On the Dynamic Mechanical Behavior of Polyimides Based on Aromatic and Alicyclic Dianhydrides", *Polymer Engineering & Science* **2003**, 43, 344.
- [19] Calleja, R.D.; Friederichs, S.; Jaimes, C.; Sanchis, M.J.; Belana, J.; Canadas, J.C.; Diego, J.A.; Mudarra, M. "Comparative Study of Mechanical and Electrical Relaxations in Poly(etherimide). Part 2", *Polymer International* **1998**, 46, 20.
- [20] Eichstadt, A.E.; Andreev, S.; Ward, T.C. "The Effect of Water on the Viscoelastic Properties of Polyimides", *Proceedings of the Annual Meeting of the Adhesion Society* **2000**, 23, 484.
- [21] Ekiner, O.M. "Phenylindane Group-Containing Polyimide Gas-Separation Membranes", *US Patent 5,015,270* **1991**.
- [22] Simmons, J.W.; Ekiner, O.M. "Preparation and Uses of Polyimide and Polyamide-Polyimide Gas Separation Membranes", *US Patent 5,232,472* **1993**.
- [23] Bos, A.; Punt, I.G.M.; Wessling, M.; Strathmann, H. "Plasticization-Resistant Glassy Polyimide Membranes for CO₂/CH₄ Separations", *Separation and Purification Technology* **1998**, 14, 27.

- [24] Wind, J.D.; Paul, D.R.; Koros, W.J. "Natural Gas Permeation in Polyimide Membranes", *Journal of Membrane Science* **2004**, *228*, 227.
- [25] Tanaka, K.; Okamoto, K.-I., "Structure and Transport Properties of Polyimides as Materials for Gas and Vapor Membrane Separation", In *Materials Science of Membranes for Gas and Vapor Separation*; Yampolskii, Y.; Pinnau, I.; Freeman, B.D., eds.; John Wiley & Sons: New York, **2006**; pp 271-291.
- [26] Kase, Y., "Gas Separation by Polyimide Membranes", In *Advanced Membrane Technology Applications*; Li, N.; Fane, A.G.; Ho, W.S.W.; Matsuura, T., eds.; John Wiley & Sons: New York, **2008**; pp 581-598.
- [27] Robeson, L.M. "The Upper Bound Revisited", *Journal of Membrane Science* **2008**, *320*, 390.
- [28] Huang, X.; Shao, L.; Meng, L.; Huang, Y. "Advances in Modification Methods of Polyimide Membranes for Gas Separation", *Mo Kexue Yu Jishu* **2009**, *29*, 101.
- [29] Simons, K.; Nijmeijer, K.; Sala, J.G.; Van Der Werf, H.; Benes, N.E.; Dingemans, T.J.; Wessling, M. "CO₂ Sorption and Transport Behavior of ODPA-Based Polyetherimide Polymer Films", *Polymer* **2010**, *51*, 3907.
- [30] Bos, A.; Punt, I.; Strathmann, H.; Wessling, M. "Suppression of Gas Separation Membrane Plasticization by Homogeneous Polymer Blending", *AIChE Journal* **2001**, *47*, 1088.
- [31] Huang, Y.; Paul, D.R. "Physical Aging of Thin Glassy Polymer Films Monitored by Gas Permeability", *Polymer* **2004**, *45*, 8377.
- [32] Madden, W.C.; Punsalan, D.; Koros, W.J. "Age Dependent CO₂ Sorption in Matrimid Asymmetric Hollow Fiber Membranes", *Polymer* **2005**, *46*, 5433.
- [33] Huang, Y.; Paul, D.R. "Physical Aging of Thin Glassy Polymer Films Monitored by Optical Properties", *Macromolecules* **2006**, *39*, 1554.
- [34] Fu, Y.-J.; Hsiao, S.-W.; Hu, C.-C.; Qui, H.-z.; Lee, K.-R.; Lai, J.-Y. "Effect of Physical Aging on Sorption and Permeation of Small Molecules in Polyimide Membranes", *Desalination* **2008**, *234*, 58.
- [35] Huang, Y.; Paul, D.R. "Experimental Methods for Tracking Physical Aging of Thin Glassy Polymer Films by Gas Permeation", *Journal of Membrane Science* **2004**, *244*, 167.
- [36] Rowe, B.W.; Freeman, B.D.; Paul, D.R. "Physical Aging of Ultrathin Glassy Polymer Films Tracked by Gas Permeability", *Polymer* **2009**, *50*, 5565.

- [37] Rowe, B.W.; Freeman, B.D.; Paul, D.R. "Influence of Previous History on Physical Aging in Thin Glassy Polymer Films as Gas Separation Membranes", *Polymer* **2010**, *51*, 3784.
- [38] Park, H.B.; Jung, C.H.; Lee, Y.M.; Hill, A.J.; Pas, S.J.; Mudie, S.T.; Van Wagner, E.; Freeman, B.D.; Cookson, D.J. "Polymers with Cavities Tuned for Fast Selective Transport of Small Molecules and Ions", *Science* **2007**, *318*, 254.
- [39] Schaefer, D.W.; Justice, R.S. "How Nano are Nanocomposites?", *Macromolecules* **2007**, *40*, 8501.
- [40] Krishnamoorti, R.; Vaia, R.A. "Polymer Nanocomposites", *Journal of Polymer Science, Part B: Polymer Physics* **2007**, *45*, 3252.
- [41] Tjong, S.C. "Structural and Mechanical Properties of Polymer Nanocomposites", *Materials Science & Engineering, R: Reports* **2006**, *R53*, 73.
- [42] Esfandiari, A.; Nazokdast, H.; Rashidi, A.-S.; Yazdanshenas, M.-E. "Review of Polymer-Organoclay Nanocomposites", *Journal of Applied Sciences* **2008**, *8*, 545.
- [43] Paul, D.R.; Robeson, L.M. "Polymer Nanotechnology: Nanocomposites", *Polymer* **2008**, *49*, 3187.
- [44] Termonia, Y. "Structure-Property Relationships in Nanocomposites", *Polymer* **2007**, *48*, 6948.
- [45] Xie, X.-L.; Mai, Y.-W.; Zhou, X.-P. "Dispersion and Alignment of Carbon Nanotubes in Polymer Matrix: A Review", *Materials Science & Engineering, R: Reports* **2005**, *R49*, 89.
- [46] Moniruzzaman, M.; Winey, K.I. "Polymer Nanocomposites Containing Carbon Nanotubes", *Macromolecules* **2006**, *39*, 5194.
- [47] Coleman, J.N.; Khan, U.; Gun'ko, Y.K. "Mechanical Reinforcement of Polymers Using Carbon Nanotubes", *Advanced Materials* **2006**, *18*, 689.
- [48] Krishnamoorti, R. "Strategies for Dispersing Nanoparticles in Polymers", *MRS Bulletin* **2007**, *32*, 341.
- [49] Priestley, R.D.; Mundra, M.K.; Barnett, N.J.; Broadbelt, L.J.; Torkelson, J.M. "Effects of Nanoscale Confinement and Interfaces on the Glass Transition Temperatures of a Series of Poly(n-methacrylate) Films", *Australian Journal of Chemistry* **2007**, *60*, 765.

- [50] Ash, B.J.; Siegel, R.W.; Schadler, L.S. "Glass-Transition Temperature Behavior of Alumina/PMMA Nanocomposites", *Journal of Polymer Science, Part B: Polymer Physics* **2004**, *42*, 4371.
- [51] Hub, C.; Harton, S.E.; Hunt, M.A.; Fink, R.; Ade, H. "Influence of Sample Preparation and Processing on Observed Glass Transition Temperatures of Polymer Nanocomposites", *Journal of Polymer Science, Part B: Polymer Physics* **2007**, *45*, 2270.
- [52] Tsagaropoulos, G.; Eisenberg, A. "Direct Observation of Two Glass Transitions in Silica-Filled Polymers. Implications for the Morphology of Random Ionomers", *Macromolecules* **1995**, *28*, 396.
- [53] Tsagaropoulos, G.; Eisenberg, A. "Dynamic Mechanical Study of the Factors Affecting the Two Glass Transition Behavior of Filled Polymers. Similarities and Differences with Random Ionomers", *Macromolecules* **1995**, *28*, 6067.
- [54] Rittigstein, P.; Priestley, R.D.; Broadbelt, L.J.; Torkelson, J.M. "Model Polymer Nanocomposites Provide an Understanding of Confinement Effects in Real Nanocomposites", *Nature Materials* **2007**, *6*, 278.
- [55] Ash, B.J.; Rogers, D.F.; Wiegand, C.J.; Schadler, L.S.; Siegel, R.W.; Benicewicz, B.C.; Apple, T. "Mechanical Properties of Al₂O₃/Polymethylmethacrylate Nanocomposites", *Polymer Composites* **2002**, *23*, 1014.
- [56] Keddie, J.L.; Jones, R.A.L.; Cory, R.A. "Size-Dependent Depression of the Glass Transition Temperature in Polymer Films", *Europhysics Letters* **1994**, *27*, 59.
- [57] Zanten, J.H.; Wallace, W.E.; Wu, W. "Effect of Strongly Favorable Substrate Interactions on the Thermal Properties of Ultrathin Polymer Films", *Physical Review E* **1996**, *53*, 2053.
- [58] Forrest, J.A.; Dalnoki-Veress, K.; Stevens, J.R.; Dutcher, J.R. "Effect of Free Surfaces on the Glass Transition Temperature of Thin Polymer Films", *Physical Review Letters* **1996**, *77*, 2002.
- [59] Forrest, J.A.; Dalnoki-Veress, K.; Dutcher, J.R. "Interface and Chain Confinement Effects on the Glass Transition Temperature of Thin Polymer Films", *Physical Review E* **1997**, *56*, 5705.
- [60] Mattsson, J.; Forrest, J.A.; Borjesson, L. "Quantifying Glass Transition Behavior in Ultrathin Free-Standing Polymer Films", *Physical Review E* **2000**, *62*, 5187.

- [61] Dalnoki-Veress, K.; Forrest, J.A.; Murray, C.; Gigault, C.; Dutcher, J.R. "Molecular Weight Dependence of Reductions in the Glass Transition Temperature of Thin, Freely Standing Polymer Films", *Physical Review E* **2001**, *63*, 031801/1.
- [62] Starr, F.W.; Schroder, T.B.; Glotzer, S.C. "Effects of a Nanoscopic Filler on the Structure and Dynamics of a Simulated Polymer Melt and the Relationship to Ultrathin Films", *Physical Review E* **2001**, *64*, 021802/1.
- [63] Kawana, S.; Jones, R.A.L. "Character of the Glass Transition in Thin Supported Polymer Films", *Physical Review E* **2001**, *63*, 021501.
- [64] Forrest, J.A. "A Decade of Dynamics in Thin Films of Polystyrene: Where Are We Now?", *European Physical Journal E* **2002**, *8*, 261.
- [65] Bansal, A.; Yang, H.; Li, C.; Cho, K.; Benicewicz, B.C.; Kumar, S.K.; Schadler, L.S. "Quantitative Equivalence Between Polymer Nanocomposites and Thin Polymer Films", *Nature Materials* **2005**, *4*, 693.
- [66] Ellison, C.J.; Mundra, M.K.; Torkelson, J.M. "Impacts of Polystyrene Molecular Weight and Modification to the Repeat Unit Structure on the Glass Transition-Nanoconfinement Effect and the Cooperativity Length Scale", *Macromolecules* **2005**, *38*, 1767.
- [67] Priestley, R.D.; Rittigstein, P.; Broadbelt, L.J.; Fukao, K.; Torkelson, J.M. "Evidence for the Molecular-Scale Origin of the Suppression of Physical Ageing in Confined Polymer: Fluorescence and Dielectric Spectroscopy Studies of Polymer-Silica Nanocomposites", *Journal of Physics: Condensed Matter* **2007**, *19*, 205120/1.
- [68] Mundra, M.K.; Donthu, S.K.; Dravid, V.P.; Torkelson, J.M. "Effect of Spatial Confinement on the Glass-Transition Temperature of Patterned Polymer Nanostructures", *Nano Letters* **2007**, *7*, 713.
- [69] Merkel, T.C.; Freeman, B.D.; Spontak, R.J.; He, Z.; Pinnau, I.; Meakin, P.; Hill, A.J. "Ultraporous, Reverse-Selective Nanocomposite Membranes", *Science* **2002**, *296*, 519.
- [70] Merkel, T.C.; Freeman, B.D.; Spontak, R.J.; He, Z.; Pinnau, I.; Meakin, P.; Hill, A.J. "Sorption, Transport, and Structural Evidence for Enhanced Free Volume in Poly (4-methyl-2-pentyne)/Fumed Silica Nanocomposite Membranes", *Chemistry of Materials* **2003**, *15*, 109.
- [71] Merkel, T.C.; He, Z.; Pinnau, I.; Freeman, B.D.; Meakin, P.; Hill, A.J. "Effect of Nanoparticles on Gas Sorption and Transport in Poly(1-trimethylsilyl-1-propyne)", *Macromolecules* **2003**, *36*, 6844.

- [72] Merkel, T.C.; He, Z.; Pinnau, I.; Freeman, B.D.; Meakin, P.; Hill, A.J. "Sorption and Transport in Poly (2,2-bis(trifluoromethyl)-4,5-difluoro-1,3-dioxole-co-tetrafluoroethylene) Containing Nanoscale Fumed Silica", *Macromolecules* **2003**, *36*, 8406.
- [73] Takahashi, S.; Paul, D.R. "Gas Permeation in Poly(Ether Imide) Nanocomposite Membranes Based on Surface-Treated Silica. Part 1: Without Chemical Coupling to Matrix", *Polymer* **2006**, *47*, 7519.
- [74] Takahashi, S.; Paul, D.R. "Gas Permeation in Poly(Ether Imide) Nanocomposite Membranes Based on Surface-Treated Silica. Part 2: With Chemical Coupling to Matrix", *Polymer* **2006**, *47*, 7535.
- [75] Matteucci, S.; Kusuma, V.A.; Kelman, S.D.; Freeman, B.D. "Gas Transport Properties of MgO Filled Poly(1-trimethylsilyl-1-propyne) Nanocomposites", *Polymer* **2008**, *49*, 1659.
- [76] Matteucci, S.; Kusuma, V.A.; Sanders, D.; Swinnea, S.; Freeman, B.D. "Gas Transport in TiO₂ Nanoparticle-Filled Poly(1-trimethylsilyl-1-propyne)", *Journal of Membrane Science* **2008**, *307*, 196.
- [77] Lin, H.; Kai, T.; Freeman, B.D.; Kalakkunnath, S.; Kalika, D.S. "The Effect of Crosslinking on Gas Permeability in Crosslinked Poly(ethylene glycol diacrylate)", *Macromolecules* **2005**, *38*, 8381.
- [78] Lin, H.; Freeman, B.D. "Materials Selection Guidelines for Membranes that Remove CO₂ from Gas Mixtures", *Journal of Molecular Structure* **2005**, *739*, 57.
- [79] Lin, H.; Freeman, B.D. "Gas and Vapor Solubility in Cross-Linked Poly(ethylene glycol diacrylate)", *Macromolecules* **2005**, *38*, 8394.
- [80] Lin, H.; Freeman, B.D. "Gas Permeation and Diffusion in Cross-Linked Poly(ethylene glycol diacrylate)", *Macromolecules* **2006**, *39*, 3568.
- [81] Lin, H.; Van Wagner, E.; Swinnea, J.S.; Freeman, B.D.; Pas, S.J.; Hill, A.J.; Kalakkunnath, S.; Kalika, D.S. "Transport and Structural Characteristics of Crosslinked Poly(ethylene oxide) Rubbers", *Journal of Membrane Science* **2006**, *276*, 145.
- [82] Raharjo, R.D.; Lin, H.; Sanders, D.F.; Freeman, B.D.; Kalakkunnath, S.; Kalika, D.S. "Relation Between Network Structure and Gas Transport in Crosslinked Poly(propylene glycol diacrylate)", *Journal of Membrane Science* **2006**, *283*, 253.

- [83] Kusuma, V.A.; Freeman, B.D.; Borna, M.A.; Kalika, D.S. "Influence of Chemical Structure of Short Chain Pendant Groups on Gas Transport Properties of Cross-linked Poly(ethylene oxide) Copolymers", *Journal of Membrane Science* **2009**, 327, 195.
- [84] Kusuma, V.A.; Matteucci, S.; Freeman, B.D.; Danquah, M.K.; Kalika, D.S. "Influence of Phenoxy-terminated Short-chain Pendant Groups on Gas Transport Properties of Cross-linked Poly(ethylene oxide) Copolymers", *Journal of Membrane Science* **2009**, 341, 84.
- [85] Kusuma, V.A.; Freeman, B.D.; Smith, S.L.; Heilman, A.L.; Kalika, D.S. "Influence of TRIS-based Co-monomer on Structure and Gas Transport Properties of Cross-linked Poly(ethylene oxide)", *Journal of Membrane Science* **2010**, 359, 25.
- [86] Kalakkunnath, S.; Kalika, D.S.; Lin, H.; Freeman, B.D. "Segmental Relaxation Characteristics of Cross-Linked Poly(Ethylene Oxide) Copolymer Networks", *Macromolecules* **2005**, 38, 9679.
- [87] Kalakkunnath, S.; Kalika, D.S.; Lin, H.; Raharjo, R.D.; Freeman, B.D. "Molecular Relaxation in Cross-linked Poly(Ethylene Glycol) and Poly(Propylene Glycol) Diacrylate Networks by Dielectric Spectroscopy", *Polymer* **2007**, 48, 579.
- [88] Kalakkunnath, S.; Kalika, D.S.; Lin, H.; Raharjo, R.D.; Freeman, B.D. "Molecular Dynamics of Poly(Ethylene Glycol) and Poly(Propylene Glycol) Copolymer Networks by Broadband Dielectric Spectroscopy", *Macromolecules* **2007**, 40, 2773.
- [89] Borna, M.A.; Kalakkunnath, S.; Kalika, D.S.; Kusuma, V.A.; Freeman, B.D. "Dynamic Relaxation Characteristics of Crosslinked Poly(ethylene oxide) Copolymer Networks: Influence of Short Chain Pendant Groups", *Polymer* **2007**, 48, 7316.
- [90] Richards, J.J.; Danquah, M.K.; Kalakkunnath, S.; Kalika, D.S.; Kusuma, V.A.; Matteucci, S.T.; Freeman, B.D. "Relation Between Structure and Gas Transport Properties of Polyethylene Oxide Networks Based on Crosslinked Bisphenol A Ethoxylate Diacrylate", *Chemical Engineering Science* **2009**, 64, 4707.
- [91] Patel, N.P.; Miller, A.C.; Spontak, R.J. "Highly CO₂-Permeable and Selective Polymer Nanocomposite Membranes", *Advanced Materials* **2003**, 15, 729.
- [92] Patel, N.P.; Miller, A.C.; Spontak, R.J. "Highly CO₂-Permeable and Selective Membranes Derived from Crosslinked Poly(Ethylene Glycol) and its Nanocomposites", *Advanced Functional Materials* **2004**, 14, 699.

- [93] Patel, N.P.; Aberg, C.M.; Sanchez, A.M.; Capracotta, M.D.; Martin, J.D.; Spontak, R.J. "Morphological, Mechanical and Gas-Transport Characteristics of Crosslinked Poly(Propylene Glycol): Homopolymers, Nanocomposites, and Blends", *Polymer* **2004**, *45*, 5941.
- [94] Matteucci, S.; Kusuma, V.A.; Swinnea, S.; Freeman, B.D. "Gas Permeability, Solubility and Diffusivity in 1,2-Polybutadiene Containing Brookite Nanoparticles", *Polymer* **2008**, *49*, 757.
- [95] Matteucci, S.; Raharjo, R.D.; Kusuma, V.A.; Swinnea, S.; Freeman, B.D. "Gas Permeability, Solubility, and Diffusion Coefficients in 1,2-Polybutadiene Containing Magnesium Oxide", *Macromolecules* **2008**, *41*, 2144.

Chapter 3

Experimental Methods

3.1 Materials

3.1.1 Matrimid[®] Polyimide

Commercial polyimide based on 3,3'-4,4'-benzophenone tetracarboxylic dianhydride and diaminophenylindane (BTDA-DAPI; Matrimid[®] 5218 from Huntsman Advanced Materials) was supplied by Air Liquide/Medal, Newport, DE. The repeat unit structure of Matrimid[®] is shown in **Figure 2.4**. Polymer films (thickness of ~ 150 μm) were prepared by solution casting onto silicon wafers using metal casting rings; all Matrimid[®] samples preparations were completed by Brandon W. Rowe in the laboratory of Prof. Don Paul at the University of Texas. The casting solvent was methylene chloride and glass plates were used as covers to slow evaporation. The films were allowed to dry for one week at ambient conditions and were subsequently held under vacuum at 100°C for four days, 200°C for one day, and then in a nitrogen purge at 330°C for 30 minutes.

3.1.2 Functionalized Aromatic Polyimides

Functionalized aromatic polyimides (APIs) were synthesized by Dr. Claudio Riberio at the University of Texas at Austin: 3,3'-dihydroxy-4,4'-diaminobiphenyl and 4,4'-(hexafluoroisopropylidene)-diphthalic anhydride [HAB-6FDA], 2,2'-bis(3-amino-4-hydroxyphenyl) hexafluoropropane and 4,4'-oxydiphthalic anhydride [APAF-ODPA], and 2,2'-bis(3-amino-4-hydroxyphenyl) hexafluoropropane and 4,4'-

(hexafluoroisopropylidene)-diphthalic anhydride [APAF-6FDA]. The chemical structure of these APIs are shown in **Figure 3.1**. Imidization of the API precursors was achieved by two different synthesis routes (chemical and thermal imidization), leading to the introduction of $-\text{OCOCH}_3$ and $-\text{OH}$ *ortho* functional groups, respectively (see Figure 3.1). These polymers were then heat treated at discrete temperatures in the range 350°C to 450°C in order to induce thermal rearrangement (TR), leading to the formation of polybenzoxazoles (see **Figure 3.2**). Chemical imidization synthesis was performed according to the experimental procedure described by Park *et al.* [1], while thermal imidization synthesis was achieved according to the procedure reported by Moy and McGrath [2]. In each case, the resulting chemical structure and corresponding molecular weight was confirmed by proton nuclear magnetic resonance (^1H NMR), attenuated total reflectance fourier-transform infrared spectroscopy (FTIR-ATR) and dilute solution viscometry studies completed at the University of Texas. Polymer test films were prepared by solution casting from chloroform (chemically-imidized samples) or tetrahydrofuran (thermally-imidized samples), followed by drying under vacuum as required to remove residual solvent.

3.1.3 PEI & PMMA Nanocomposites

Poly (ether imide) [PEI] resin pellets were obtained from GE Plastics (Ultem[®] 1000). Poly (methyl methacrylate) [PMMA] pellets were obtained from Altuglas International (Plexiglas[®] V826). The corresponding repeat unit structures for these polymers are presented in **Figure 3.3**. Silica nanoparticles were purchased from Aldrich. Commercial fumed silicas with modified surfaces were obtained from Cabot Corporation: Cab-o-sil[®] TS-530, TS-610, and TS-720. The surface chemistry for each of these nanoparticles is

presented in **Figure 3.4**. Solvents used for nanocomposite preparation (dichloromethane; dimethylformamide) were purchased from Fisher Scientific. For the PEI-based nanocomposites, PEI pellets (10 wt%) were dissolved in dichloromethane followed by addition of an appropriate proportion of nanoparticles. The solution was cast into a shallow container and allowed to evaporate under ambient conditions. The blend was then dried under vacuum to remove residual solvent and the resulting samples were compression molded to achieve uniform films of desired thickness. For the PMMA-based nanocomposites, PMMA pellets (10 wt%) were dissolved in dimethylformamide followed by addition of an appropriate proportion of nanoparticles; only a single series of PMMA composites was investigated, based on inclusion of the TS-610 particles. The PMMA nanocomposite formulations were recovered via precipitation in water, and then filtered, dried, and compression molded to produce uniform films of desired thickness.

3.1.4 Crosslinked PEO Nanocomposites

Crosslinked poly(ethylene oxide) nanocomposite networks were prepared by UV photopolymerization of poly(ethylene glycol) diacrylate [PEGDA] in the presence metal oxide nanoparticles (see **Figure 3.5**). Poly(ethylene glycol) diacrylate crosslinker (PEGDA) and 1 hydroxyl-cyclohexyl phenyl ketone (HCPK) photoinitiator were obtained from Aldrich Chemical Company, Milwaukee, WI. Spherical MgO nanoparticles were obtained from Nanoscale Materials Inc., Manhattan, KS. SiO₂ nanoparticles were obtained from Aldrich. PEGDA, HCPK (0.1 wt% based on PEGDA) and nanoparticles were mixed in the desired proportions and sonicated to eliminate bubbles. In select cases, toluene was added to the pre-polymerization mixture to aid in nanoparticle dispersion. Samples were crosslinked via UV photopolymerization using a

Spectrolinker XL-1000 crosslinker; the resulting film thickness was ~ 1.0 mm for dynamic mechanical specimens and ~ 0.30 mm for samples prepared for dielectric measurement.

3.2 Dynamic Mechanical Analysis (DMA)

3.2.1 DMA Theory

The mechanical response of a viscoelastic material is time-dependent. Over short timescales the material will behave as an elastic solid, while for sufficiently long observational timescales the material will behave as a viscous liquid. Storage modulus, E , is a common mechanical property used to track mechanical behavior and is a measure of the stiffness of a material. For a static system, E is defined as [3]:

$$E = \frac{\sigma}{e} \quad [3.1]$$

where σ is the stress and e is the strain. The typical material response of an amorphous viscoelastic material (modulus vs. temperature) is shown in **Figure 2.1**.

For a dynamic perturbation that is periodic in time, the applied stress can be represented as follows:

$$\sigma = \sigma_o \sin(\omega t) \quad [3.2]$$

where σ_o is the stress amplitude and ω is the frequency (rad/s).

For a purely elastic material, the strain response will assume the same form:

$$e = e_o \sin(\omega t) \quad [3.3]$$

If the material is viscoelastic, there will be a lag in the strain response by some fixed phase angle, δ :

$$\sigma = \sigma_o \sin(\omega t + \delta) \quad [3.4]$$

$$e = e_o \sin(\omega t) \quad [3.5]$$

In expanded form, the equation of the stress is as follows:

$$\sigma = \sigma_o \sin(\omega t) \cos(\delta) + \sigma_o \cos(\omega t) \sin(\delta) \quad [3.6]$$

The modulus can be written in terms of two dynamic components:

$$E_1 = \frac{\sigma_o \cos(\delta)}{e_o} \quad [3.7a]$$

$$E_2 = \frac{\sigma_o \sin(\delta)}{e_o} \quad [3.7b]$$

where E_1 is the storage modulus (in-phase elastic component) which is fully recovered upon unloading and E_2 is the loss modulus (out-of-phase viscous component) which is lost to viscous dissipation.

The stress can be re-written as:

$$\sigma = e_o E_1 \sin(\omega t) + e_o E_2 \cos(\omega t) \quad [3.8]$$

with phase angle,

$$\tan \delta = \frac{E_2}{E_1} = \text{loss factor} \quad [3.9]$$

3.2.2 Time-Temperature Superposition

Time-temperature superposition is based on the empirical observation that for many polymer response characteristics, time and temperature are interchangeable. It assumes that for a given property such as storage modulus, the same material response can be obtained by varying the intrinsic timescale of the material (*i.e.*, by variation in temperature) or by altering the observational timescale (e.g., by changing the perturbation frequency). In **Figure 3.6**, typical stress relaxation curves are shown plotted as modulus versus frequency at fixed temperatures. The shift factor, a_T , is the horizontal displacement which allows the individual curves to join smoothly into a master curve based on a selected reference temperature (see **Figure 3.7**). Time-temperature superposition is used to extend the range of observed viscoelastic behavior as a function of time at specific temperatures. It avoids the impractical aspects of measuring polymer behavior over long periods of time at a specified temperature by utilizing the fact that at higher temperatures (and longer times) the polymer response will be the same [4].

3.2.3 Kohlrausch-Williams-Watts (KWW) Model

Storage and loss modulus master curves can be described using the Kohlrausch-Williams-Watts (KWW) “stretched exponential” relaxation time distribution function, $\phi(t)$, as follows [5]:

$$\phi(t) = \exp\left[-\left(t/\tau_o\right)^{\beta_{KWW}}\right] \quad [3.10]$$

where τ_o is the relaxation time and β_{KWW} is the distribution or breadth parameter. The value of β_{KWW} can range from 0 to 1, with lower values reflecting broad transitions

affected by a constrained environment. Series approximations reported by Williams et al. express modulus and loss for the KWW model in the frequency domain, and these equations were used as the basis for curve fits applied to TTS master curves for the determination of β_{KWW} [5].

3.2.4 The DMA Instrument

Dynamic mechanical analysis (DMA) was conducted at the University of Kentucky Center for Applied Energy Research using a dynamic mechanical analyzer (model Q800) from TA Instruments - Waters LLC. The Q800 has an interchangeable clamping assembly designed to accommodate a variety of materials with different characteristics. The clamps can be classified as tensioning or non-tensioning. Tensioning clamps require the sample to be under a constant force (*i.e.*, pre-load force) at all times. Examples of tensioning modes include: compression, film tension, 3-point bending, and penetration. Non-tensioning modes include single cantilever and dual cantilever. The Q800 records seven experimental variables (temperature, time, stress, strain, displacement, frequency, and force). It enables many material properties to be determined including modulus, creep, damping, glass transitions, stress relaxations, and softening points. Material types can include solids, gels, viscous liquids, films, and fibers. For this study, a film tension clamping configuration was used as illustrated in **Figure 3.8a**.

In addition to the measurements described above, dynamic mechanical analysis (DMA) in non-tensioning mode was performed using a Polymer Laboratories Dynamic Mechanical Thermal Analyzer (DMTA-MkII). Single cantilever geometry was used as illustrated in **Figure 3.8b** [6].

3.2.5 Sample Preparation and Experimental Procedures

All experiments using the TA Q800 in film tension mode were conducted in a nitrogen environment. Liquid nitrogen was used as coolant to control sub-ambient temperatures. Samples were cut in rectangular strips with typical dimensions of 1-2 mm in width, .07-1.2 mm in thickness, and 10-25 mm in length. System parameters included: (i) preload force (~125%), (ii) clamping torque (2 lb_f-in [0.23 N-m]), and (iii) strain amplitude (2-10 microns). Single frequency temperature sweeps (1 Hz) ranged from -150°C to 500°C at rates from 1 to 3°C/min. Multi-frequency test runs were conducted using discrete frequencies ranging from 0.1 Hz to 30 Hz at temperatures from -150°C to 500°C (10°C increments).

Experiments using the DMTA-MkII in single cantilever mode were conducted in a nitrogen environment with liquid nitrogen as the coolant to control sub-ambient temperatures. Samples were cut in rectangular strips with typical dimensions of 10 mm in width, 1 mm in thickness, and 30 mm in length. System parameters included: (i) 4X strain, (ii) knife edge spreader clamp, (iii) small frame, and (iv) clamp torque (0.18–0.25 N-m). Temperature sweeps were conducted from -120°C to 100°C at rates of 1 or 1.5°C/min over a frequency range of 0.1 to 10 Hz.

3.3 Broadband Dielectric Spectroscopy (BDS)

3.3.1 Dielectric Theory

Dielectrics are materials that may be polarized when exposed to an external electric field and this polarization causes a shift in the charge equilibrium of the material. Positive

charges in the dielectric are aligned in the direction of the external field and negative charges are aligned in the opposite direction (see **Figure 3.9**). Polarization is one of several dielectric properties that can be measured from dielectric spectroscopy analysis; types of polarization include: 1) induced dipole polarization, 2) orientation polarization, 3) interfacial polarization, and 4) charge migration polarization.

Mechanisms of induced dipole polarization include electronic and atomic polarization. Electronic polarization results from the displacement of electrons from their equilibrium position relative to the positive nucleus. Atomic polarization results from equilibrium displacement of atoms that share electrons unequally. Unlike induced dipole polarization, orientation polarization results from permanent dipoles and is dependent on the constitution and conformation of the dielectric; orientation polarization forms the basis for studying the motional transitions in polymeric materials. Interfacial polarization occurs in heterogeneous materials such as nanocomposites where there can be an accumulation of charges at interfaces between phases (Maxwell-Wagner-Sillars polarization). Charge migration polarization can contribute to conduction and arises from migrating charges such as ionic impurities and proton transfer along hydrogen bonds [7,8].

3.3.1.1 Static Measurements

When an electric field with strength (E) is applied across a parallel-plate capacitor with area (A) and plates separated by a distance d (much smaller than the plate dimensions), the capacitance of a dielectric medium positioned between the plates is given by:

$$C = \frac{\sigma A}{Ed} = \frac{Q}{V} \quad [3.11]$$

where σ is the charge density, Q is the magnitude of charge on each plate, and V is the potential difference across the plates due to the charge.

The relative static permittivity, ϵ_s , is defined as:

$$\epsilon_s = \frac{C}{C_0} \quad [3.12]$$

where C_0 is the measured capacitance of the same configuration under vacuum. The electric displacement (D) and polarization (P) of the dielectric material are related to field strength according to the following [8]:

$$D = E + 4\pi P \quad [3.13]$$

$$D = \epsilon_s E \quad [3.14]$$

$$P = \frac{E(\epsilon_s - 1)}{4\pi} \quad [3.15]$$

3.3.1.2 Dynamic Measurements

When a dielectric is placed in an alternating electric field the strength of the field $E(t)$ and the electric displacement $D(t)$ are described as follows:

$$E(t) = E_o \exp(i\omega t) \quad [3.16]$$

$$D(t) = D_o \exp i(\omega t - \delta) \quad [3.17]$$

where E_o and D_o are system constants, ω is the angular frequency, and t is time. $D(t)$ is normally out of phase with $E(t)$ by the phase angle δ . In complex notation, the dielectric constant (ϵ^*) is expressed as:

$$\epsilon^* = \frac{D(t)}{E(t)} = \frac{D_o}{E_o} \exp(-i\delta) = \epsilon_o(\cos\delta - i\sin\delta) \quad [3.18]$$

$$\epsilon^* = (\epsilon_o \cos\delta) - i(\epsilon_o \sin\delta) = \epsilon' - i\epsilon'' \quad [3.19]$$

and

$$\tan\delta = \frac{\epsilon''}{\epsilon'} \quad [3.20]$$

where ϵ' is the dielectric constant or permittivity and ϵ'' is the dielectric loss; $\tan \delta$ is the dissipation factor or loss tangent and is independent of sample geometry [9].

3.3.2 Dynamic Relaxation Models

Several empirical equations have been developed to model the dielectric relaxation response of polymeric materials. The Debye relaxation corresponds to the single relaxation time response of an ideal, non-interacting population of dipoles to an alternating external electric field. It is usually expressed in terms of the complex permittivity (ϵ^*) of the medium as a function of the applied frequency (ω):

$$\epsilon^*(\omega) = \epsilon_U + \frac{\Delta\epsilon}{1 + i\omega\tau} \quad [3.21]$$

where ε_U is the unrelaxed dielectric constant at the high frequency limit, $\Delta\varepsilon = \varepsilon_R - \varepsilon_U$, ε_R is the relaxed (*i.e.*, static) dielectric constant at low frequency, and τ is the characteristic relaxation time.

For most polymeric materials, the motional relaxations observed via orientation polarization are non-Debye in character and encompass a broad distribution of relaxation times. In many cases, the individual relaxations can be described using the Havriliak-Negami (HN) modification of the single-relaxation time Debye expression:

$$\varepsilon^* = \varepsilon' - i\varepsilon'' = \varepsilon_U + \frac{\varepsilon_R - \varepsilon_U}{[1 + (i\omega\tau_{HN})^a]^b} \quad [3.22]$$

where ε_R and ε_U represent the relaxed ($\omega \rightarrow 0$) and unrelaxed ($\omega \rightarrow \infty$) values of the dielectric constant for each relaxation, $\omega = 2\pi f$ is the frequency, τ_{HN} is the characteristic relaxation time for the dielectric, and a and b represent the broadening and skewing parameters, respectively, which account for non-Debye relaxation behavior. Limiting values of a and b convert the HN expression to other, well-established modifications of the Debye equation; e.g. the Cole-Cole model (broadening only, $b = 1$) and the Davidson-Cole model (skewing only, $a = 1$). When both a and b are equal to one, the HN expression reduces to the Debye equation.

3.3.3 The BDS Instrument

Dielectric spectroscopy was performed using the Novocontrol “Concept 40” broadband dielectric spectrometer (Hundsangen, Germany). The Novocontrol is designed to measure molecular response and relaxation properties of dielectric materials while

exposed to an alternating electrical field; the frequency range for the measurements in this work was from 0.1 Hz to 3 MHz. Dielectric constant and loss were calculated directly from the measured sample impedance as a function of frequency and temperature. Measurements were performed in a nitrogen environment and sub-ambient temperatures were achieved using liquid nitrogen as the cooling medium. The sample holder is shown in **Figure 3.10**.

3.3.4 Sample Preparation

Prior to measurement, each film was coated on both sides with concentric silver electrodes using a VEECO 7700 Series High Vacuum Evaporator. The thermal evaporation of silver shot (Alfa Aesar) ensures uniform electrical contact across the film surface.

3.3.5 Experimental Procedures

Samples were mounted between gold plated platens and positioned in the Novocontrol Quatro Cryosystem. Dielectric constant (ϵ') and loss (ϵ'') were recorded in the frequency domain (0.1 Hz to 3 MHz) at 10°C isothermal intervals from -150 to 380°C.

3.4 Density Determinations

Bulk density measurements were conducted by hydrostatic weighing at 25°C using a conventional density determination kit (Denver Instruments); deionized ultrafiltered water (Fisher Sci.) or *n*-heptane was employed as the auxiliary liquid, depending on the nature of the polymer under investigation. A minimum of three replicate measurements were completed for each sample tested.

3.5 Thermogravimetric Analysis

A TA Instruments Q500 was used for Thermogravimetric Analysis studies (TGA; University of Texas at Austin). The TGA measures the amount and rate of weight change in a material as a function of increasing temperature, or isothermally as a function of time, in a controlled environment. It is often used to characterize materials that exhibit weight changes due to decomposition, oxidation, or dehydration. In this study, experiments were conducted in a nitrogen atmosphere.

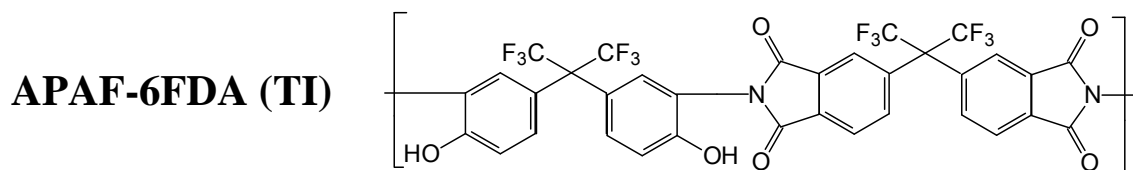
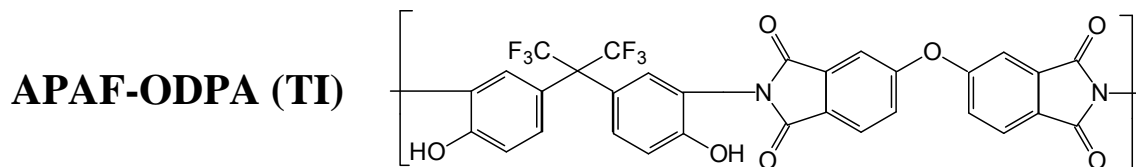
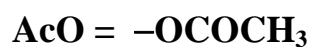
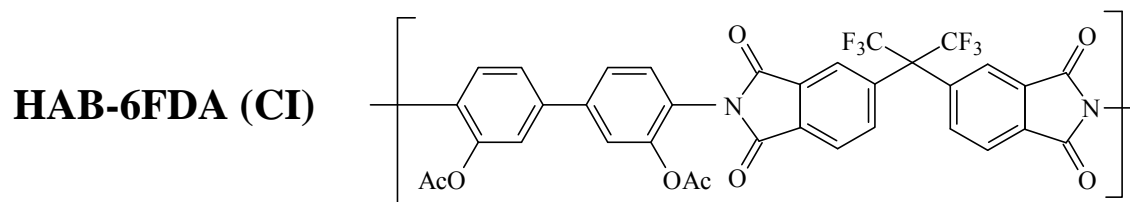


Figure 3.1: Chemical structures for aromatic polyimides prepared via chemical imidization (CI) or thermal imidization (TI).

HAB-6FDA (CI)

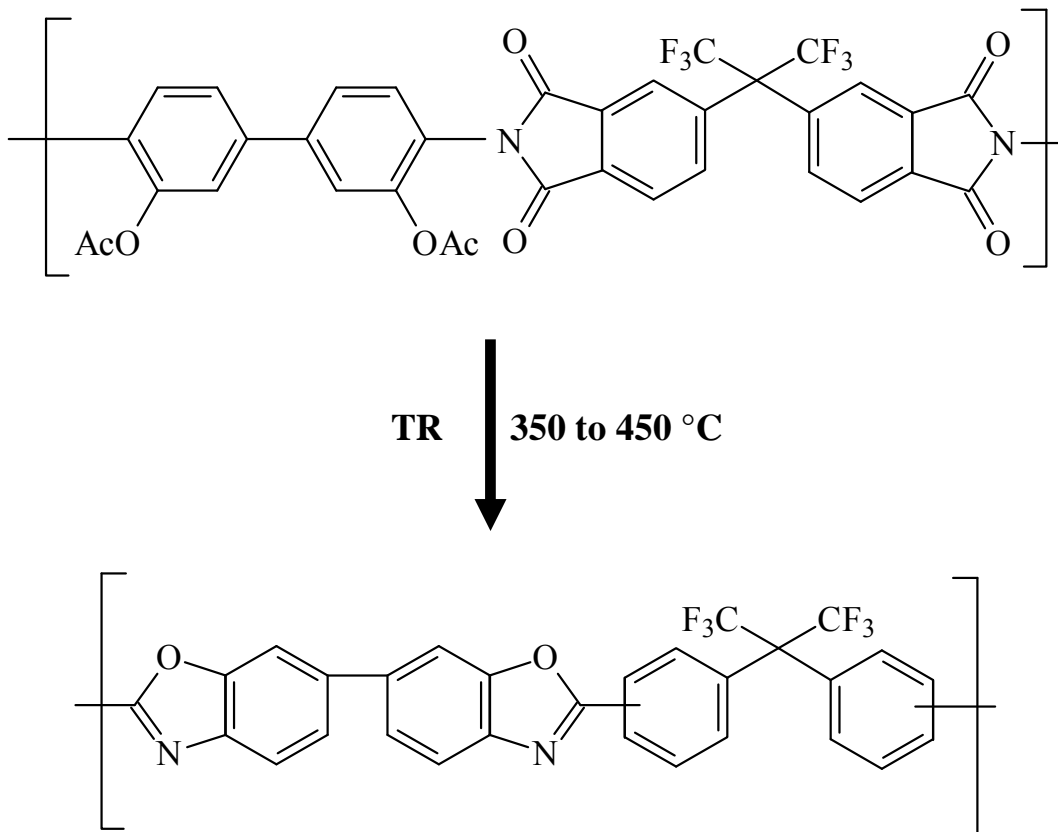


Figure 3.2a: TR conversion structures (PBOs) for aromatic polyimides prepared via chemical imidization (CI) or thermal imidization (TI): **HAB-6FDA-CI**

APAF-ODPA (TI)

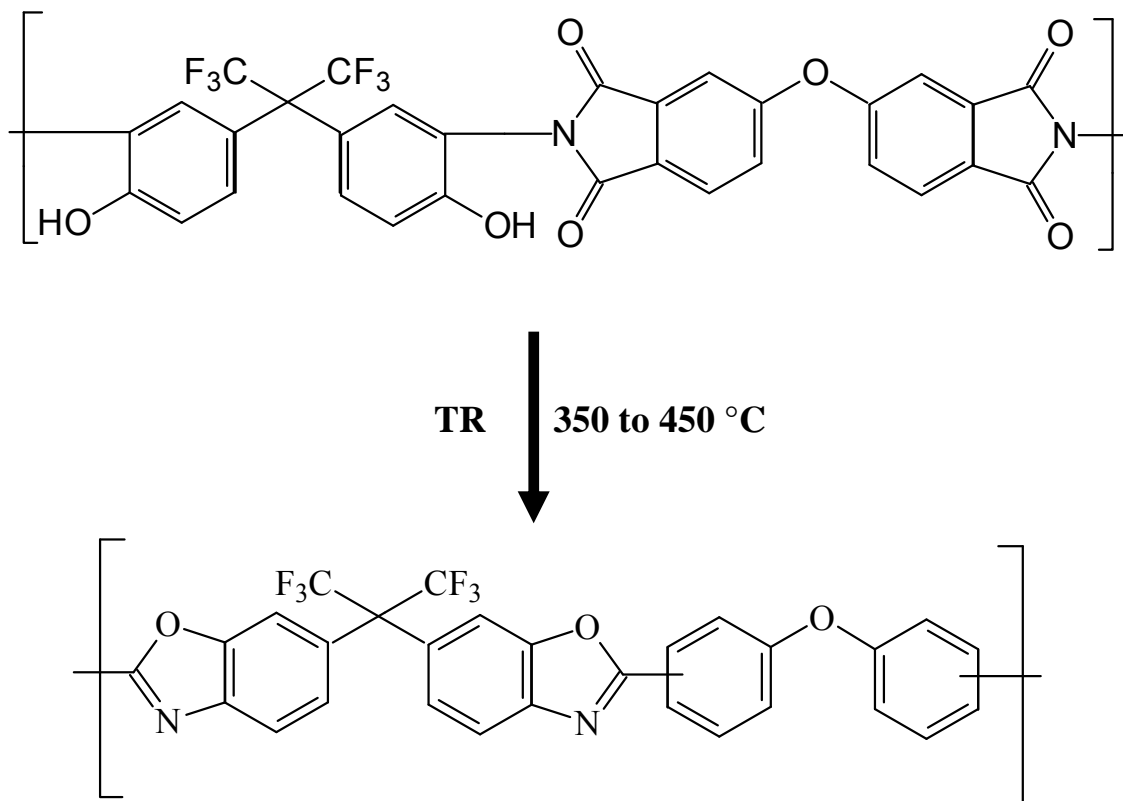


Figure 3.2b: TR conversion structures (PBOs) for aromatic polyimides prepared via chemical imidization (CI) or thermal imidization (TI): **APAF-ODPA-TI**

APAF-6FDA (TI)

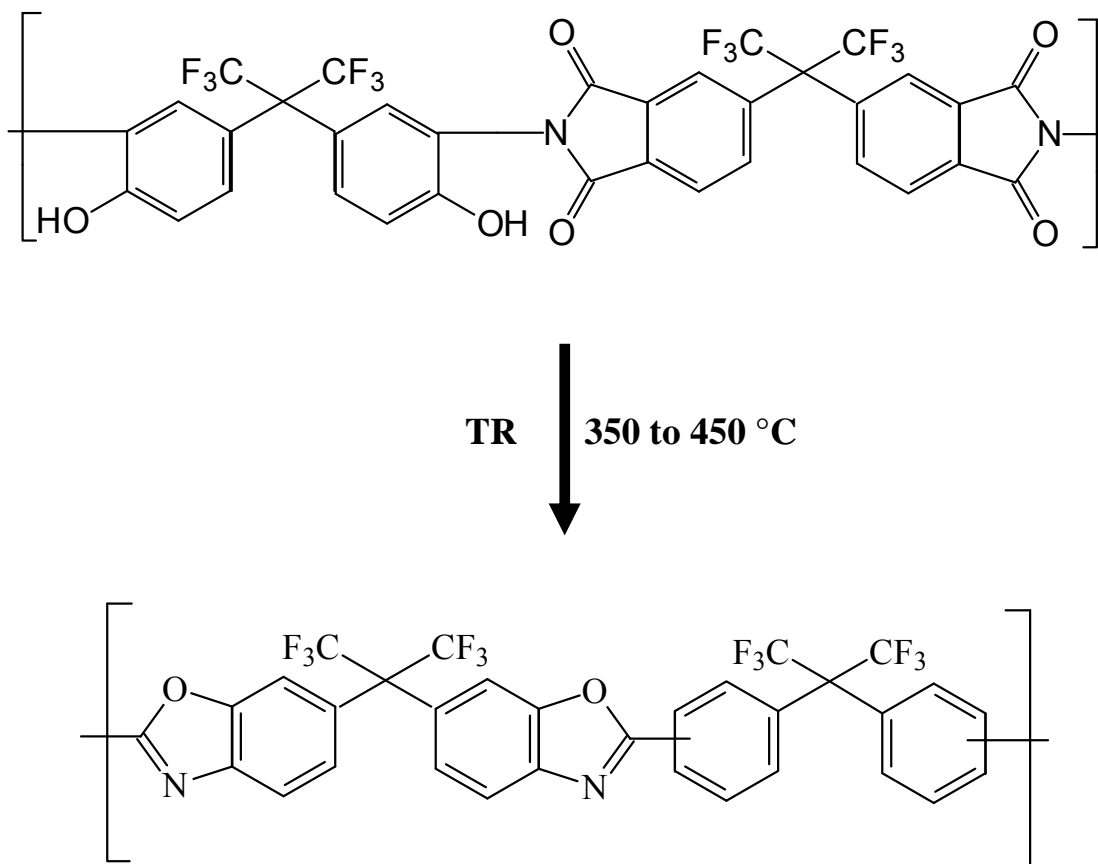
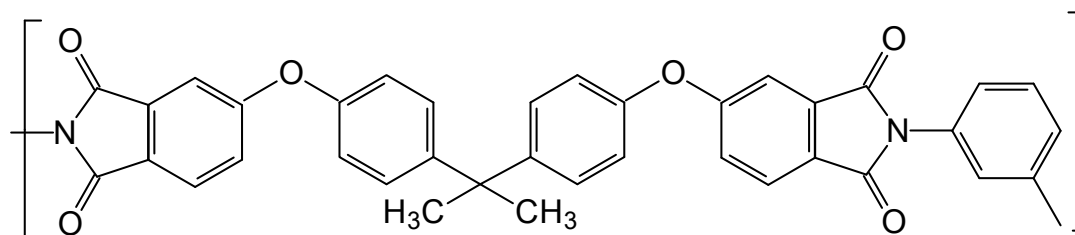


Figure 3.2c: TR conversion structures (PBOs) for aromatic polyimides prepared via chemical imidization (CI) or thermal imidization (TI): **APAF-6FDA-TI**

PEI



PMMA

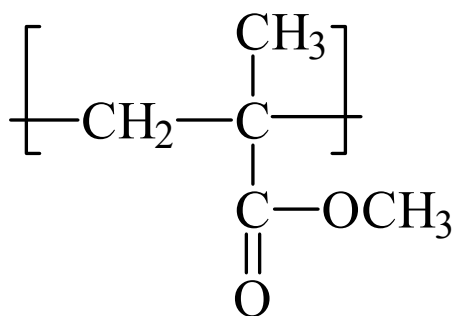


Figure 3.3: Chemical structures for poly (ether imide) [PEI] and poly (methyl methacrylate) [PMMA].

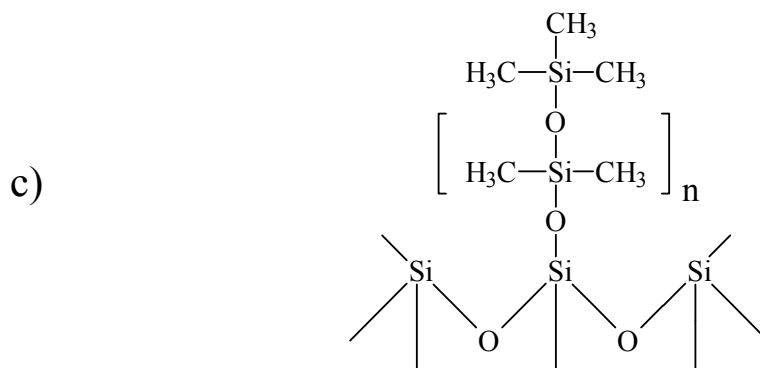
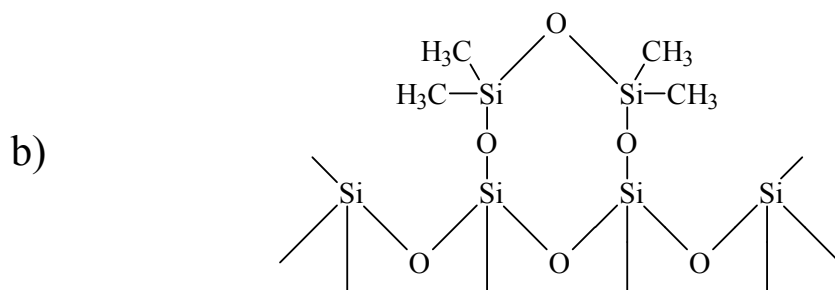
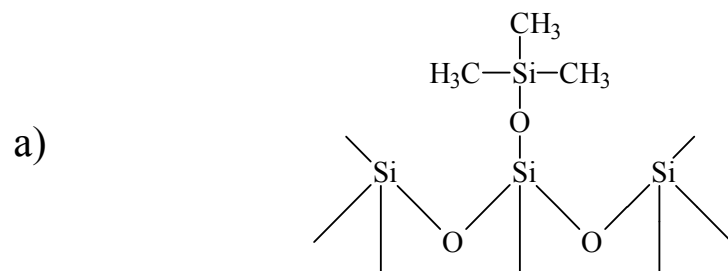


Figure 3.4: Surface chemistry of fumed silica nanoparticles: a) TS-530; b) TS-610; c) TS-720.

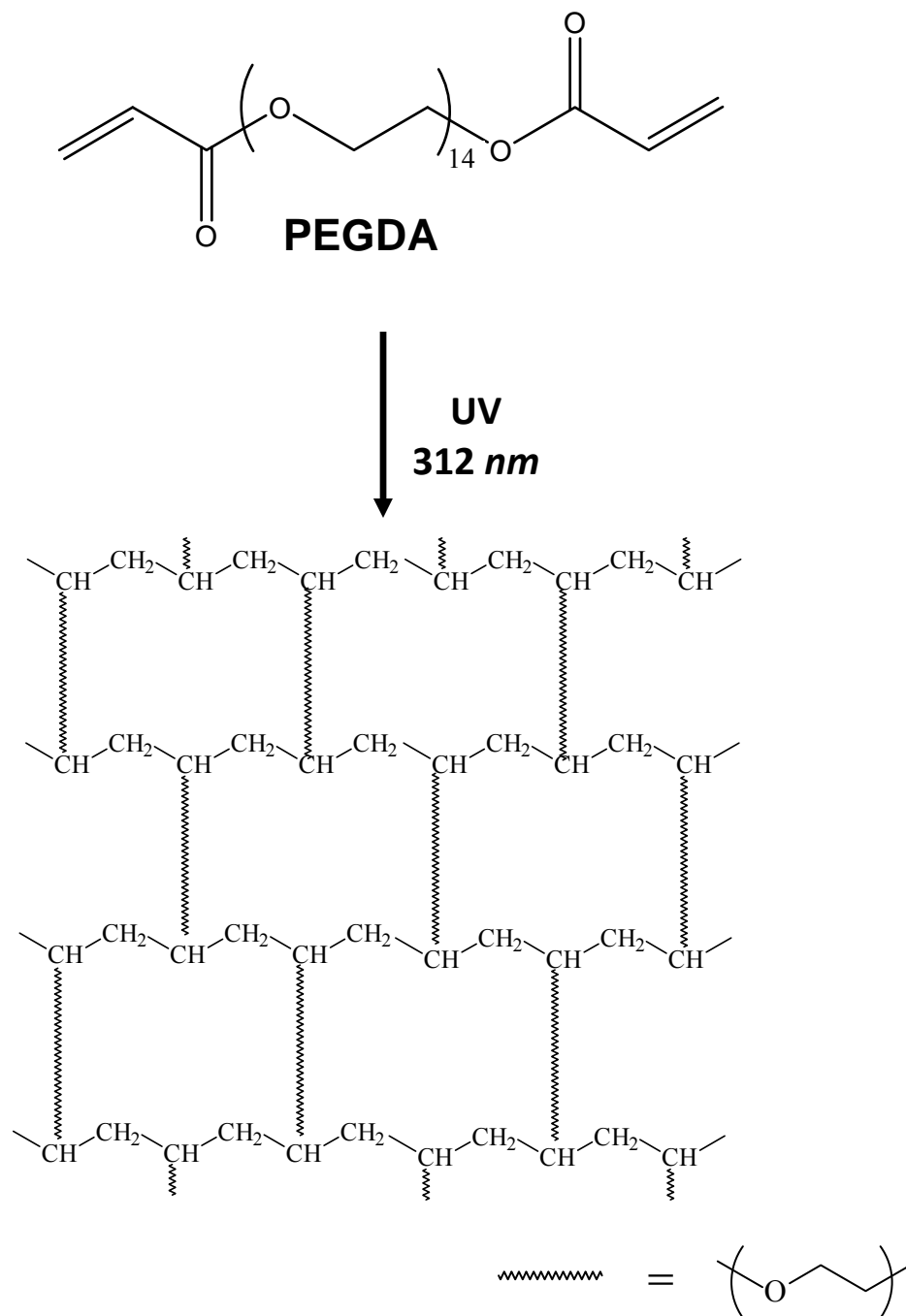


Figure 3.5: Chemical structure for cross-linked poly(ethylene glycol) diacrylate [XLPEGDA].

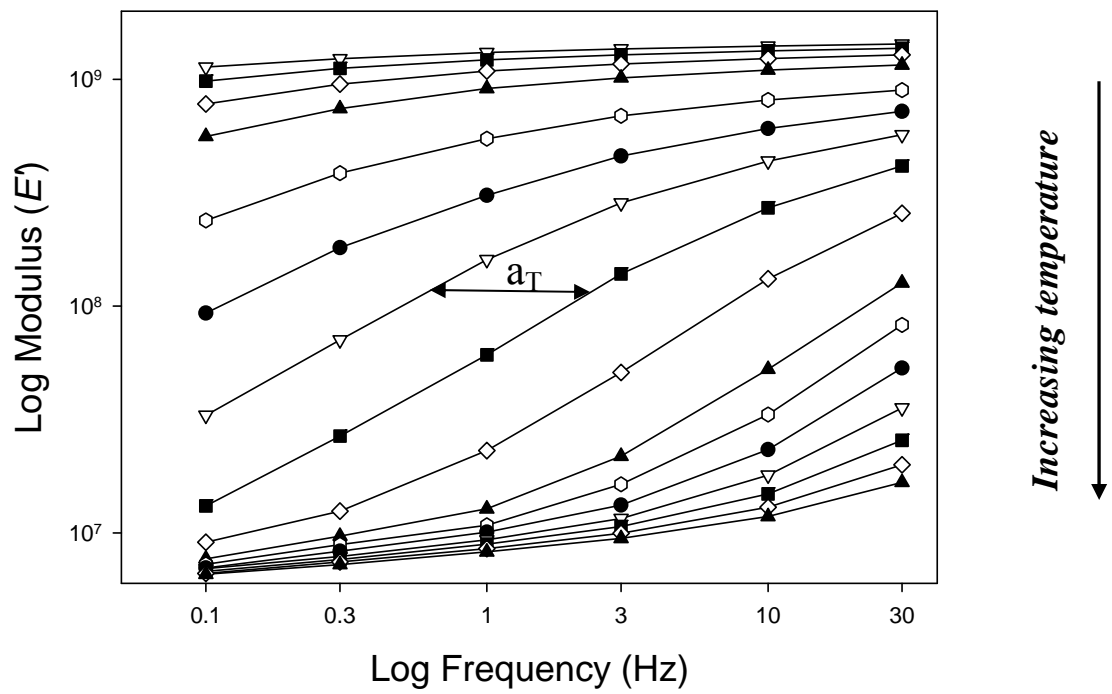


Figure 3.6: Typical viscoelastic response curves on a frequency basis.

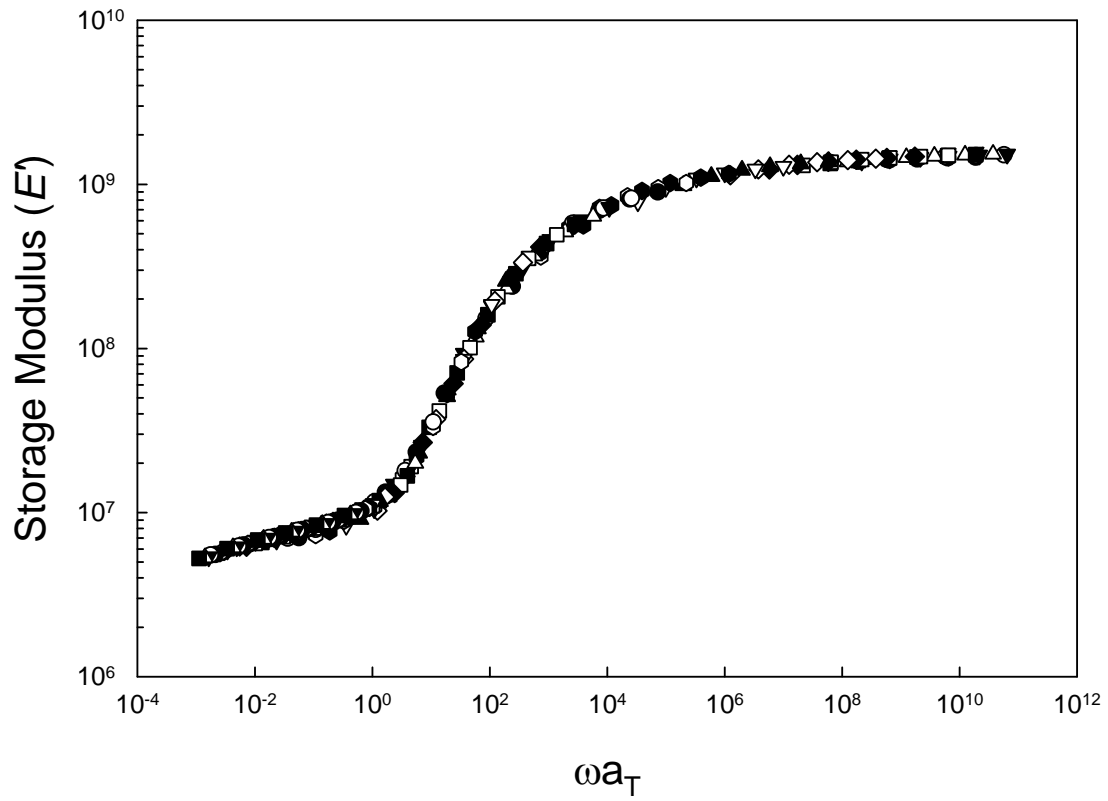


Figure 3.7 Storage modulus master curve obtained via time-temperature superposition.

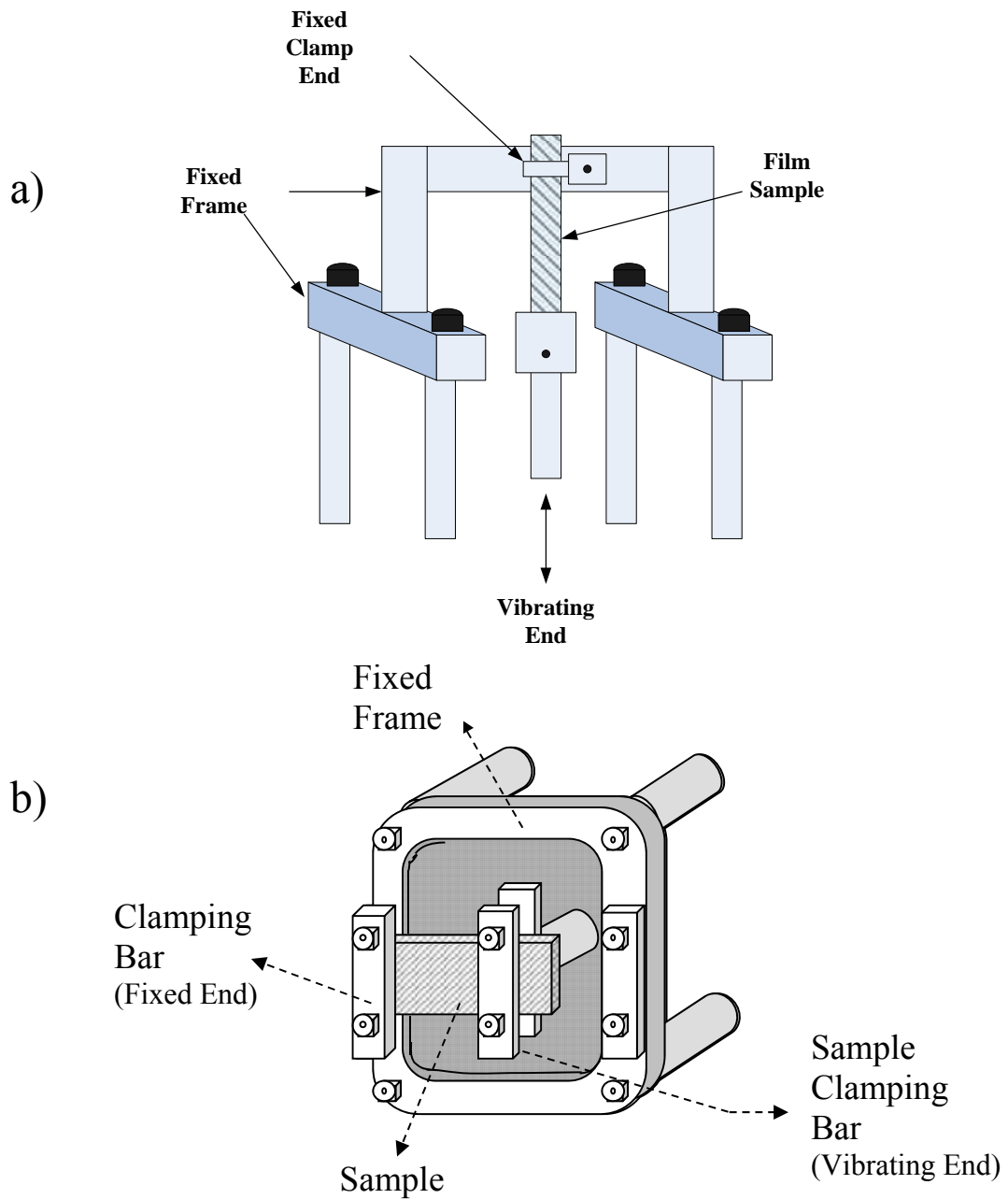


Figure 3.8: Test configurations for dynamic mechanical analysis: a) TA Instruments dynamic mechanical analyzer (Model Q800) in film tension clamping configuration. b) Polymer Laboratories Dynamic Mechanical Thermal Analyzer (DMTA-MkII) in single cantilever geometry [6].

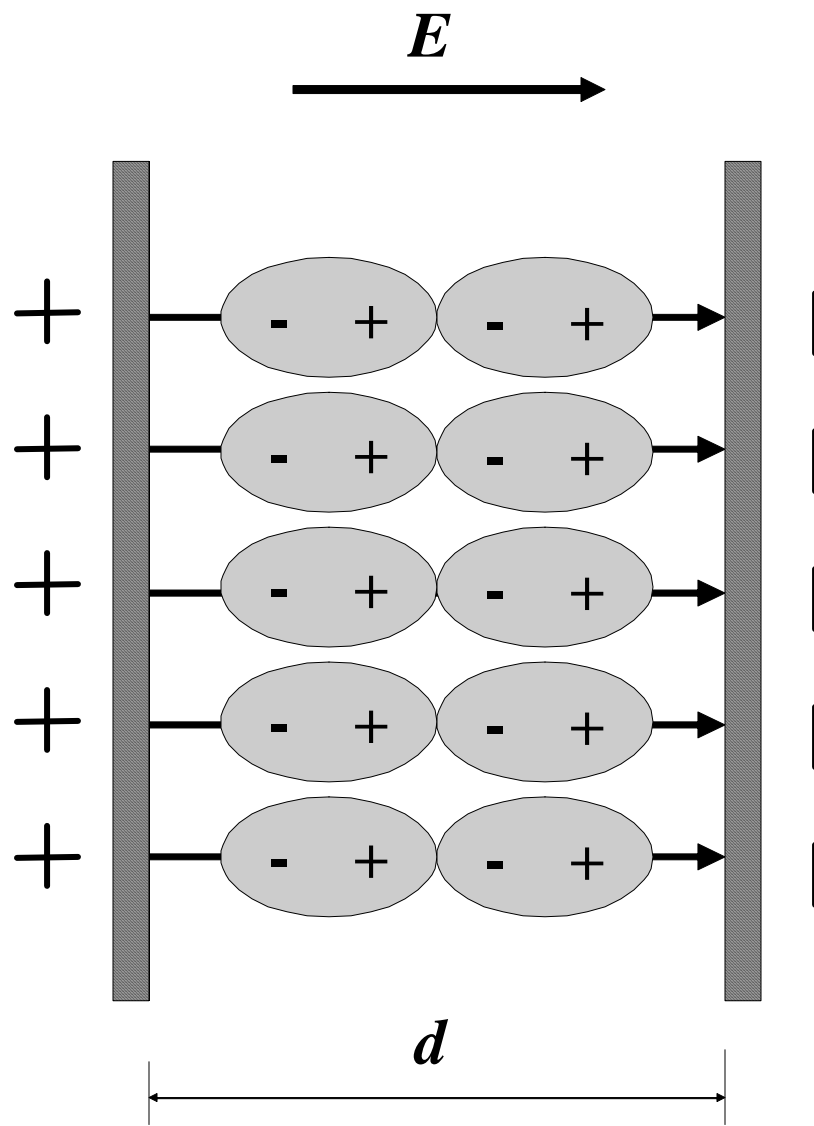


Figure 3.9: Charge separation in a parallel-plate capacitor with dielectric material of thickness d , in an electric field E .

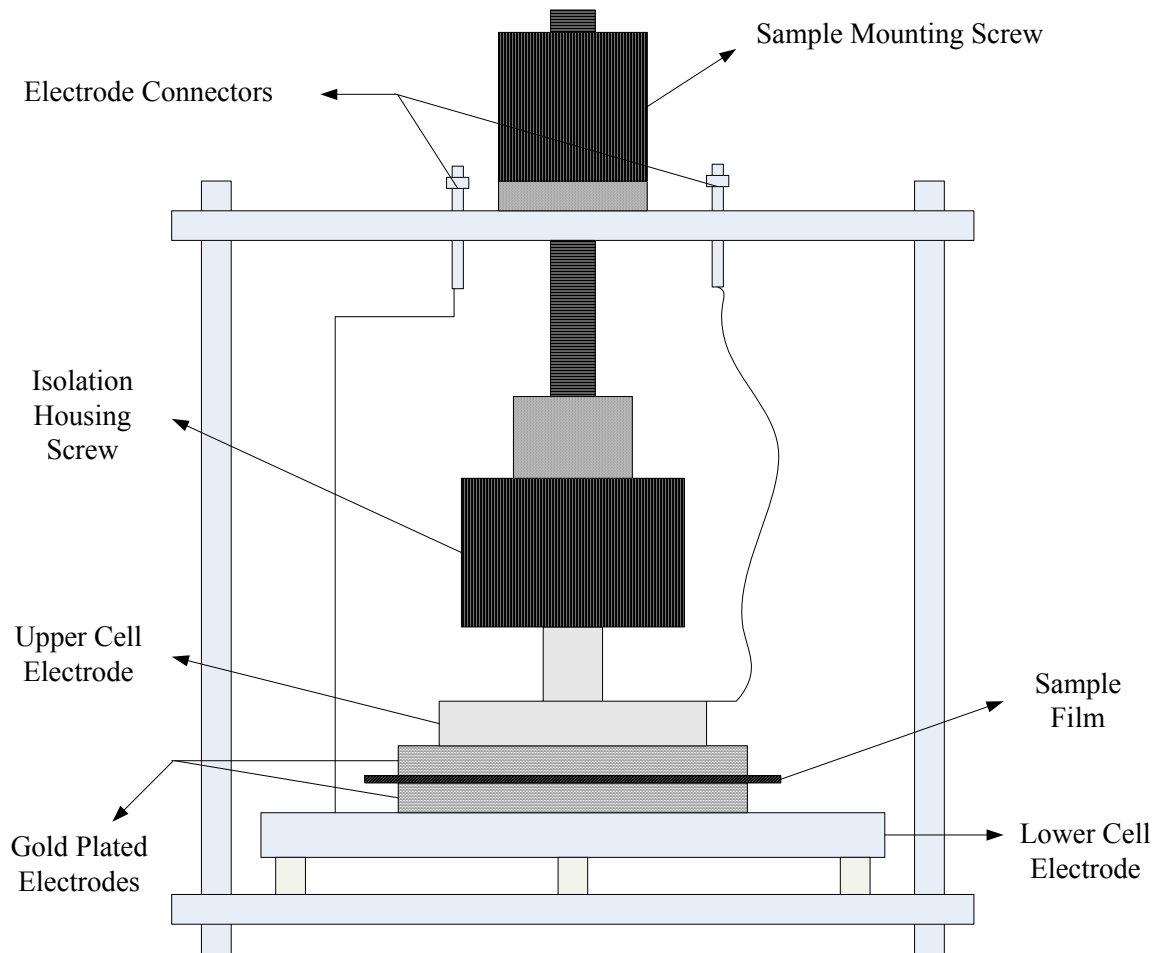


Figure 3.10: Novocontrol “Concept 40” Broadband Dielectric Spectrometer sample cell (Adapted from [6]).

References

- [1] Park, H.B.; Jung, C.H.; Lee, Y.M.; Hill, A.J.; Pas, S.J.; Mudie, S.T.; Van Wagner, E.; Freeman, B.D.; Cookson, D.J. "Polymers with Cavities Tuned for Fast Selective Transport of Small Molecules and Ions", *Science* **2007**, *318*, 254.
- [2] Moy, T.M.; McGrath, J.E. "Synthesis of Hydroxyl-Containing Polyimides Derived from 4,6-Diaminoresorcinol Dihydrochloride and Aromatic Tetracarboxylic Dianhydrides", *Journal of Polymer Science, Part A: Polymer Chemistry* **1994**, *32*, 1903.
- [3] Young, R.J.; Lovell, P.A. *Introduction to Polymers*, 3rd edition; CRC Press, **2009**.
- [4] Ferry, J.D. *Viscoelastic Properties of Polymers*, 3rd edition; John Wiley and Sons: New York, **1980**.
- [5] Williams, G.; Watts, D.C.; Dev, S.B.; North, A.M. "Further Considerations of Non Symmetrical Dielectric Relaxation Behaviour Arising From a Simple Empirical Decay Function", *Transactions of the Faraday Society* **1971**, *67*, 1323.
- [6] Kalakkunnath, S. "*Viscoelastic Relaxation Characteristics of Rubbery Polymer Networks and Engineering Polyesters*"; Ph.D. Dissertation University of Kentucky: Lexington, KY, **2007**.
- [7] Mijovic, J., "Dielectric Spectroscopy of Reactive Network-Forming Polymers", In *Broadband Dielectric Spectroscopy*; Kremer, F.; Schönhals, A., eds.; Springer-Verlag: Berlin, **2003**; pp 349-384.
- [8] McCrum, N.G.; Read, B.E.; Williams, G. *Anelastic and Dielectric Effects in Polymer Solids*; John Wiley and Sons, 1967, reprinted by Dover Publications: London, **1991**.
- [9] Menczel, J.D.; Prime, R.B.; Editors. *Thermal analysis of polymers: Fundamentals and applications*; John Wiley & Sons, Inc., **2009**.

Chapter 4

Dynamic Relaxation Characteristics of Matrimid[®] Polyimide

This chapter is based on the following published work:

Comer, A.C.; Kalika, D.S.; Rowe, B.W.; Freeman, B.D.; Paul, D.R. "Dynamic relaxation characteristics of Matrimid polyimide", *Polymer* **2009**, *50*, 891.

4.1 Introduction

Polymers below their glass transition temperature, T_g , are non-equilibrium materials that evolve over time towards an equilibrium state. This process, known as physical aging, is manifested by changes in physical properties of the polymer and has been studied extensively for bulk materials [1-3]. Physical aging is strongly dependent on the system temperature, which affects both segmental mobility and displacement from equilibrium [4]. Molecular motions that persist below the glass transition, related to secondary transitions, allow physical aging to proceed by small localized rearrangements towards equilibrium [2].

It has been suggested that physical aging does not continue at temperatures below the sub-glass transition range, because the localized motions related to these processes become frozen. However, evidence of low-temperature aging (*i.e.*, below the sub-glass transition) has been reported [5,6]. For example, Lee and McGarry showed that cooperative segmental motions exist at temperatures below T_β in polystyrene, as evidenced by isothermal volume relaxation [6]. By studying the effect of secondary relaxations on physical aging, additional insight regarding the molecular mechanisms responsible for aging may be obtained and

improved performance predictions, as well as strategies to control and possibly arrest physical aging, can be developed.

Matrimid[®] is a high T_g , amorphous thermoplastic polyimide comprised of 3,3'-4,4'-benzophenone tetracarboxylic dianhydride (BTDA) and diaminophenylindane (DAPI); see **Figure 2.4** [7]. Matrimid is a useful material for the creation of gas separation membranes [8-10]. However, the performance of these membranes decreases over time due to physical aging [11-13]. In an effort to more fully understand the mechanisms responsible for physical aging in the BTDA-DAPI polyimide, a comprehensive study of the dynamic relaxation characteristics of the commercial polymer has been undertaken. Specifically, dynamic mechanical analysis (DMA) and broadband dielectric spectroscopy (BDS) have been used to determine the glass-rubber and sub-glass transition properties of the Matrimid polyimide. This detailed investigation provides valuable information regarding the nature of the underlying motional processes responsible for these transitions, and their potential relationship to physical aging.

Characterization of the dynamic relaxation processes of polyimides as a function of constituent backbone structure has been an area of extensive activity. Dynamic mechanical and dielectric relaxation techniques have been widely applied to establish transition temperatures, relative relaxation intensity, and the time-temperature characteristics of the motional transitions encountered in these materials [14-28]. To date, however, a detailed report of the sub-glass and glass-rubber relaxation properties of BTDA-DAPI (*i.e.*, Matrimid) has not appeared.

A number of authors have summarized the common relaxation features of polyimides [22,26,28]. Typically, three relaxation processes are observed with increasing temperature designated γ , β and α , respectively, with α corresponding to the glass-rubber relaxation. For polyimides based on the BTDA dianhydride, T_γ (*re*: dynamic mechanical peak at 1 Hz) is usually in the vicinity of -110 to -90°C, and T_β is observed at 80 to 130°C [23,28]. Owing to the local character of the sub-glass relaxations, their time-temperature relations can be described by a constant activation energy according to the Arrhenius relation. For the γ process, the apparent activation energy (E_A) is approximately 40-60 kJ/mol, and for the β process, $E_A = 130-160$ kJ/mol. While the γ and β sub-glass relaxations are nominally local and non-cooperative in nature, the exact molecular mechanisms underlying these relaxations has been the subject of some discussion [22]. In the case of the γ transition, the presence of residual water in the polymer appears to play an important role, with numerous studies reporting a direct correlation between water content and the intensity of the relaxation [15,16,28]. However, there is sufficient evidence to suggest that for many systems, detection of the γ transition is not solely dependent on the presence of coupled water molecules, and may reflect limited motions such as phenyl ring oscillations [20,22]. For the β transition in polyimides, various mechanisms have been postulated involving motions that while still essentially local in character, encompass larger portions of the repeat unit that respond in a correlated manner [17,18,22]. A recent review by Ngai and Paluch examines in detail the dynamic properties of sub-glass relaxations, and in particular the characteristics of secondary relaxations in glass formers with varying degrees of flexibility. In more rigid systems, the origin of the β relaxation is linked to small amplitude motions that ultimately involve the entire repeat segment [29].

4.2 Experimental

4.2.1 Materials

Commercial polyimide based on 3,3'-4,4'-benzophenone tetracarboxylic dianhydride and diaminophenylindane (BTDA-DAPI; Matrimid[®] 5218 from Huntsman Advanced Materials) was generously supplied by Air Liquide/Medal, Newport, DE. The polymer was provided in the form of flakes, and was used as-received in this study. The structure of Matrimid is shown in Figure 2.4.

4.2.2 Sample Preparation

Polymer films (thickness of ~ 150 μm) were prepared by solution casting onto silicon wafers using metal casting rings; all samples were prepared by Brandon Rowe at the University of Texas at Austin. The casting solvent was methylene chloride and glass plates were used as covers to slow evaporation. The films were allowed to dry for one week at ambient conditions and were subsequently held under vacuum at 100°C for four days, 200°C for one day, and then in a nitrogen purge at 330°C for 30 minutes. This drying procedure was designed to maximize solvent removal without crosslinking the material, which can occur when the polymer is exposed to high temperatures in the vicinity of T_g for extended times [30]. Solubility tests performed on samples subjected to the drying protocol indicated no evidence of crosslinking. Upon completion of the solvent-removal procedure, the samples were stored at ambient temperature and humidity. Prior studies on water uptake in annealed Matrimid films indicate an equilibrium water content of approximately 1.5 wt% for these test samples (50% relative humidity, see ref. [31]).

4.2.3 Dynamic Mechanical Analysis

Dynamic mechanical analysis was performed using a TA Instruments Q800 DMA configured in tensile geometry. Storage and loss modulus (E' ; E'') were measured both in temperature sweep mode (1 Hz; 3°C/min), as well as in frequency sweep mode (0.1 to 30 Hz) at discrete temperatures ranging from -150 to 425°C. All measurements were performed under nitrogen atmosphere.

4.2.4 Broadband Dielectric Spectroscopy

Dielectric spectroscopy was performed using the Novocontrol “Concept 40” broadband dielectric spectrometer (Hundsangen, Germany). Prior to measurement, concentric silver electrodes were vacuum-evaporated on each polymer sample using a VEECO thermal evaporation system. Samples were subsequently mounted between gold platens and positioned in the Novocontrol Quatro Cryosystem. Dielectric constant (ϵ') and loss (ϵ'') were recorded in the frequency domain (1 Hz to 1 MHz) at 10°C isothermal intervals from -150 to 300°C (*i.e.*, sub-glass transition range). A high level of conduction was encountered at temperatures $> 300^\circ\text{C}$, precluding a full analysis of the glass-rubber relaxation via dielectric methods.

4.3 Results and Discussion

4.3.1 Relaxation Properties of Matrimid Polyimide

The overall dynamic mechanical relaxation properties of the BTDA-DAPI polyimide are reported as storage and loss modulus (1 Hz) vs. temperature in **Figure 4.1**. Matrimid shows three distinct relaxation peaks in E'' with increasing temperature, consistent with the results

for similar polymers [28]; the relaxations are labeled as γ , β and α , respectively, where α corresponds to the glass transition. The peak temperatures are: -112°C (T_{γ}), 80°C (T_{β}) and 313°C (T_{α}). Dielectric loss data (ϵ'') are compared with the mechanical loss results across the sub-glass transition range in **Figure 4.2**. The dielectric results also show two distinct sub-glass transitions, and the position and breadth of each relaxation are in close correspondence to the dynamic mechanical curve. Based on the relative peak heights of the sub-glass transitions, the β process would appear to be somewhat more prominent in the dynamic mechanical measurement.

4.3.2 Sub-glass Relaxation Processes

Detailed dynamic mechanical results for the γ and β transitions (0.1 Hz to 30 Hz) are presented in **Figure 4.3**; please note the different temperature scales associated with the individual graphs. The maxima in E'' from the isochronal curves are the basis for the Arrhenius plots (f [Hz] vs. $1000/T$ [K]) presented in **Figure 4.4**. Over the limited range of accessible frequencies, both the γ and β dynamic mechanical data sets display linear Arrhenius behavior. The slope of the data reflects the apparent activation energy in each case: $E_A(\gamma) = 43$ kJ/mol and $E_A(\beta) = 156$ kJ/mol. These values are in good agreement with the ranges reported for polyimides based on BTDA, as discussed above [28].

Dielectric data for the γ and β transitions are presented as dielectric loss vs. frequency at discrete temperatures in **Figure 4.5**. The individual relaxations can be described using the Havriliak-Negami (HN) modification of the single-relaxation time Debye expression:

$$\varepsilon^* = \varepsilon' - i\varepsilon'' = \varepsilon_U + \frac{\varepsilon_R - \varepsilon_U}{[1 + (i\omega\tau_{HN})^a]^b} \quad [4.1]$$

where ε_R and ε_U represent the relaxed ($\omega \rightarrow 0$) and unrelaxed ($\omega \rightarrow \infty$) values of the dielectric constant for each relaxation, $\omega = 2\pi f$ is the frequency, τ_{HN} is the relaxation time for each process, and a and b represent the broadening and skewing parameters, respectively [32,33]. When the parameters $a = b = 1$, Eq. (1) reverts to the Debye form. The WINFIT software package provided with the Novocontrol spectrometer was used to obtain HN best fits for the ε'' vs. frequency data at each temperature; see solid curves in Figure 4.5. HN parameters determined for the individual relaxations are plotted vs. temperature in **Figure 4.6**, with $\Delta\varepsilon = \varepsilon_R - \varepsilon_U$ corresponding to the dielectric relaxation intensity. For the sub-glass γ transition, both broadening and high-frequency skewing are evident, with $a \sim 0.5$ and $b \sim 0.4$, respectively. In the case of the β transition, the dielectric dispersion is observed to be symmetric in the frequency domain, such that the data can be satisfactorily fit using the Cole-Cole form of Eq. (1), with the skewing parameter (b) equal to unity [34]. The β relaxation is observed to narrow with increasing temperature (*i.e.*, broadening exponent (a) increases with temperature), indicating a tighter distribution of relaxation times at higher temperature. The relaxation intensity ($\Delta\varepsilon$) is comparable in magnitude for both sub-glass relaxations, and decreases with temperature reflecting an apparent loss of net dipolar correlation with increasing thermal energy.

Relaxation times associated with the individual dielectric dispersions were determined from the HN fits. Specifically, the relaxation times (τ_{MAX}) associated with the peak maxima in Figure 4.5 can be derived from the HN relaxation time (τ_{HN}) at each temperature [35]:

$$\tau_{MAX} = \tau_{HN} \left[\frac{\sin\left(\frac{\pi ab}{2 + 2b}\right)}{\sin\left(\frac{\pi a}{2 + 2b}\right)} \right]^{1/a} \quad [4.2]$$

For the β relaxation, the skewing parameter (b) was taken equal to 1, such that $\tau_{MAX} = \tau_{HN}$. The frequency maxima for the dielectric relaxations, $f_{MAX} = [2\pi\tau_{MAX}]^{-1}$, are plotted vs. reciprocal temperature (*i.e.*, Arrhenius plots) in Figure 4.4.

Across the γ relaxation range, the dielectric data follow a linear Arrhenius relation that is identical to the result from the dynamic mechanical studies. The combined dynamic mechanical and dielectric data span nearly seven orders of magnitude in relaxation time with an apparent activation energy of 43 kJ/mol. The consistency of the dynamic mechanical and dielectric data suggests that the DMA and BDS techniques are probing the same underlying motions. Examination of the backbone structure of the BTDA-DAPI polymer (*re*: Figure 2.4) reveals that the dielectric dispersion response most likely originates from motions involving the dianhydride segment, given the concentration of permanent dipoles, as well as the potential for interactions with residual water molecules, in this portion of the repeat unit. In the case of the β transition, the dielectric data again show a linear Arrhenius behavior (see Figure 4.4b), but the dielectric results do not match the time-temperature relation established by the dynamic mechanical measurements. For the dielectric probe, $E_A(\beta) = 99$ kJ/mol, which is significantly less than the value obtained via DMA (156 kJ/mol). Further, when extrapolated to the low-frequency range, the dielectric relation predicts peak temperatures (T_β) that are lower than those obtained via dynamic mechanical testing. This outcome (*i.e.*, downward offset in dielectric peak temperatures relative to dynamic mechanical result) is

typical of sub-glass relaxation data obtained for a wide range of flexible and rigid polymers, as demonstrated in the extensive compilation of McCrum et al. [36].

The linear Arrhenius quality of both the γ and β processes is indicative of a localized, relatively non-cooperative molecular origin for these relaxations that is characteristic of sub-glass polymer relaxations in general. Additional insight with respect to the character of sub-glass relaxations can be obtained according to the approach described by Starkweather [37,38], wherein the apparent activation energy associated with each relaxation is related to the relaxation temperature (T') and its corresponding activation entropy (ΔS^+) at a frequency of 1 Hz:

$$E_A = RT' [1 + \ln(kT' / 2\pi h)] + T'\Delta S^+ \quad [4.3a]$$

where k is Boltzmann's constant and h is Planck's constant. For simple, non-cooperative relaxations, Starkweather suggests that $\Delta S^+ \rightarrow 0$, with the resulting equation providing a limiting relationship between activation energy and relaxation temperature for isolated, non-interactive motional processes:

$$E_A = RT' [1 + \ln(k / 2\pi h) + \ln(T')] \quad [4.3b]$$

A plot of activation energy vs. temperature for the sub-glass transitions in Matrimid is presented in **Figure 4.7**; the solid line in the plot reflects the $\Delta S^+ = 0$ non-cooperative limit. For the γ transition, the activation energy obtained from the DMA and BDS measurements falls very close to the zero-entropy limit, reflecting the essentially non-cooperative character of this relaxation as probed by both methods. This result is consistent with similar analyses of the polyimide γ process as reported in the literature [23]. For the β transition, two important features are evident in Figure 4.7: (i) the results from the DMA and BDS

measurements are positioned well above the zero-entropy line, indicating some degree of cooperative character inherent to the relaxation as detected by both techniques, and (ii) the dynamic mechanical E_A value shows a much higher degree of offset, suggesting that the DMA measurement is capable of detecting a range of motions that encompasses a higher level of cooperativity as compared to the dielectric probe. Considering the structure of the Matrimid molecule and the location of permanent dipoles within the repeat unit, one possible explanation for the contrasting dielectric and dynamic mechanical results is that the measured dielectric response is limited to motions of the BTDA dianhydride segment, while the dynamic mechanical response reflects longer-range correlated motions involving both portions of the repeat. The longer-range motions captured by the dynamic mechanical data would likely engender a higher degree of intra- and intermolecular cooperativity, as shown in Figure 4.7. The offset in activation energy reported here for the dynamic mechanical β transition is comparable to the results for other polyimides [23,28].

4.3.3 Glass-rubber Relaxation Process

Figure 4.9 shows detailed dynamic mechanical results for the α relaxation range; the observed two order of magnitude decrease in storage modulus is consistent with assignment of this relaxation to the glass-rubber transition. Time-temperature superposition was performed in order to obtain master curves of storage and loss modulus vs. frequency across the α transition [39]. The storage modulus master curve was obtained strictly by horizontal shifting of the data and is plotted as E' vs. ωa_T in **Figure 4.9a**, where ω is the applied test frequency and a_T is the dimensionless shift factor. A reference temperature of 307°C was selected which corresponds to a central relaxation time, $\langle\tau\rangle$, equal to 1 sec. A similar master

curve for loss modulus could be obtained by a combination of horizontal shifting (same a_T values as above) and vertical shifting; the result is shown in **Figure 4.9b**.

Both the storage and loss master curves for the α transition could be described using the Kohlrausch-Williams-Watts (KWW) “stretched exponential” relaxation time distribution function:

$$\phi(t) = \exp[-(t/\tau_o)^{\beta_{KWW}}] \quad [4.4]$$

where τ_o is the relaxation time and β_{KWW} is the distribution or breadth parameter. β_{KWW} can range from 0 to 1, with $\beta_{KWW} = 1$ corresponding to a single relaxation time Debye response. Lower values of β typically reflect increased intermolecular cooperativity as influenced by the chemical structure of the polymer, as well as potential constraints owing to the presence of crystallinity or crosslinks [40]. Series approximations reported by Williams et al. express modulus and loss for the KWW model in the frequency domain, and these equations were used as the basis for the curve fits reported here [41]. The solid curves shown in Figure 4.9 correspond to a single KWW fit with a corresponding distribution parameter, $\beta_{KWW} = 0.34$.

The time-temperature character of the glass-rubber relaxation can be assessed by the construction of a cooperativity plot, a normalized Arrhenius plot where the shift factor ($a_T = \tau/\tau_\alpha$) is plotted as $\log(a_T)$ vs. T_α/T in the vicinity of the glass transition. In this context, T_α is the experimental temperature that corresponds to a central relaxation time (τ_α) of 100 sec. The cooperativity plot for Matrimid based on the dynamic mechanical results is presented in **Figure 4.10** with $T_\alpha = 296^\circ\text{C}$. The data display non-Arrhenius curvature when plotted against reciprocal temperature that is consistent with the cooperative character of the glass-

rubber relaxation; the solid curve corresponds to a WLF (Williams-Landel-Ferry) best fit to the data [39].

The time-temperature sensitivity of the Matrimid polymer across the glass transition can be expressed in terms of its dynamic fragility. Polymers that display severe degradation of structure with temperature are designated as fragile liquids and their relaxation typically reflects a high level of intermolecular coupling, often as a result of a less flexible backbone or the presence of sterically cumbersome pendant groups. By contrast, polymers with smooth, more flexible backbones tend to experience reduced intermolecular constraint and as a result display less time-temperature sensitivity and correspondingly lower fragility [40]. The fragility index, m , quantifies the time-temperature sensitivity of the polymer glass transition based on the slope of the cooperativity curve evaluated at $T = T_\alpha$:

$$m = \left. \frac{d \log(\tau)}{d(T_\alpha / T)} \right|_{T=T_\alpha} = \left. \frac{d \log(a_T)}{d(T_\alpha / T)} \right|_{T=T_\alpha} \quad [4.5]$$

The value of m depends upon the definition of T_α : for the glass transition, the convention is to assign T_α such that the corresponding relaxation time, $\tau(T_\alpha) = 100$ sec. Values of the fragility index determined on this basis range from $m = 16$ (strong limit) to $m \geq 200$ (fragile limit) [42]. Tabulations of dynamic fragility have been reported in the literature for a variety of polymers and small molecules [42-44]. For simple polyethylene, $m = 46$, while for vinyl polymers with pendant substituents, the fragility index is considerably higher (*e.g.*, $m = 137$ for polypropylene; 191 for PVC) [43]. Linear amorphous polymers with stiffer backbones also show relatively high fragility values; for polycarbonate, $m = 132$ [42]. Based on the

dynamic mechanical data presented in Figure 4.10, a fragility index of $m = 115$ is obtained for Matrimid polyimide.

Bohmer et al. reported an inverse correlation between the fragility index (m) and the stretching exponent (β_{KWW}) that is valid across a number of material families, with higher values of m corresponding to a stronger degree of non-exponentiality (*i.e.*, lower values of β_{KWW} and greater intermolecular coupling) [42]. The parameters measured for Matrimid polyimide ($m = 115$; $\beta_{KWW} = 0.34$) exhibit a reasonably good correspondence with the correlation bounds presented by Bohmer; examination of the values reported in Ref. [42] shows a cluster of data for a subset of polymers with $\beta_{KWW} \sim 0.35$, and m ranging from 120 to 145. Thus, the relatively rigid nature of the Matrimid backbone is observed to correlate with both relaxation breadth and a somewhat fragile time-temperature character consistent with the overall behavior reported for a range of polymers.

4.4 Conclusions

The dynamic relaxation properties of BTDA-DAPI (Matrimid[®]) polyimide were investigated using dynamic mechanical and dielectric methods. Matrimid displayed two sub-glass relaxations with increasing temperature centered at -112°C (T_{γ}) and 80°C (T_{β}) based on the measured maxima in mechanical loss modulus at 1 Hz. Application of the analysis proposed by Starkweather indicated that the γ transition was non-cooperative in nature, and both DMA and BDS measurements provided an apparent activation energy of 43 kJ/mol that was consistent with values reported for similar polyimides. The β transition had a more cooperative character, and comparison of dynamic mechanical and dielectric Arrhenius data indicated a higher apparent activation energy for the DMA tests ($E_A = 156$ kJ/mol) as

compared to the BDS studies (99 kJ/mol). It was postulated that the dynamic mechanical probe was sensitive to a wider range of sub-glass motions across the β relaxation range encompassing a higher level of cooperative response. The glass-rubber relaxation ($T_\alpha = 313^\circ\text{C}$) was evaluated by time-temperature superposition; the resulting dynamic mechanical master curves were fit using the KWW stretched exponential function, with a corresponding exponent $\beta_{KWW} = 0.34$. A cooperativity plot was used to establish the dynamic fragility of the polymer. The value of the fragility index ($m = 115$) reflected the relatively rigid character of the polyimide backbone, and the observed relation between fragility and β_{KWW} was consistent with the correlation reported in the literature for a wide variety of polymers.

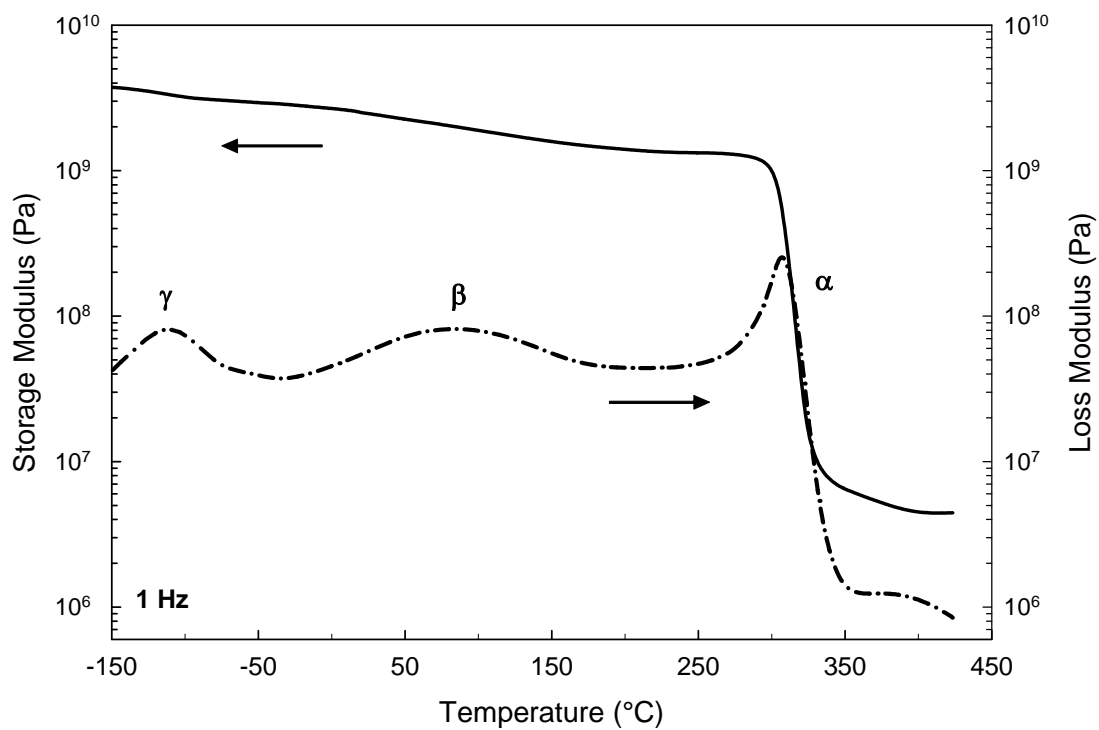


Figure 4.1: Storage modulus (— , Pa) and loss modulus (- · - , Pa) vs. temperature (°C) for Matrimid[®] polyimide. Frequency of 1 Hz, heating rate of 3°C/min.

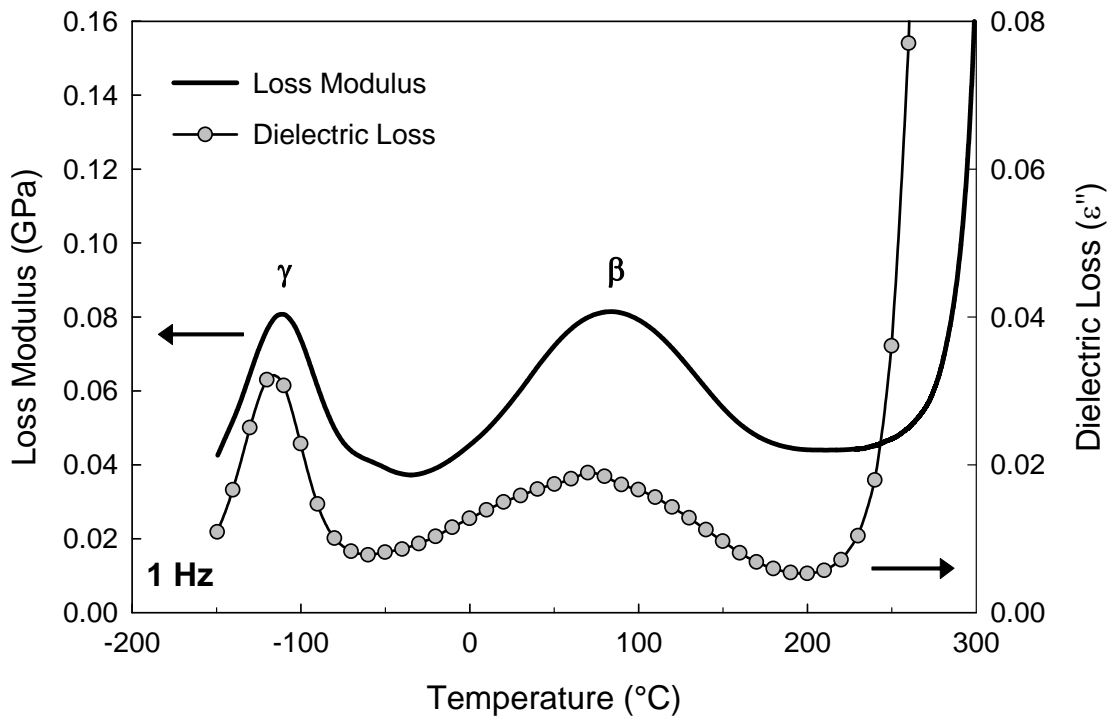


Figure 4.2: Dynamic mechanical loss modulus (— , GPa) and dielectric loss (●) vs. temperature (°C) for Matrimid[®] polyimide across the sub-glass transition region. Frequency of 1 Hz.

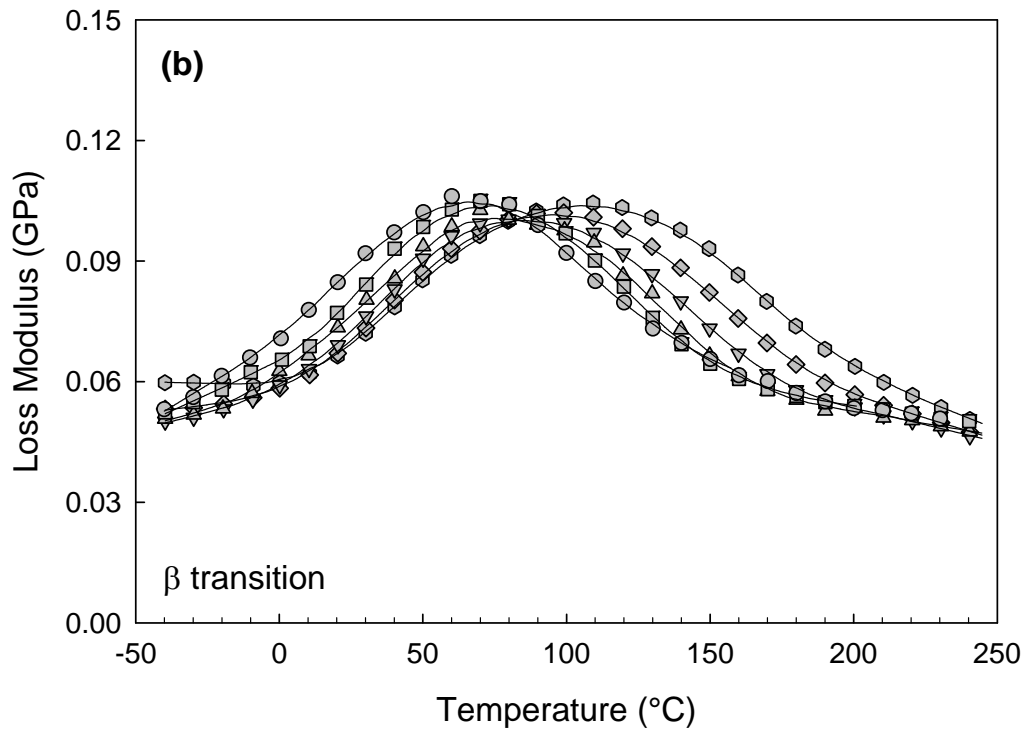
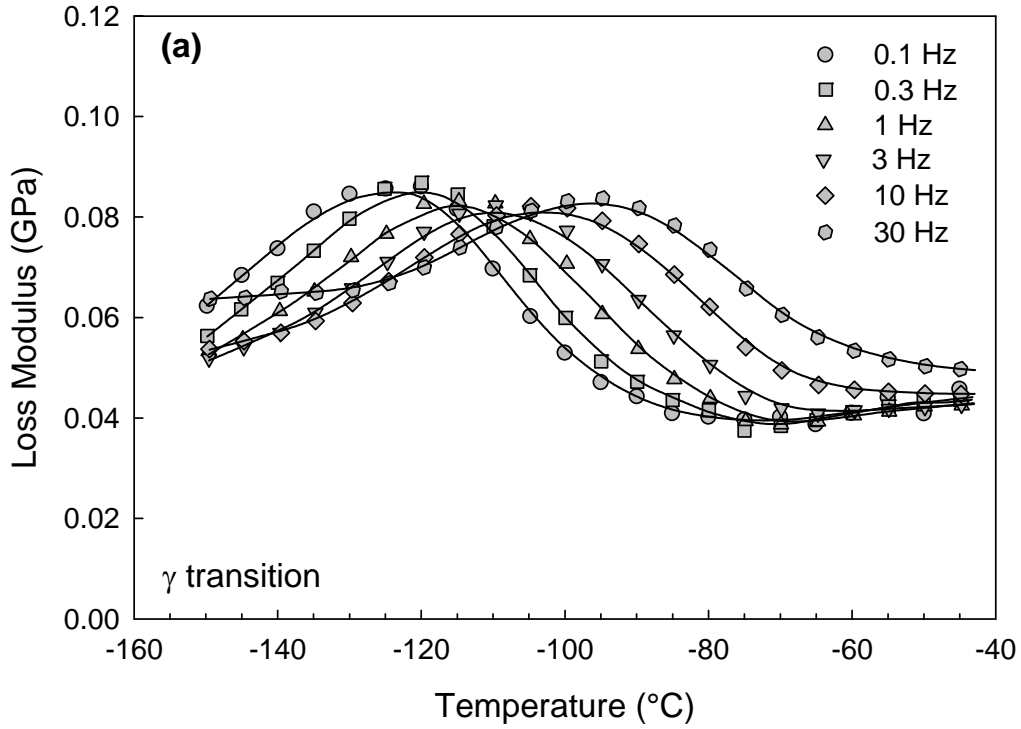


Figure 4.3: Loss modulus (GPa) vs. temperature (°C) for Matrimid[®] polyimide. (a) γ transition; (b) β transition. Curves are provided as a guide to the eye.

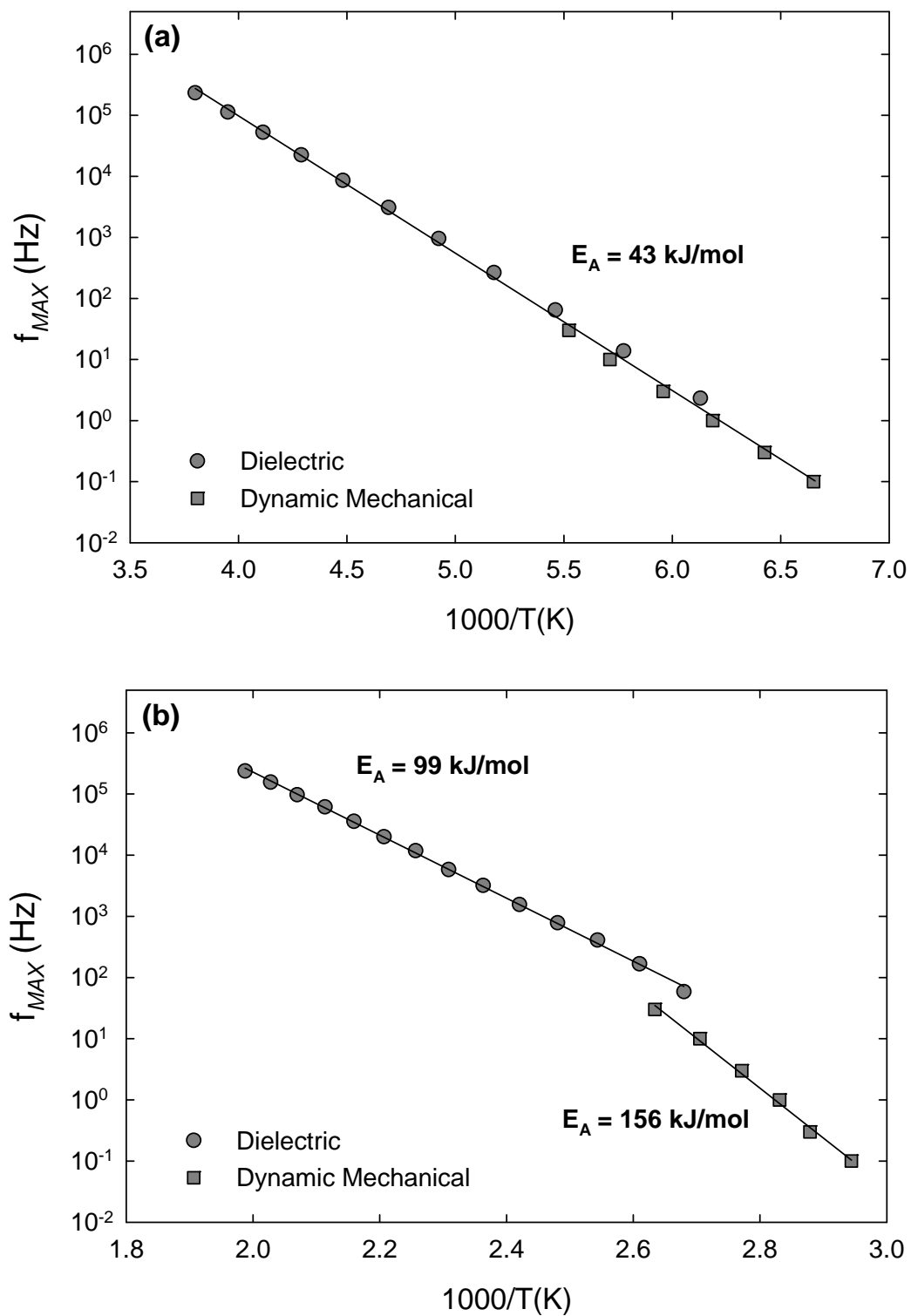


Figure 4.4: Arrhenius plots of $\log(f_{MAX})$ vs. $1000/T$ (K) based on dynamic mechanical and dielectric results: (a) γ transition; (b) β transition.

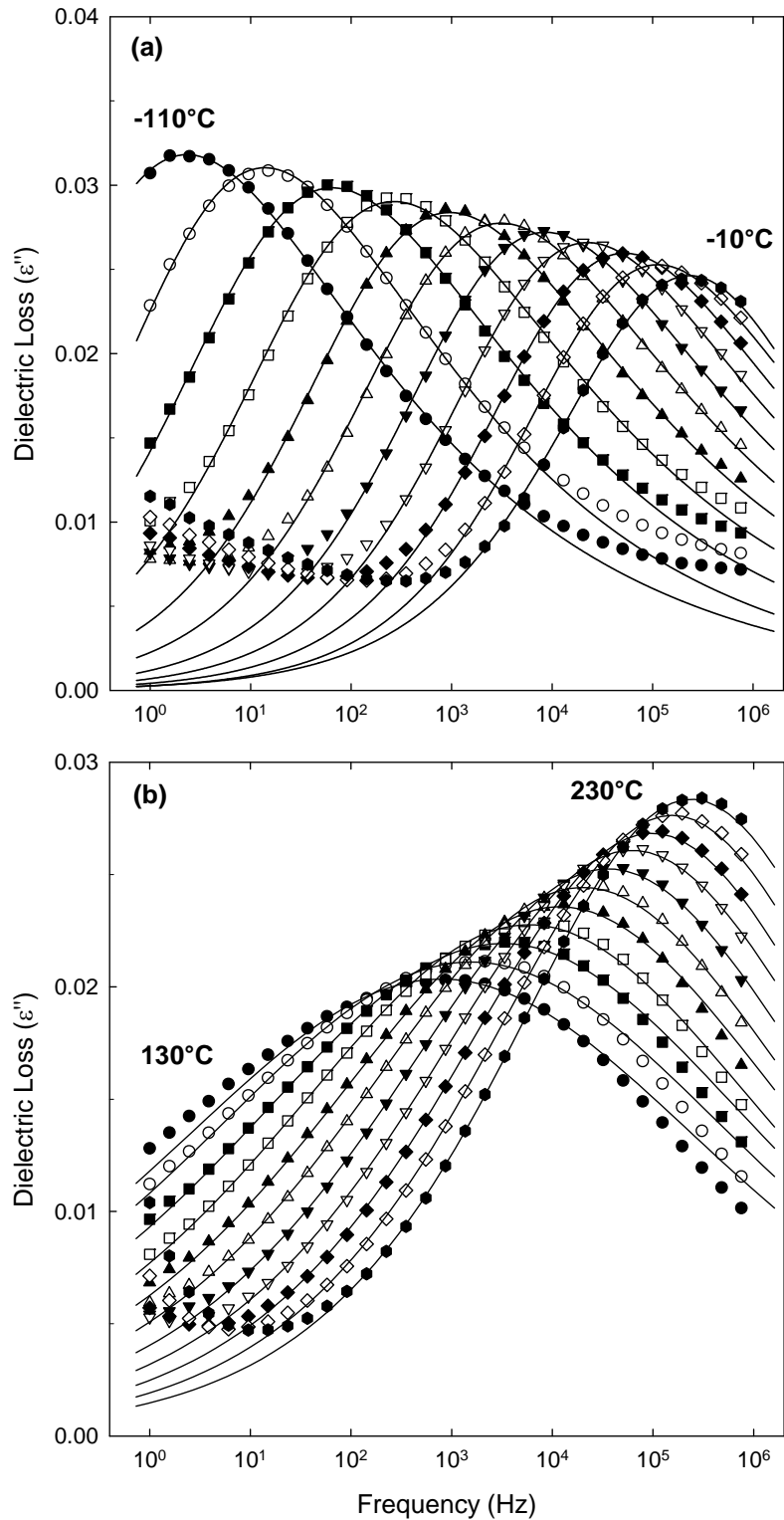


Figure 4.5: Dielectric loss vs. frequency (Hz) for Matrimid[®] polyimide. (a) γ transition; (b) β transition. Data are presented at 10°C intervals. Solid curves are Havriliak-Negami (HN) best fits to the data.

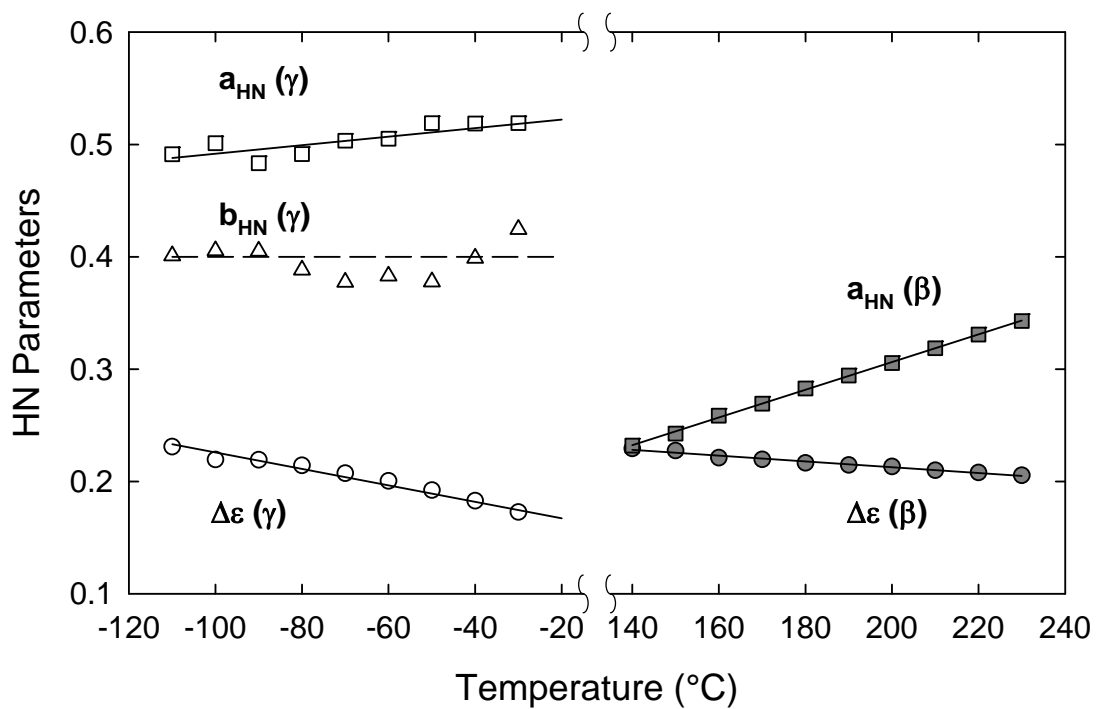


Figure 4.6: Havriliak-Negami (HN) parameters vs. temperature (°C) for γ and β transition regions. a_{HN} : broadening parameter; b_{HN} : skewing parameter; $\Delta\epsilon$: dielectric relaxation intensity.

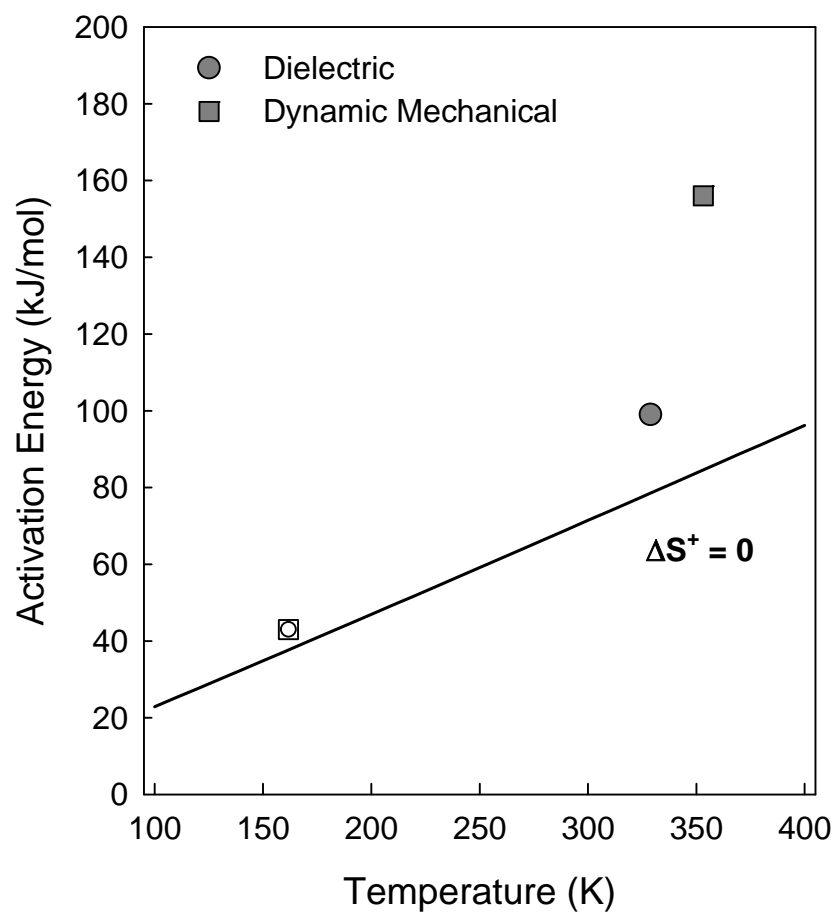


Figure 4.7: Apparent activation energy (kJ/mol) vs. relaxation temperature (K) at 1 Hz based on dynamic mechanical and dielectric results. Solid line represents $\Delta S^+ = 0$ limit (re: Eq. 4.3b). Unfilled symbols: γ transition. Filled symbols: β transition.

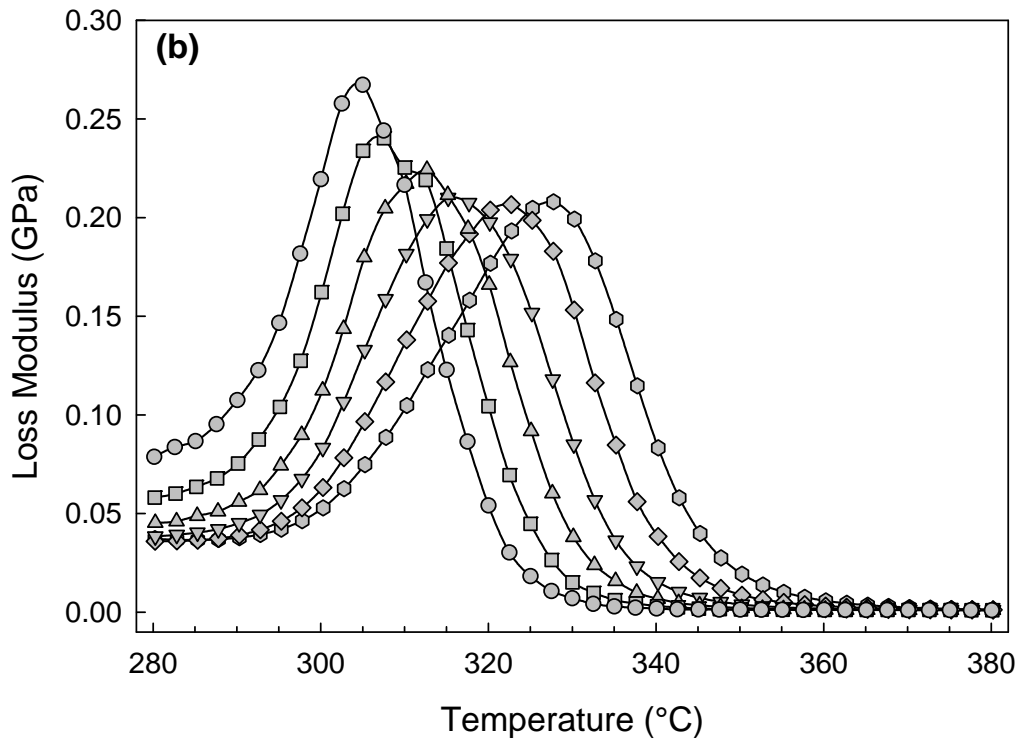
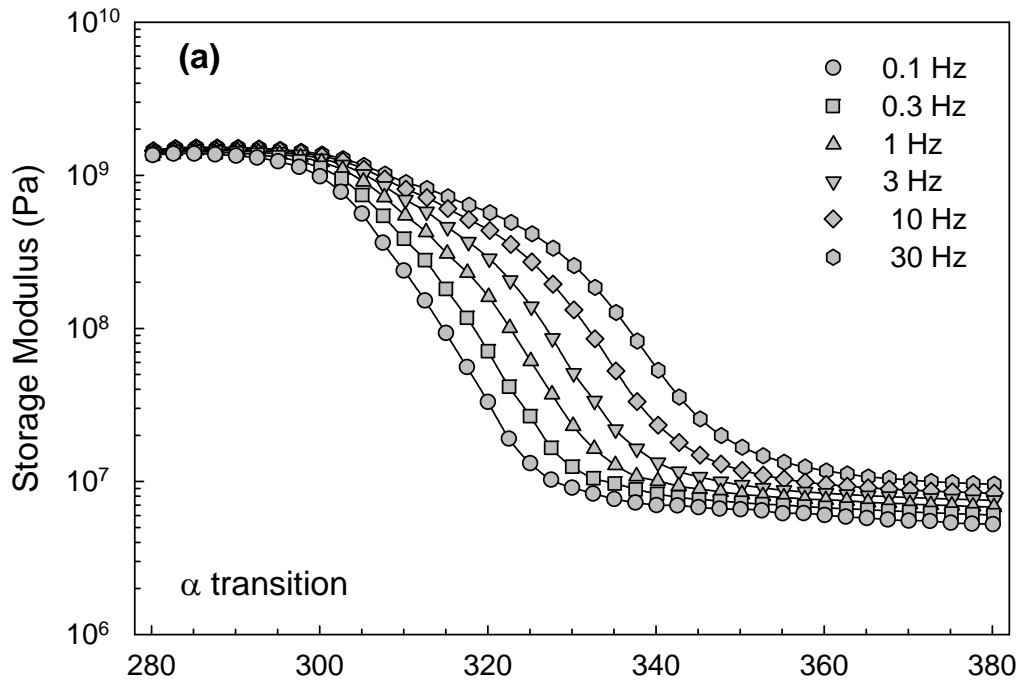


Figure 4.8: Storage modulus and loss modulus vs. temperature (°C) for Matrimid[®] polyimide in the vicinity of the glass-rubber (α) relaxation.

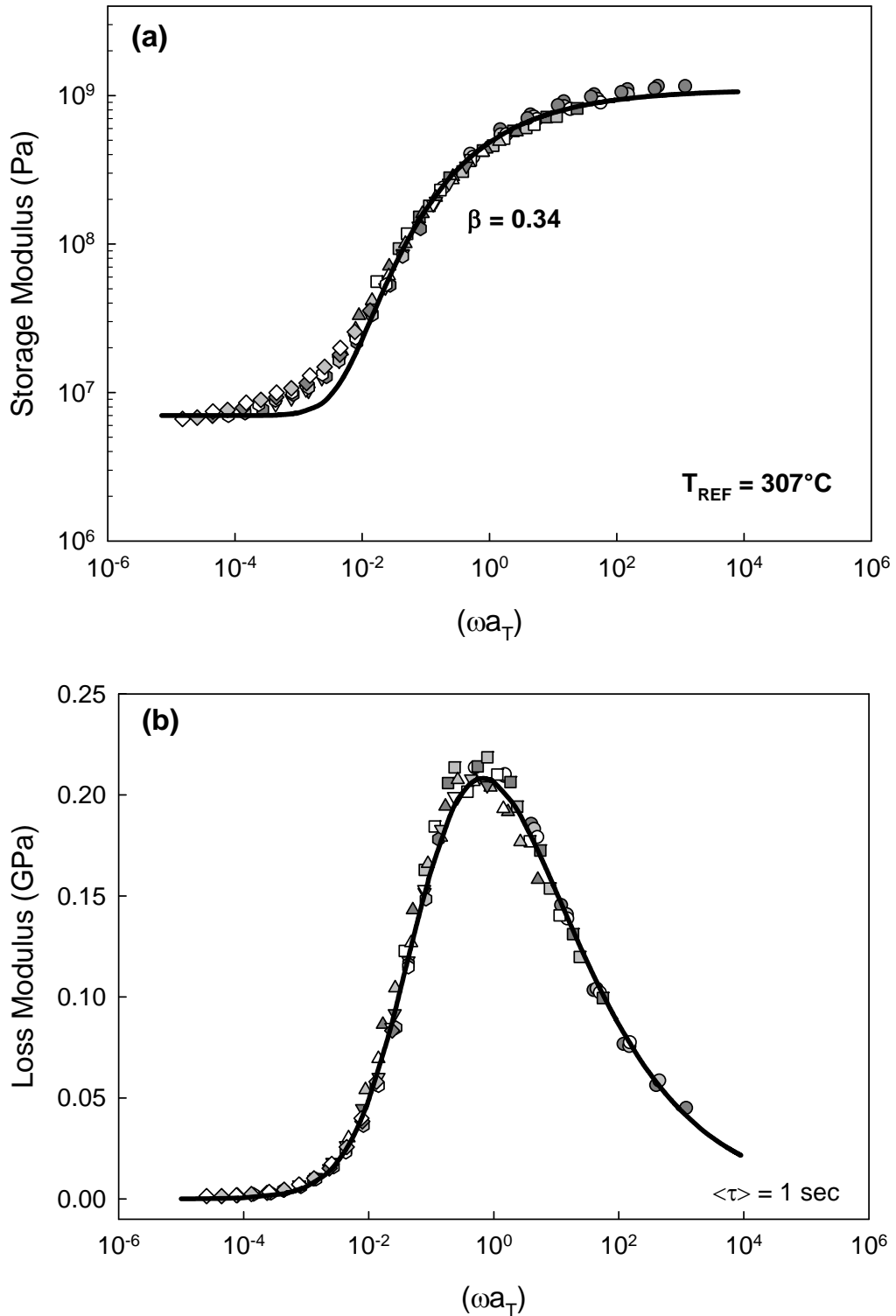


Figure 4.9: Dynamic mechanical time-temperature master curves at a reference temperature of 307°C ($\langle \tau \rangle = 1 \text{ sec}$); glass-rubber relaxation. (a) Storage modulus; (b) Loss modulus. Solid curves represent KWW best fit.

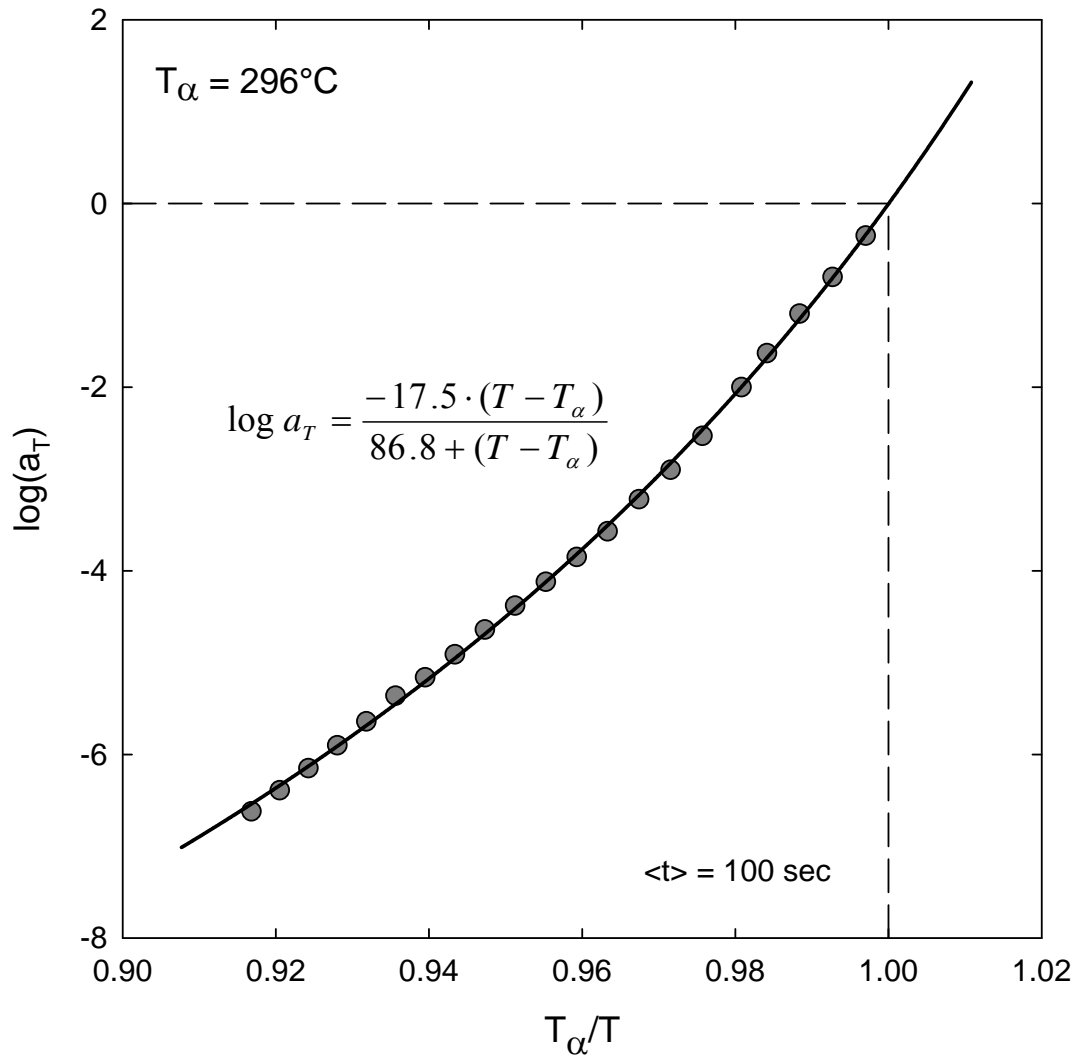


Figure 4.10: Cooperativity plot of $\log(a_T)$ vs. T_{α}/T based on dynamic mechanical measurements. $T_{\alpha} = 296^{\circ}\text{C}$ ($\langle \tau \rangle = 100 \text{ sec}$). Solid curve is WLF fit.

References

- [1] Struik, L.C.E. *Physical Aging in Amorphous Polymers and Other Materials*; Elsevier: Amsterdam, **1978**.
- [2] Hutchinson, J.M. "Physical Aging of Polymers", *Progress Polymer Science* **1995**, *20*, 703.
- [3] Hodge, I.M. "Physical Aging in Polymer Glasses", *Science* **1995**, *267*, 1945.
- [4] Drozdov, A.D. "The Effect of Temperature on Physical Aging of Glassy Polymers", *Journal of Applied Polymer Science* **2001**, *81*, 3309.
- [5] Venditti, R.A.; Gillham, J.K. "Physical Aging Deep in the Glassy State of a Fully Cured Polyimide", *Journal of Applied Polymer Science* **1992**, *45*, 1501.
- [6] Lee, H.H.D.; McGarry, F.J. "The Origin of the Beta Transition and its Influence on Physical Aging", *Polymer* **1993**, *34*, 4267.
- [7] Bateman, J.; Gordon, D.A. "Soluble Polyimides Derived from Phenylindane Diamines and Dianhydrides", *US Patent 3,856,752* **1974**.
- [8] Bos, A.; Punt, I.G.M.; Wessling, M.; Strathmann, H. "Plasticization-Resistant Glassy Polyimide Membranes for CO₂/CH₄ Separations", *Separation and Purification Technology* **1998**, *14*, 27.
- [9] Ekiner, O.M. "Phenylindane Group-Containing Polyimide Gas-Separation Membranes", *US Patent 5,015,270* **1991**.
- [10] Simmons, J.W.; Ekiner, O.M. "Preparation and Uses of Polyimide and Polyamide-Polyimide Gas Separation Membranes", *US Patent 5,232,472* **1993**.
- [11] Madden, W.C.; Punsalan, D.; Koros, W.J. "Age Dependent CO₂ Sorption in Matrimid Asymmetric Hollow Fiber Membranes", *Polymer* **2005**, *46*, 5433.
- [12] Huang, Y.; Paul, D.R. "Physical Aging of Thin Glassy Polymer Films Monitored by Gas Permeability", *Polymer* **2004**, *45*, 8377.
- [13] Huang, Y.; Paul, D.R. "Physical Aging of Thin Glassy Polymer Films Monitored by Optical Properties", *Macromolecules* **2006**, *39*, 1554.
- [14] Lim, T.; Frosini, V.; Zaleckas, V.; Morrow, D.; Sauer, J.A. "Mechanical Relaxation Phenomena in Polyimide and Poly(2,6-dimethyl-p-phenylene oxide) from 100K to 700K", *Polymer Engineering and Science* **1973**, *13*, 51.

- [15] Perena, J.M. "Dynamic Mechanical Relaxations in Polyimide and Polyamideimide", *Angewandte Makromolekulare Chemie* **1982**, *106*, 61.
- [16] Xu, G.; Gryte, C.C.; Nowick, A.S.; Li, S.Z.; Pak, Y.S.; Greenbaum, S.G. "Dielectric Relaxation and Deuteron NMR of Water in Polyimide Films", *Journal of Applied Physics* **1989**, *66*, 5290.
- [17] Sun, Z.; Dong, L.; Zhuang, Y.; Cao, L.; Ding, M.; Feng, Z. "Beta Relaxation in Polyimides", *Polymer* **1992**, *33*, 4728.
- [18] Arnold, F.E., Jr.; Bruno, K.R.; Shen, D.; Eashoo, M.; Lee, C.J.; Harris, F.W.; Cheng, S.Z.D. "The Origin of β Relaxations in Segmented Rigid-Rod Polyimide and Copolyimide Films", *Polymer Engineering and Science* **1993**, *33*, 1373.
- [19] Coburn, J.C.; Soper, P.D.; Auman, B.C. "Relaxation Behavior of Polyimides Based on 2,2'-Disubstituted Benzidines", *Macromolecules* **1995**, *28*, 3253.
- [20] Cheng, S.Z.D.; Chalmers, T.M.; Gu, Y.; Yoon, Y.; Harris, F.W.; Cheng, J.; Fone, M.; Koenig, J.L. "Relaxation Processes and Molecular Motion in a New Semicrystalline Polyimide", *Macromolecular Chemistry and Physics* **1995**, *196*, 1439.
- [21] Kim, Y.H.; Moon, B.S.; Harris, F.W.; Cheng, S.Z.D. "Polymerization, Structure and Thermal Properties of ODPA-DMB Polyimide Films", *Journal of Thermal Analysis and Calorimetry* **1996**, *46*, 921.
- [22] Habas, J.P.; Peyrelasse, J.; Grenier-Loustalot, M.F. "Rheological Study of a High-Performance Polyimide. Interpretation of the Secondary Mechanical Relaxations of a Nadimide Crosslinked System", *High Performance Polymers* **1996**, *8*, 515.
- [23] Li, S.; Hsu, B.L.; Li, F.; Li, C.Y.; Harris, F.W.; Cheng, S.Z.D. "A Study of Polyimide Thermoplastics Used as Tougheners in Epoxy Resins - Structure, Property and Solubility Relationships", *Thermochimica Acta* **1999**, *340-341*, 221.
- [24] Li, F.; Fang, S.; Ge, J.J.; Honigfort, P.S.; Chen, J.C.; Harris, F.W.; Cheng, S.Z.D. "Diamine Architecture Effects on Glass Transitions, Relaxation Processes and Other Material Properties in Organo-Soluble Aromatic Polyimide Films", *Polymer* **1999**, *40*, 4571.
- [25] Li, F.; Ge, J.J.; Honigfort, P.S.; Fang, S.; Chen, J.-C.; Harris, F.W.; Cheng, S.Z.D. "Dianhydride Architectural Effects on the Relaxation Behaviors and Thermal and Optical Properties of Organo-Soluble Aromatic Polyimide Films", *Polymer* **1999**, *40*, 4987.

- [26] Qu, W.; Ko, T.M.; Vora, R.H.; Chung, T.S. "Effect of Polyimides with Different Ratios of Para- to Meta- Analogous Fluorinated Diamines on Relaxation Process", *Polymer* **2001**, *42*, 6393.
- [27] Eichstadt, A.E.; Ward, T.C.; Bagwell, M.D.; Farr, I.V.; Dunson, D.L.; McGrath, J.E. "Synthesis and Characterization of Amorphous Partially Aliphatic Polyimide Copolymers Based on Bisphenol-A Dianhydride", *Macromolecules* **2002**, *35*, 7561.
- [28] Bas, C.; Tamagna, C.; Pascal, T.; Alberola, N.D. "On the Dynamic Mechanical Behavior of Polyimides Based on Aromatic and Alicyclic Dianhydrides", *Polymer Engineering & Science* **2003**, *43*, 344.
- [29] Ngai, K.L.; Paluch, M. "Classification of Secondary Relaxation in Glass-Formers Based on Dynamic Properties", *Journal of Chemical Physics* **2004**, *120*, 857.
- [30] Rowe, B.W. "*Physical Aging of Thin and Ultrathin Glassy Polymer Films*"; Ph.D. Dissertation University of Texas at Austin: Austin, TX, **2010**.
- [31] Rowe, B.W.; Freeman, B.D.; Paul, D.R. "Effect of Sorbed Water and Temperature on the Optical Properties and Density of Thin Glassy Polymer Films on a Silicon Substrate", *Macromolecules* **2007**, *40*, 2806.
- [32] Havriliak, S.; Negami, S. "Complex Plane Analysis of α -Dispersions in Some Polymer Systems", *Journal of Polymer Science, Polymer Symposia* **1966**, *14*, 99.
- [33] Havriliak, S.; Havriliak, S.J. *Dielectric and Mechanical Relaxation in Materials*; Hanser: Cincinnati, **1997**.
- [34] Cole, K.S.; Cole, R.H. "Dispersion and Absorption in Dielectrics. I. Alternating-Current Characteristics", *Journal of Chemical Physics* **1941**, *9*, 341.
- [35] Schönhal, A.; Kremer, F., "Analysis of Dielectric Spectra", In *Broadband Dielectric Spectroscopy*; Kremer, F.; Schönhal, A., eds.; Springer-Verlag: New York, **2003**; pp 59-98.
- [36] McCrum, N.G.; Read, B.E.; Williams, G. *Anelastic and Dielectric Effects in Polymer Solids*; John Wiley and Sons, 1967, reprinted by Dover Publications: London, **1991**.
- [37] Starkweather, H.W. "Simple and Complex Relaxations", *Macromolecules* **1981**, *14*, 1277.
- [38] Starkweather, H.W. "Aspects of Simple, Noncooperative Relaxations", *Polymer* **1991**, *32*, 2443.
- [39] Ferry, J.D. *Viscoelastic Properties of Polymers*, 3rd edition; John Wiley and Sons: New York, **1980**.

- [40] Ngai, K.L.; Roland, C.M. "Chemical Structure and Intermolecular Cooperativity: Dielectric Relaxation Results", *Macromolecules* **1993**, *26*, 6824.
- [41] Williams, G.; Watts, D.C.; Dev, S.B.; North, A.M. "Further Considerations of Non Symmetrical Dielectric Relaxation Behaviour Arising From a Simple Empirical Decay Function", *Transactions of the Faraday Society* **1971**, *67*, 1323.
- [42] Bohmer, R.; Ngai, K.L.; Angell, C.A.; Plazek, D.J. "Nonexponential Relaxations in Strong and Fragile Glass Formers", *Journal of Chemical Physics* **1993**, *99*, 4201.
- [43] Roland, C.M.; Santangelo, P.G.; Ngai, K.L. "The Application of the Energy Landscape Model to Polymers", *Journal of Chemical Physics* **1999**, *111*, 5593.
- [44] Huang, D.; McKenna, G.B. "New Insights into the Fragility Dilemma in Liquids", *Journal of Chemical Physics* **2001**, *114*, 5621.

Chapter 5

Relaxation Characteristics of Aromatic Polyimides

5.1 Introduction

A new class of thermally-modified aromatic polyimides has recently been identified as a promising membrane material for processes requiring high permeability and selectivity in combination with intrinsic thermal and chemical resistance properties. These membranes are based on soluble aromatic polyimides with *ortho*-positioned functional groups; exposure of the polyimides to thermal rearrangement (TR) at 350°C to 450°C leads to fully-aromatic, insoluble polybenzoxazoles (PBOs) with exceptional thermal and chemical resistance characteristics. The thermal conversion step produces fundamental changes in molecular connectivity and conformation that alter chain packing, resulting in a narrow distribution of free volume elements and unique “hourglass” shaped cavities. It is the distinctive shape and distribution of these cavities that appear to be responsible for the unprecedented gas separation performance reported by Park et al [1].

Three distinct aromatic polyimides (APIs) were synthesized by Dr. Claudio Ribeiro at the University of Texas at Austin based on the reaction of diamine-dianhydride pairs intentionally selected to introduce *ortho*-positioned functional groups along the polymer backbone: i.e., 3,3'-dihydroxy-4,4'-diamino-biphenyl (HAB) and 2,2-bis(3-amino-4-hydroxyphenyl)-hexafluoropropane (APAF) diamines; 2,2'-bis-(3,4-dicarboxyphenyl) hexafluoropropane dianhydride (6FDA) and 4,4'-oxydiphthalic anhydride (ODPA) dianhydrides (see **Figure 5.1**). Specific API polymers under consideration were HAB-6FDA, APAF-ODPA, and APAF-6FDA. Imidization of the API precursors was achieved

by two different routes (chemical vs. thermal imidization), leading to the introduction of acetate ($-\text{OCOCH}_3$) or hydroxyl ($-\text{OH}$) *ortho* functional groups, respectively (see **Figure 5.2**). These polymers were then subject to thermal exposure at discrete temperatures in the range 350°C to 450°C in order to achieve thermal rearrangement to polybenzoxazoles (**Figure 5.3**).

5.2 Experimental

5.2.1 Polymer Synthesis

5.2.1.1 API Polymers Prepared via Chemical Imidization

Polyimides containing *ortho*-positioned acetate groups ($-\text{OCOCH}_3$) were synthesized via chemical imidization by combining HAB or APAF (diamine) and ODPa or 6FDA (dianhydride) in a two-step polycondensation according to the experimental procedure described by Park et al [1]. Each polyimide test film was then cast from chloroform solution (CHCl_3) and thermally treated in two stages: (i) a drying step under vacuum followed by (ii) a TR conversion step. Under certain heating conditions, the acetate groups in the polymer backbone were susceptible to thermal degradation to hydroxyls. The chemical structures and corresponding molecular weights of the synthesized polymers were confirmed via infrared spectroscopy, nuclear magnetic resonance and dilute solution viscometry.

5.2.1.2 API Polymers Prepared via Thermal Imidization

Polyimides containing *ortho*-positioned hydroxyl groups ($-\text{OH}$) were synthesized via thermal imidization by combining HAB or APAF and ODPa or 6FDA according to the

procedure described by Moy and McGrath [2]. Film casting required dissolution in tetrahydrofuran (THF), and cast films were subject to vacuum drying to ensure full removal of solvent prior to TR conversion. The TR conversion step was performed in a tubular furnace under inert atmosphere at the University of Texas. Here again, all chemical structures were confirmed via IR, NMR and dilute solution viscometry.

5.2.2 Dynamic Mechanical Analysis

Dynamic mechanical analysis was performed using a TA Instruments Q800 DMA configured in tensile geometry. Storage and loss modulus (E' ; E'') were measured both in temperature sweep mode (1 Hz; 3°C/min), as well as in frequency sweep mode (0.1 to 30 Hz) at discrete temperatures ranging from -150 to 500°C. All measurements were performed under nitrogen atmosphere.

5.2.3 Broadband Dielectric Spectroscopy

Dielectric spectroscopy was performed using the Novocontrol “Concept 40” broadband dielectric spectrometer (Hundsangen, Germany). Prior to measurement, concentric silver electrodes were vacuum-evaporated on each polymer sample using a VEECO thermal evaporation system. Samples were subsequently mounted between gold platens and positioned in the Novocontrol Quatro Cryosystem. Dielectric constant (ϵ') and loss (ϵ'') were recorded in the frequency domain (0.1 Hz to 3 MHz) at 10°C isothermal intervals from -150 to 300°C (*i.e.*, sub-glass transition range). A high level of conduction was encountered at temperatures $> 300^\circ\text{C}$, precluding a full analysis of the glass-rubber relaxation via dielectric methods.

5.3 Results and Discussion

5.3.1 HAB-6FDA Polyimide

5.3.1.1 Thermal Stability

The chemically-imidized (CI) API polymers contain *ortho*-positioned acetate (-OCOCH₃) groups that are susceptible to chemical degradation at elevated temperature and conversion to hydroxyls, as shown in **Figure 5.4**. If this degradation occurs below the onset of the TR conversion process (*i.e.*, below T_g), the generation of degradation products (primarily acetic acid) and their presence in the polymer test film has the potential to influence the measured thermomechanical properties of the polymer. In the case of the HAB-6FDA polymer, the potential for degradation can be assessed by monitoring the weight loss associated with this process. The theoretical weight loss for acetate conversion is approximately 12 wt %, while the weight loss associated with complete TR conversion is about 24 wt%. Thermal gravimetric analysis (TGA) and ¹H NMR were performed on the HAB-6FDA (CI) polymer to assess the temperature range across which acetate conversion occurs. For the TGA studies, the samples were chemically imidized and the resulting synthesized polymer was used directly for the TGA measurements, without additional solvent exposure (*re*: film casting). The initial sample was held at 250°C for 10 hours. Each subsequent sample was held at 250°C for 3 hours, followed by a 1 hour hold at 300°C, 350°C, 370°C, or 400°C. The results, as shown in **Figure 5.5**, indicate no significant weight loss (*i.e.*, acetate degradation) at 250°C. The sample exposed to 300°C for one hour shows a relatively gradual weight change over time, with a total loss of approximately 4%. Independent ¹H NMR studies performed on

this sample at the University of Texas confirmed that some degree of acetate-to-hydroxyl conversion had occurred in the polymer, but there was no evidence of TR conversion to the polybenzoxazole structure. For those samples exposed to higher annealing temperatures ($\geq 350^{\circ}\text{C}$), a much sharper weight loss is evident that signals the onset of TR conversion in these polymers, as confirmed by ^1H NMR.

All (chemically-imidized) HAB-6FDA (CI) series samples characterized via dynamic mechanical analysis and dielectric spectroscopy were cast from CHCl_3 and thermally conditioned by holding under vacuum at 220°C for five days, followed by three hours at 250°C . The polymers were then subject to thermal (“TR”) exposure for one hour at 300°C , 350°C , or 400°C .

5.3.1.2 Dynamic Mechanical Analysis

Dynamic mechanical results for chemically imidized HAB-6FDA exposed to 300°C for one hour are shown in **Figure 5.6**. Three motional relaxation processes are observed with increasing temperature (designated γ , β , α , respectively), consistent with other aromatic polyimides. The peak temperatures at 1 Hz are -111°C (T_{γ}), 165°C (T_{β}), and 307°C (T_{α}). Here, the γ and β processes correspond to localized sub-glass motions of limited range, while the α process corresponds to the glass-rubber relaxation. At temperatures above 330°C , a recovery in modulus is evident that corresponds to the onset of thermal rearrangement (TR process) during the DMA heating sweep, leading to generation of a highly-rigid PBO structure. The TR process appears as a high-temperature shoulder on the glass transition $\tan \delta$ peak.

Expanded dynamic mechanical results for HAB-6FDA-TR300 (CI) are shown in **Figure 5.7**. This run was conducted across a series of six test frequencies ranging from 0.1 Hz to 30 Hz. The two sub-glass relaxations (γ , β) and the glass-rubber relaxation (α) are evident as frequency-dependent processes, wherein the relaxation temperature is offset to higher values with increasing measurement frequency. It should be noted that above the glass transition (*i.e.*, above $\sim 325^\circ\text{C}$), all features in the dynamic mechanical sweep are frequency *independent*. This is consistent with the chemical conversion associated with the TR process (recovery in E' from 325°C to 375°C). At temperatures above 450°C , an additional frequency-independent increase in modulus is observed that reflects the onset of thermal degradation during the DMA scan, as confirmed by independent TGA studies.

The relative maxima in $\tan \delta$ as a function of temperature were used as the basis for establishing time-temperature relations across the sub-glass relaxations. The results for the HAB-6FDA-TR (CI) series (300°C , 350°C , and 400°C) are shown in the form of Arrhenius plots in **Figure 5.8**, where the β relaxation peaks correspond to the higher-temperature feature in these curves (see discussion of sub-glass relaxations, below). The apparent activation energies for the γ and β relaxations are comparable to the values obtained for other polyimides, as discussed in Chapter 4.

Dynamic mechanical results for the HAB-6FDA-TR (CI) series of samples are shown in **Figure 5.9**, and demonstrate the influence of prior TR conversion on suppressing the glass transition in those polymers that have a substantial degree of PBO character along the polymer backbone (re: 350°C and 400°C exposures). For the HAB-6FDA-TR350 (CI) sample, the API glass transition process is essentially absent, with a small additional amount of thermal rearrangement indicated by the modest increase in modulus at scan

temperatures above 350°C. In this case, the limited additional TR conversion during the DMA scan appears as a broad peak in $\tan\delta$ centered at about 380°C. Finally, for the HAB-6FDA-TR400 (CI) film, only the γ and β processes are evident, indicating complete suppression of the glass transition event associated with the original API polymer. No further thermal rearrangement is evident in the DMA sweep.

Figure 5.10 shows $\tan \delta$ results for the HAB-6FDA-TR (CI) series across the sub-glass transition region. For the γ transition, the imposition of TR exposure appears to have no influence on either the position or intensity of the observed relaxation. For the β transition, the TR conversion leads to a reduction in relaxation intensity, and the emergence of a lower-temperature feature shifted 80°C to 100°C below the position of the β process in the TR300 sample; a dual-transition character is evident in both the TR350 and TR400 $\tan \delta$ curves. The shift of the β transition to lower temperatures appears to reflect localized motions involving backbone moieties that are more compact in the TR-converted polymer, as compared to the as-prepared API (re: **Figure 5.3** structures).

5.3.1.3 Broadband Dielectric Spectroscopy

Dielectric spectroscopy data for the HAB-6FDA-TR300 (CI) sample (isochronal curves; -150°C to 300°C, frequency range 0.1 Hz to 3 MHz) are presented in **Figure 5.11**. Both sub-glass relaxation processes (γ and β) are evident in the results as indicated by the distinct, step-wise, increases in dielectric constant and corresponding peaks in dielectric loss. At temperatures approaching 300°C, a strong increase in dielectric loss is observed owing to the onset of the glass transition and conduction within the sample. A

comparison of the dielectric results for the HAB-6FDA-TR300 and TR400 samples is presented as dielectric loss versus frequency in **Figure 5.12**. Examination of the γ transition data for the TR300 and TR400 films indicates little change in relaxation intensity or position with TR conversion. For the β transition, however, a dramatic reduction in relaxation intensity is observed for the TR400 sample, suggesting added motional constraint, but also a significant reduction in the net dipole moment associated with the β process in the thermally-converted polymer.

A comparison of the 1 Hz data from DMA and dielectric ($\tan \delta$ vs. temperature) is provided in **Figure 5.13**. While the position and intensity of the γ relaxation peak are comparable for both measurement techniques, it is observed that the intensity of the β relaxation is much lower in the dielectric curve. This suggests that the β process may result primarily from restricted, correlated motions of the -6FDA- dianhydride moiety, which is symmetric and encompasses limited polarity. However, the relatively bulky character of the -6FDA- unit is apparently responsible for significant viscoelastic loss (*i.e.*, β relaxation process) as detected by dynamic mechanical measurements.

5.3.2 APAF-ODPA Polyimide

5.3.2.1 Thermal Stability

APAF-ODPA polyimides prepared via chemical imidization are susceptible to acetate degradation (re: HAB-6FDA characterization discussed above). Similar to the HAB-6FDA series, TGA and NMR studies were performed on the APAF-ODPA (CI) polymer to assess the acetate conversion temperature range; the TGA results are shown in

Figure 5.14. The initial sample was held at 250°C for 10 hours. Subsequent samples were held for 1 hour at 300°C or 350°C, or 10 hours at 400°C or 450°C. The results show that at 250°C acetate degradation and conversion to hydroxyls (corresponding to an apx. 4% weight loss after 10 hours) is underway; this is in contrast to the HAB-6FDA polyimide, which showed no degradation at 250°C. At 300°C the weight loss is more significant and supporting NMR analysis confirms that acetate conversion is nearly complete in the APAF-ODPA-CI polymer. Solution-based NMR analysis could not be performed on samples exposed to higher annealing temperatures ($\geq 350^\circ\text{C}$) because the samples were insoluble as a result of TR conversion.

5.3.2.2 Dynamic Mechanical Analysis

All chemically imidized APAF-ODPA samples were cast from CHCl_3 and then dried by holding under vacuum at 200°C for five days prior to TR exposure. Dynamic mechanical $\tan \delta$ results for the chemically imidized APAF-ODPA polymers are shown in **Figure 5.15**; tested films included an as-prepared sample (exposure to 200°C, only), and samples exposed to 350°C and 400°C for one hour. The γ , β , and α relaxation processes are observed with increasing temperature, consistent with other aromatic polyimides. The sample treated at 200°C (no thermal rearrangement) appears to be strongly plasticized, as indicated by the high intensity and relatively low-temperature position of the α relaxation peak. The apparent plasticization of the sample could be due to residual chloroform from the film casting process, but may also reflect the generation of acetic acid in the polymer matrix due to acetate degradation during the DMA heating sweep. For the TR samples (350°C or 400°C for one hour), the prior high temperature exposure is presumably

sufficient to convert all acetate groups to hydroxyl, and to initiate thermal rearrangement to PBO. A reduced glass-rubber (α) peak was measured for the sample annealed at 350°C (TR350), and full suppression of the α relaxation was observed for the sample exposed to 400°C (TR400).

Chemically imidized APAF-ODPA samples were conditioned at 200°C for five days. These samples were also annealed at 250°C for different hold times (3 hours; 24 and 72 hours). The dynamic mechanical results ($\tan \delta$ vs. temperature) for these films are compared in **Figure 5.16**. The sharp, high-intensity glass-transition peak observed for the 200°C sample is consistent with a high level of ongoing plasticization. Sample conditioning at 250°C reduces this effect; the data suggest that conditioning at 24 hours drives sufficient conversion of the acetate groups to eliminate the influence of plasticization on the DMA results. The 24 hour conditioned sample shows a glass transition peak at $\sim 330^\circ\text{C}$ (1 Hz), with the TR re-arrangement process centered at 440°C; results for the 72 hour sample are nearly identical. A comparison of DMA results for the chemically imidized and thermally imidized APAF-ODPA samples is presented in **Figure 5.17**. With appropriate thermal conditioning, both polymers display the same $\tan \delta$ peak temperature.

All thermally imidized APAF-ODPA series samples were cast from THF and then held under vacuum at 220°C for five days, and then at 350°C for one hour prior to TR exposure. The DMA results for the APAF-ODPA-TR (TI) series are shown in **Figure 5.18**. Three relaxations (γ , β , α) are observed with $\tan \delta$ peak temperatures at 1 Hz of -97°C (T_γ), 165°C (T_β), and 331°C (T_α), respectively. Examination of storage modulus

and $\tan \delta$ across the range 325° to 475°C reveals a sharp drop in E' (and peak in $\tan \delta$) indicative of the glass-rubber relaxation, followed by a recovery in modulus that reflects stiffening of the polymer backbone as it undergoes thermal rearrangement during the DMA scan (*i.e.*, TR process). Both the TR400 and TR450 samples display well-defined glass transitions: as prior exposure temperature increases (350, 400, 450°C), the intensity of the glass transition peak is reduced, and it shifts to higher temperatures (see Figure 5.18B). However, even at 450°C, the one hour exposure time does not appear to produce enough thermal rearrangement along the polymer backbone to fully suppress the longer-range, flexible motions inherent to the glass-rubber relaxation.

An expanded view of the sub-glass transition region for the APAF-ODPA-TR series is shown in **Figure 5.19**. Two trends are evident that reflect the influence of thermal rearrangement on the local motions inherent to the sub-glass processes: (i) the γ relaxation peak decreases strongly with TR exposure and shifts to slightly lower temperatures, and (ii) the β relaxation peak moves downward by $\sim 80^\circ\text{C}$.

In order to further elucidate the thermal rearrangement characteristics of the APAF-ODPA films, dynamic mechanical samples were exposed to extended annealing at 400°C (8 h) and 450°C (4 h). Results for the APAF-ODPA sample held at 400°C for 8 hours are reported in **Figure 5.20**. The additional annealing (beyond 1 h) led to an increase in the glass transition peak temperature and a reduction in $\tan \delta$ intensity consistent with a higher degree of thermal rearrangement in the sample prior to DMA testing. However, 8 hours at 400°C were not sufficient to fully rearrange the sample, as evidenced by the persistence of the glass-rubber transition in the dynamic mechanical data. For the sample

exposed to 450°C (4 h), however, virtually “full” conversion was achieved, as manifested in the mechanical properties of the polymer. The modulus data shown in **Figure 5.21** indicate complete suppression of the glass-rubber transition event through to the onset of degradation at ~ 500°C.

5.3.2.3 Broadband Dielectric Spectroscopy

Dielectric results for the APAF-ODPA-TR (TI) series across the sub-glass region are shown in **Figure 5.22**. The trend in the γ relaxation is similar to that in the DMA results, showing a strong decrease in the peak intensity with TR exposure, and a shift to slightly lower temperatures. The β relaxation is weak with little sensitivity to thermal exposure history.

A comparison of the DMA and dielectric results for APAF-ODPA-TR350 (TI) is shown in **Figure 5.23**. The similar characteristics of the γ relaxation indicate that the molecular motions probed by both DMA and dielectric analysis originate from the same moieties. As discussed above with respect to HAB-6FDA, the weak dielectric β relaxation response suggests that the β relaxation may correlate primarily with local motions encompassing the dianhydride unit (–ODPA–), which is relatively bulky (accounting for the strong DMA response) but also symmetric and largely non-polar in character.

5.3.3 APAF-6FDA Polyimide

5.3.3.1 Dynamic Mechanical Analysis

All chemically imidized APAF-6FDA series samples were cast from CHCl_3 and thermally treated by holding under vacuum at 200°C for five days before TR exposure for one hour at 350°C or 400°C . Dynamic mechanical results for this series are shown in **Figure 5.24**. The γ , β , and α relaxation processes are observed with increasing temperature, consistent with other aromatic polyimides. The glass-rubber (α) transition persists up to exposure temperatures of 400°C (TR400; 1 hour), in contrast to the chemically imidized APAF-ODPA sample, where α was fully suppressed after one hour at 400°C .

The thermally imidized APAF-6FDA series samples were cast from THF and then thermally treated by holding under vacuum at 220°C for five days and then 350°C for one hour prior to TR exposure. Dynamic mechanical results for the thermally imidized APAF-6FDA-TR series are shown in **Figure 5.25**. The characteristics of the APAF-6FDA results are similar to those obtained for the APAF-ODPA (TI) polymer: three motional transitions (γ , β , α) are observed with increasing temperature, followed by a separate high-temperature peak that reflects sample stiffening associated with thermal rearrangement. The $\tan \delta$ peak temperatures at 1 Hz are -96°C (T_γ), 215°C (T_β), and 337°C (T_α).

TR exposure of 400°C for one hour (TR400) leads to a positive offset in the glass transition, indicative of partial thermal rearrangement along the polymer chain backbone.

Upon annealing at 450°C for one hour (TR450), full suppression of the glass transition event is achieved. This stands in contrast to the results for the APAF-ODPA polymer, where thermal exposure well beyond one hour at 450°C was necessary to fully suppress the glass-rubber relaxation process.

An expanded view of the dynamic mechanical results in the vicinity of the sub-glass relaxations is provided in **Figure 5.26**. For the γ transition, the base polymer shows a transition temperature (T_γ) which is nearly identical to the value obtained for the APAF-ODPA polymer. Previous comparisons (both dynamic mechanical and dielectric) between HAB-6FDA and APAF-ODPA suggested that the γ transition could be correlated with uncoupled, local motions associated with the diamine portion of the polymer repeat. The close match in T_γ observed here is consistent with this scenario, given that both APAF-ODPA and APAF-6FDA contain the same diamine moiety. Upon thermal rearrangement, the intensity of the γ transition is reduced, and essentially disappears for TR exposure at 450°C (TR450); a similar trend was observed for APAF-ODPA.

Examination of the β transition region in Figure 5.26 reveals a very broad peak that appears to encompass more than one underlying relaxation process. The β relaxation peak ($T_\beta = 215^\circ\text{C}$) has an additional feature at $\sim 165^\circ\text{C}$, which is the nominal transition temperature reported for both HAB-6FDA and APAF-ODPA. Although the DMA-dielectric comparisons presented above suggest an apparent correlation between the β transition and motions associated with the dianhydride portion of the API repeat, this interpretation should be approached with caution. The relatively complex character of

the β loss curve suggests multiple, and most likely coupled motional mechanisms. Upon TR exposure, some of this underlying complexity seems to be removed, and an overall downward shift in the β relaxation is observed, similar to the trends encountered with both HAB-6FDA and APAF-ODPA.

A comparison of the sub-glass $\tan \delta$ curves for thermally imidized APAF-ODPA and APAF-6FDA is provided in **Figure 5.27**. The γ relaxation position for both polymers at all TR conversions is invariant, and at the highest TR conversion (TR450) the γ relaxation curves collapse on one another. Again, this is consistent with the γ relaxation originating from motions involving the (–APAF–) diamine unit common to both polymers.

5.3.3.2 Broadband Dielectric Spectroscopy

Dielectric results for the APAF-6FDA-TR (TI) series in the sub-glass region are shown in **Figure 5.28**. The results are similar to the APAF-ODPA-TR (TI) series showing a strong decrease in the γ peak with TR exposure and a shift to slightly lower temperatures; the β relaxation is weak with little sensitivity to thermal exposure history.

A comparison of the dielectric and DMA results for APAF-6FDA-TR350 (TI) is shown in **Figure 5.29**. The weak β relaxation response as detected by the dielectric probe is indicative of motions encompassing symmetric moieties with relatively low net dipolar content (i.e., –6FDA–). This is contrasted by the stronger dynamic mechanical response, which reflects the bulk viscoelastic processes required to accommodate these same

motions. A similar contrast in β relaxation intensity was observed for both HAB-6FDA and APAF-ODPA.

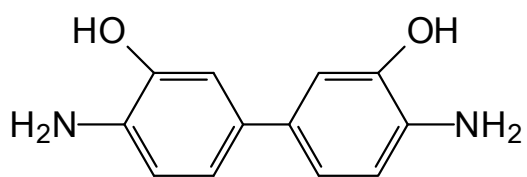
5.4 Influence of Ambient Moisture on API Sub-glass Relaxations

As indicated above, all DMA measurements completed on the polyimides (including Matrimid) were conducted on samples allowed to equilibrate to ambient laboratory temperature and humidity prior to testing. However, residual moisture has been identified in some studies as contributing to or responsible for the sub-glass relaxations observed in aromatic polyimides [3]. Selected samples in this study were evaluated by DMA analysis to observe the effects of drying. The samples were mounted in the DMA and dried *in situ* by briefly exposing the sample to temperatures above 200°C in an inert atmosphere. The results comparing the treated (dried) and untreated (wet) samples are shown in **Figure 5.30**. The plots indicate that for all dried samples examined, (*i.e.*, HAB-6FDA-TR400 (CI), APAF-ODPA-TR350 (TI), and APAF-6FDA-TR350 (TI)) the γ relaxation is no longer present. This would suggest that: (i) the water molecules themselves are responsible for the molecular motions associated with the γ transition; (ii) the presence of the water molecules are affecting chain mobility which results in the observed γ relaxation, or (iii) a combination of these two mechanisms. Moisture has little effect on the β relaxation, with only a slight shoulder evident for HAB-6FDA-TR400 (CI) and APAF-ODPA-TR350 (TI). In the case of APAF-6FDA-TR350 (TI), the shoulder is also present, but broader. These moisture effects were shown to be reversible when dried samples were exposed to ambient air overnight, and the γ relaxation reappeared in the subsequent DMA scans (see **Figure 5.31**).

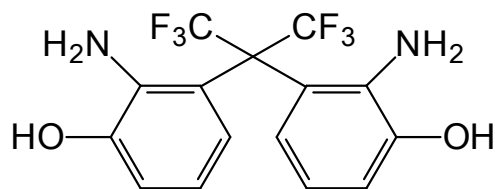
5.5 Conclusions

The application of dynamic mechanical and dielectric thermal analysis methods provides essential insight regarding the thermal stability and TR conversion characteristics of API polymers developed for application in the context of both hydrocarbon (pervaporation) and selective gas separations. Crucial to this effort are sample preparation strategies that eliminate or minimize complications that may impact the measured dynamic properties of the polymers; *e.g.*, residual solvent in cast film specimens, or ongoing chemical transformations at temperatures prior to the TR threshold. By carefully controlling these factors, we have established a body of data across three model series of API polymers that forms the basis for a clearer understanding of the TR conversion process and its relation to polymer structure and sample thermal history. The impact of thermal rearrangement on the sub-glass processes is of particular interest, as these limited-range motions are especially sensitive to the local environments and variations in backbone flexibility that govern transport phenomena on a molecular level. Future studies in this regard will aim to more definitively establish the underlying origin of these local relaxations in an effort to better correlate backbone modifications with membrane performance properties.

a) Diamine Structures

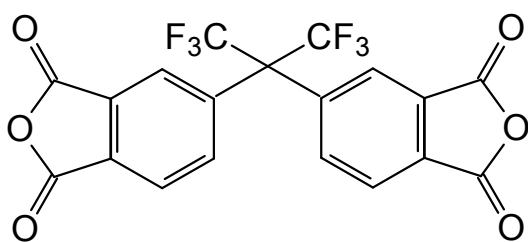


HAB

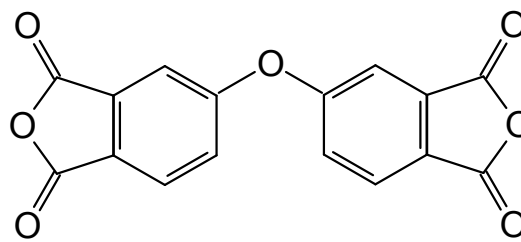


APAF

b) Dianhydride Structures



6FDA



ODPA

Figure 5.1: Chemical structures for a) diamines and b) dianhydrides.

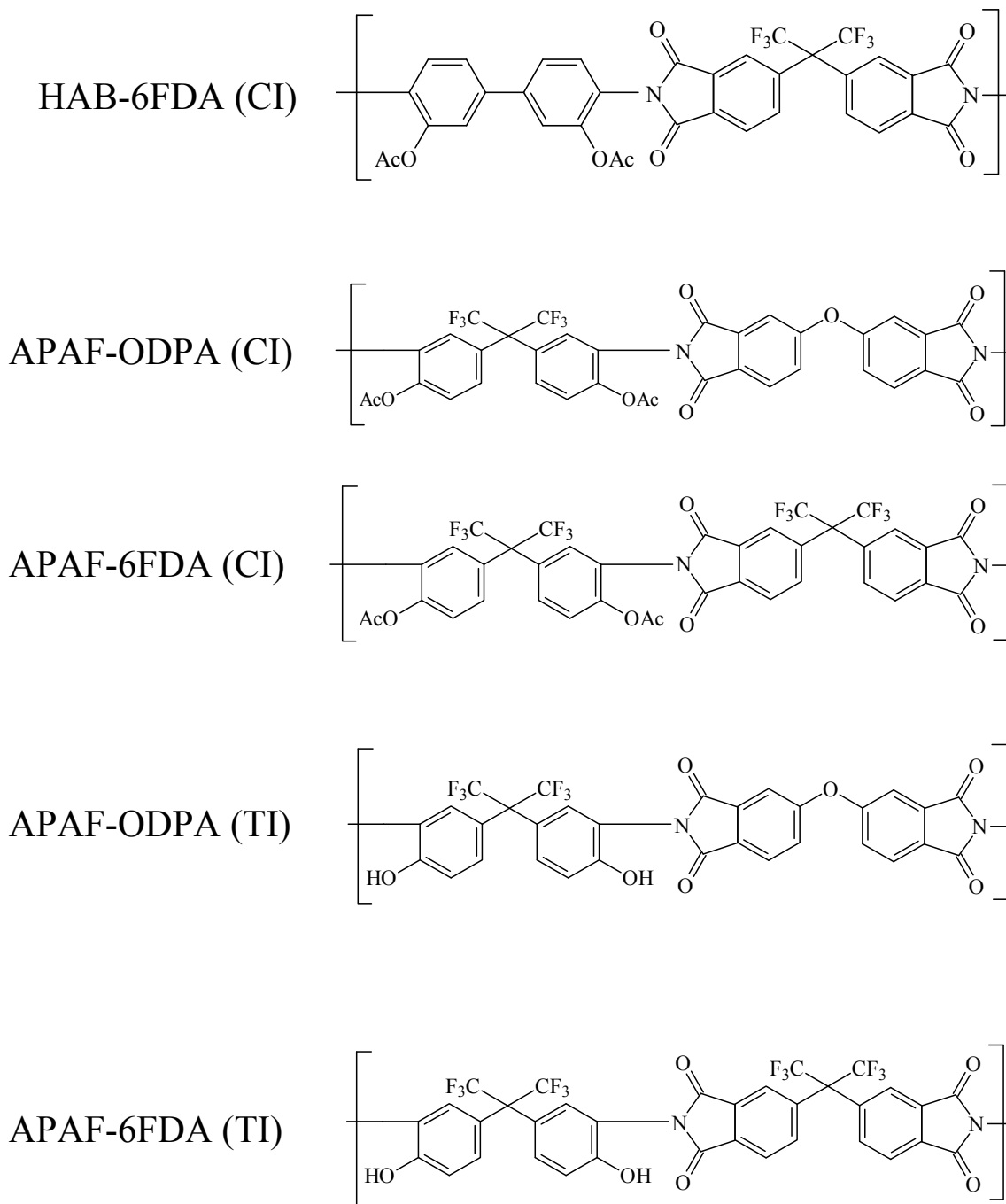


Figure 5.2: Chemical structures for aromatic polyimides prepared via chemical imidization (CI) and thermal imidization (TI).

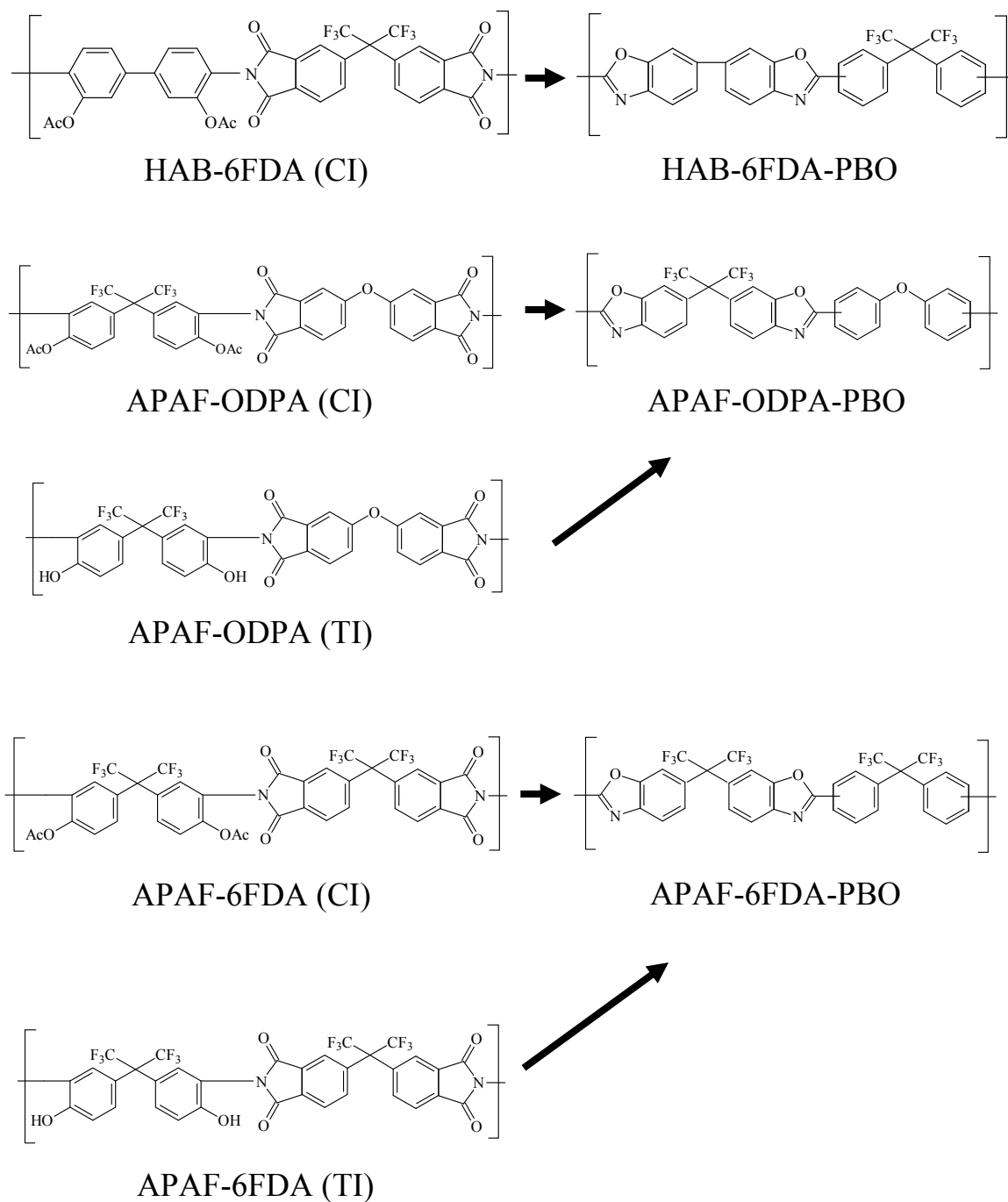
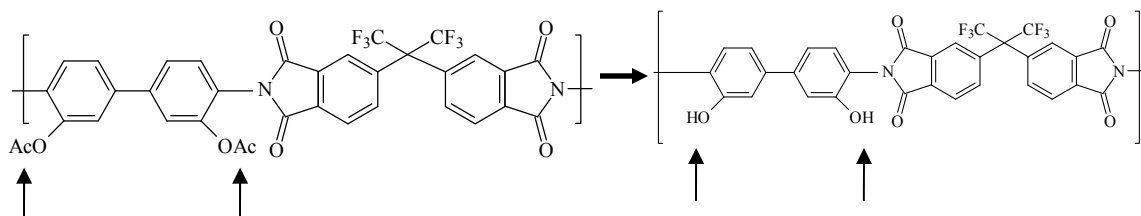


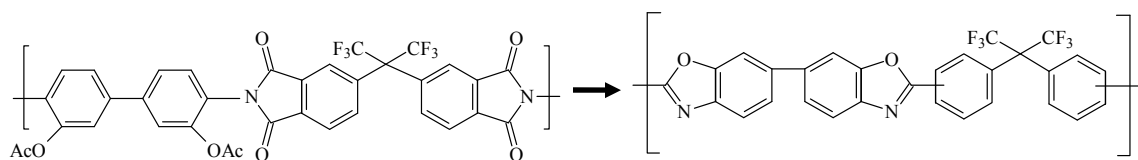
Figure 5.3: TR conversion structures (PBOs) for aromatic polyimides initially prepared via chemical imidization (CI) and thermal imidization (TI).

HAB-6FDA: Potential for acetate degradation



Theoretical weight loss ~ 12%

HAB-6FDA: TR process



Theoretical weight loss ~ 24%

Figure 5.4: HAB-6FDA theoretical weight loss (chemically imidized): acetate degradation and TR conversion.

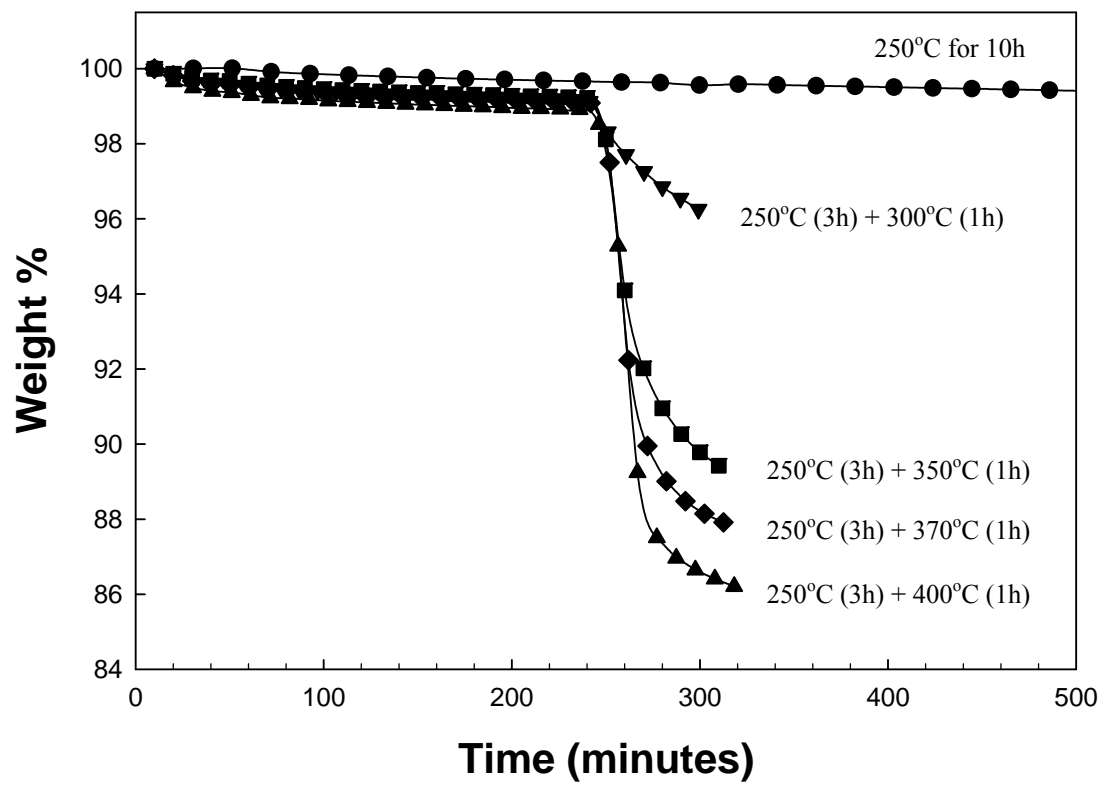


Figure 5.5: Chemically imidized HAB-6FDA exposed to various thermal histories and plotted as weight % retained vs. time (minutes). Ramp time to isothermal hold (250°C) approximately 60 minutes. (TGA studies completed by Dr. Claudio Ribeiro).

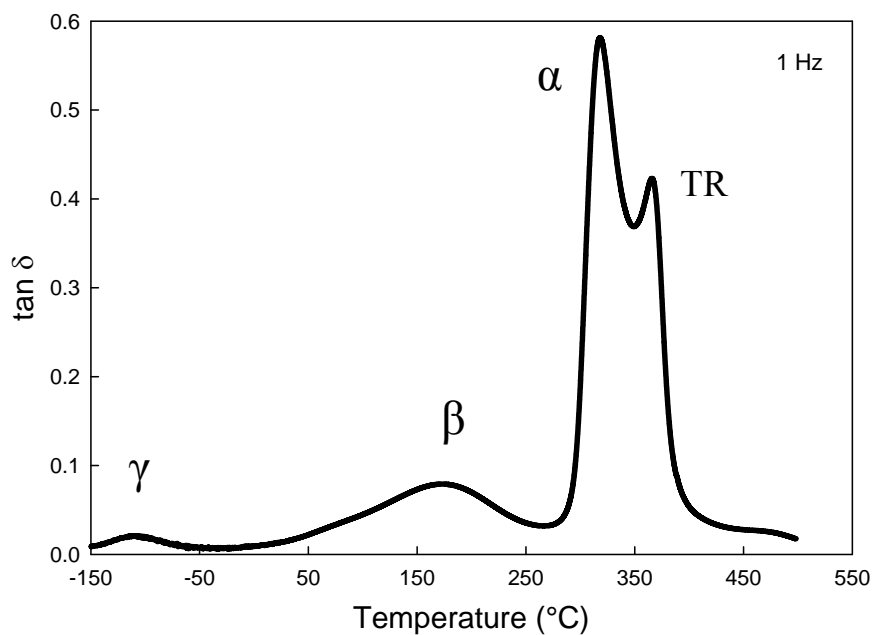
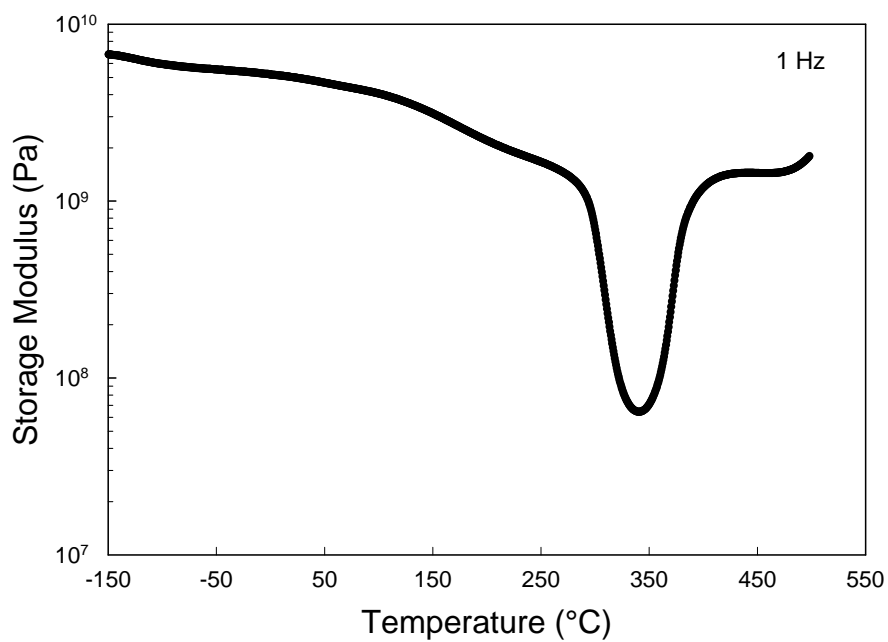


Figure 5.6: Storage modulus and $\tan \delta$ vs. temperature for chemically imidized HAB-6FDA-TR300. Sample was held at 250°C for 3 hours and then at 300°C for 1 hour. Frequency of 1 Hz; heating rate of 3°C/min.

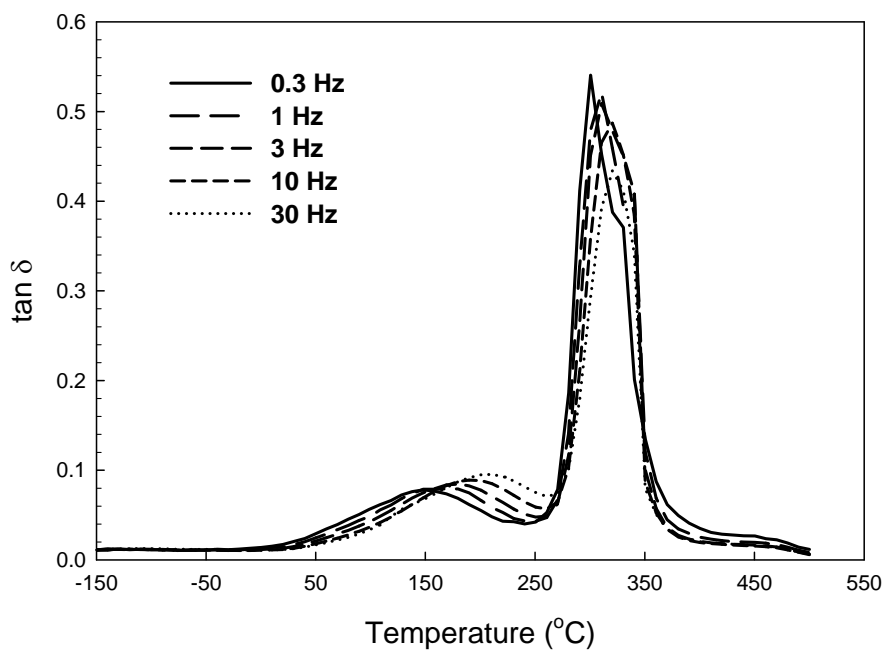
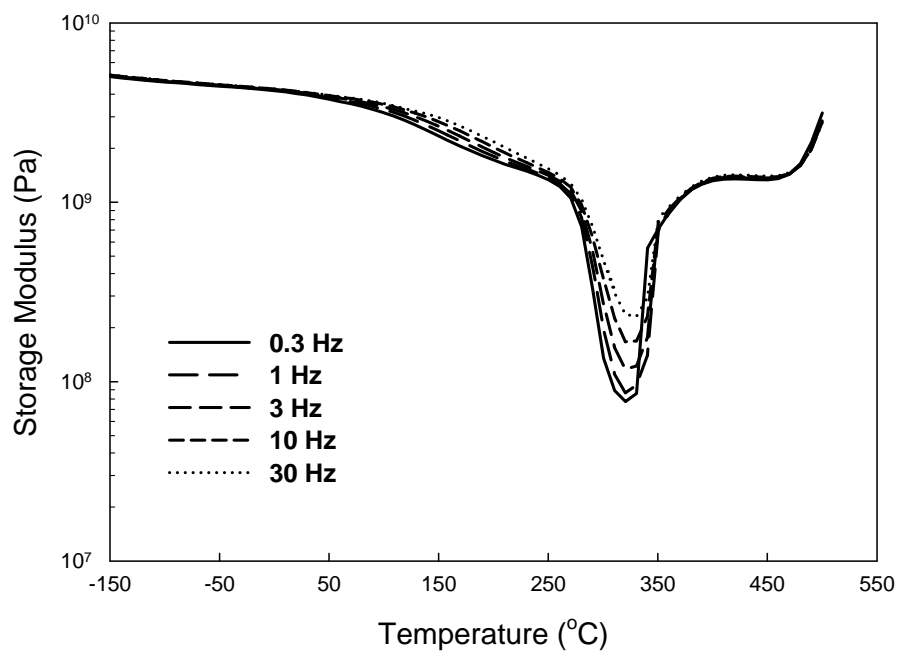


Figure 5.7: Multi-frequency plots of storage modulus and $\tan \delta$ vs. temperature for chemically imidized HAB-6FDA-TR300.

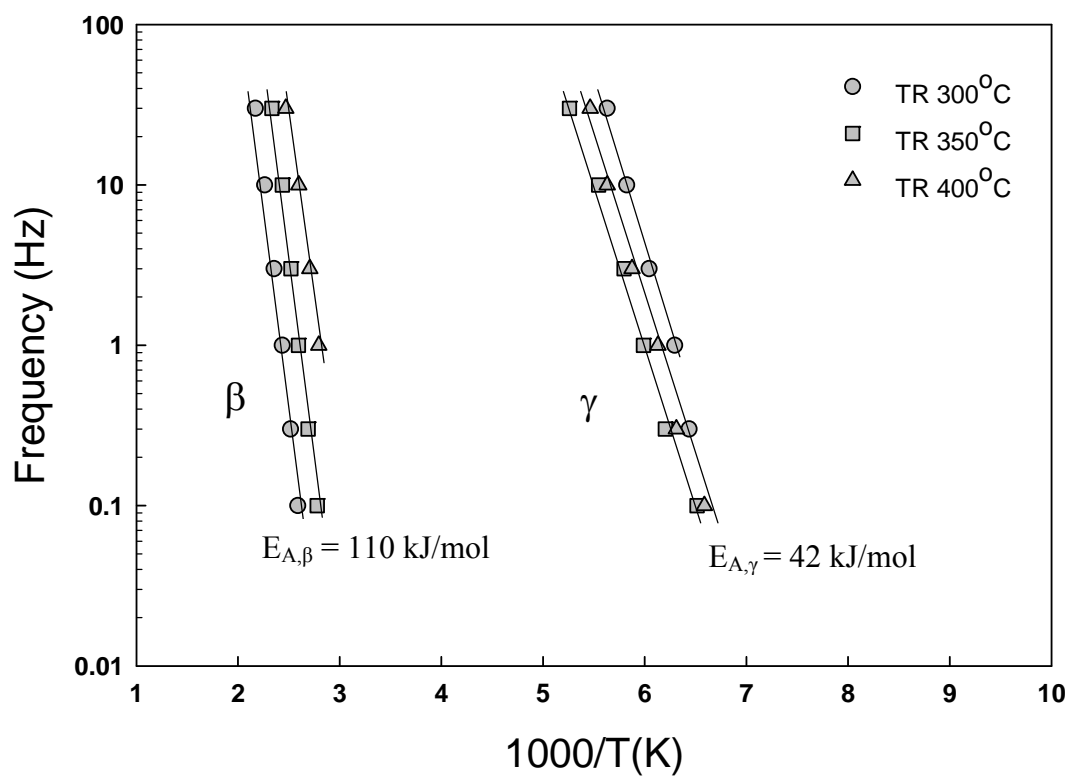


Figure 5.8: Arrhenius plot (dynamic mechanical sub-glass transitions) for chemically imidized HAB-6FDA TR series (TR exposure at given temperature for one hour).

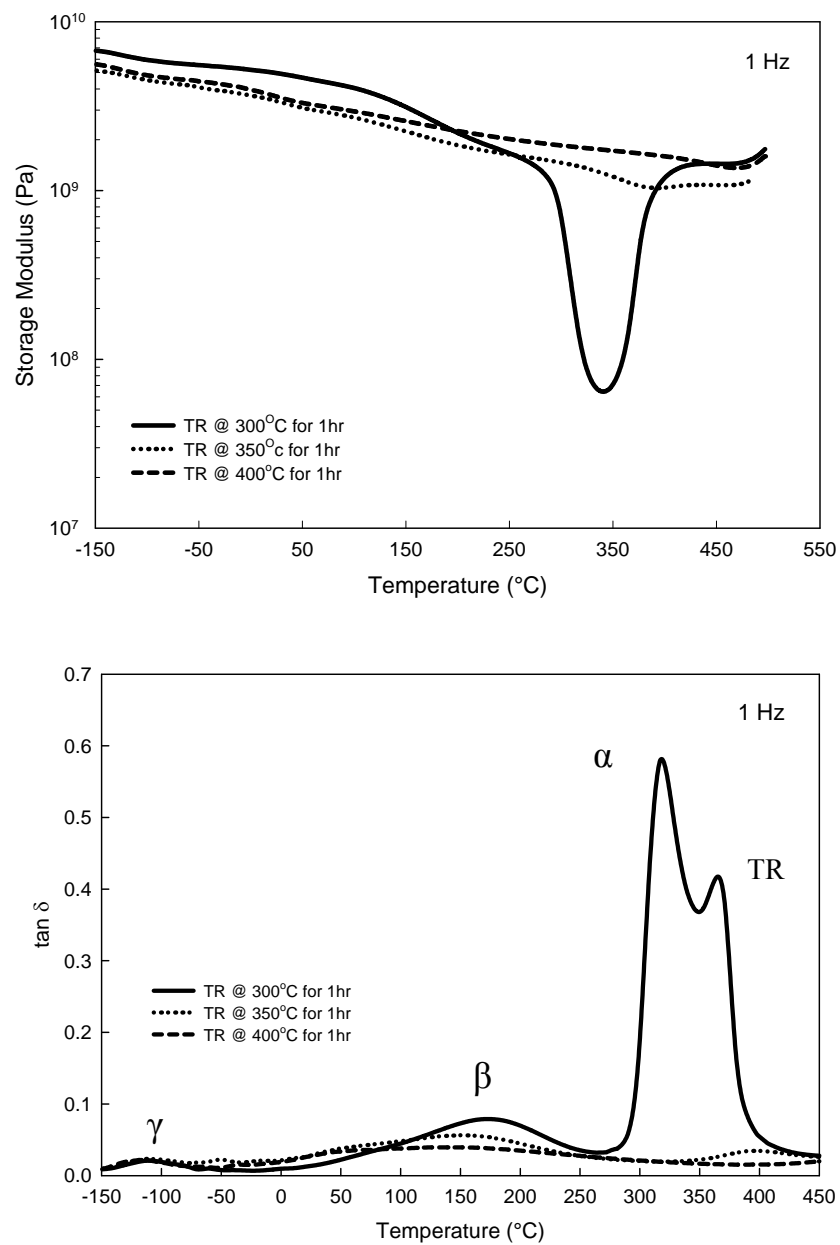


Figure 5.9: Storage modulus and $\tan \delta$ vs. temperature for chemically imidized HAB-6FDA TR series. Sample was held at 250°C for 3 hours and then at 300°C for 1 hour. Frequency of 1 Hz; heating rate of 3°C/min.

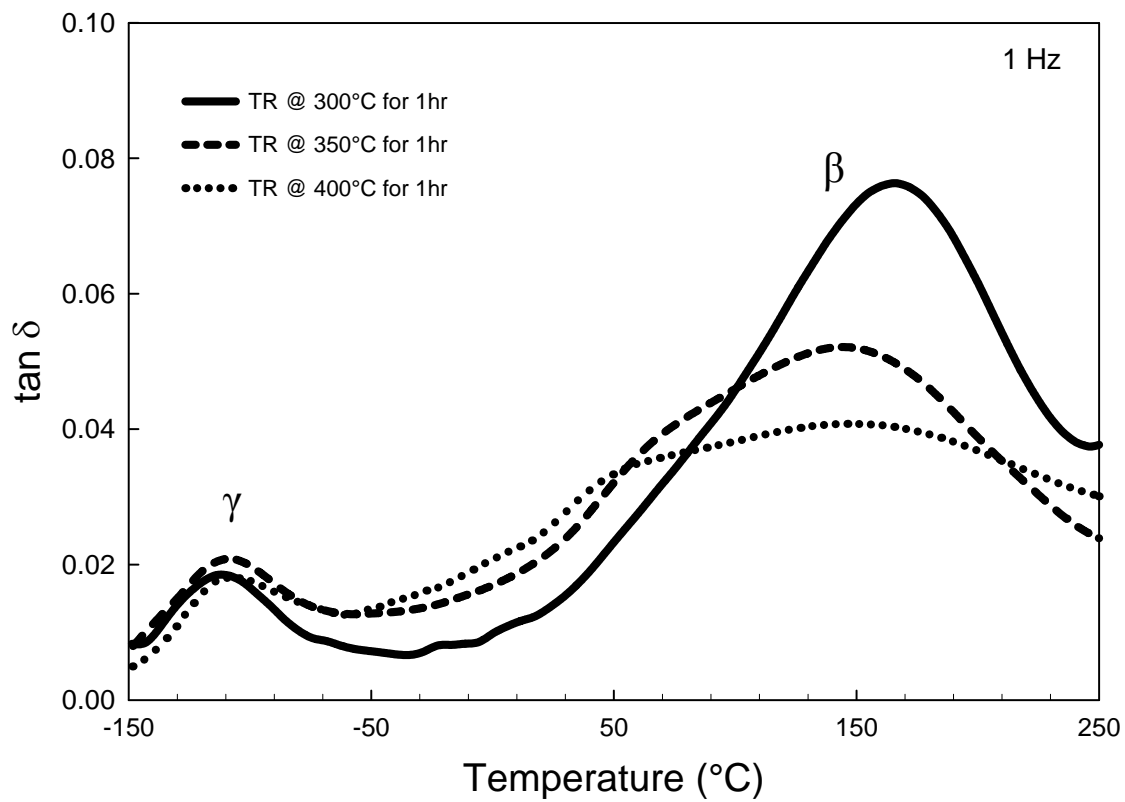


Figure 5.10: $\tan \delta$ vs. temperature for chemically imidized HAB-6FDA TR series in the sub-glass region. DMA analysis at 1 Hz and heating rate of $3^{\circ}\text{C}/\text{min}$.

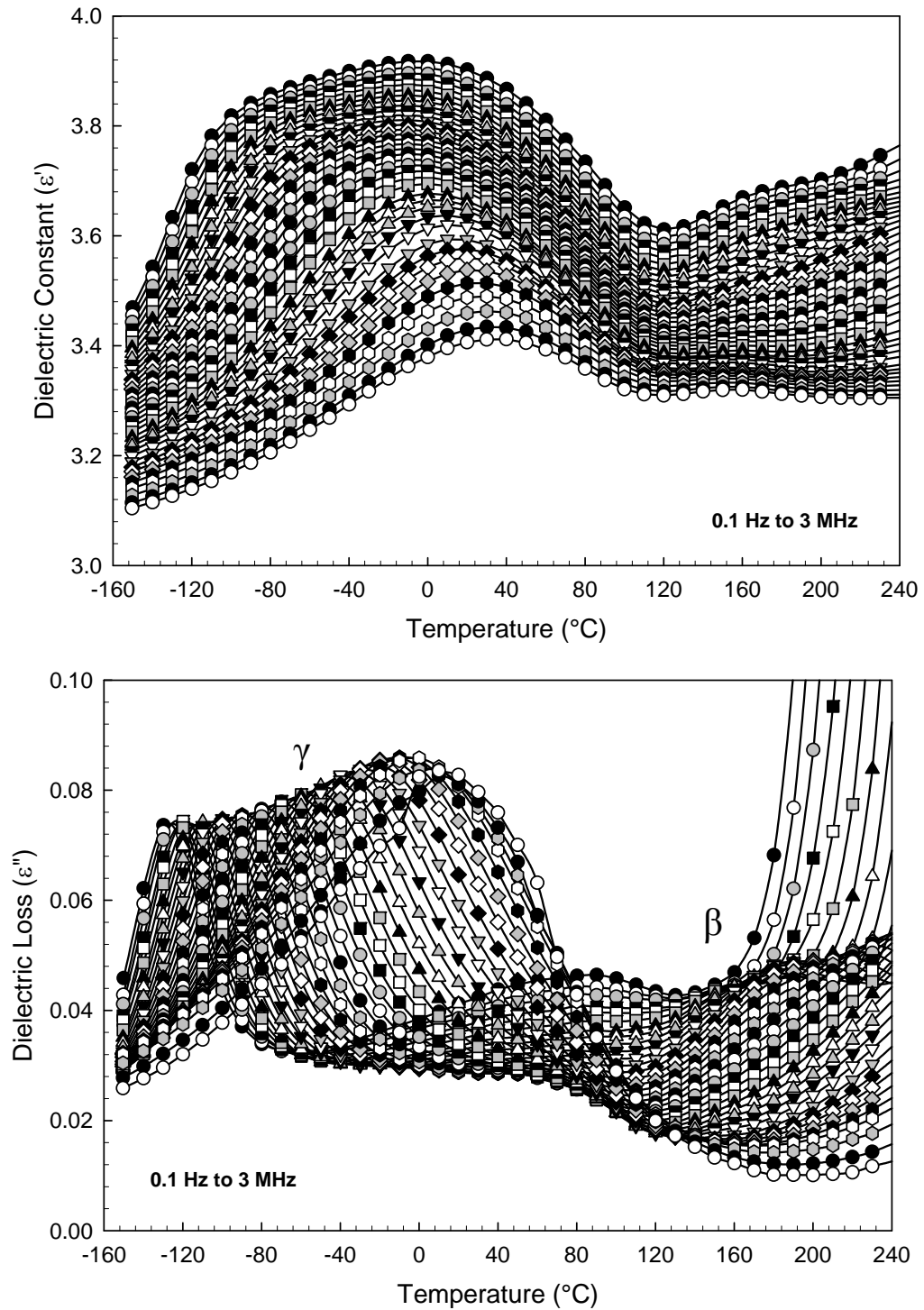


Figure 5.11: Dielectric properties vs. temperature for chemically imidized HAB-6FDA-TR 300. Frequencies from 0.1 Hz to 3MHz.

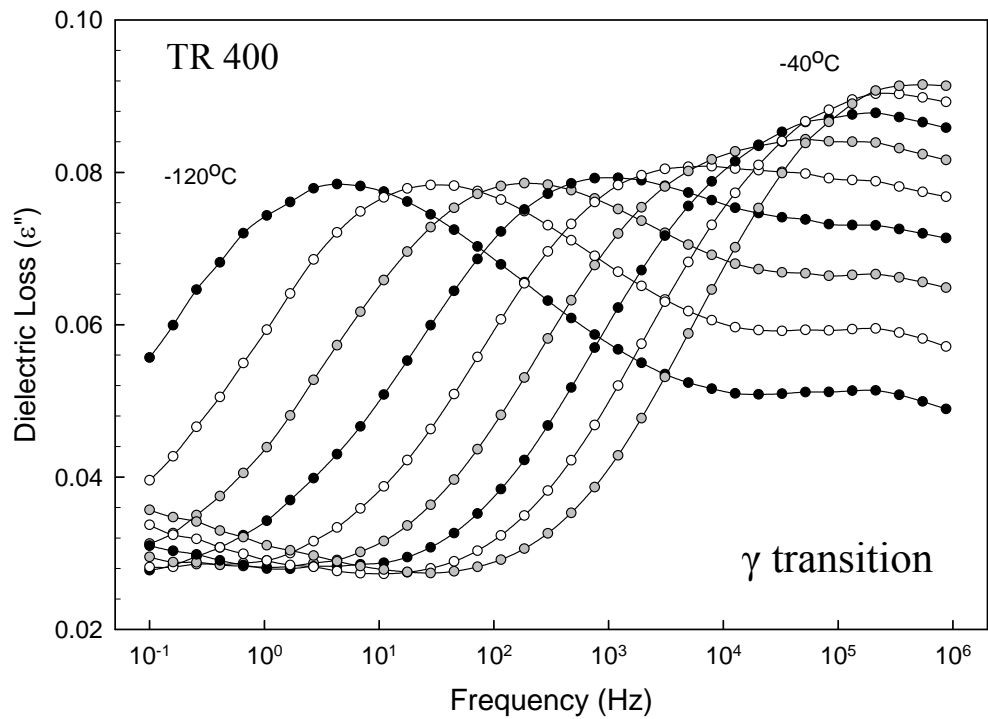
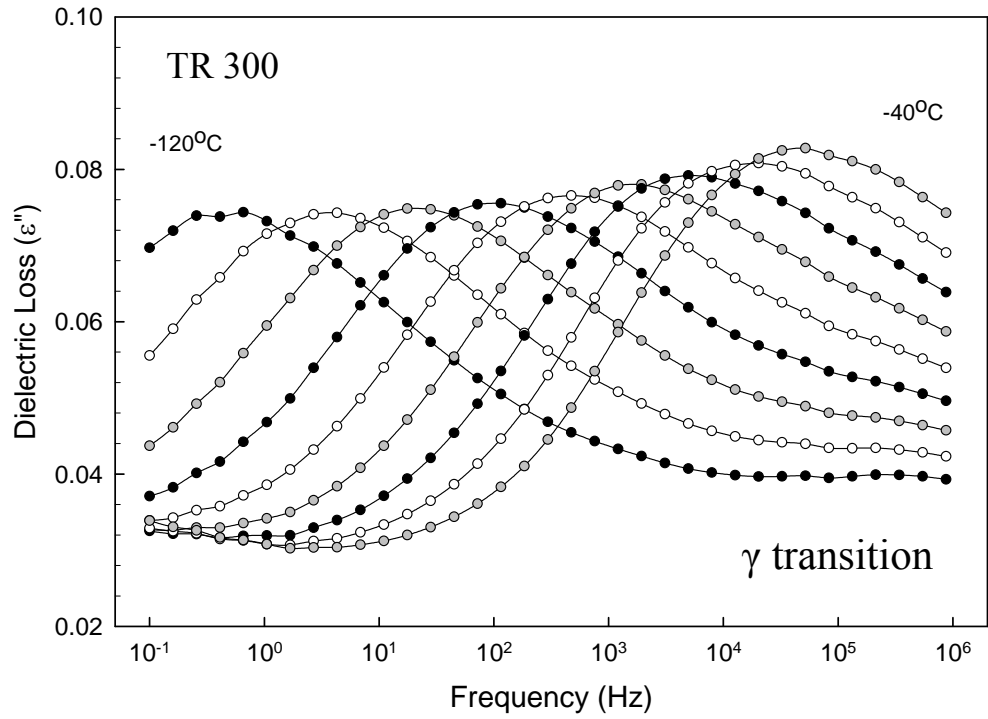


Figure 5.12A: Dielectric loss vs. frequency for chemically imidized HAB-6FDA; γ transition. TR @ 300°C for 1hr, TR @ 400°C for 1hr.

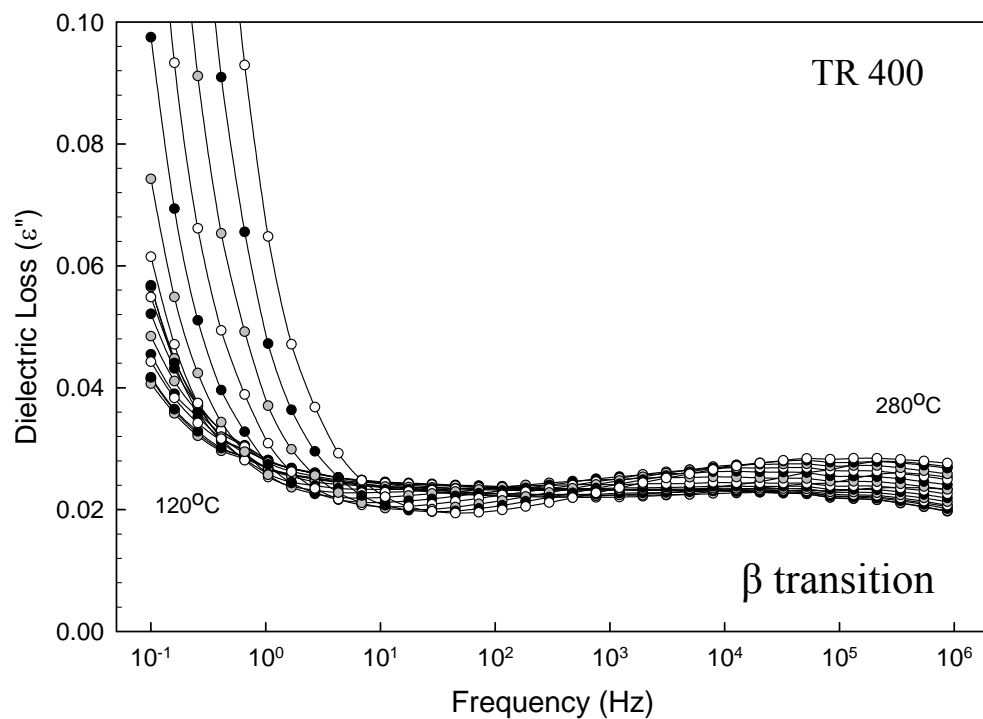
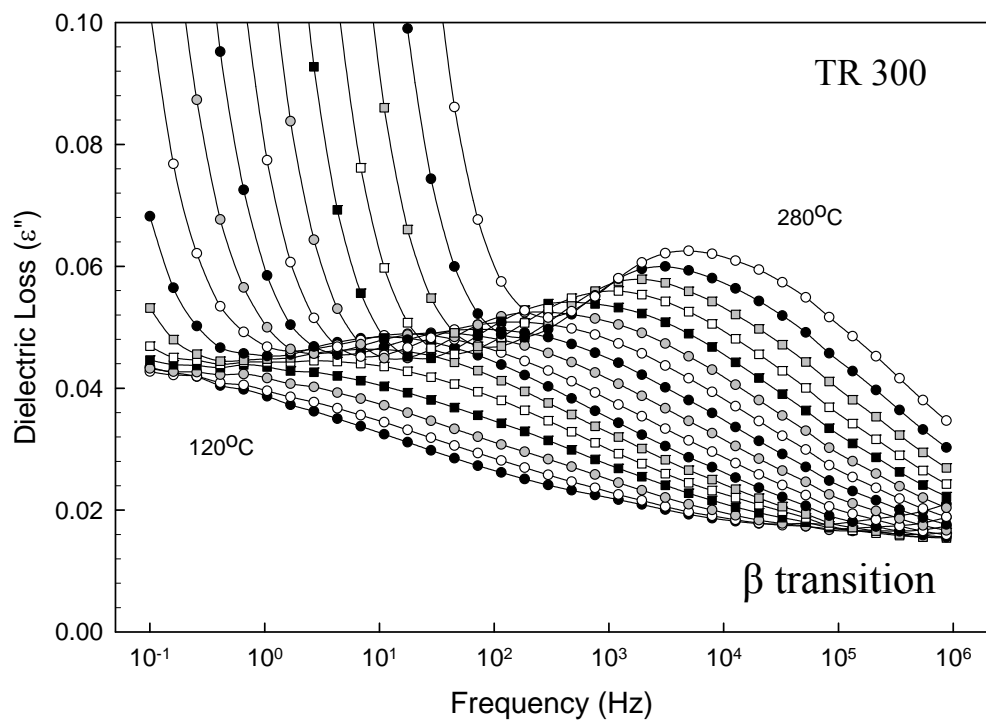


Figure 5.12B: Dielectric loss vs. frequency for chemically imidized HAB-6FDA; β transition. TR @ 300°C for 1hr, TR @ 400°C for 1hr.

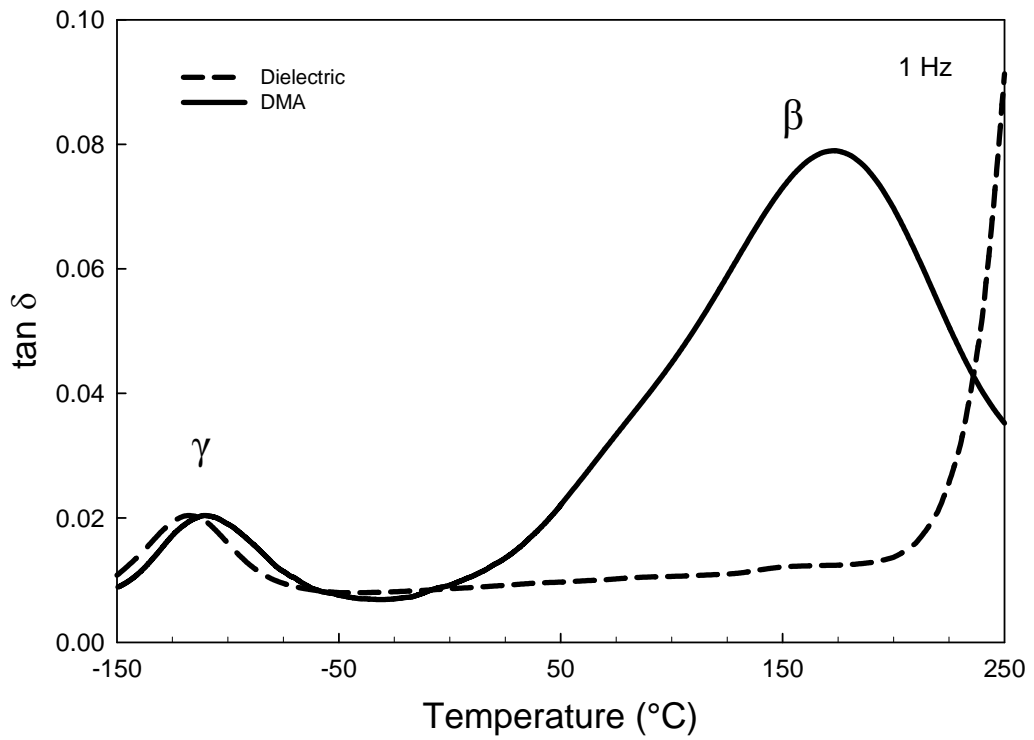


Figure 5.13: $\tan \delta$ vs. temperature for chemically imidized HAB-6FDA-TR300.

Dielectric and DMA results at 1 Hz.

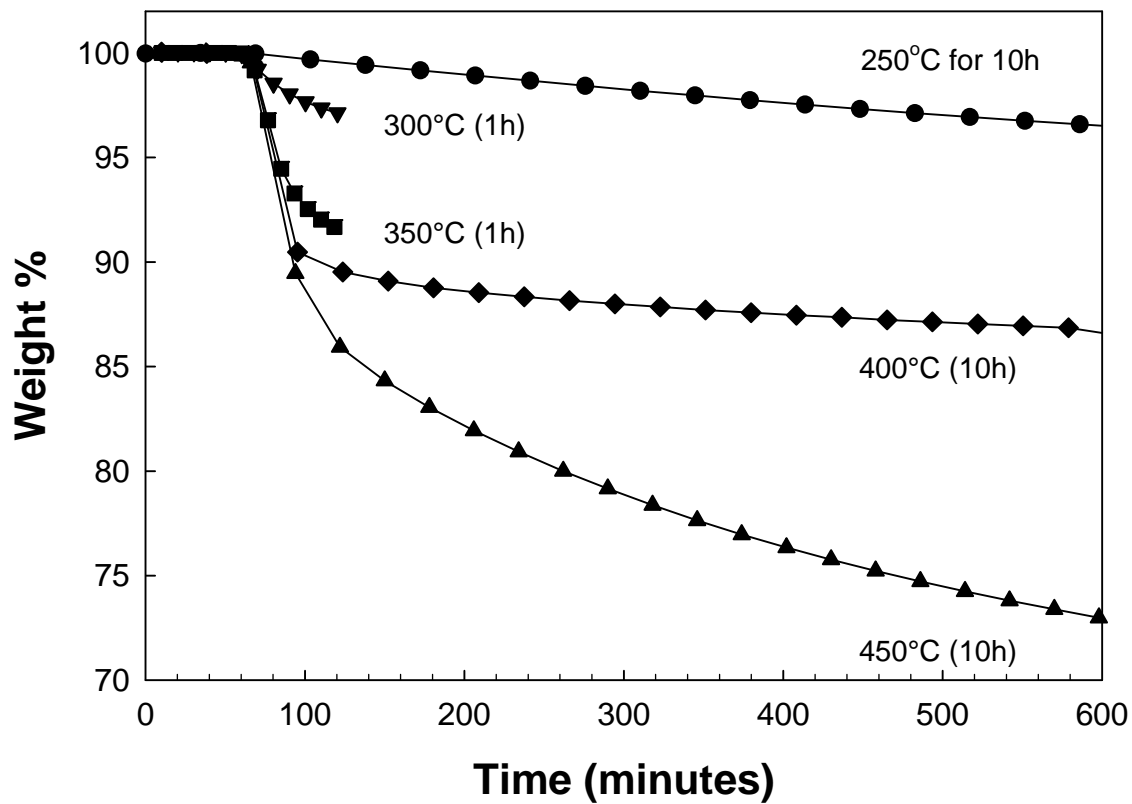


Figure 5.14: Chemically imidized APAF-ODPA exposed to various thermal histories and plotted as weight % retained *vs.* time (minutes). Heating rate to isothermal hold temperature $\sim 5^{\circ}\text{C}/\text{min}$. (TGA studies completed by Dr. Claudio Ribeiro).

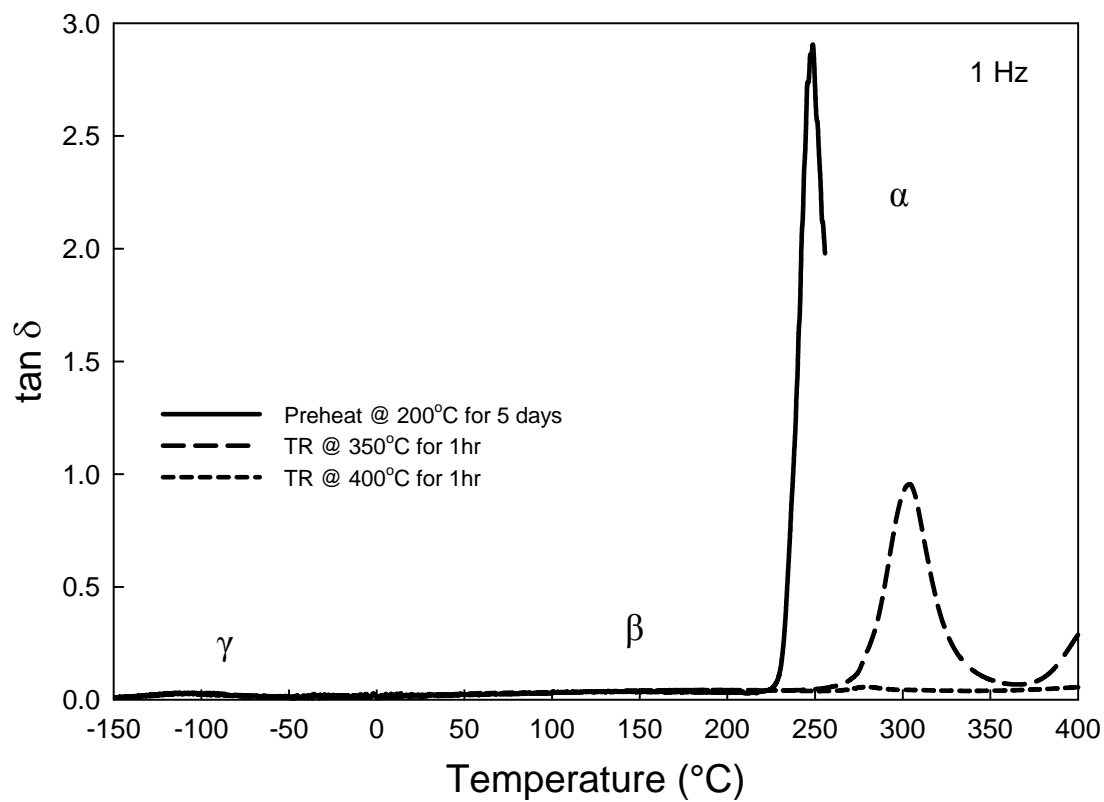


Figure 5.15: Dynamic mechanical $\tan \delta$ vs. temperature for chemically imidized APAF-ODPA TR series. All samples were exposed to vacuum drying at 200°C prior to TR exposure. Frequency of 1 Hz; heating rate of 3°C/min.

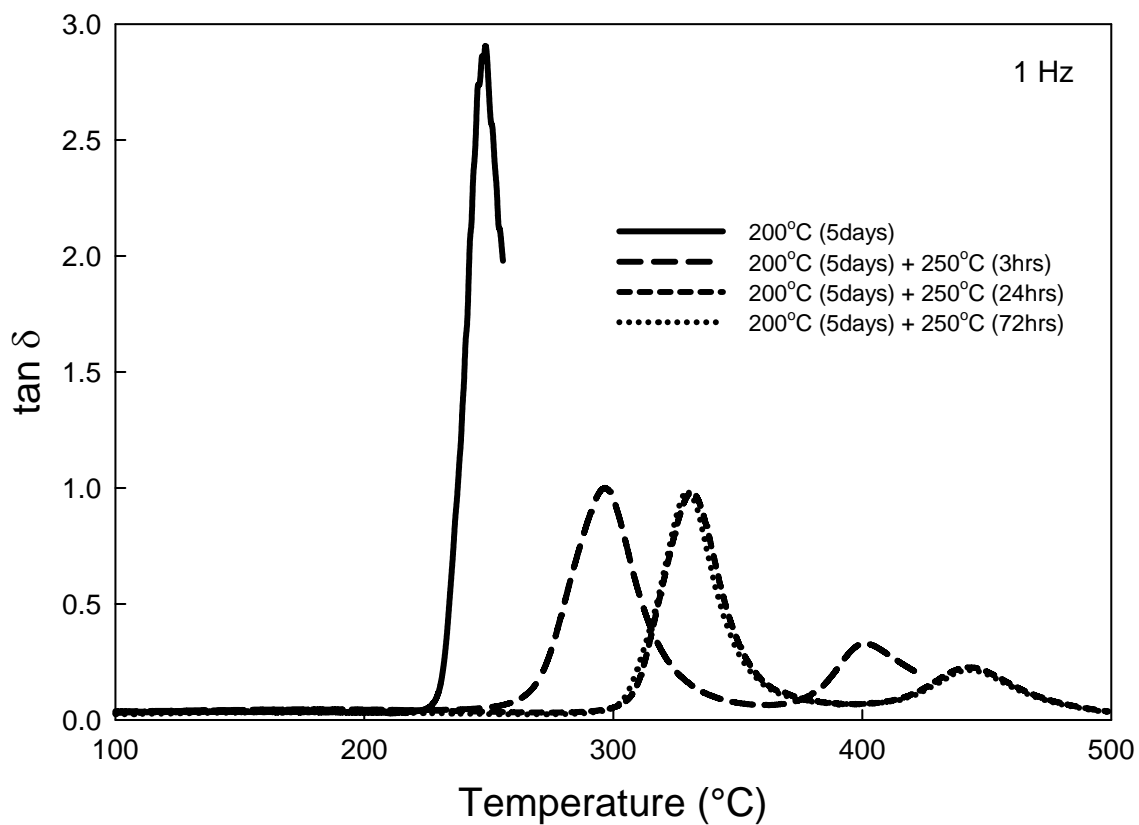


Figure 5.16: Dynamic mechanical results (tan δ vs. temperature) for APAF-ODPA samples synthesized via chemical imidization and exposed to various thermal histories as indicated. Frequency of 1 Hz; heating rate of 3 $^{\circ}\text{C}/\text{min}$.

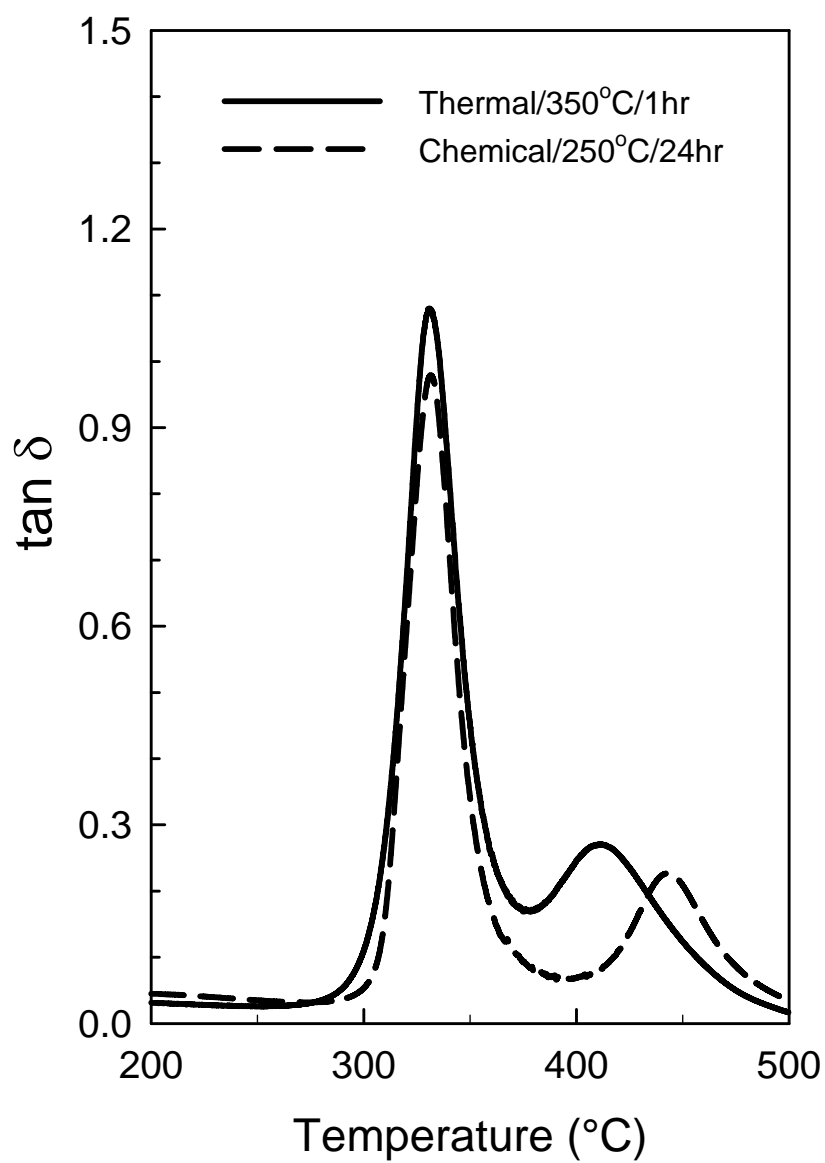


Figure 5.17: Comparison of dynamic mechanical $\tan \delta$ for APAF-ODPA samples synthesized via chemical and thermal imidization; sample histories as indicated. Frequency of 1 Hz.

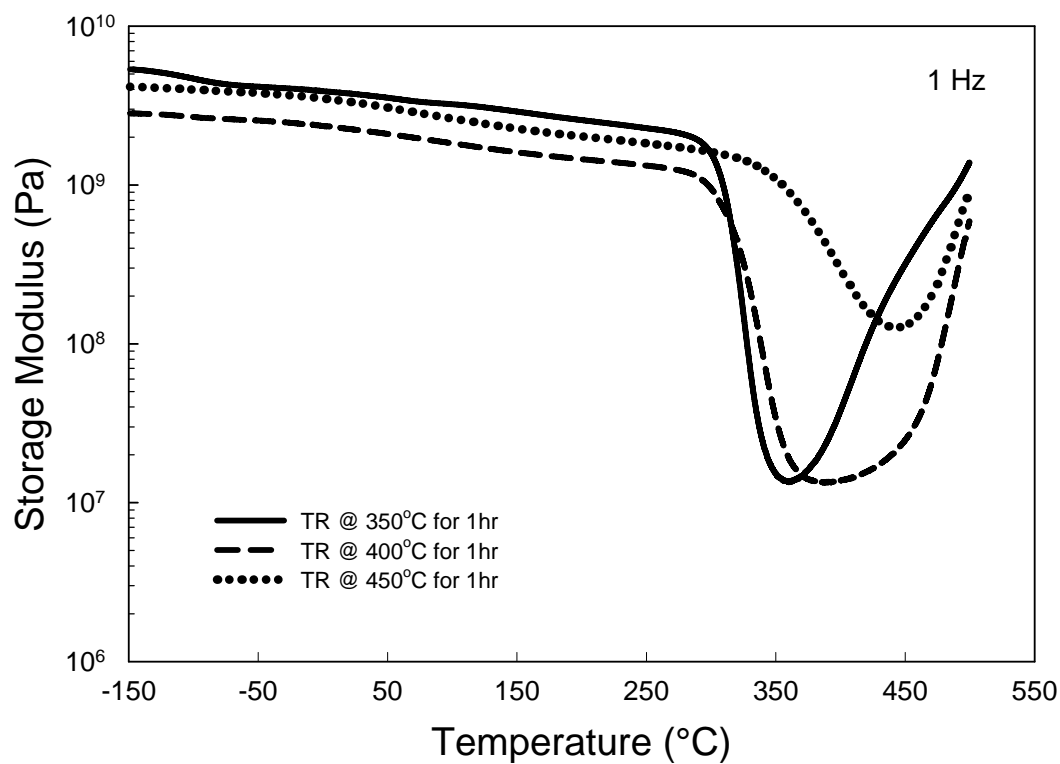


Figure 5.18A: Dynamic mechanical properties for thermally imidized APAF-ODPA TR series: storage modulus results. All samples were exposed to vacuum drying at 220°C prior to TR exposure. Frequency of 1 Hz; heating rate of 3°C/min.

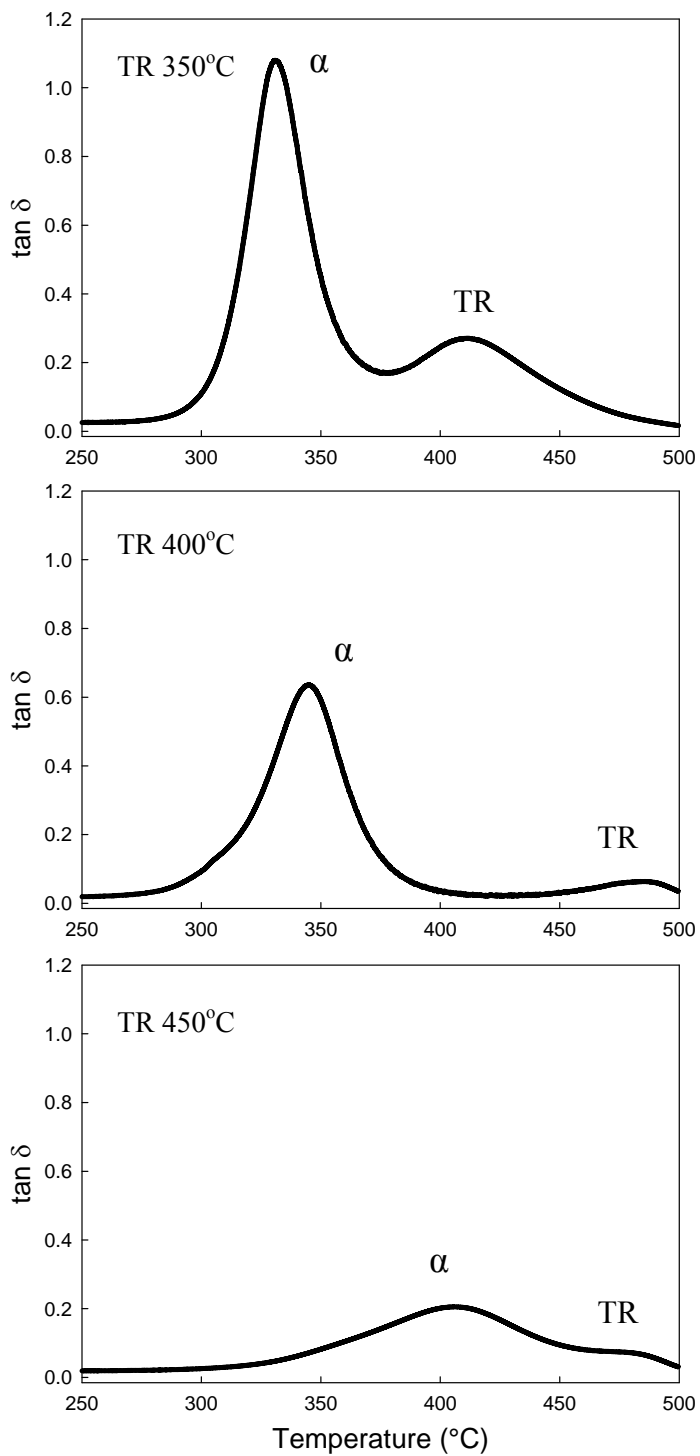


Figure 5.18B: Dynamic mechanical properties for thermally imidized APAF-ODPA TR series: $\tan \delta$ results. All samples were exposed to vacuum drying at 220 $^{\circ}\text{C}$ prior to TR exposure. Frequency of 1 Hz; heating rate of 3 $^{\circ}\text{C}/\text{min}$.

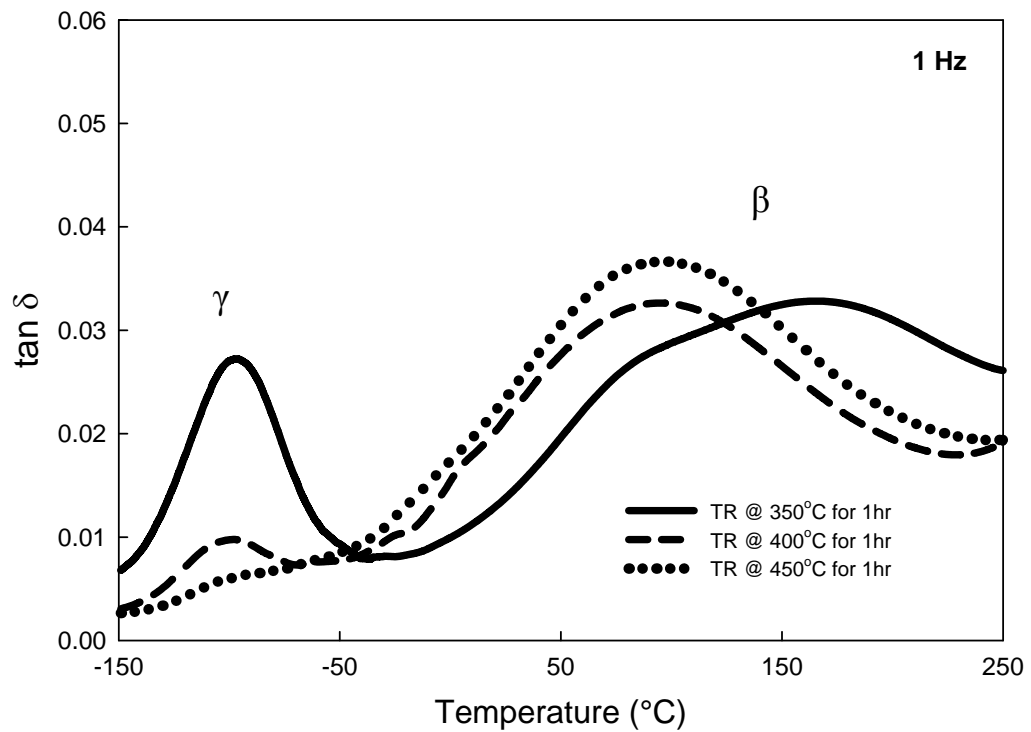


Figure 5.19: $\tan \delta$ vs. temperature for thermally imidized APAF-ODPA TR series in the sub-glass region. DMA analysis at 1 Hz and heating rate of $3^{\circ}\text{C}/\text{min}$.

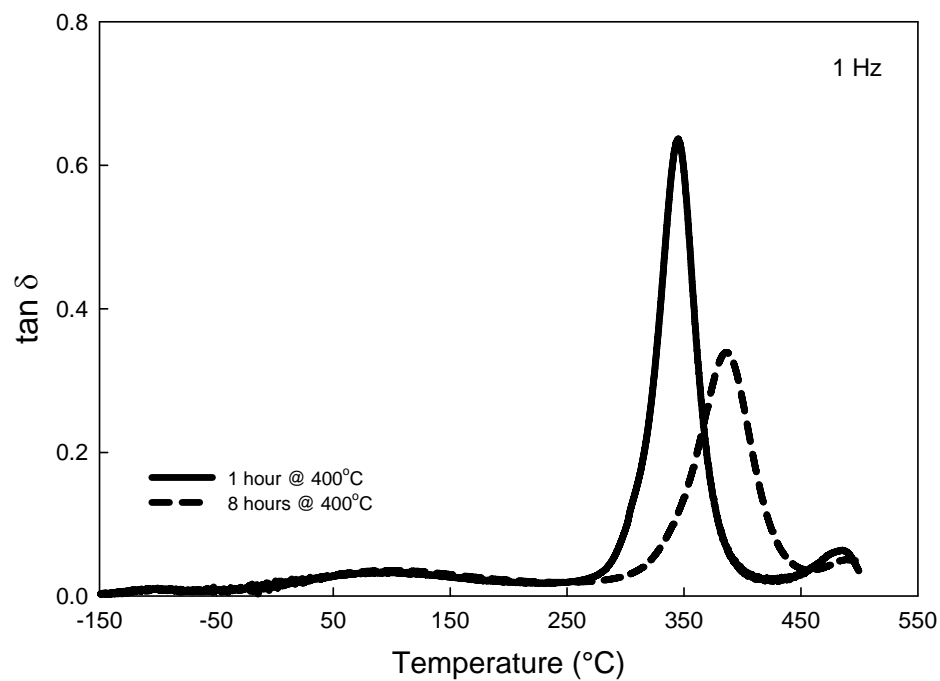
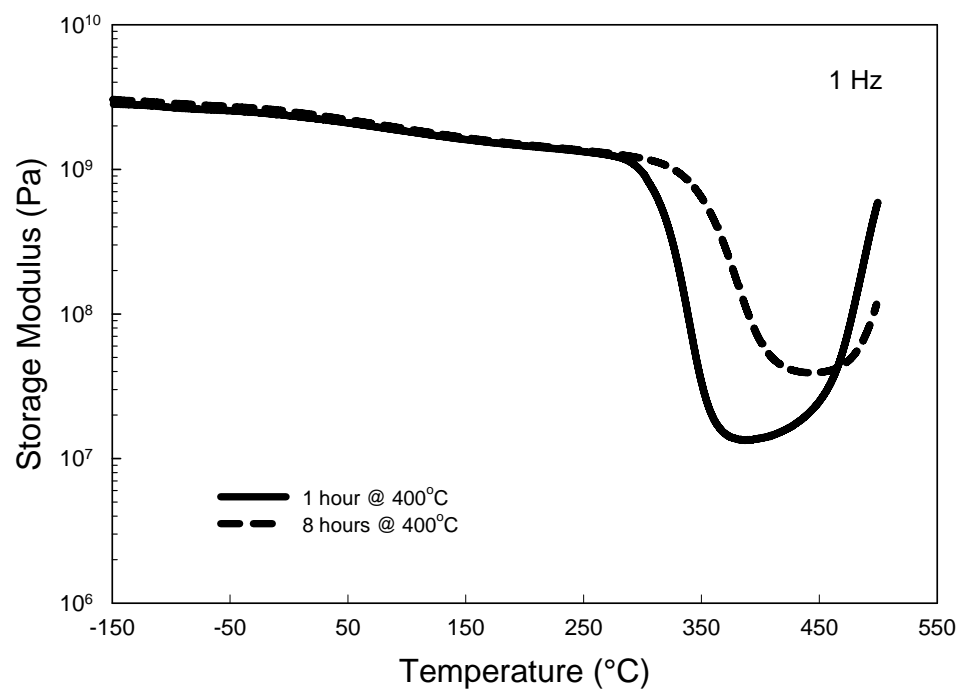


Figure 5.20: Storage modulus and $\tan \delta$ vs. temperature for thermally imidized APAF-ODPA-TR400 at different hold times. DMA analysis at 1 Hz.

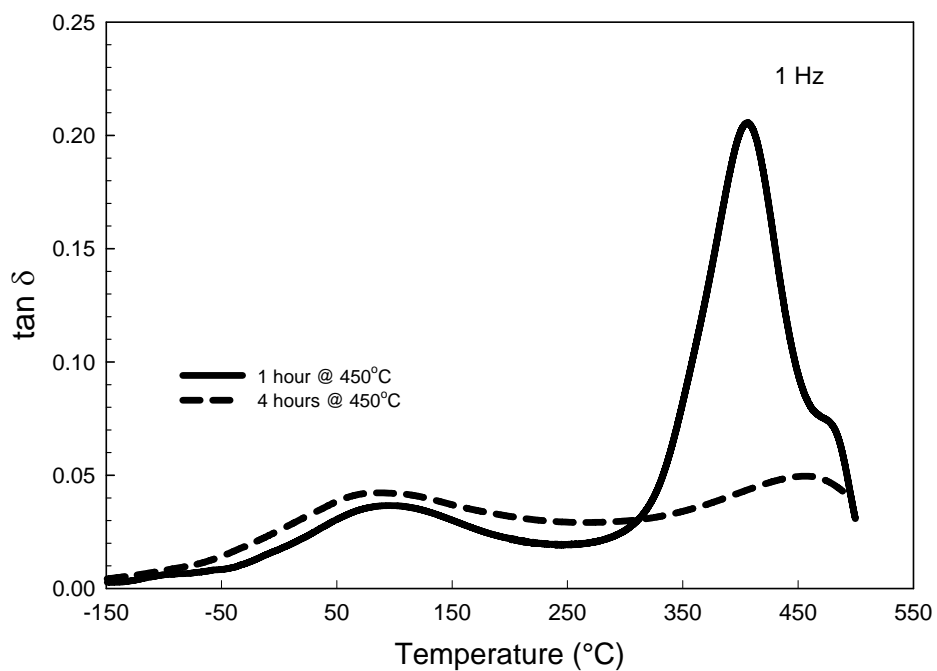
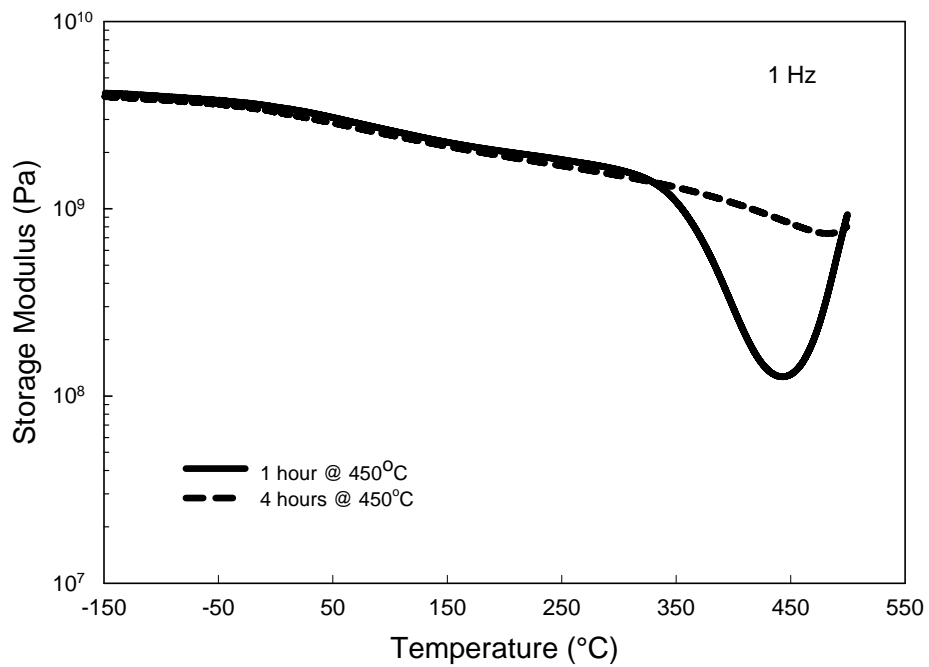


Figure 5.21: Storage modulus and $\tan \delta$ vs. temperature for thermally imidized APAF-ODPA-TR450 at different hold times. DMA analysis at 1 Hz.

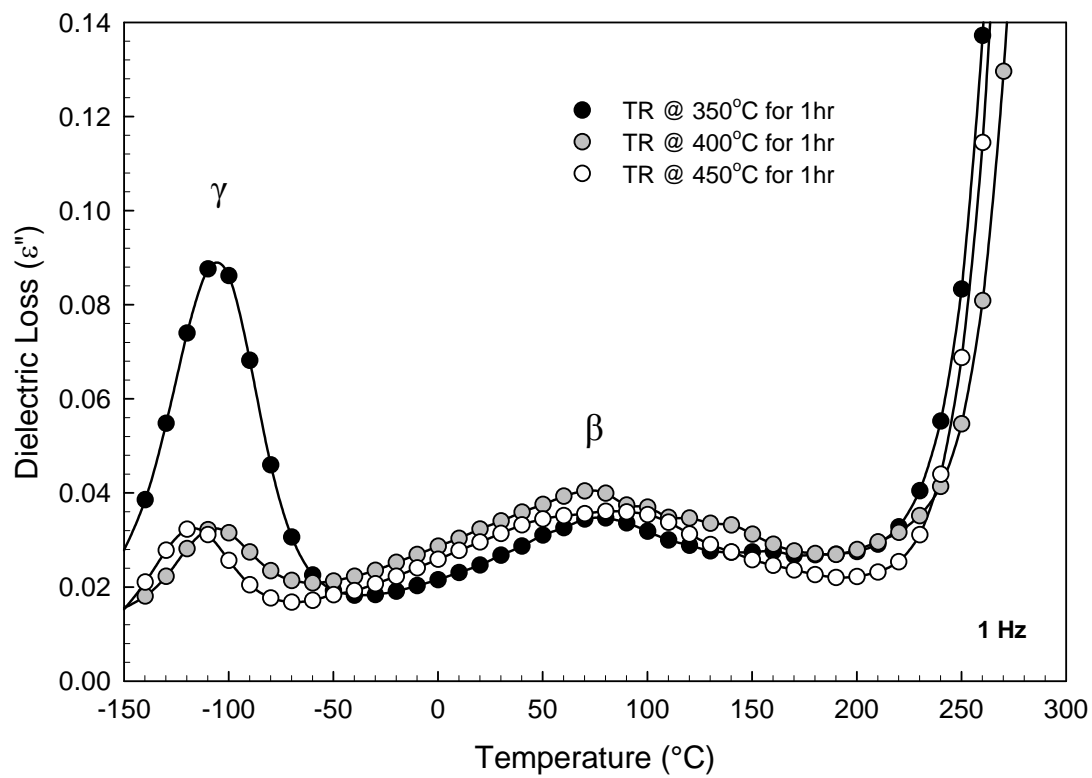


Figure 5.22: Dielectric loss vs. temperature for thermally imidized APAF-ODPA TR series.

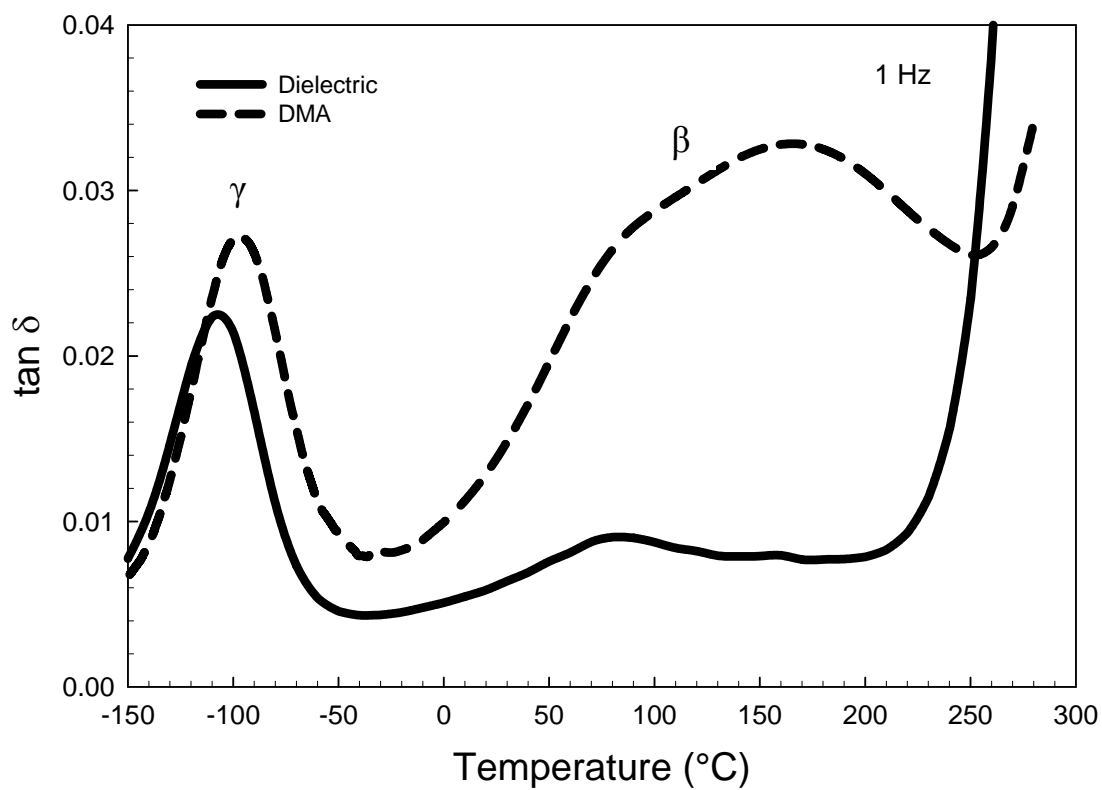


Figure 5.23: $\tan \delta$ vs. temperature for thermally imidized APAF-ODPA-TR 350.

Dielectric and DMA results; frequency of 1 Hz.

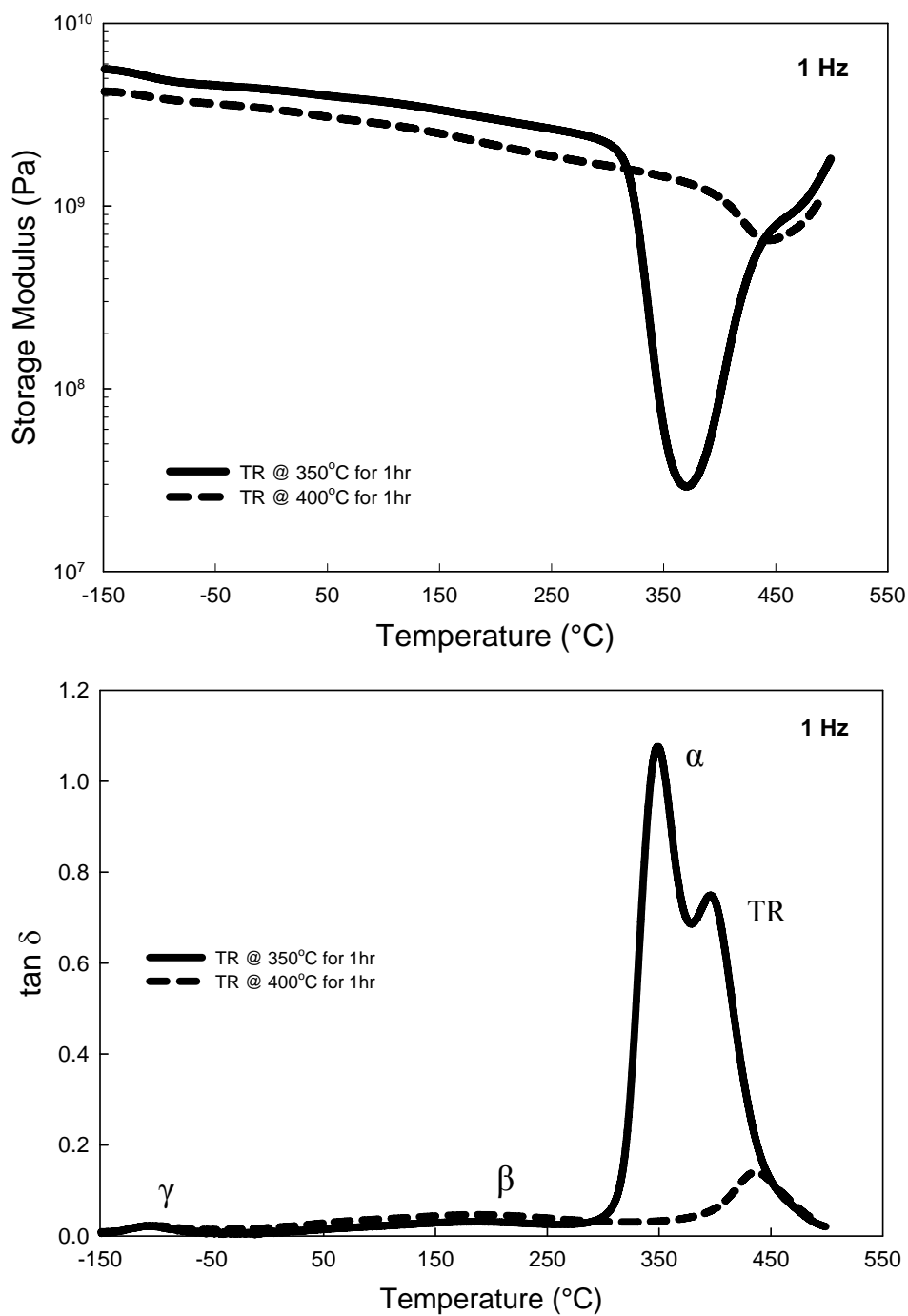


Figure 5.24: Storage modulus and $\tan \delta$ vs. temperature for chemically imidized APAF-6FDA TR series. All samples were exposed to vacuum drying at 200°C prior to TR exposure. Frequency of 1 Hz; heating rate of 3°C/min.

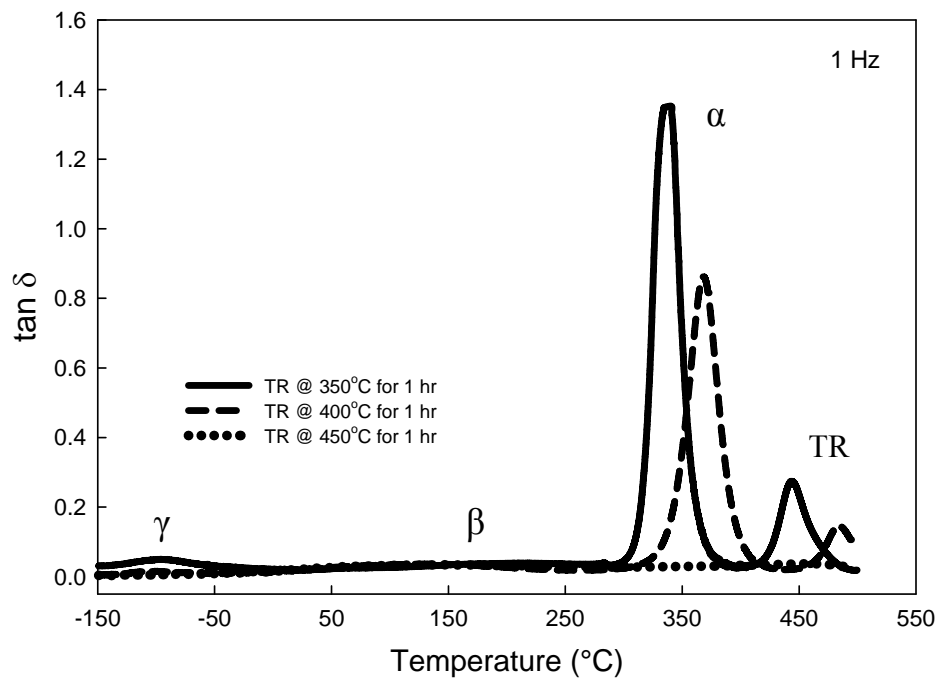
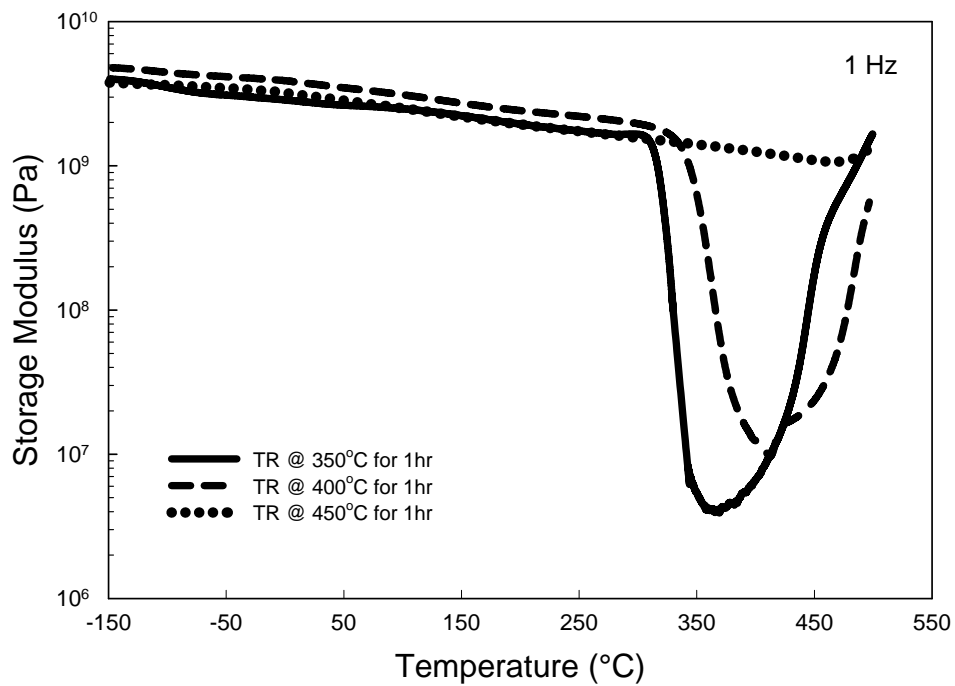


Figure 5.25: Storage modulus and $\tan \delta$ vs. temperature for thermally imidized APAF-6FDA TR series. All samples were exposed to vacuum drying at 220°C prior to TR exposure. Frequency of 1 Hz; heating rate of 3°C/min.

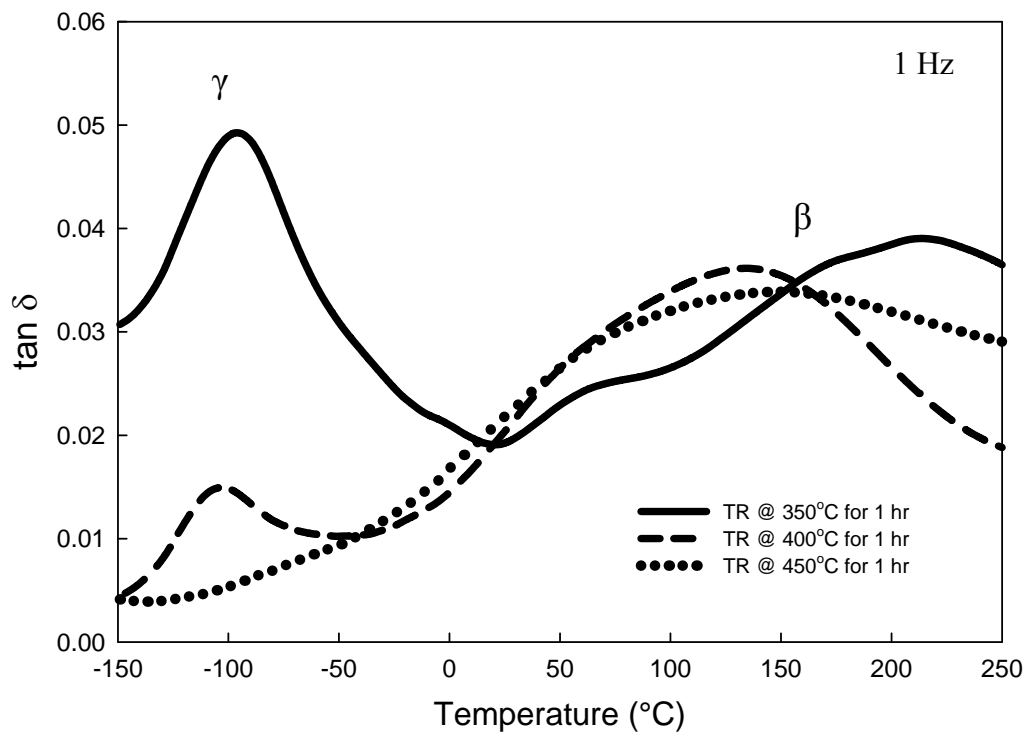


Figure 5.26: Tan δ vs. temperature for thermally imidized APAF-6FDA TR series in the sub-glass region. DMA results at 1 Hz and heating rate of 3 $^{\circ}\text{C}/\text{min}$.

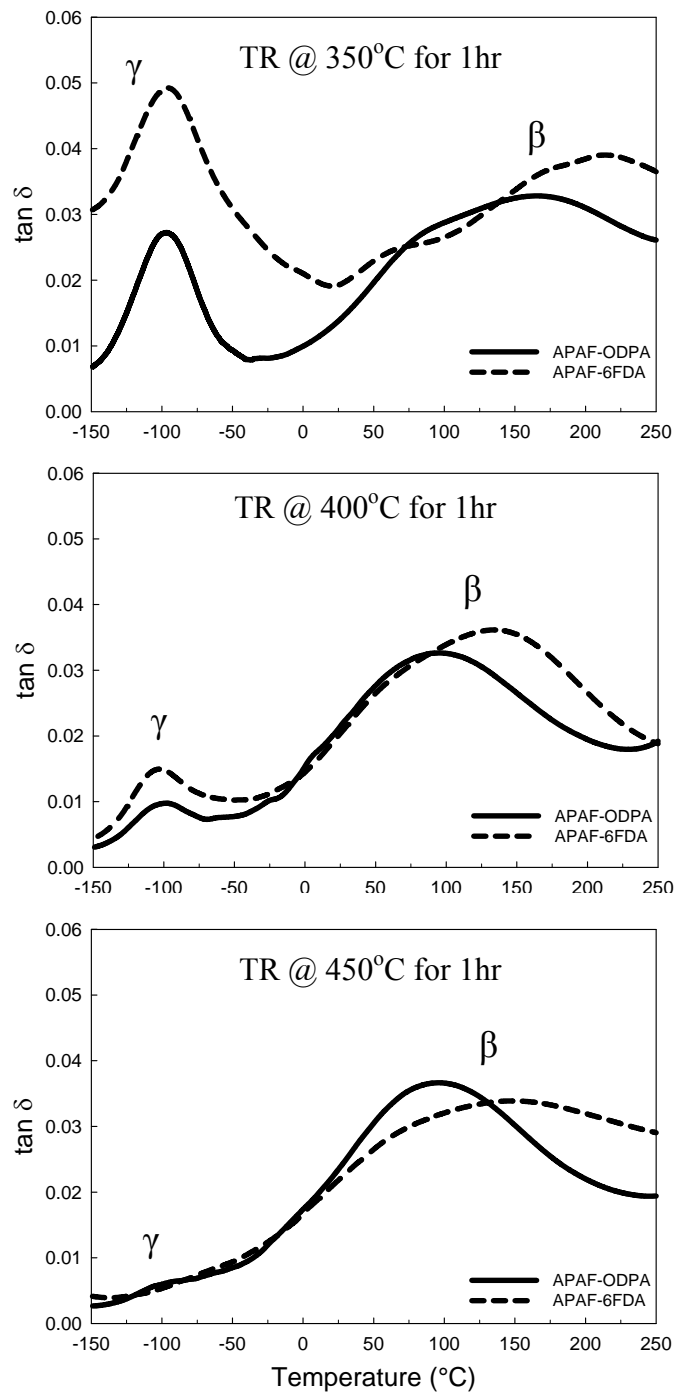


Figure 5.27: $\tan \delta$ vs. temperature for thermally imidized APAF-ODPA and APAF-6FDA TR series in sub-glass region. Frequency of 1 Hz; heating rate of 3°C/min.

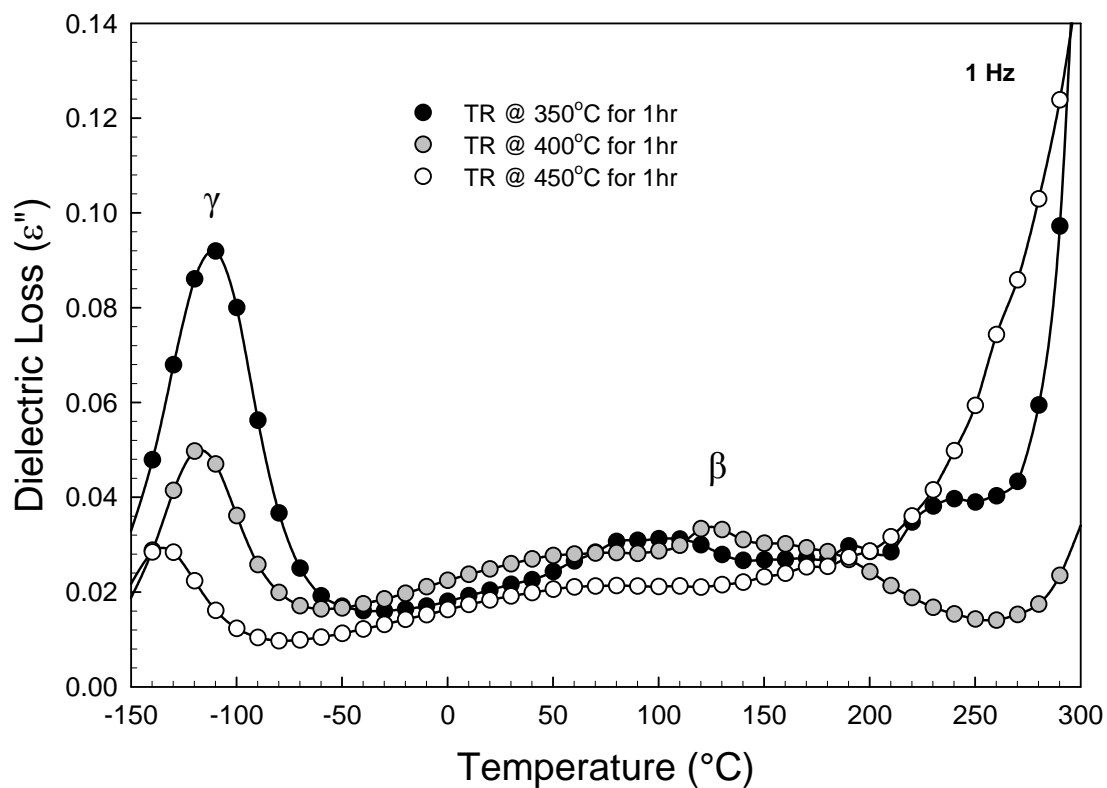


Figure 5.28: Dielectric loss vs. temperature for thermally imidized APAF-6FDA TR series in sub-glass region. Frequency at 1 Hz.

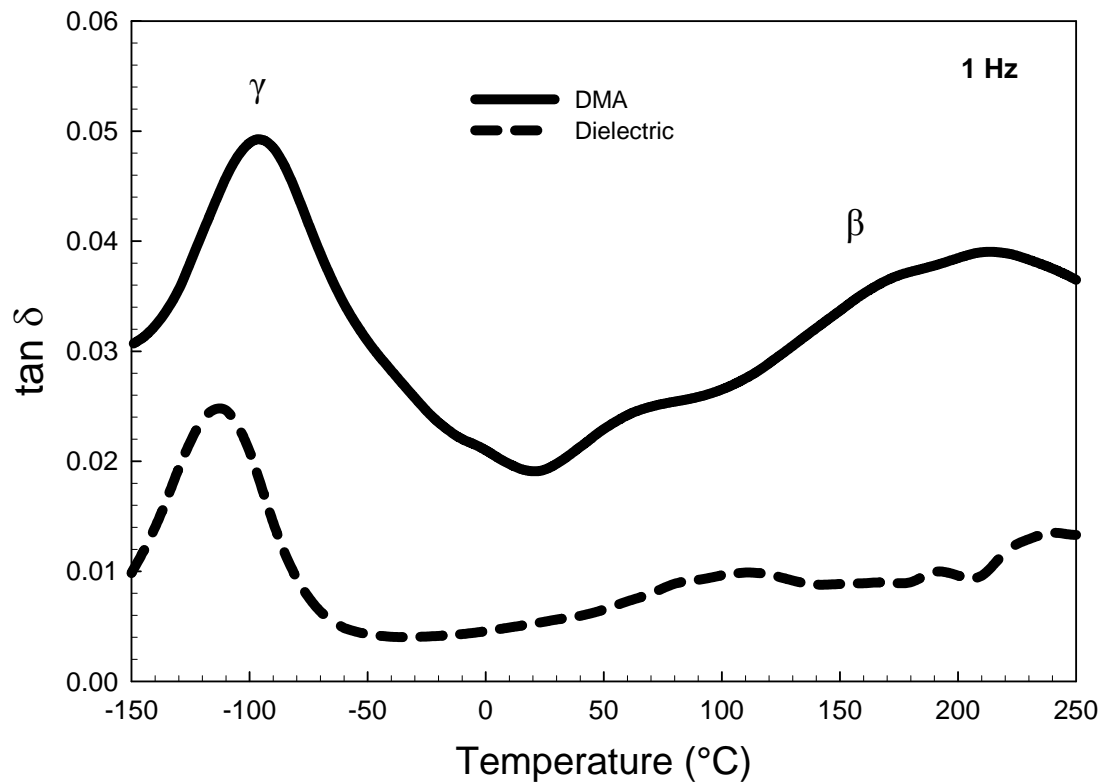


Figure 5.29: $\tan \delta$ vs. temperature for thermally imidized APAF-6FDA-TR 350.

Dielectric and DMA results at 1 Hz.

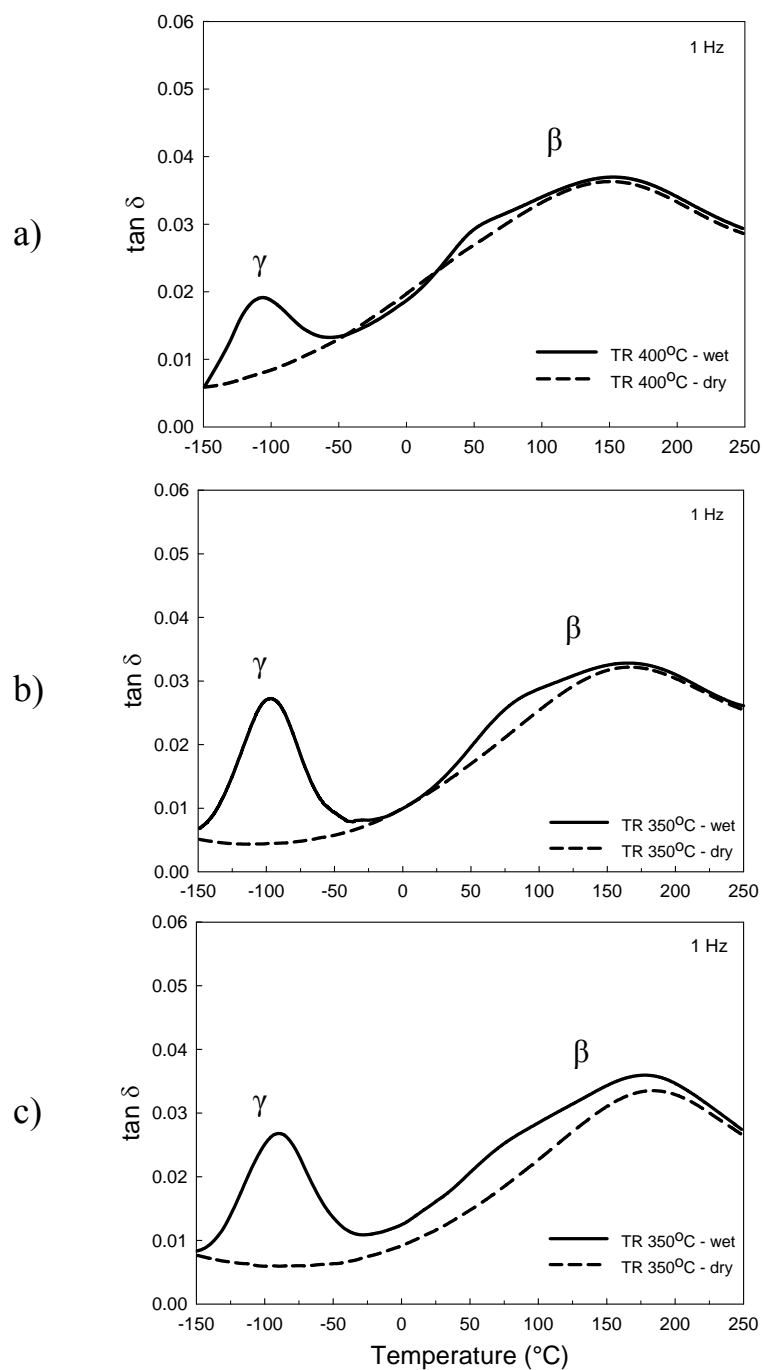


Figure 5.30: $\tan \delta$ vs. temperature for sub-glass relaxations showing effects of moisture: a) Chemically imidized HAB-6FDA-TR 400, b) Thermally imidized APAF-ODPA-TR 350, c) Thermally imidized APAF-6FDA-TR 350. DMA results at 1 Hz.

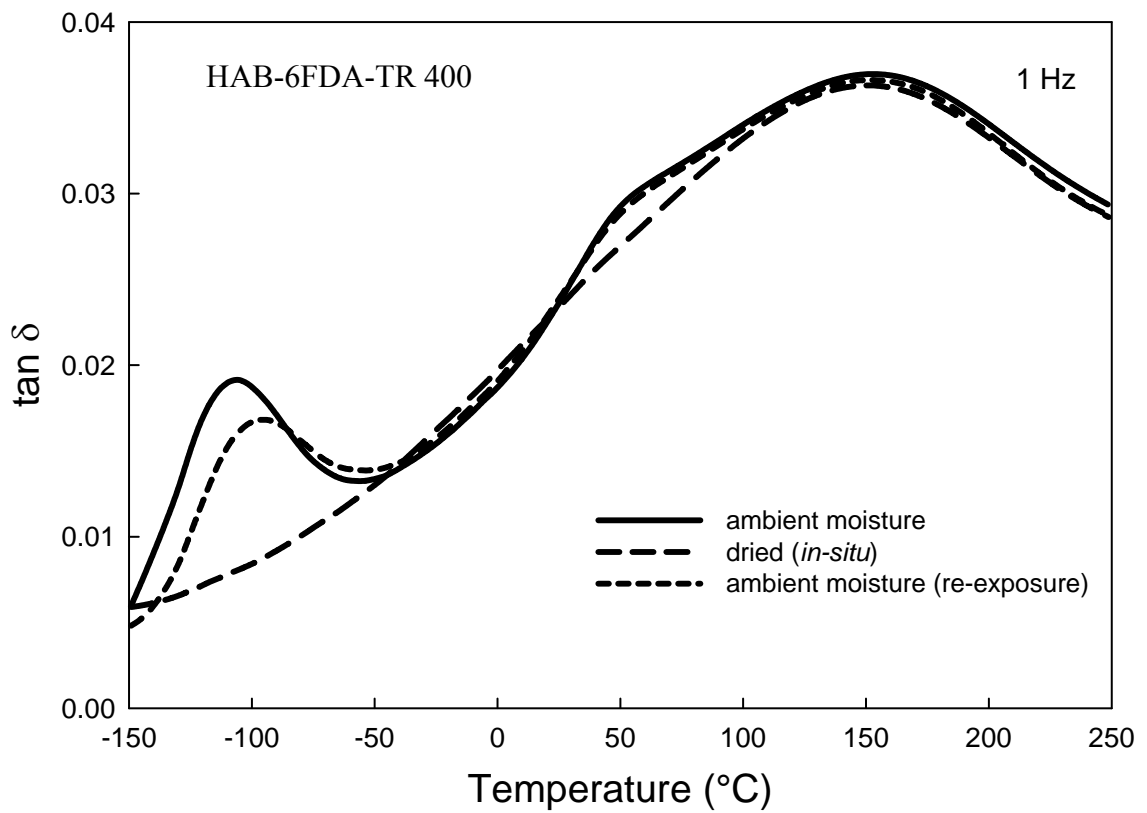


Figure 5.31: Tan δ vs. temperature for sub-glass relaxations showing the reversibility of moisture effects: chemically imidized HAB-6FDA-TR400. DMA results at 1 Hz.

References

- [1] Park, H.B.; Jung, C.H.; Lee, Y.M.; Hill, A.J.; Pas, S.J.; Mudie, S.T.; Van Wagner, E.; Freeman, B.D.; Cookson, D.J. "Polymers with Cavities Tuned for Fast Selective Transport of Small Molecules and Ions", *Science* **2007**, *318*, 254.

- [2] Moy, T.M.; McGrath, J.E. "Synthesis of Hydroxyl-Containing Polyimides Derived from 4,6-Diaminoresorcinol Dihydrochloride and Aromatic Tetracarboxylic Dianhydrides", *Journal of Polymer Science, Part A: Polymer Chemistry* **1994**, *32*, 1903.

- [3] Eichstadt, A.E.; Andreev, S.; Ward, T.C. "The Effect of Water on the Viscoelastic Properties of Polyimides", *Proceedings of the Annual Meeting of the Adhesion Society* **2000**, *23*, 484.

Chapter 6

Dynamic Relaxation Characteristics of Polymer Nanocomposites Based on Poly (ether imide) and Poly (methyl methacrylate)

This chapter is based on the following published work:

Comer, A.C.; Heilman, A.L.; Kalika, D.S. "Dynamic relaxation characteristics of polymer nanocomposites based on poly(ether imide) and poly(methyl methacrylate)", *Polymer* **2010**, *51*, 5245.

6.1 Introduction

Polymer nanocomposites, *i.e.* inorganic-organic hybrid materials that contain nanoscale filler with characteristic dimensions at or below 100 nm, have been the subject of extensive study owing to their potentially superior performance properties as compared to conventional filled plastics. Over the last two decades, a broad body of experimental and theoretical work has emerged that explores the relationships between filler size and geometry, surface chemistry, and nanocomposite morphology and their influence on ultimate performance characteristics; many aspects of this work have been summarized in the numerous review papers available in the literature [1-9].

An important factor in understanding the potential enhancement of bulk properties in polymer nanocomposites is the extent to which the presence of nanoscale filler alters the characteristics of the surrounding polymer matrix phase [9]. The introduction of spherical nanoscale particles, for example, leads to the creation of vast amounts of particle-polymer surface area that can strongly influence polymer chain mobility in the vicinity of the solid-polymer interface. The quality of particle-polymer interactions, as

well as physical confinement effects, are often manifested by shifts in the glass transition temperature (T_g), as well as changes in the underlying time-temperature characteristics of the glass-rubber and sub-glass relaxation processes [10]. In situations where favorable interactions are established between the nanoparticles and the polymer matrix, positive offsets in T_g are typically observed, as well as the possible appearance of a second, higher T_g corresponding to the presence of a distinct, constrained population of chain segments in the vicinity of the particle surface [11-18]. For particle-polymer combinations with poor wetting characteristics, reductions in T_g with nanoparticle loading have been reported [19-22].

In this chapter, we examine the dynamic relaxation characteristics of glassy polymer nanocomposites based on amorphous poly(ether imide) [PEI] and poly(methyl methacrylate) [PMMA] filled with fumed silica nanoparticles. Four series of PEI composites are investigated, encompassing native SiO_2 particles, and three commercial silicas produced with various surface treatments intended to render them hydrophobic in character. The preparation and morphology of the PEI composites were previously described by Takahashi and Paul, who explored the relationships between particle dispersion, potential internal void formation and gas transport properties as a function of nanoparticle loading and surface chemistry [23,24]. In the current work, we assess the influence of the particles on the glass-rubber and sub-glass relaxations of PEI and PMMA composites using dynamic mechanical and dielectric spectroscopy methods. Of particular interest is the observation of dual glass-rubber relaxations in these composites, a behavior discussed by Tsagaropoulos and Eisenberg [13,14]. In their study on a variety of favorably-interacting polymer-silica systems, Tsagaropoulos and Eisenberg saw that

silica particle (7 nm diameter) loadings on the order of 10 wt% and higher led to the emergence of two distinct T_g events as measured by dynamic mechanical analysis: a bulk T_g corresponding to the glass transition of the unfilled polymer, and a second, higher T_g offset by ~ 40 to 100°C . The relative intensity and position of these relaxations were interpreted according to the overall loading of the nanoparticles, and the respective populations of loosely-bound and more tightly-bound polymer segments near the particle surface. In the work presented here, the generality of the dual- T_g response will be considered for both the PEI- and PMMA-based composites, as well as any potential perturbation of the sub-glass relaxations measured for these systems.

6.2 Experimental

6.2.1 Materials

Poly (ether imide) [PEI] resin pellets were obtained from GE Plastics (Ultem[®] 1000). Poly (methyl methacrylate) [PMMA] pellets were obtained from Altuglas International (Plexiglas[®] V826). Silica nanoparticles (99.5% purity; 10 nm diameter) were purchased from Aldrich, with a reported BET surface area of 590 to 690 m^2/g and density of 2.2 g/cm^3 . Commercial fumed silicas with modified surfaces were obtained from Cabot Corporation: Cab-o-sil[®] TS-530, TS-610, and TS-720. The surface chemistry for each of these nanoparticles is presented in **Figure 3.4**, and details on particle properties are provided in Ref. [23]. The series of particles encompasses nominal diameters from ~ 10 to 30 nm, with corresponding densities of 2.2 (TS-530), 2.2 (TS-610) and 1.8 g/cm^3 (TS-720), respectively. Solvents used for nanocomposite preparation (dichloromethane; dimethylformamide) were purchased from Fisher Scientific.

6.2.2 Sample Preparation

PEI-based nanocomposites: PEI pellets (10 wt%) were dissolved in dichloromethane by magnetic stirring at room temperature for one hour. Nanoparticles in appropriate proportion were added to the polymer solution and subject to vigorous mechanical mixing for 10 minutes; the blend was then poured into an open, shallow container and solvent was allowed to evaporate at ambient conditions for ~ 24 hours. The resulting composites were placed under vacuum and held at 100°C (24 h), 200°C (24 h), and then briefly above T_g (220°C; 30 min.) to ensure full removal of solvent. Finally, the samples were consolidated via compression molding to achieve uniform films of desired thickness. Molding temperatures ranged from 260°C to 320°C depending on filler loading, with melt exposure times < 5 min. Film thickness was ~ 0.7 mm for dynamic mechanical specimens and ~ 0.3 mm for samples prepared for dielectric measurement. The precise thickness of each film was determined using a digital micrometer with precision to $\pm 1 \mu\text{m}$.

PMMA-based nanocomposites: PMMA pellets (10 wt%) were dissolved in DMF by magnetic stirring, followed by addition of an appropriate proportion of nanoparticles; only a single series of PMMA composites was investigated, based on inclusion of the TS-610 particles. The nanocomposite formulations were recovered via precipitation: the polymer/particle solution was poured into a running laboratory blender filled with water, and the precipitated blend was filtered as a coarse powder. Samples were then dried under vacuum at 70°C (24 h), 110°C (4 h), and 130°C (30 min.) to facilitate removal of water and residual DMF. Compression molding (220°C) was used to produce uniform films for dynamic mechanical (0.7 mm) and dielectric (0.3 mm) studies.

6.2.3 Film Density

Bulk density measurements of PEI nanocomposite films were conducted by hydrostatic weighing at 25°C using a conventional density determination kit (Denver Instruments); deionized ultrafiltered water (Fisher Sci.) was employed as the auxiliary liquid. A minimum of three replicate measurements were completed for each sample tested.

6.2.4 Dynamic Mechanical Analysis

Dynamic mechanical analysis was performed using a TA Instruments Q800 DMA configured in tensile geometry. Storage modulus (E') and loss tangent ($\tan \delta$) were recorded both in temperature sweep mode (1 Hz; 3°C/min) and frequency sweep mode (0.1 to 30 Hz) at temperatures ranging from 150 to 350°C (PEI-based films) and 35 to 260°C (PMMA-based films). All measurements were performed under nitrogen atmosphere.

6.2.5 Broadband Dielectric Spectroscopy

Dielectric measurements were conducted using the Novocontrol Broadband Dielectric Spectrometer. To promote electrical contact during measurement, concentric 33 mm diameter silver electrodes were applied to each sample film using a VEECO thermal evaporation system. Samples were subsequently mounted between gold platens and positioned in the Novocontrol Quatro Cryosystem. Dielectric constant (ϵ') and loss (ϵ'') were recorded at discrete temperatures ranging from -150 to 380°C (PEI-based films) and -120° to 230°C (PMMA-based films). Test frequencies ranged from 0.1 Hz to 3 MHz.

6.3 Results and Discussion

6.3.1 Nanocomposite Density

The incorporation of nanoscale particles into a polymer matrix provides a range of variables that can be exploited for the enhancement of material properties. A crucial aspect of nanocomposite performance is the dispersion of the filler particles within the polymer matrix, as polymer nanocomposites are susceptible to particle agglomeration and potential network formation [25]. Extensive agglomeration within the matrix, accompanied by polymer de-wetting at the particle surface, may lead to the entrapment of voids and defects. Takahashi and Paul recently addressed this issue for a series of PEI-based composites incorporating commercially-available fumed silicas with chemical surface modifications intended to render the particles more hydrophobic in character and thereby more compatible with the PEI matrix [23,24]. Detailed electron microscopy studies revealed moderate to high levels of particle agglomeration in both solution-cast and melt-processed PEI nanocomposites [23]. The morphology of these composites was correlated with bulk density measurements intended to assess the potential formation of internal voids as related to processing history and particle-polymer interaction.

For the studies reported here, we have prepared PEI nanocomposites using components identical to those employed by Takahashi and Paul. Density results for our composites are presented as a function of particle loading in **Figure 6.1**, and are compared to densities predicted based on strict volume additivity (see solid lines in Figure 6.1). The density of unfilled PEI was measured as 1.27 g/cm^3 , which is in agreement with the value reported by the manufacturer [26]. Figure 6.1a presents nanocomposite results for native

SiO₂ and the TS-530 and TS-610 particles ($\rho_F = 2.2 \text{ g/cm}^3$), while Figure 6.1b presents results for composites containing TS-720 ($\rho_F = 1.8 \text{ g/cm}^3$).

Examination of Figure 6.1 shows that the PEI composites based on inclusion of TS-610 and TS-720 adhere closely to the volume additivity prediction for loadings up to 20 wt% filler. The results for the TS-610 composites are in close agreement with data reported by Takahashi and Paul, who observed the best overall dispersion quality for the TS-610 particles [23]. Density values for the composites containing TS-530 and native SiO₂ display negative deviations from additivity that increase with particle loading, and that suggest the entrapment of voids or gaps within the composite. For the highest particle loadings, a maximum void volume fraction of approx. 3% is indicated, again consistent with the results reported in Ref. [23].

6.3.2 PEI Composites - Dynamic Mechanical Analysis

Dynamic mechanical results (E' ; $\tan \delta$ vs. temperature) for the series of composites based on PEI and TS-610 particles are presented in **Figure 6.2**. Across the glassy region, the introduction of nanoscale filler leads to a progressive increase in storage modulus, with E' increasing by a factor of two for a loading of 30 wt% particles. At loadings $\geq 15 \text{ wt\%}$, a two-step incremental drop in modulus is evident with increasing temperature that is indicative of a dual- T_g response, and the plateau modulus that is obtained at the highest measurement temperatures shows a strong positive correlation with particle loading. Examination of the $\tan \delta$ results for this series reveals a sharp “bulk polymer” glass transition peak at $\sim 225^\circ\text{C}$ (T_{g1}); the peak intensity decreases systematically with particle loading, but the position of the peak is nearly invariant across the range of composite

compositions studied. At higher temperatures, a broad maximum in $\tan \delta$ is indicated, suggesting a second glass-rubber relaxation process (T_{g2}) corresponding to the motional response of polymer chain segments impeded to some degree owing to their proximity to the nanoparticle surface. The intensity of this higher-temperature relaxation event decreases with increasing filler content, and the position of the maximum in $\tan \delta$ shifts to lower temperatures with increased loading. It should be noted that the results for unfilled PEI presented in Figure 6.2 correspond to a sample prepared via the same solution-based process used for the nanocomposite specimens. Comparison of these data with dynamic mechanical results obtained for an exclusively melt-processed PEI sample showed no difference in the modulus or $\tan \delta$ curves, indicating that the drying protocol performed during sample preparation was sufficient in removing residual solvent that could plasticize the matrix and thereby shift T_{g1} to lower temperatures. A summary of $\tan \delta$ peak temperatures (1 Hz) for the various composites is provided in **Table 6.1**.

The trends in dynamic mechanical data for the PEI/TS-610 composites show numerous similarities to the dual- T_g behavior reported by Tsagaropoulos and Eisenberg, and can be satisfactorily explained according to the qualitative model that they proposed [14]. Specifically, it is suggested that the glass-rubber relaxation response of the polymer composites is governed by the distribution of polymer chain segments across three relaxation environments: bulk polymer (essentially unperturbed by the presence of the nanoparticles), loosely-bound polymer, and tightly-bound polymer immobilized at the particle surface. T_{g1} corresponds to the glass transition response involving bulk polymer that is only minimally impacted by inclusion of the particles; the decrease in $\tan \delta$ peak intensity with increasing loading (T_{g1}) reflects not only the replacement of polymer with

solid filler, but also the transformation of some fraction of the surrounding polymer matrix into loosely- and tightly-bound populations. The segmental relaxation of the loosely-bound population (*i.e.*, polymer chain segments hindered by their proximity to the particle surface as well as potential physical confinement effects) is reflected in the higher-temperature relaxation event, T_{g2} . In addition, it is postulated that a subset of polymer segments, the tightly-bound population, is so strongly constrained at the particle surface that these segments are unable to undergo the large-scale motions inherent to the glass-rubber relaxation. The relative position and intensity of the T_{g2} event reflect the progressive transformation of loosely-bound polymer to tightly-bound polymer with increased overall loading: as particle content increases (and average interparticle distance decreases), growing local constraints reduce the relative fraction of loosely-bound segments capable of participating in the glass-rubber relaxation process. This is manifested in an overall decrease in T_{g2} relaxation intensity with increased loading, as well as a shift in peak position to *lower* temperatures, as the most restricted of the loosely-bound segments are converted into tightly-bound polymer.

Dynamic mechanical results for the PEI composites based on native SiO_2 particles are presented in **Figure 6.3**. As compared to the PEI/TS-610 series, the PEI/ SiO_2 composites display a lower overall degree of mechanical reinforcement, especially at loadings ≤ 20 wt% SiO_2 . The dual- T_g response behavior that is clearly established in the PEI/TS-610 samples at 15 wt% loading is not fully evident in the PEI/ SiO_2 composites until a loading of at least 25 wt%. This may indicate a lower degree of particle dispersion across the PEI/ SiO_2 series, and potentially weaker interaction between the PEI matrix and the unmodified SiO_2 surface. As reported in Figure 1, density data for the PEI/ SiO_2 series

show the strongest negative deviation from volume additivity amongst the various PEI composites, possibly reflecting a lower degree of compatibility (and hence greater agglomeration and void formation) between the PEI thermoplastic and the hydrophilic particles.

A comparison of the dynamic mechanical curves for the four PEI-based nanocomposites is presented in **Figure 6.4** (15 wt% filler loading). Across the data sets, there is minimal variation in the characteristics of the bulk polymer glass transition event, T_{g1} . At temperatures above T_{g1} , the PEI/SiO₂ sample shows only limited mechanical reinforcement, while a dual- T_g response is evident in each of the PEI/Cab-o-sil materials. Incorporation of TS-720 particles, which appear to present the most strongly hydrophobic surface, leads to the highest measured value of rubbery modulus above T_{g2} . This correlates with the lowest intensity $\tan \delta$ peak for the T_{g2} event, suggesting that the PEI/TS-720 composite contains the highest proportion of tightly-bound polymer segments at the particle surface. The loosely-bound segments that are capable of participating in the T_{g2} process are presumably further removed from the TS-720 surface and less constrained as compared to the loosely-bound populations present in the TS-530 and TS-610 composites. As a result, the T_{g2} peak for the TS-720 system is positioned at a lower temperature as compared to the TS-530 and TS-610 composites (see full listing of T_{g1} and T_{g2} values as a function of composition in Table 6.1).

Representative dynamic mechanical curves of $\tan \delta$ vs. temperature at various measurement frequencies (PEI/TS-610; 30 wt% filler) are shown in **Figure 6.5**; the range of frequencies is 0.1 to 30 Hz. Both transitions (*i.e.*, peaks in $\tan \delta$) shift to higher

temperatures with increasing frequency, consistent with their origin as motional relaxation processes. Plots of $\log(\text{frequency})$ vs. reciprocal temperature, based on the measured maxima in $\tan \delta$ from the isochronal curves, are provided in **Figure 6.6** for the PEI/TS-610 series. Across the limited range of frequencies accessible with the dynamic mechanical instrument, data for both the T_{g1} and T_{g2} transitions follow the Arrhenius relation, as indicated by the straight-line fits included in the figure. For the T_{g1} glass transition event, the peak temperatures of the composite specimens are shifted to slightly higher values as compared to unfilled PEI (see also Table 6.1), but all data sets reflect a single apparent activation energy, $E_A = 880$ kJ/mol. For the T_{g2} relaxation, a much lower activation energy is indicated over the various composite loadings ($E_A = 220$ kJ/mol), with the data points positioned according to the observed shifts in T_{g2} to lower temperatures with increased loading. The smaller activation energy encountered for the T_{g2} process is consistent with the results of Tsagaropoulos and Eisenberg [14], who measured E_A values that were two to three times lower than the activation energy for the T_{g1} transition at low to moderate filler loadings.

The time-temperature character of the glass transition events in the PEI composites was further explored by the construction of modulus-frequency master curves based on time-temperature superposition [27]. **Figure 6.7** shows E' vs. ωa_T master curves for the PEI/TS-610 series at a reference temperature of 225°C , where ω is the applied frequency ($\omega = 2\pi f$, with f expressed in Hz) and a_T is the dimensionless shift factor. The master curves capture the dual relaxation behavior of the PEI composites and the progressive increase in mechanical reinforcement with filler loading. In an effort to quantify the relative breadth of the relaxations, each component was fit to the Kohlrausch-Williams-

Watts (KWW) stretched exponential function, with determination of the KWW distribution parameter, β_{KWW} [28]. The value of β_{KWW} can range from 0 to 1, with lower values reflecting broad transitions influenced by intermolecular coupling, crosslinks, particle-polymer interactions and physical confinement. The inset to Figure 6.7 shows a representative dual KWW curve fit for the 30 wt% composite. For all composite compositions, the bulk glass-rubber relaxation could be described by a single value of the distribution parameter, $\beta_{\text{KWW}} = 0.30$. The higher-temperature transition, corresponding to the relaxation of loosely-bound polymer segments in the vicinity of the particles, broadened with increasing polymer loading: β_{KWW} values for the higher-temperature process were 0.30 for the 10 and 15 wt% samples, 0.20 for the 20 wt% composite, and 0.15 for the 25 and 30 wt% loadings, respectively (PEI/TS-610 series). The low values of β_{KWW} measured at the highest filler loadings reflect the increasingly heterogeneous relaxation environment of the polymer chain segments as influenced by their interactions with the particles, as well as local physical confinement with decreasing overall interparticle distance.

6.3.3 PMMA Composites - Dynamic Mechanical Analysis

In order to assess the generality of the dual- T_g response, a series of PMMA/TS-610 specimens was examined by dynamic mechanical analysis; dual- T_g behavior for the combination of PMMA with native silica (10 and 20 wt%) was previously reported in Ref. [14]. Dynamic mechanical results for the PMMA/TS-610 series are presented in **Figure 6.8**. Unfilled PMMA displays a glass transition centered at 130°C (peak in $\tan \delta$ at 1 Hz), and increasing particle loading leads to a strong decrease in the intensity of the

$\tan \delta$ peak, as well as a modest shift in T_g to lower temperatures. A dual- T_g response is indicated only at the highest particle loading examined (30 wt%), with the “ T_{g2} ” process manifested by an extremely broad maximum in $\tan \delta$ and a corresponding peak temperature of $\sim 200^\circ\text{C}$. The failure to observe dual- T_g character at lower loadings may be a reflection of the lower degree of compatibility inherent to the combination of PMMA with the hydrophobically-modified TS-610, as compared to native SiO_2 .

6.3.4 PEI Composites – Dielectric Spectroscopy

Broadband dielectric measurements can serve as a valuable complement to dynamic mechanical studies for the investigation of sub-glass and glass-rubber relaxation processes in polymer composites, as they provide time-temperature information across an exceptionally wide range of test frequencies (*i.e.*, ≥ 6 to 8 orders of magnitude). Dielectric results for unfilled PEI are plotted as dielectric loss (ϵ'') vs. temperature in **Figure 6.9**. Three distinct relaxation processes are evident with increasing temperature: the sub-glass γ and β processes, and the glass-rubber α process. At a test frequency of 1 kHz, the corresponding relaxation temperatures are -60°C (γ), 120°C (β) and 240°C (α), respectively. The features encompassed in Figure 6.9 are consistent with previous reports on the relaxation characteristics of the PEI thermoplastic [29-32].

Representative plots of dielectric loss vs. frequency at discrete temperatures in the range of the γ , β , and α relaxations are presented for the PEI composites in **Figure 6.10** (PEI/TS-610; 20 wt% filler). The dielectric dispersions are fit according to the Havriliak-Negami (HN) modification of the Debye equation in order to establish the central relaxation times (τ_{MAX}) associated with each process [33]; details of the analysis are

available in Kalakkunnath et al. [34]. A comparison of the α relaxation response for the PEI/TS-610 composites at 260°C is presented in **Figure 6.11**. The addition of filler particles leads to a systematic decrease in the intensity of the dielectric loss, but the location of the α relaxation is unchanged by the presence of the particles. This outcome is consistent with the results obtained via dynamic mechanical analysis (T_{g1} process), for which the peak position of the bulk polymer relaxation was essentially independent of increasing filler content.

Attempts to detect a second, higher-temperature glass-rubber relaxation process using dielectric relaxation spectroscopy were unsuccessful, owing to ionic conduction and the strong interfacial polarization response encountered in the composite samples at temperatures $> T_{g1}$. In heterogeneous materials above the glass transition, the polarization of mobile charges at interfacial boundaries can lead to contributions to dielectric constant and loss that far exceed the magnitude of the orientational polarizations associated with local and longer-scale segmental motions [35]. This was the case with the PEI- and PMMA-based composites, wherein the high intensity of interfacial polarization effectively masked the detection of possible higher-temperature relaxations associated with a constrained segmental population.

Arrhenius plots based on the dielectric measurements are presented in **Figure 6.12**, with f_{MAX} for each temperature determined from the isothermal HN fits as $f_{MAX} = [2\pi\tau_{MAX}]^{-1}$. For each of the three relaxations, the data indicate no variation as a function of particle loading in the composite. The linear Arrhenius character of the time-temperature data for the γ and β processes is consistent with non-cooperative motions of limited length scale

[30]; the apparent activation energies for the sub-glass processes are $E_A = 45$ kJ/mol (γ) and 84 kJ/mol (β), respectively. The invariance of the measured relaxation times with composition suggests that the underlying dipolar reorientations associated with the γ and β transitions are sufficiently localized to remain unperturbed by the presence of the nanoscale particles, even at the highest loadings investigated.

The α relaxation data reported in Figure 6.12 correspond to the “ T_{gl} ” glass transition. **Figure 6.13** shows the dielectric α relaxation data plotted over a much narrower range of $1/T$, and combined with dynamic mechanical data established from maxima in the loss modulus as a function of temperature. When viewed on this basis, the data again reveal minimal variation in relaxation peak location as a function of particle loading, other than a slight positive shift in relaxation temperature for the composites as compared to the unfilled PEI resin. The curvature evident in the combined data (when plotted on an Arrhenius basis) is consistent with the underlying cooperative character of the bulk polymer glass-rubber relaxation. Good overall agreement is obtained between the dielectric and dynamic mechanical methods, and the entire data set can be adequately described by a single Williams-Landel-Ferry (WLF) relation [27], where $C_1 = 11.2$, $C_2 = 62\text{K}$ and $T_{REF} = 490\text{K}$ (relative to a reference frequency of 1 Hz).

6.3.5 PMMA Composites – Dielectric Spectroscopy

Dielectric studies of PMMA and the PMMA/TS-610 composites were performed to assess the potential influence of nanoparticles on the time-temperature relaxation behavior of the PMMA matrix. Representative results (ϵ'' vs. temperature) for the 20 wt% PMMA/TS-610 composite are presented in **Figure 6.14** and display three

relaxations with increasing temperature, designated γ , β and α , respectively. The molecular origins for the PMMA relaxations are well-established, with the weak γ transition corresponding to isolated rotation of the main-chain methyl group, the β transition corresponding to local ester side-group rotations, and the α transition corresponding to the glass-rubber relaxation [36,37]. At higher temperatures and frequencies, the β and α relaxations merge into a single dielectric dispersion peak. Arrhenius plots for PMMA and the composites are provided in **Figure 6.15** (dielectric data, only). The γ and β processes show linear Arrhenius behavior and corresponding activation energies that are consistent with the local, non-cooperative origins of these relaxations, with $E_A = 44$ kJ/mol for the γ transition and $E_A = 81$ kJ/mol for the β transition. The α relaxation can be described by the WLF form (see plot). As was the case with the PEI-based formulations, the time-temperature response behavior of the PMMA composites is independent of filler content, and matches the results obtained for the unfilled PMMA resin. Here again, it was not possible to differentiate a potential higher-temperature glass-rubber relaxation event, owing to strong conduction and interfacial polarization in the PMMA composites at temperatures above T_g .

6.4 Conclusions

The dynamic relaxation characteristics of PEI- and PMMA-based polymer nanocomposites were investigated as a function of nanoparticle loading and surface chemistry. For the PEI composites, four series of specimens were studied based on the inclusion of native SiO_2 particles, as well as commercial particles prepared with hydrophobic surface modifications. Density measurements showed close adherence to

volume additivity, especially for the TS-610 and TS-720 particles, indicating minimal entrapment of void volume in the preparation of the composites. Dynamic mechanical measurements revealed a dual- T_g relaxation behavior. The lower-temperature transition (T_{g1}) corresponded to the relaxation of bulk, unperturbed polymer segments in the matrix, and was positioned very close to the transition temperature of the unfilled thermoplastic. The higher-temperature transition (T_{g2}) corresponded to the relaxation of loosely-bound chain segments constrained to some degree by their proximity to the particle surface. The location and intensity of the higher-temperature transition was influenced by the conversion of loosely-bound polymer to tightly-bound polymer at higher particle loadings; the immobilization of some portion of the loosely-bound segments at higher loadings led to a decrease in the intensity of the T_{g2} relaxation event, and a shift in the position of the loss maximum to lower temperatures. The dual- T_g response was well-established in the PEI/Cab-o-sil composites at filler loadings ≥ 15 wt%. For the less compatible PEI/SiO₂ combination, a dual- T_g response was observed at loadings ≥ 25 wt%.

Dielectric measurements were used to probe the influence of the filler particles on the polymer response across the sub-glass relaxation region, as well as in the vicinity of the glass transition. For both the PEI and PMMA composites, the introduction of nanoscale filler had no effect on the dielectric time-temperature characteristics of the local sub-glass relaxations. The position of the bulk polymer glass transition was also independent of filler content, in agreement with the dynamic mechanical measurements; the combined dynamic mechanical and dielectric data sets were observed to follow a single, cooperative (*i.e.*, WLF) expression for all composite loadings. Efforts to distinguish a

second, higher-temperature dielectric glass transition in the composites were unsuccessful, owing to the high level of interfacial polarization response that was encountered.

Table 6.1: Glass transition temperatures for PEI / nanoparticle composites as a function of particle loading (wt%). T_g values correspond to maxima in dynamic mechanical $\tan \delta$ at a frequency of 1 Hz.

wt% filler	TS-530		TS-610		TS-720	
	T_{g1} [°C]	T_{g2} [°C]	T_{g1} [°C]	T_{g2} [°C]	T_{g1} [°C]	T_{g2} [°C]
0	224	--	224	--	224	--
10	226	321	226	325	226	306
15	226	305	227	316	226	297
20	227	293	226	313	226	287
25	226	289	227	293	224	283
30	226	291	227	289	224	279

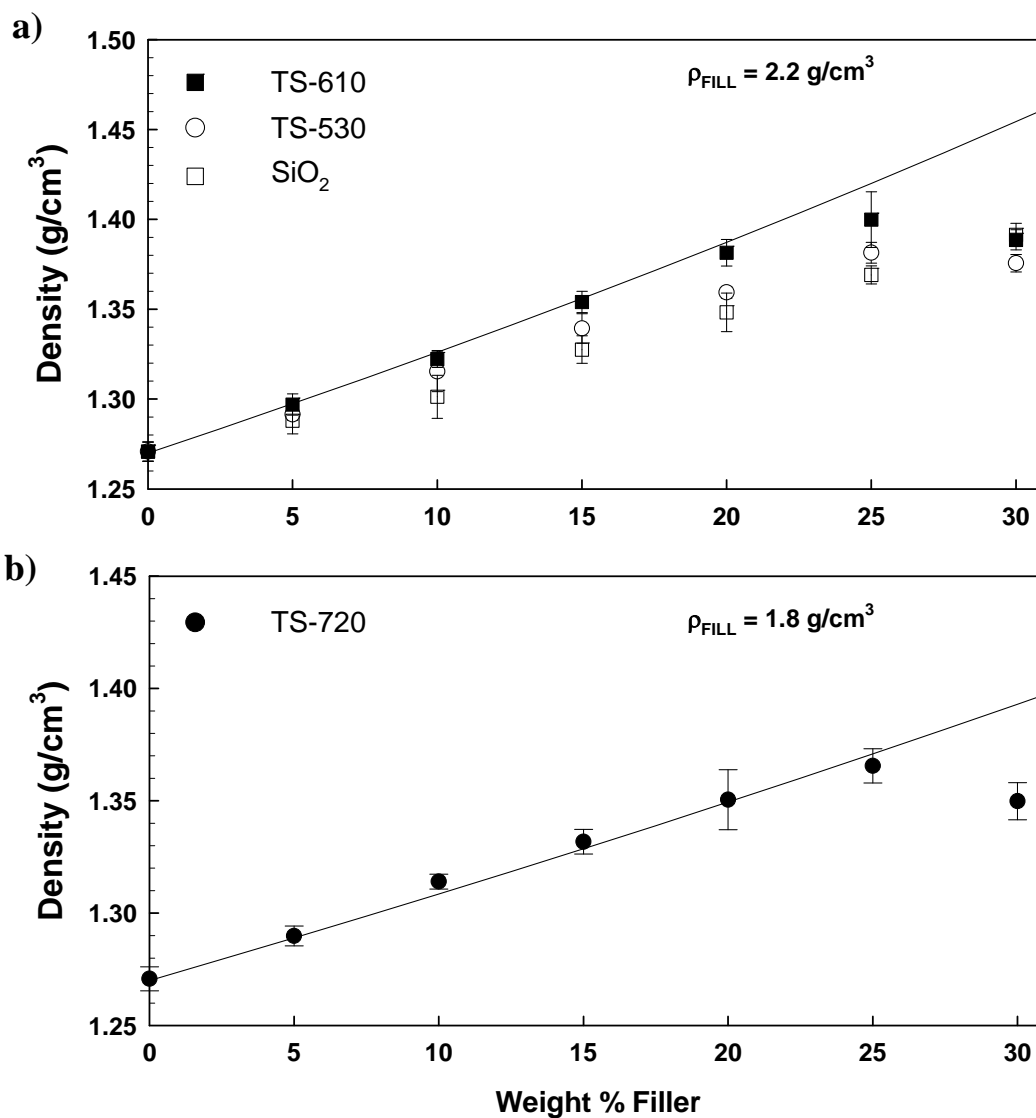


Figure 6.1: Density (g/cm^3) vs. weight percent filler for PEI nanocomposites. Solid curves correspond to volume additivity prediction. a) Filler density = 2.2 g/cm^3 [TS-610; TS-530; SiO_2]; b) Filler density = 1.8 g/cm^3 [TS-720].

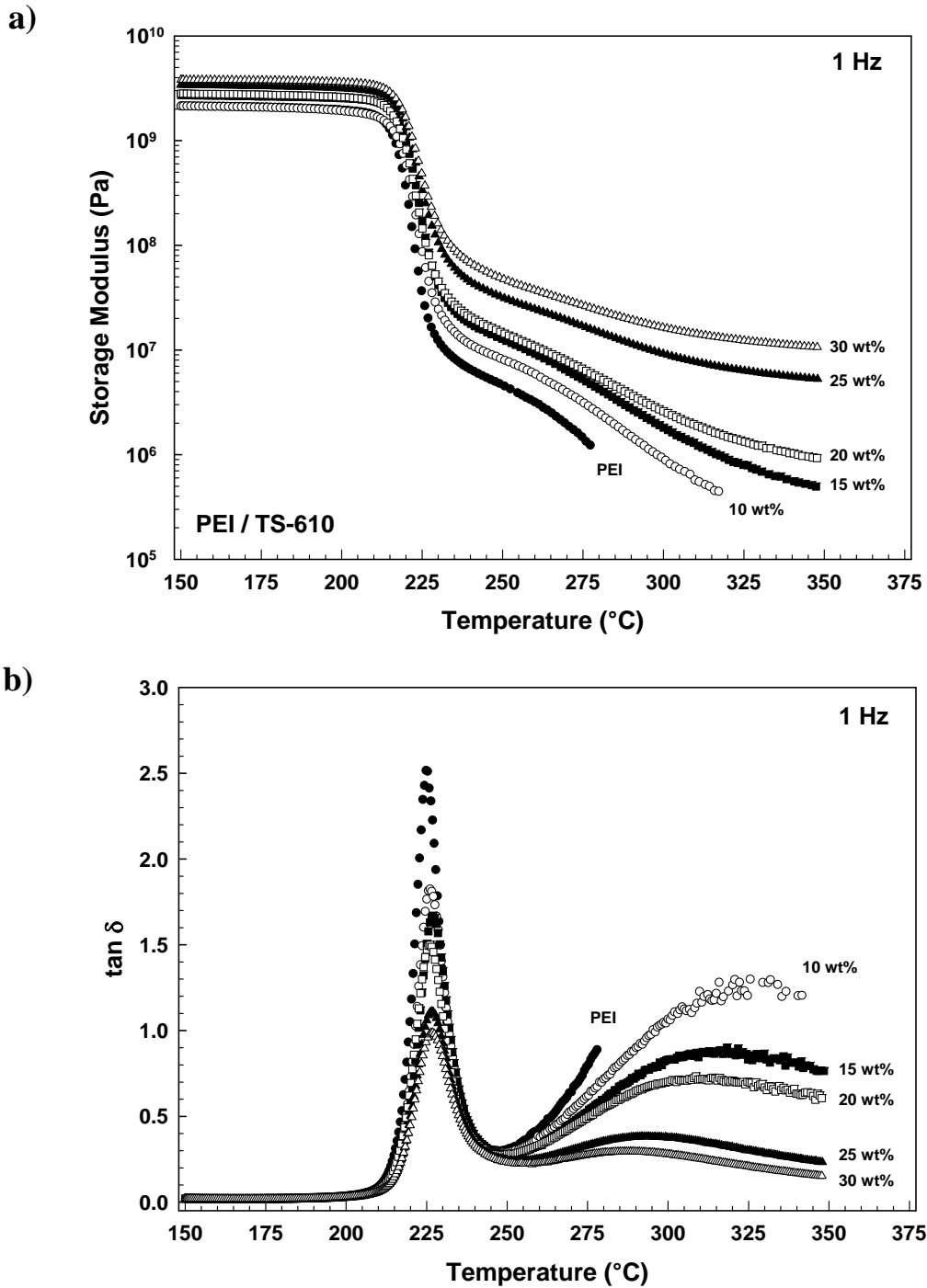


Figure 6.2: Dynamic mechanical properties vs. temperature (°C) for PEI/TS-610 nanocomposites. a) storage modulus (Pa); b) $\tan \delta$. Frequency of 1 Hz; heating rate of 3°C/min.

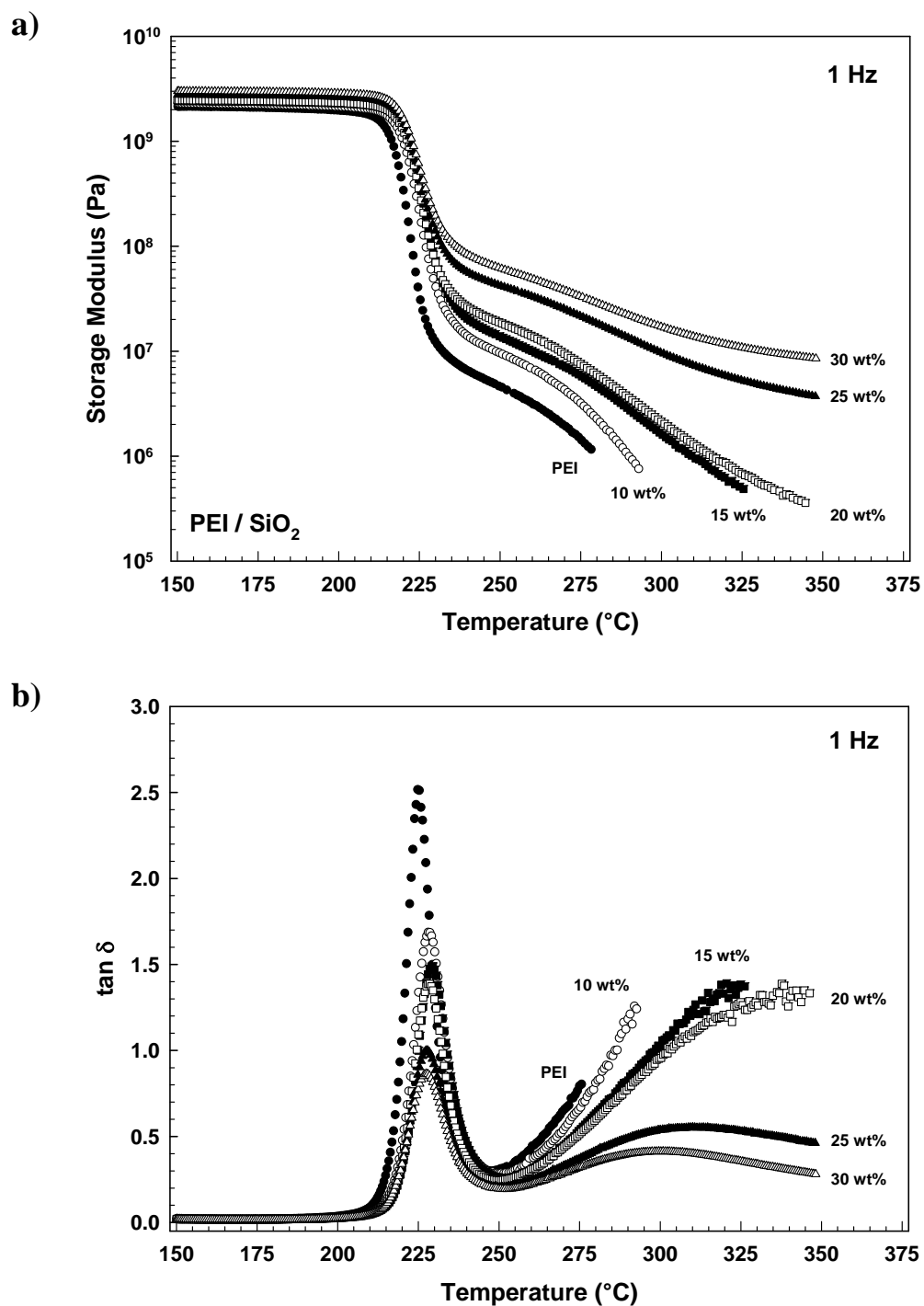


Figure 6.3: Dynamic mechanical properties vs. temperature (°C) for PEI/SiO₂ nanocomposites. a) storage modulus (Pa); b) tan δ . Frequency of 1 Hz; heating rate of 3°C/min.

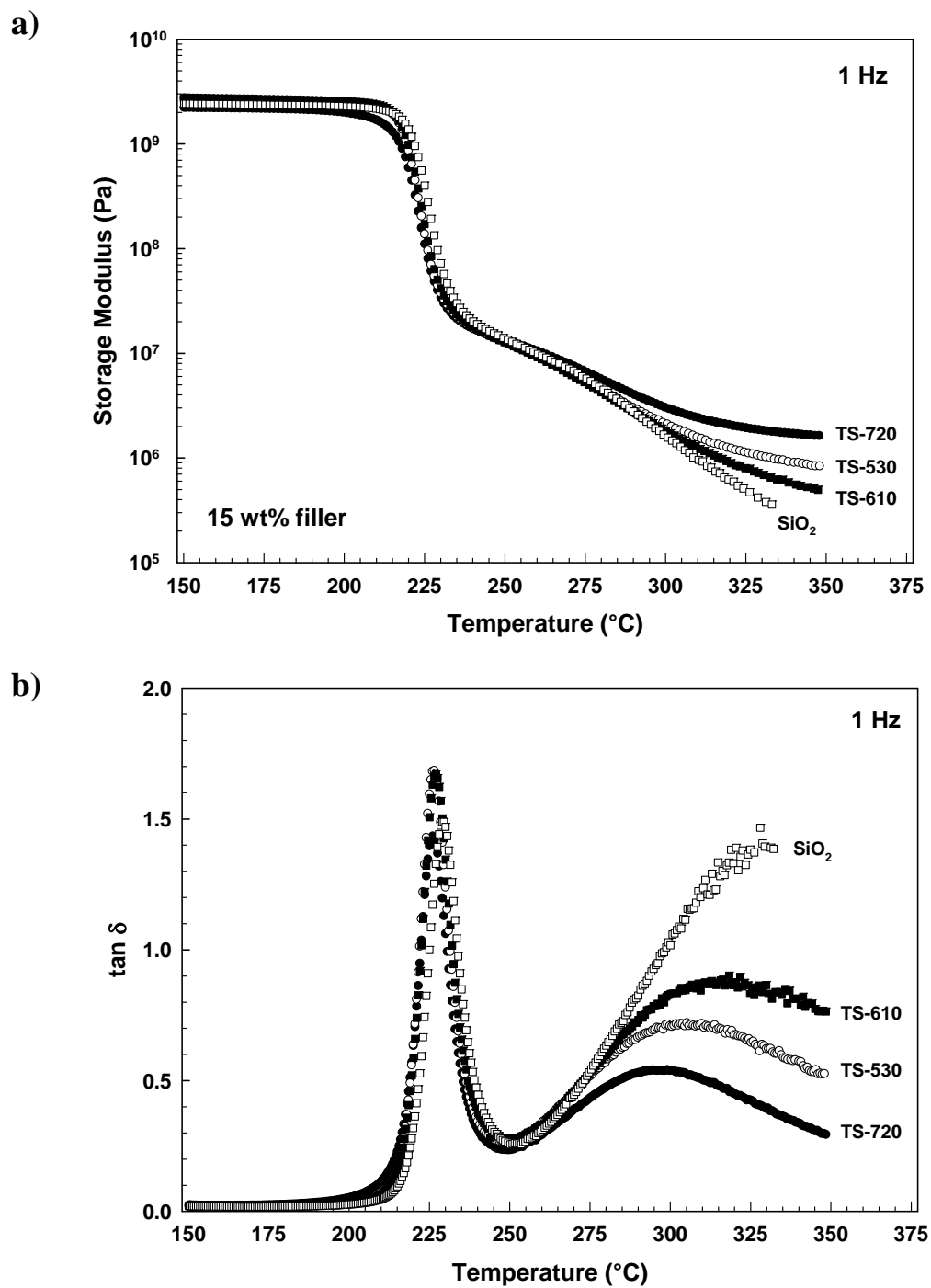


Figure 6.4: Dynamic mechanical properties vs. temperature (°C) for PEI nanocomposites with particle loading of 15 wt%: SiO₂; TS-530; TS-610; TS-720. a) storage modulus (Pa); b) tan δ . Frequency of 1 Hz; heating rate of 3°C/min.

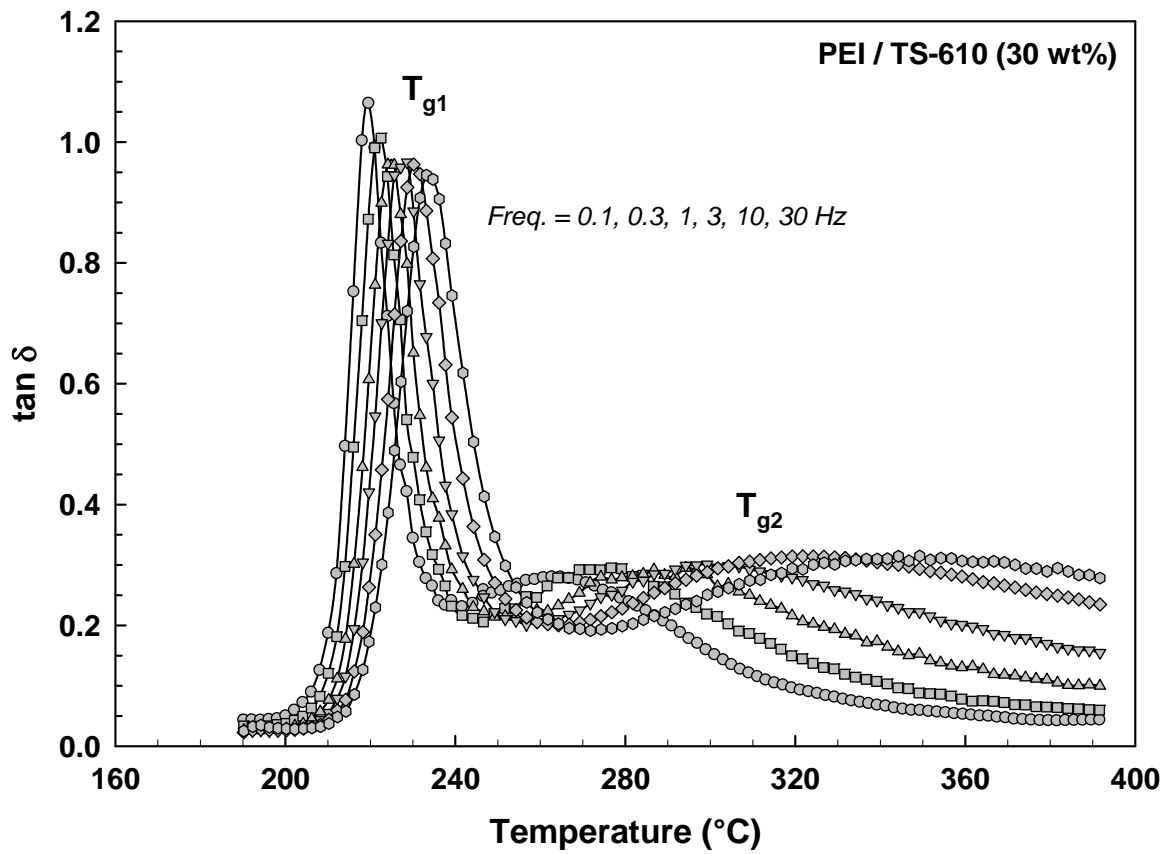


Figure 6.5: Dynamic mechanical tan δ vs. temperature ($^{\circ}\text{C}$) for PEI/TS-610 (30 wt%) nanocomposite. Frequencies of 0.1, 0.3, 1, 3, 10, 30 Hz.

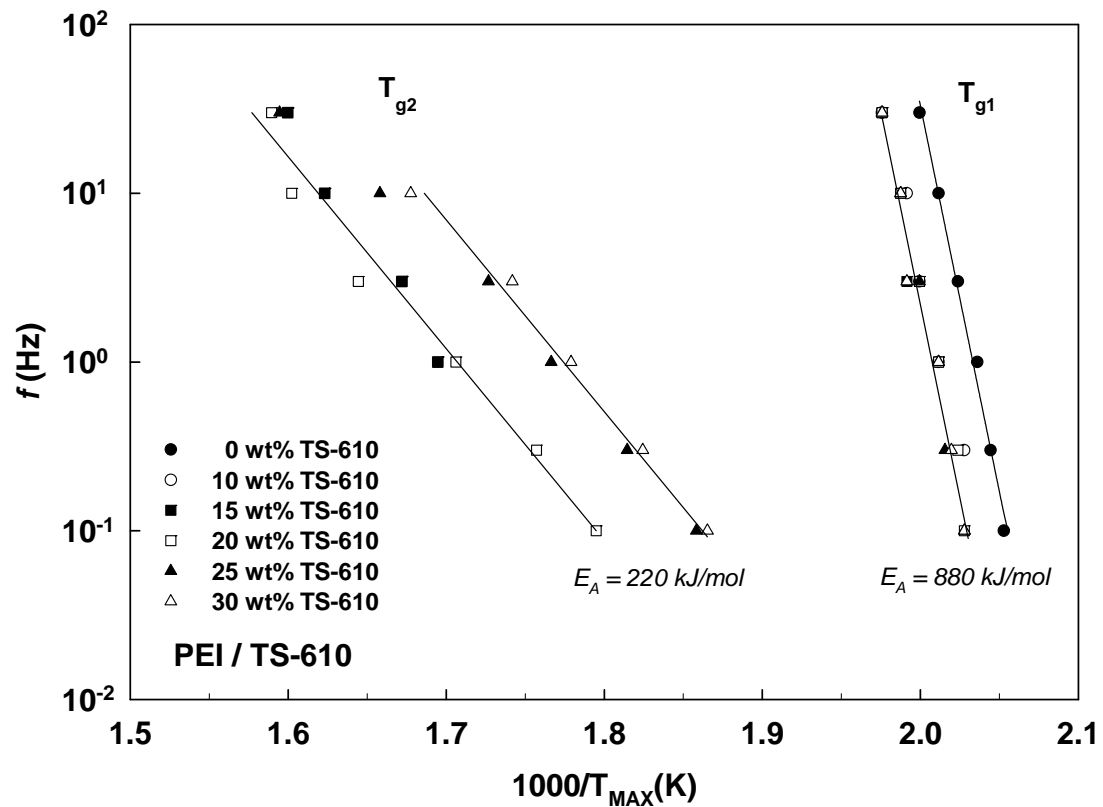


Figure 6.6: Arrhenius plots of f (Hz) vs. $1000/T_{MAX}$ (K) for PEI/TS-610 nanocomposites based on maxima in dynamic mechanical $\tan \delta$.

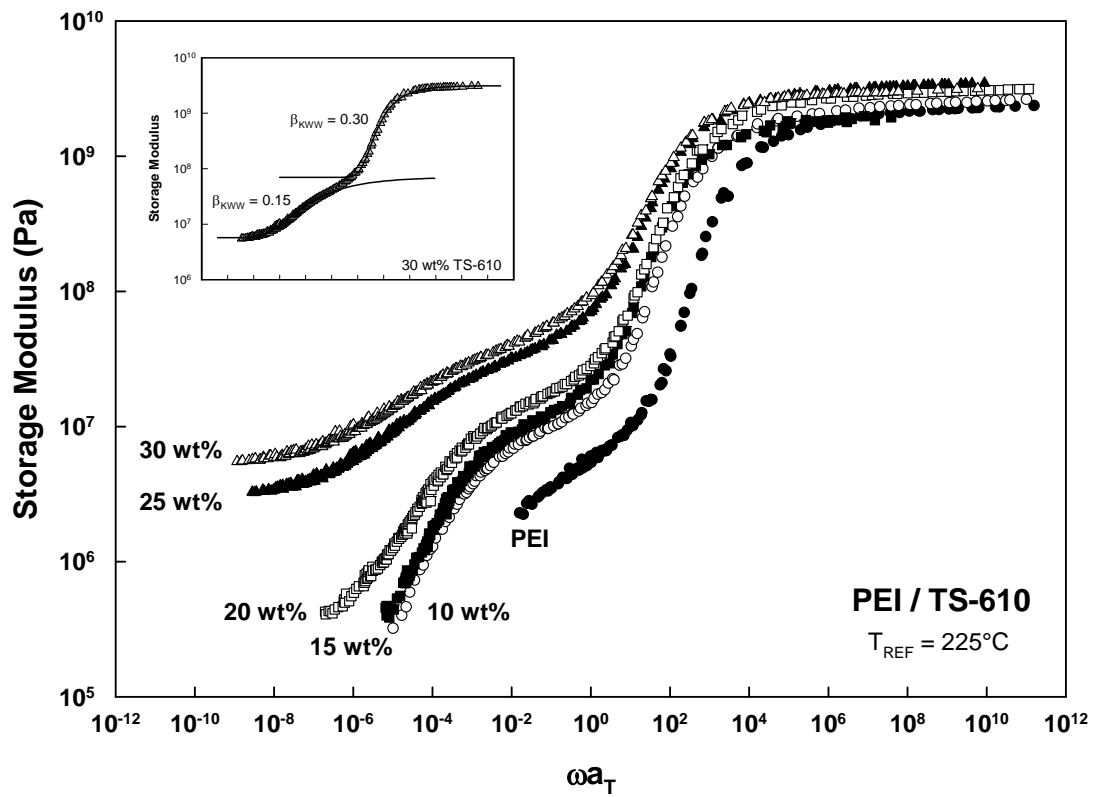


Figure 6.7: Time-temperature master curves (E' vs. ωa_T) for PEI/TS-610 nanocomposites. Reference temperature of 225°C. *Inset:* dual KWW curve fits for 30 wt% TS-610 composite.

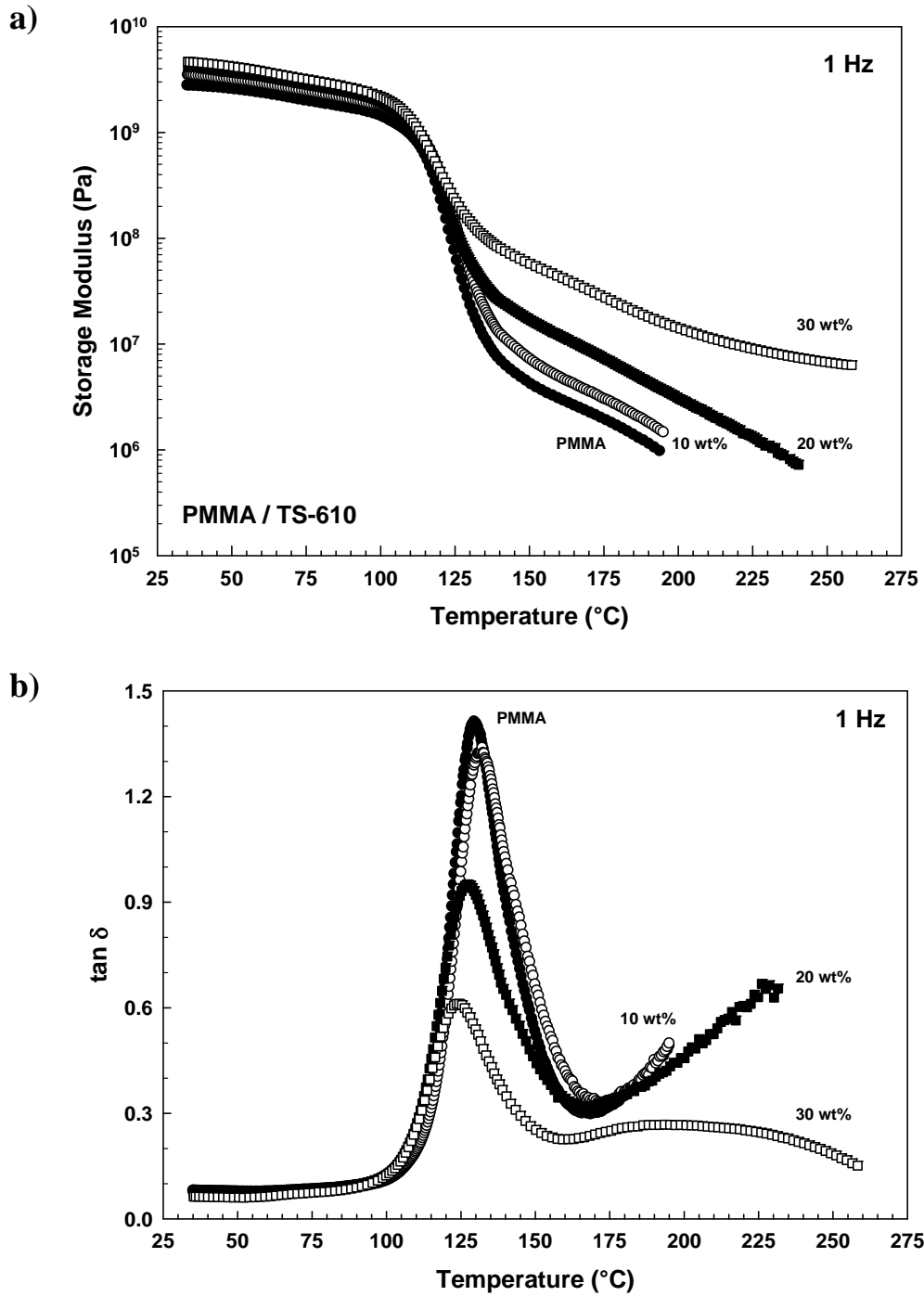


Figure 6.8: Dynamic mechanical properties vs. temperature (°C) for PMMA/TS-610 nanocomposites. a) storage modulus (Pa); b) tan δ . Frequency of 1 Hz; heating rate of 3°C/min.

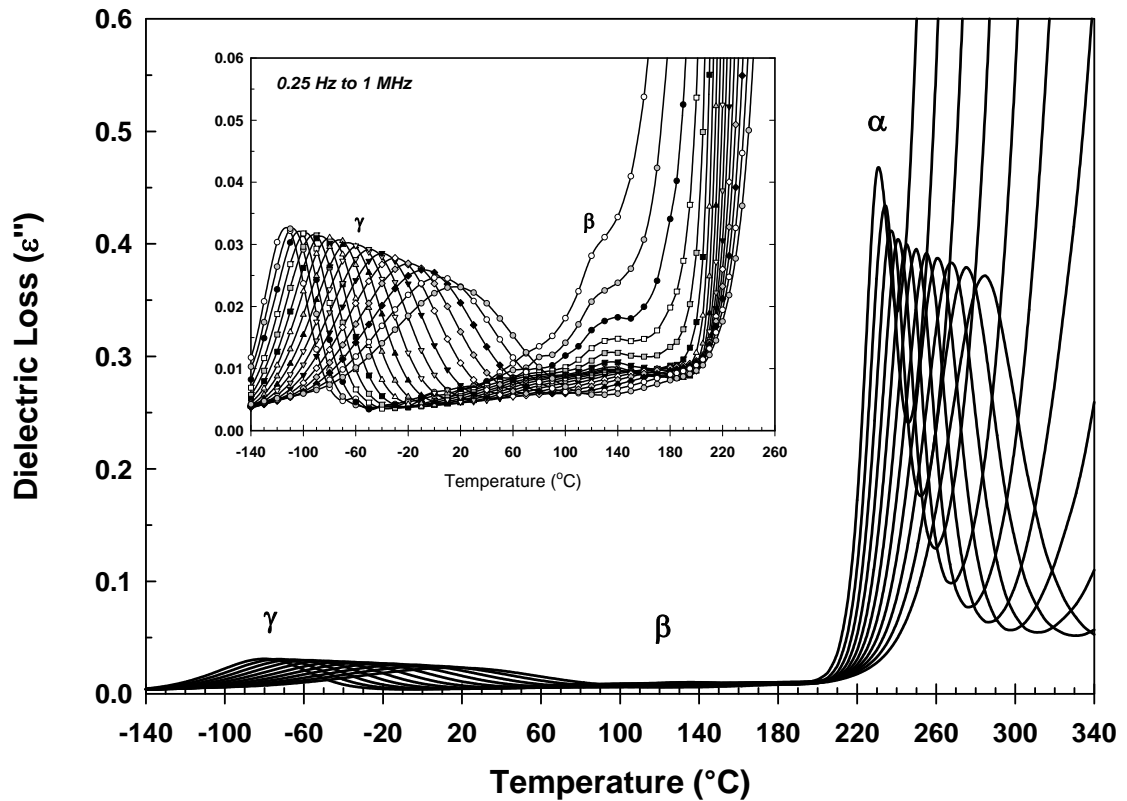


Figure 6.9: Dielectric loss (ϵ'') vs. temperature for unfilled PEI; selected frequencies from 75 Hz to 1 MHz. *Inset:* expanded view of dielectric loss across the sub-glass region (0.25 Hz to 1 MHz).

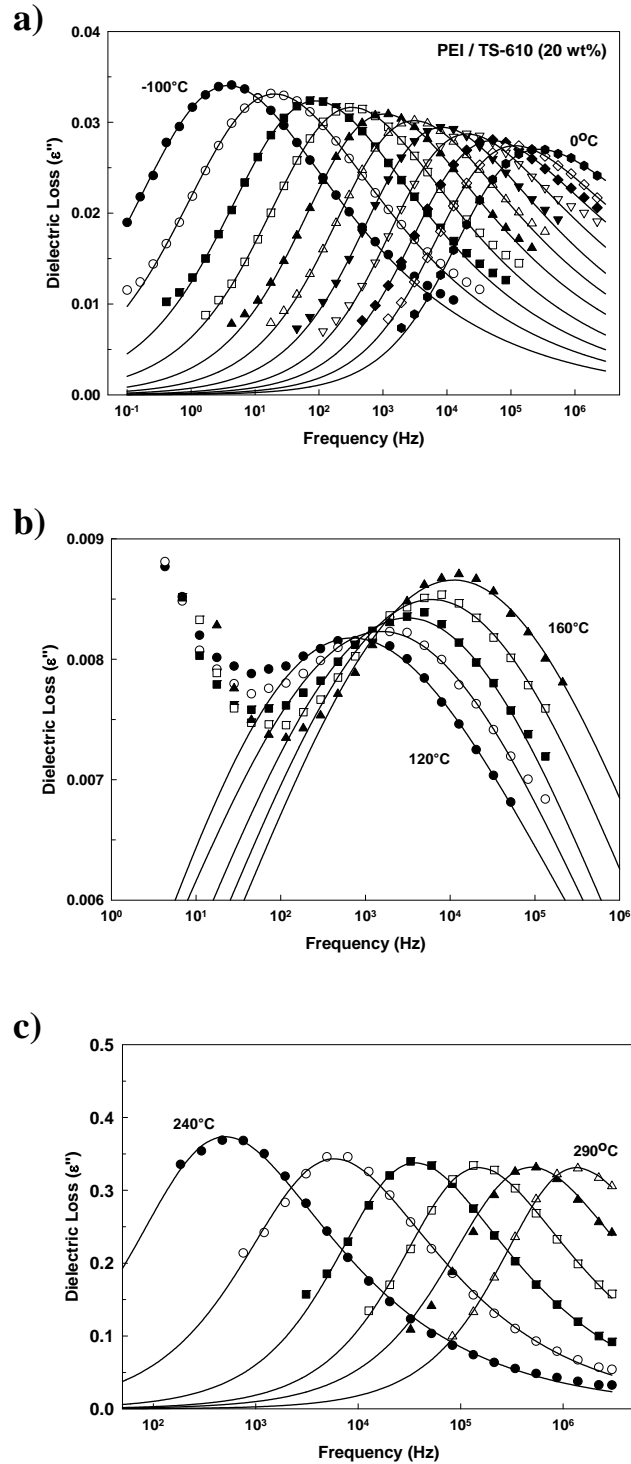


Figure 6.10: Dielectric loss (ϵ'') vs. frequency (Hz) for PEI/TS-610 (20 wt%) nanocomposite. Results are reported at 10°C intervals; solid curves correspond to HN best-fits. a) sub-glass γ transition; b) sub-glass β transition; c) glass-rubber α transition.

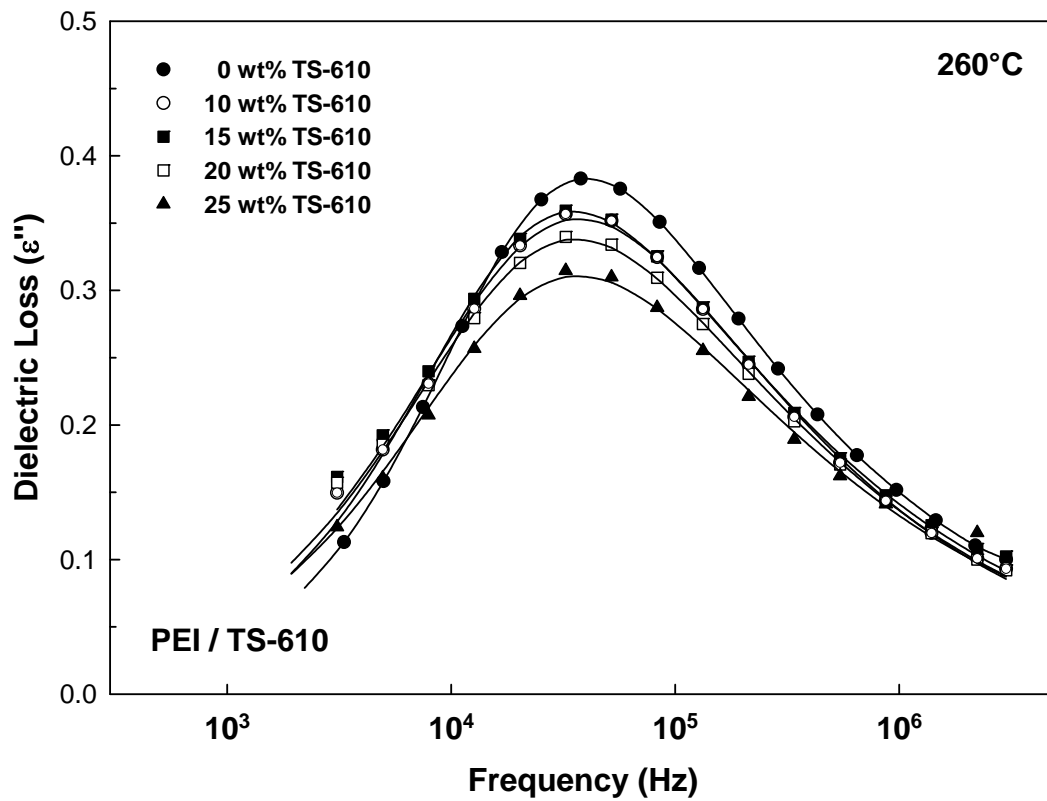


Figure 6.11: Dielectric loss (ϵ'') vs. frequency (Hz) for PEI/TS-610 nanocomposites at 260°C (glass-rubber relaxation). Solid curves correspond to HN best-fits.

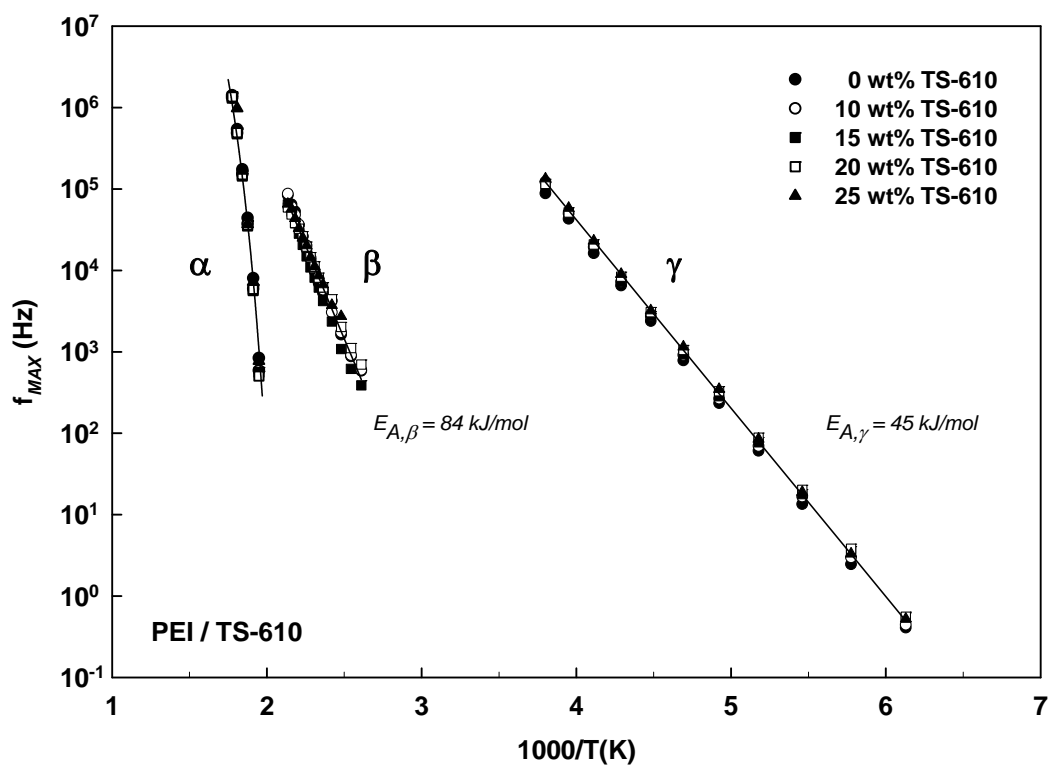


Figure 6.12: Arrhenius plots of f_{MAX} (Hz) vs. $1000/T(K)$ for PEI/TS-610 nanocomposites based on maxima in dielectric loss.

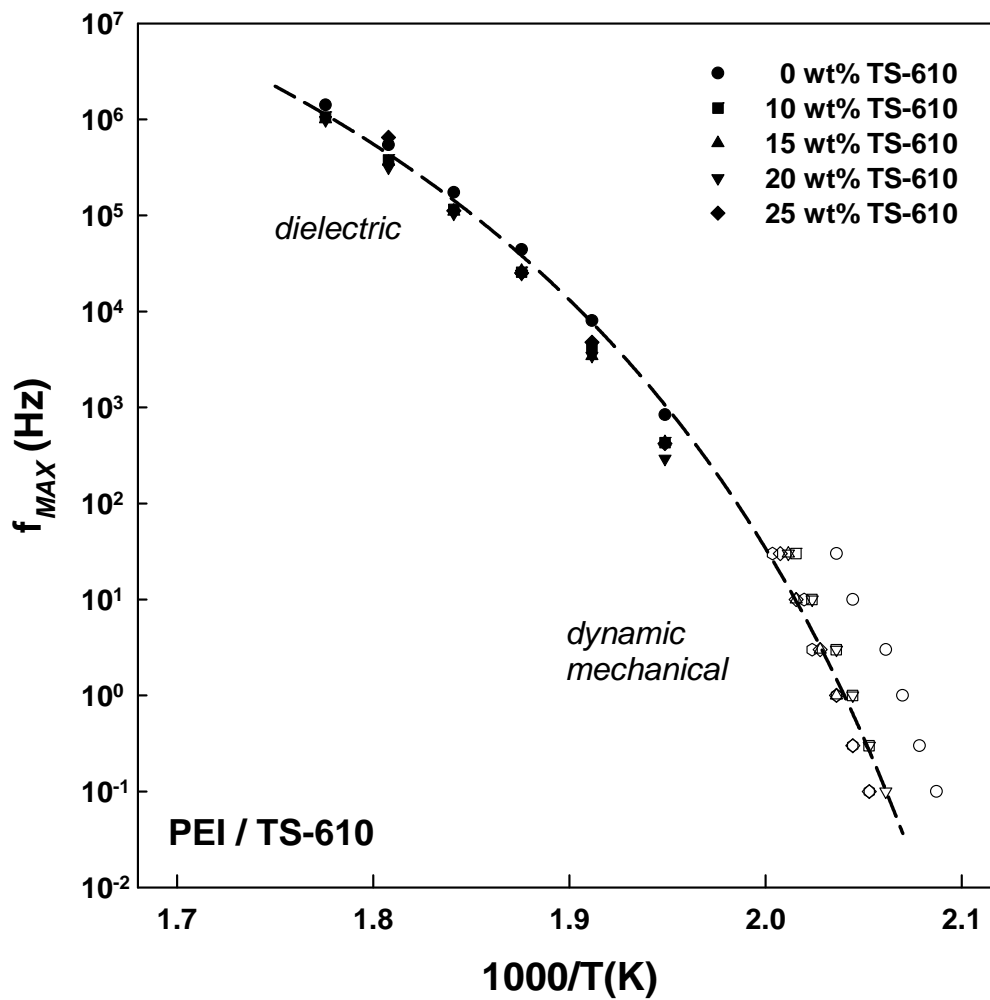


Figure 6.13: Arrhenius plots of f_{MAX} (Hz) vs. $1000/T(K)$ for PEI/TS-610 nanocomposites across the glass-rubber relaxation. Dashed curve represents WLF best-fit. Unfilled symbols correspond to dynamic mechanical measurements; filled symbols correspond to dielectric measurements.

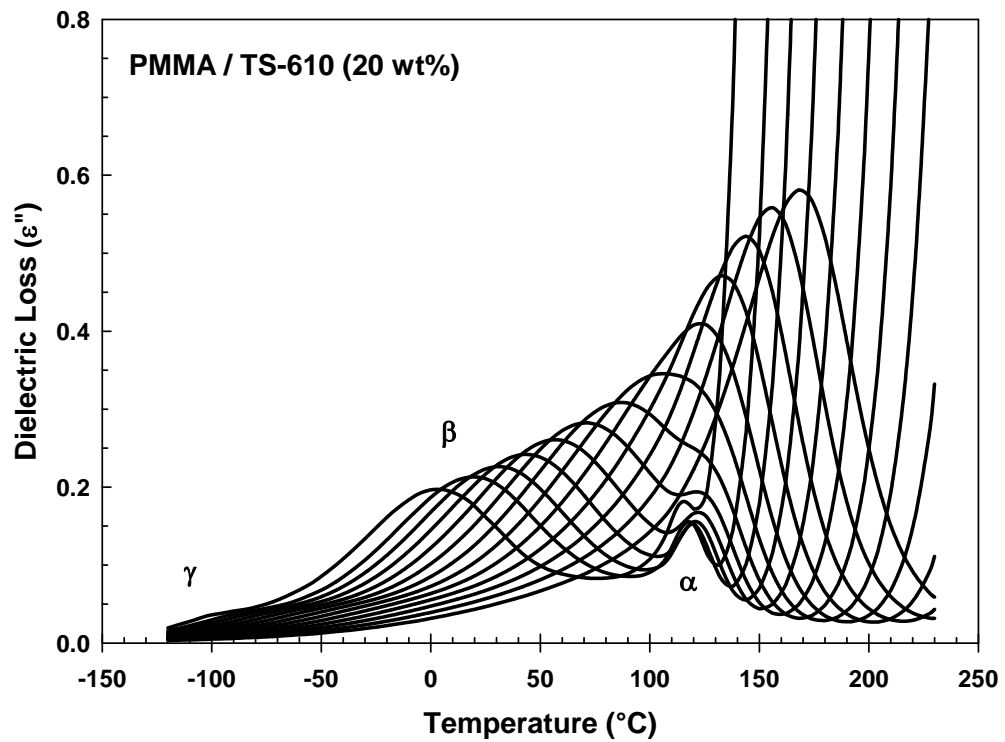


Figure 6.14: Dielectric loss (ϵ'') vs. temperature for PMMA/TS-610 nanocomposite; selected frequencies from 0.5 Hz to 1 MHz.

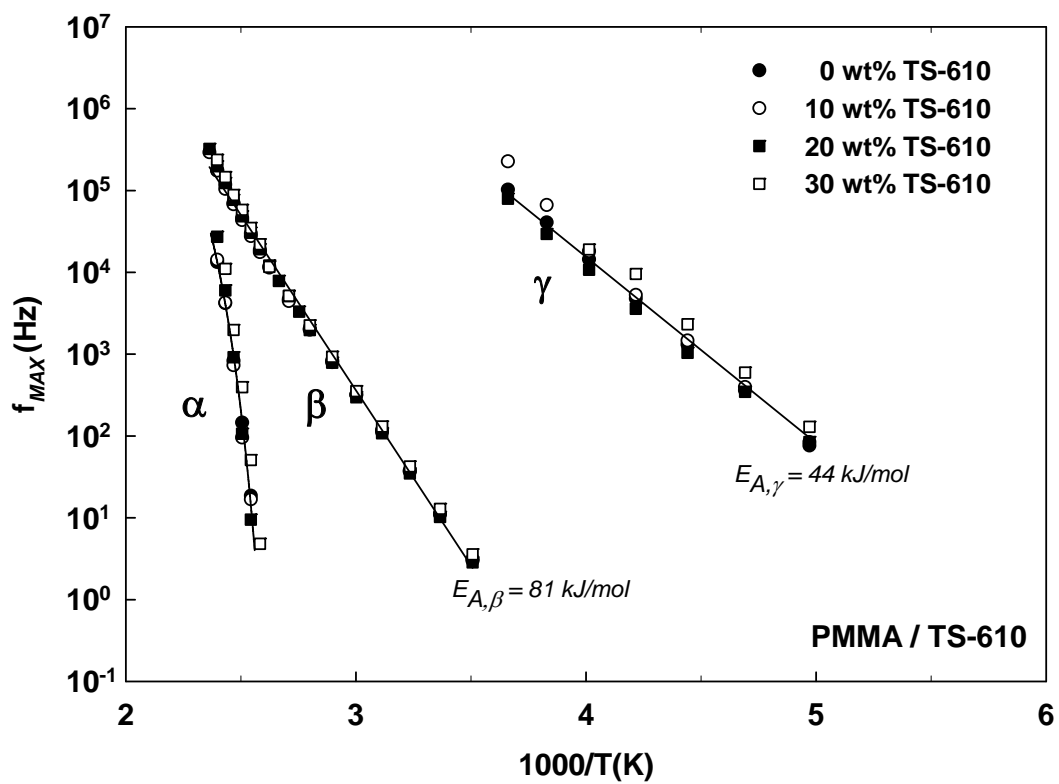


Figure 6.15: Arrhenius plots of f_{MAX} (Hz) vs. $1000/T$ (K) for PMMA/TS-610 nanocomposites based on maxima in dielectric loss.

References

- [1] Vaia, R.A.; Giannelis, E.P. "Polymer Nanocomposites: Status and Opportunities", *MRS Bulletin* **2001**, 26, 394.
- [2] Jordan, J.; Jacob, K.I.; Tannenbaum, R.; Sharaf, M.A.; Jasiuk, I. "Experimental Trends in Polymer Nanocomposites: A Review", *Materials Science and Engineering, A: Structural Materials: Properties, Microstructure and Processing* **2005**, 393, 1.
- [3] Tjong, S.C. "Structural and Mechanical Properties of Polymer Nanocomposites", *Materials Science & Engineering, R: Reports* **2006**, R53, 73.
- [4] Balazs, A.C.; Emrick, T.; Russell, T.P. "Nanoparticle Polymer Composites: Where Two Small Worlds Meet", *Science* **2006**, 314, 1107.
- [5] Crosby Alfred J.; Jong-Young, L. "Polymer Nanocomposites: The "Nano" Effect of Mechanical Properties", *Polymer Reviews* **2007**, 47, 217.
- [6] Schaefer, D.W.; Justice, R.S. "How Nano are Nanocomposites?", *Macromolecules* **2007**, 40, 8501.
- [7] Winey, K.I.; Vaia, R.A. "Polymer nanocomposites", *MRS Bulletin* **2007**, 32, 314.
- [8] Paul, D.R.; Robeson, L.M. "Polymer Nanotechnology: Nanocomposites", *Polymer* **2008**, 49, 3187.
- [9] Jancar, J.; Douglas, J.F.; Starr, F.W.; Kumar, S.K.; Cassagnau, P.; Lesser, A.J.; Sternstein, S.S.; Buehler, M.J. "Current Issues in Research on Structure-Property Relationships in Polymer Nanocomposites", *Polymer* **2010**, 51, 3321.
- [10] Robertson, C.G.; Roland, C.M. "Glass Transition and Interfacial Segmental Dynamics in Polymer-Particle Composites", *Rubber Chemistry and Technology* **2008**, 81, 506.
- [11] Yim, A.; Chahal, R.S.; St. Pierre, L.E. "Effect of Polymer-Filler Interaction Energy on the T_g (glass transition temperature) of Filled Polymers", *Journal of Colloid and Interface Science* **1973**, 43, 583.
- [12] Reid, C.G.; Greenberg, A.R. "Influence of Silica Reinforcement Upon the Glass-Transition Behavior of Acrylic Polymers", *Journal of Applied Polymer Science* **1990**, 39, 995.

- [13] Tsagaropoulos, G.; Eisenberg, A. "Direct Observation of Two Glass Transitions in Silica-Filled Polymers. Implications for the Morphology of Random Ionomers", *Macromolecules* **1995**, *28*, 396.
- [14] Tsagaropoulos, G.; Eisenberg, A. "Dynamic Mechanical Study of the Factors Affecting the Two Glass Transition Behavior of Filled Polymers. Similarities and Differences with Random Ionomers", *Macromolecules* **1995**, *28*, 6067.
- [15] Arrighi, V.; McEwen, I.; Qian, H.; Prieto, M. "The Glass Transition and Interfacial Layer in Styrene-Butadiene Rubber Containing Silica Nanofiller", *Polymer* **2003**, *44*, 6259.
- [16] Fragiadakis, D.; Pissis, P.; Bokobza, L. "Glass Transition and Molecular Dynamics in Poly(dimethylsiloxane)/Silica Nanocomposites", *Polymer* **2005**, *46*, 6001.
- [17] Fragiadakis, D.; Pissis, P. "Glass Transition and Segmental Dynamics in Poly(dimethylsiloxane)/Silica Nanocomposites Studied by Various Techniques", *Journal of Non-Crystalline Solids* **2007**, *353*, 4344.
- [18] Chen, L.; Zheng, K.; Tian, X.; Hu, K.; Wang, R.; Liu, C.; Li, Y.; Cui, P. "Double Glass Transitions and Interfacial Immobilized Layer in in-Situ-Synthesized Poly(vinyl alcohol)/Silica Nanocomposites", *Macromolecules* **2010**, *43*, 1076.
- [19] Ash, B.J.; Siegel, R.W.; Schadler, L.S. "Glass-Transition Temperature Behavior of Alumina/PMMA Nanocomposites", *Journal of Polymer Science, Part B: Polymer Physics* **2004**, *42*, 4371.
- [20] Bansal, A.; Yang, H.; Li, C.; Cho, K.; Benicewicz, B.C.; Kumar, S.K.; Schadler, L.S. "Quantitative Equivalence Between Polymer Nanocomposites and Thin Polymer Films", *Nature Materials* **2005**, *4*, 693.
- [21] Bansal, A.; Yang, H.; Li, C.; Benicewicz, B.C.; Kumar, S.K.; Schadler, L.S. "Controlling the Thermomechanical Properties of Polymer Nanocomposites by Tailoring the Polymer-Particle Interface", *Journal of Polymer Science, Part B: Polymer Physics* **2006**, *44*, 2944.
- [22] Rittigstein, P.; Torkelson, J.M. "Polymer-Nanoparticle Interfacial Interactions in Polymer Nanocomposites: Confinement Effects on Glass Transition Temperature and Suppression of Physical Aging", *Journal of Polymer Science, Part B: Polymer Physics* **2006**, *44*, 2935.
- [23] Takahashi, S.; Paul, D.R. "Gas Permeation in Poly(Ether Imide) Nanocomposite Membranes Based on Surface-Treated Silica. Part 1: Without Chemical Coupling to Matrix", *Polymer* **2006**, *47*, 7519.

- [24] Takahashi, S.; Paul, D.R. "Gas Permeation in Poly(Ether Imide) Nanocomposite Membranes Based on Surface-Treated Silica. Part 2: With Chemical Coupling to Matrix", *Polymer* **2006**, *47*, 7535.
- [25] Krishnamoorti, R. "Strategies for Dispersing Nanoparticles in Polymers", *MRS Bulletin* **2007**, *32*, 341.
- [26] "G.E. Plastics: Technical Data Sheet for Ultem Resin 1000", *G.E. Plastics: Technical Data Sheet for Ultem Resin 1000*; **2003**.
- [27] Ferry, J.D. *Viscoelastic Properties of Polymers*, 3rd edition; John Wiley and Sons: New York, **1980**.
- [28] Williams, G.; Watts, D.C.; Dev, S.B.; North, A.M. "Further Considerations of Non Symmetrical Dielectric Relaxation Behaviour Arising From a Simple Empirical Decay Function", *Transactions of the Faraday Society* **1971**, *67*, 1323.
- [29] Goodwin, A.A.; Simon, G.P. "Glass Transition Behavior of Poly(ether ether ketone)/Poly(ether imide) Blends", *Polymer* **1996**, *37*, 991.
- [30] Goodwin, A.; Marsh, R. "Dielectric and Dynamic Mechanical Relaxation of Poly(ether ether ketone)/Poly(ether imide) Blends Below the Glass Transition", *Macromolecular Rapid Communications* **1996**, *17*, 475.
- [31] Bristow, J.F.; Kalika, D.S. "Investigation of Semicrystalline Morphology in Poly(ether ether ketone)/Poly(ether imide) Blends by Dielectric Relaxation Spectroscopy", *Polymer* **1997**, *38*, 287.
- [32] Jenkins, M.J. "Relaxation Behaviour in Blends of PEEK and PEI", *Polymer* **2000**, *41*, 6803.
- [33] Havriliak, S.; Havriliak, S.J. *Dielectric and Mechanical Relaxation in Materials*; Hanser: Cincinnati, **1997**.
- [34] Kalakkunnath, S.; Kalika, D.S.; Lin, H.; Raharjo, R.D.; Freeman, B.D. "Molecular Relaxation in Cross-linked Poly(Ethylene Glycol) and Poly(Propylene Glycol) Diacrylate Networks by Dielectric Spectroscopy", *Polymer* **2007**, *48*, 579.
- [35] Steeman, P.A.M.; van Turnhout, J., "Dielectric Properties of Inhomogeneous Media", In *Broadband Dielectric Spectroscopy*; Kremer, F.; Schönhals, A., eds.; Springer-Verlag: Berlin, **2003**; pp 495-522.
- [36] McCrum, N.G.; Read, B.E.; Williams, G. *Anelastic and Dielectric Effects in Polymer Solids*; John Wiley and Sons, 1967, reprinted by Dover Publications: London, **1991**.

[37] Hedvig, P. *Dielectric Spectroscopy of Polymers*; John Wiley and Sons: New York, **1977**.

Chapter 7

Glass-Transition and Gas-Transport Characteristics of Polymer Nanocomposites Based on Crosslinked Poly(ethylene oxide)

This chapter is based on the following published work:

Comer, A.C., Kalika, D.S., Kusuma, V.A., Freeman, B.D. "Glass-Transition and Gas-Transport Characteristics of Polymer Nanocomposites Based on Crosslinked Poly(ethylene oxide)", *Journal of Applied Polymer Science* **2010**, *117*, 2395.

7.1 Introduction

The removal of acid gases such as carbon dioxide from light gas mixtures via membrane separation technology is an area of intense interest due to the relevance of such separations for a range of industrial processes. Recently, a series of rubbery copolymer membranes based on crosslinked poly(ethylene oxide) [XLPEO] has been investigated for use in CO₂/light gas separations [1,2]. The polymers display high CO₂ permeability and favorable CO₂/light gas selectivity owing to their rubbery character and the presence of polar ether oxygens in the polymer network that interact preferentially with CO₂ [3]. Strategic copolymerization of XLPEO has been used to tailor the free volume and chemical composition of the networks, leading to the establishment of material design rules for the optimization of gas separation performance in these CO₂-selective membranes [4-8].

The introduction of nanoscale structure in polymers via the inclusion of inorganic nanoparticles provides a range of variables that can be exploited for the enhancement of material properties. In the case of gas separation membranes, recent studies have

demonstrated improvements in gas separation performance that can be achieved upon the incorporation of metal oxide nanoparticles into glassy and rubbery polymers, with the presence of the filler leading to changes in both the diffusivity and solubility characteristics of the membranes. For example, the introduction of hydrophobic fumed silica into glassy, high free-volume poly(4-methyl-2-pentyne) produces a disruption in polymer chain packing that leads to a subtle, angstrom-level increase in the free volume available for penetrant transport, resulting in a systematic increase in diffusivity with filler loading [9,10]. The enhancement in gas transport properties is higher in samples containing smaller nanoparticles, suggesting the importance of surface-to-volume ratio in these materials. Similarly, the incorporation of metal oxide nanoparticles into rubbery 1,2-polybutadiene generates a marked increase in permeability that reflects a combination of higher penetrant solubility due to physical adsorption, as well as increased diffusivity [11,12]. The enhancement in diffusivity for the polybutadiene composites is due primarily to the presence of a substantial void volume fraction detected in the solvent-cast samples.

Given the potential of XLPEO network polymers for use as CO₂-selective membranes and the commercial availability of very small metal oxide-based nanoparticles, it is of interest to explore possible enhancements in XLPEO gas separation performance due to incorporation of metal oxide nanoparticles; *e.g.* magnesium oxide (MgO) and silica (SiO₂). When assessing the influence of nanoparticles on gas transport, it is important to consider the extent to which the particles perturb the surrounding polymer, as changes in polymer chain mobility affect size discrimination and the corresponding penetrant diffusivity characteristics of the matrix. In rubbery polymers, segmental mobility is

responsible for the creation of transient free volume elements by which gas diffusion occurs. The glass transition temperature, T_g , can be used as an indicator of overall segmental mobility, and a number of authors have reported correlations wherein measured light gas permeability and diffusivity decrease systematically with increasing T_g across a range of rubbery polymers [13].

The vast amount of particle-polymer surface area created in nanocomposites can have a substantial influence on the segmental mobility of the polymer chains, owing to both particle-polymer interactions as well as physical confinement effects; these perturbations to the bulk polymer chain dynamics are often manifested by changes in T_g . Over the last several decades, there have been numerous reports examining the glass transition characteristics of filled polymers reinforced with materials such as carbon black or silica, and more recently such systems have been studied within the context of nanoscale phenomena. In filled polymers, the inclusion of inorganic particles often leads to an increase in the glass transition temperature due to favorable interactions between the particle surface and the polymer chains that restrict chain mobility [14]. Investigators have reported positive offsets in T_g , as well as the emergence of a second (higher) T_g corresponding to the presence of a distinct, constrained population of chain segments in the vicinity of the particle surface [15-19]. For systems that exhibit poor wetting, T_g reductions have also been encountered [20,21]. In certain cases, a direct correlation has been demonstrated between the T_g values measured for bulk composites, and the influence of physical confinement on T_g observed for ultra-thin polymer films [22-24].

In this chapter, we examined the glass transition and gas permeability characteristics of a series of rubbery polymer nanocomposites based on crosslinked poly (ethylene glycol)

diacrylate [PEGDA]. Nanocomposite samples were prepared by UV photopolymerization of PEGDA in the presence of varying amounts of nominally spherical MgO or SiO₂ nanoparticles. The glass-rubber relaxation characteristics of the resulting polymers were assessed using dynamic mechanical analysis and dielectric spectroscopy. Gas permeability results are reported for CO₂, CH₄, O₂ and H₂, along with gas diffusion and solubility coefficients. In addition, the influence of sample preparation in the presence of toluene as a potential particle dispersion aid is reported.

7.2 Experimental

7.2.1 Materials

Poly(ethylene glycol) diacrylate crosslinker (PEGDA; nominal molecular weight of 700 g/mol) and 1 hydroxyl-cyclohexyl phenyl ketone (HCPK) photoinitiator were obtained from Aldrich Chemical Company, Milwaukee, WI. The molecular weight and polydispersity of the PEGDA were characterized previously, indicating a number-average molecular weight (M_n) of 743 g/mol consistent with a monomeric repeat length, $n \sim 14$ (see ref. [4]). Spherical MgO nanoparticles (99.2% purity) were obtained from Nanoscale Materials Inc., Manhattan, KS. The manufacturer reports an effective density for these particles of 2.4 g/cm³ and a BET surface area of 600 m²/g, corresponding to a nominal particle diameter of ~ 3 nm.[11] SiO₂ nanoparticles (99.5% purity; 10 nm diameter) were obtained from Aldrich, with a reported BET surface area of 590 to 690 m²/g and density of 2.2 g/cm³. Toluene (HPLC grade) was purchased from Fisher Scientific, Pittsburgh, PA. All gases were obtained from Airgas Southwest Inc. (Corpus

Christi, TX), with purity of at least 99.9% (except for methane: 99.0%), and were used as received.

7.2.2 Sample Preparation

PEGDA, HCPK (0.1 wt% based on PEGDA) and nanoparticles were magnetically mixed in the desired proportions for at least 20 min., followed by sonication in an ultrasonic water bath for 10 min. to eliminate bubbles (Model FS60, Fisher Scientific). In cases where toluene was added to aid particle dispersion (*i.e.*, at higher particle loadings), PEGDA, HCPK, and toluene were first magnetically mixed for at least 20 min., followed by addition of nanoparticles and mixing for an additional 20 min. prior to degassing. All mixtures were then subjected to planetary mixing for 3 min. at 2000 rpm in a Thinky Planetary Mixer Model AR-250 (Thinky Corporation, Laguna Hills, CA).

Samples were crosslinked via UV photopolymerization using a Spectrolinker XL-1000 crosslinker (Spectronics Corporation, Westbury, NY). The mixture was sandwiched between parallel quartz plates with controlled spacing and exposed to 312 nm UV light for 90s at 3 mW/cm², as per the method for XLPEGDA polymerization described previously [4,25]. After crosslinking, the films were stored under vacuum at 25°C for at least 24 hrs. before further study. Films prepared with toluene diluent were immediately covered after crosslinking to control the rate of toluene evaporation; after initial drying in the fume hood, these samples were held under vacuum at room temperature (25°C). Thickness of the resulting nanocomposite films was ~ 1.0 mm for dynamic mechanical specimens, and ~ 0.30 mm for samples prepared for dielectric measurement and

permeability tests; the precise thickness of each film was determined using a digital micrometer with precision to $\pm 1 \mu\text{m}$.

7.2.3 Film Density

Bulk density measurements of the crosslinked nanocomposite films were conducted by hydrostatic weighing at 25°C using a conventional density determination kit (Denver Instruments, CO); *n*-heptane was employed as the auxiliary liquid. A minimum of three replicate measurements were completed for each sample tested.

7.2.4 Dynamic Mechanical Analysis

Dynamic mechanical analysis was performed using a Polymer Laboratories DMTA (Amherst, MA) operating in single cantilever bending geometry. All specimens were dried under vacuum at room temperature for at least 24 hrs. prior to measurement, and sample mounting procedures were designed to minimize exposure to ambient moisture. Storage modulus (E') and loss tangent ($\tan \delta$) were recorded at a heating rate of $1^\circ\text{C}/\text{min}$. with test frequencies of 0.1, 1, and 10 Hz. Each measurement was carried out under an inert (N_2) atmosphere.

7.2.5 Broadband Dielectric Spectroscopy

Dielectric measurements were conducted using the Novocontrol Broadband Dielectric Spectrometer (Hundsangen, Germany). To promote electrical contact during measurement, concentric 33 mm silver electrodes were applied to each sample film using a VEECO (Plainview, NY) thermal evaporation system. Samples were subsequently mounted between gold platens and positioned in the Novocontrol Quatro Cryosystem.

Dielectric constant (ϵ') and loss (ϵ'') were recorded at a heating rate of 2 °C/min with test frequencies ranging from 1 Hz to 2 MHz.

7.2.6 Gas Transport Measurements

Pure gas permeability measurements were conducted by Victor Kusuma at the University of Texas at Austin. Pure gas permeability values for CO₂, CH₄, O₂ and H₂ were determined using a constant volume/variable pressure apparatus [26,27]. The gas flux was measured from the steady-state pressure rise in a pre-evacuated downstream vessel of fixed volume when pure gas was applied on the upstream side at a known high pressure (3 to 15 atm. for the studies conducted here); the samples were partially masked with impermeable aluminum tape on the upstream face of each film to accurately define the surface area available for mass transport and to prevent damage to the film during testing. Permeability values were calculated from the steady-state flux measurements [6], while diffusion coefficients were estimated via time lag measurements of transient gas flux [27,28]. The corresponding gas solubility coefficients were determined according to the solution-diffusion model, as $S = P/D$ [29]. The permeability values obtained for CH₄, O₂ and H₂ were independent of upstream pressure, while CO₂ exhibited plasticization with increasing pressure (see ref. [4]). In order to compare the inherent permeability of the polymers to different gases, permeability values are reported at infinite dilution (*i.e.*, extrapolated to an upstream pressure, $p \rightarrow 0$), consistent with our previous studies. All experiments were performed at 35°C.

7.3 Results and Discussion

7.3.1 Dynamic Mechanical Analysis

The UV photopolymerization of the PEGDA ($n = 14$) crosslinker in the presence of various loadings of nanoparticles produced three-dimensional nanocomposite networks, consistent with the results obtained for the PEGDA-based formulations studied previously [4]. Independent differential scanning calorimetry studies (not shown) indicated that the polymer matrix was fully amorphous, with no evidence of crystallization.

Dynamic mechanical results for the PEGDA/MgO and PEGDA/SiO₂ nanocomposite films are presented in **Figures 7.1 and 7.2**, respectively, with storage modulus (E') and loss tangent ($\tan \delta$) plotted versus temperature at a frequency of 1 Hz. The 100% XLPEGDA (unfilled) network displays a glassy modulus of ~ 2.5 GPa and a glass-rubber transition peak temperature of -35°C (T_{α} ; 1 Hz). The rubbery modulus for XLPEGDA (0°C) is ~ 50 MPa. The introduction of MgO nanoparticles has only a minimal influence on the glassy modulus of the network (*i.e.*, less than 5% enhancement), but produces a strong systematic increase in the rubbery modulus with particle loading, owing to the larger difference in the inherent moduli of the included and matrix phases in this region [14,30]. The observed increase in rubbery modulus with loading is accompanied by a systematic decrease in the intensity of $\tan \delta$ and a shift in peak position to higher temperatures; *i.e.*, a progressive increase in the glass-rubber relaxation temperature. Similar results are obtained for the PEGDA/SiO₂ system (see Figure 7.2), but with a slightly greater ($\sim 15\%$) enhancement in glassy modulus with loading evident below T_g .

In nanocomposite systems with favorable particle-polymer interactions, increases in T_g with filler loading are often observed, the magnitude of the increase reflecting a number of inter-related material factors that include: particle size and corresponding interfacial surface area, particle loading and its implications for the average polymer layer thickness surrounding each particle, the particle-polymer interaction energy, and the relative stiffness of the polymer [22-24]. The measured dynamic mechanical peak temperatures for the PEGDA-based nanocomposites are reported in **Figure 7.3** as a function of loading. Across the range of compositions examined, an overall increase in T_α of $\sim 6^\circ\text{C}$ is observed. The trend is essentially the same for both systems. Further, there is no evidence to suggest the emergence of a second, distinct glass transition process in the composite samples (re: Tsagaropoulos and Eisenberg [18]).

The rubbery modulus measured for the various nanocomposites is plotted versus volume percent filler in **Figure 7.4**. Here, the volume fraction of filler (ϕ_F) is determined from:

$$\phi_F = \frac{w_F}{w_F + \frac{\rho_F}{\rho_P}(1 - w_F)} \quad (7.1)$$

where w_F is the weight fraction particles and ρ_P is the density of the XLPEGDA polymer matrix, taken to be 1.183 g/cm^3 [4]. According to their respective suppliers, the densities of the filler particles (ρ_F) are 2.4 g/cm^3 for MgO and 2.2 g/cm^3 for SiO₂.

The modulus data presented in Figure 7.4 can be described using a modified version of the Mooney equation, which in its original form describes the viscosity of colloidal

suspensions containing rigid spherical particles [31]. In the context of the mechanical modulus, the Mooney equation can be expressed as:

$$\ln\left(\frac{E}{E_p}\right) = \frac{k_E \phi_F}{1 - \phi_F / \phi_M} \quad (7.2)$$

where E is the measured rubbery modulus of the composite, E_p is the modulus of the polymer matrix (50 MPa; see Figure 7.1), ϕ_F is the volume fraction of the filler, k_E is the Einstein coefficient, and ϕ_M is the maximum volume fraction of the filler. The value of the Einstein coefficient depends upon the quality of the particle-matrix interaction, as well as particle distribution (*i.e.*, dispersed vs. agglomerated spheres). For dispersed spheres with no slippage at the interface, $k_E = 2.5$, with higher values obtained in agglomerated systems. Likewise, ϕ_M depends upon the packing geometry and the extent of agglomeration, with a maximum value of 0.74 corresponding to an ideal close-packed arrangement [14]. For the data shown in Figure 7.4, best-fit curves are obtained with k_E and ϕ_M serving as adjustable parameters. A single value for ϕ_M is obtained for both systems ($\phi_M = 0.45$), with $k_E = 4.8$ (MgO) and 5.8 (SiO₂), respectively. The parameter values indicate that the modulus-filler relation is influenced to some degree by particle agglomeration within the crosslinked PEGDA matrix, the effect being slightly stronger in the case of the PEGDA/SiO₂ composites [14].

Time-temperature superposition was applied to the dynamic mechanical results to obtain modulus-frequency master curves for the composites at a reference temperature of -40°C [32]. The results are presented in **Figure 7.5** (PEGDA/MgO composites) with E' plotted vs. ωa_T , where ω is the applied test frequency ($\omega = 2\pi f$, with f expressed in Hz) and a_T is the dimensionless shift factor. The relative positions of the curves along the horizontal

axis reflect the effective glass-rubber relaxation time for the samples, with higher MgO loadings leading to longer relaxation times and correspondingly higher glass transition temperatures. The time-temperature master curves could be satisfactorily described using the Kohlrausch-Williams-Watts (KWW) “stretched exponential” relaxation time distribution function:

$$\alpha(t) = \exp\left[-(t/\tau_o)^{\beta_{KWW}}\right] \quad (7.3)$$

where τ_o is the central relaxation time and β_{KWW} is the distribution parameter. β_{KWW} ranges from 0 to 1, with values close to unity corresponding to a narrow, single relaxation time response, and lower values reflecting broader transitions influenced by intermolecular coupling, crosslinks, and the presence of crystallinity or other internal constraints. For the data shown in Figure 7.5, series approximations reported by Williams et al. were used as the basis for the KWW curve fits [33]. A single value for the broadening parameter, $\beta_{KWW} = 0.25 \pm 0.01$, was sufficient to describe the relaxation response for both the PEGDA/MgO and PEGDA/SiO₂ composite series, independent of particle loading. That is, no significant broadening of the XLPEGDA glass-rubber relaxation was encountered with the addition of increasing levels of nanoparticles in these composites.

7.3.2 Broadband Dielectric Spectroscopy

Broadband dielectric spectroscopy can serve as a valuable complement to dynamic mechanical measurements for the elucidation of relaxation processes (*e.g.* the glass transition) in polymer systems. Dielectric spectroscopy relies on the detection of dipolar reorientations along the polymer molecules as the basis for establishing motional

transitions, and modern dielectric instruments provide for measurements across an exceptionally wide range of test frequencies. However, in heterogeneous media, the measured dielectric response is complicated by the occurrence of interfacial polarization, which results due to the build-up of charges at the internal boundaries within the material [34]. The contributions to dielectric constant and loss from interfacial polarization can be substantial, and are most pronounced at low frequencies and temperatures above the glass transition. Although a number of theories have emerged that describe interfacial polarization effects as a function of the electrical properties of the individual constituents, their shape and distribution, the quantitative application of these models is often difficult owing to the complexity of the morphology encountered in bulk composite materials.

The dielectric relaxation properties of unfilled XLPEGDA and related copolymers have been studied in detail, and are reported in a series of prior publications [35-37]. Representative dielectric results for the nanocomposites (PEGDA + 30wt% MgO) are given in **Figure 7.6**. Examination of dielectric constant vs. temperature reveals three polarization processes that appear as incremental increases in ϵ' : a merged sub-glass (β) process at low temperatures ($\sim -100^\circ\text{C}$), the glass-rubber (α) relaxation with onset temperature at $\sim -50^\circ\text{C}$, and interfacial polarization at temperatures beyond the α transition. Relative maxima in dielectric loss are observed for each of the three processes; at lower frequencies, the interfacial contribution to ϵ'' largely obscures the orientational polarization response associated with the glass transition.

A comparison of the dielectric results for XLPEGDA and the PEGDA/MgO series of nanocomposites is presented in **Figure 7.7**. Plots of ϵ' vs. temperature at 130 Hz clearly

show the increasing magnitude of the interfacial polarization component with increasing MgO content; note the absence of this contribution for the unfilled XLPEGDA network. At 130 Hz, there is considerable overlap of the glass transition and interfacial polarization processes, and it is difficult to discern any clear trend in glass transition temperature with increasing MgO loading. The inset plot, however, shows dielectric loss data at 85 kHz (XLPEGDA + 30wt% MgO composite), where there is greater separation between the glass-rubber and interfacial processes. Here, the loss peak associated with the glass transition in the composite is offset upwards by about 8°C as compared to the unfilled polymer network, a result that is in good agreement with the T_g trends obtained from the dynamic mechanical studies.

7.3.3 Nanocomposite Density

The measurement of bulk density for polymer nanocomposite samples can often provide insight as to the nature of the particle dispersion within the polymer matrix. In particular, negative deviations from volume additivity are often indicative of the presence of voids or defects around the filler particles, or the possible formation of agglomerates, features that can have a strong influence on the mechanical and gas transport properties of the composite [38]. For example, gas transport studies on rubbery 1,2-polybutadiene (PB) nanocomposites reported by Matteucci et al. revealed greater than ten-fold increases in CO₂, CH₄ and N₂ permeability in samples loaded with increasing amounts of MgO nanoparticles (up to 27 vol%) [11]. This trend, which runs counter to conventional composite models that predict a reduction in permeability with the incorporation of impermeable filler, was found to correlate with the presence of a substantial void volume fraction in the PB/MgO composites as indicated by density measurements. Bulk density

values for the composites displayed a strong negative deviation relative to predictions based on simple volume additivity, with apparent void volume estimated to be as high as approximately 50%.

Density measurements for the PEGDA/MgO and PEGDA/SiO₂ nanocomposites are reported as a function of particle loading in **Figure 7.8**; each plot includes the prediction for composite density based strictly on volume additivity (ρ_{ADD}):

$$\rho_{\text{ADD}} = \rho_{\text{F}}\phi_{\text{F}} + \rho_{\text{P}}\phi_{\text{P}} \quad (7.4)$$

where ϕ_{F} and ϕ_{P} are the respective filler and polymer volume fractions, and ρ_{F} and ρ_{P} are the corresponding densities ($\rho_{\text{F}} = 2.4 \text{ g/cm}^3$ (MgO), 2.2 g/cm^3 (SiO₂); $\rho_{\text{P}} = 1.183 \text{ g/cm}^3$, as per above). For the PEGDA/MgO composites synthesized without any added diluent, the measured density closely follows the volume additivity model for loadings up to 30 wt% MgO, suggesting relatively little void volume formation during the preparation of these materials. In the case of the PEGDA/SiO₂ composites, a small negative deviation from volume additivity is observed at higher loadings. Estimated void volume fractions range from 0.011 (10 wt% SiO₂) to 0.026 (30 wt% SiO₂).

Additional studies were completed on PEGDA/MgO nanocomposites crosslinked in the presence of toluene, which was added to possibly aid in the dispersion of the nanoparticles prior to UV exposure [11]. The addition of toluene to the prepolymerization mixture has the potential to alter not only the distribution of nanoparticles, but also the properties of the surrounding XLPEGDA matrix. Photopolymerization in the presence of diluent can lead to intramolecular cyclization or loop formation in the polymer network and a corresponding decrease in the effective

crosslink density [39,40]. In a separate publication, the influence of toluene on the characteristics of XLPEGDA networks is studied in detail [41]: photopolymerization of PEGDA crosslinker in the presence of increasing amounts of toluene leads to a systematic reduction in the rubbery modulus of the networks owing to the formation of loops (*i.e.*, “wasted” crosslinks), and this is accompanied by a modest decrease in bulk density ($\rho_P = 1.171 \text{ g/cm}^3$ for samples prepared with 40 wt% toluene). Density values for PEGDA/MgO nanocomposites prepared with varying levels of toluene are included in Figure 7.8a, with toluene content expressed relative to the amount of PEGDA crosslinker in the prepolymerization mixture. For all samples, a negative deviation in bulk density is observed relative to nanocomposites prepared under “neat” conditions. The observed deviation is considerably larger than the density decrease encountered for unfilled XLPEGDA prepared with toluene and may reflect a change in the underlying composite morphology, possibly leading to an increase in particle agglomeration and/or greater void volume within the material. The implications of this result with respect to gas permeability in the samples are discussed below.

7.3.4 Gas Transport

The remarkable increases in gas permeability observed by Matteucci et al. [11,12] for nanoparticle composites based on rubbery 1,2-polybutadiene suggest that similar enhancements could potentially be achieved in CO₂-selective XLPEGDA membrane networks. The inclusion of MgO is of particular interest, as the nanoparticles are basic in character, and have the capacity to adsorb CO₂. In the case of the PB/MgO composites, reversible penetrant sorption by the nanoparticles was a significant factor in determining

gas transport characteristics, both in terms of the gas solubility behavior of the materials, as well as their resultant permeability.

Permeability measurements for the PEGDA/MgO nanocomposites were conducted for CO₂, CH₄, O₂ and H₂ at 35°C and pressures ranging from 3 to 15 atm. The values were extrapolated to an upstream pressure equal to 0, with the reported quantity corresponding to penetrant permeability at infinite dilution. While the measured permeabilities for CH₄, O₂ and H₂ were independent of upstream pressure, CO₂ permeability for the various samples at 15 atm. was ~ 20 to 30% higher than the infinite dilution permeability. Results for the XLPEGDA composites as a function of MgO loading are presented in **Figure 7.9**. For all gases tested, a systematic decrease in permeability is observed with increasing MgO content, accompanied by a small reduction in CO₂/light gas selectivity. The trend of the data follows models that describe molecular transport through a polymer matrix containing impermeable spherical filler particles, *i.e.*, Maxwell's equation [42,43]:

$$\frac{P_C}{P_P} = \frac{(1 - \phi_F)}{(1 + \frac{\phi_F}{2})} \quad (7.5)$$

where P_C is the permeability of the composite and P_P is the permeability of the pure polymer network. The results for CH₄, O₂ and H₂ show good agreement with the Maxwell model (see Figure 7.9), and are consistent with data reported by Patel et al. for PEGDA crosslinked in the presence of modified fumed silica [44,45]. The results for CO₂ permeability in the PEGDA/MgO composites are positioned below the Maxwell prediction, indicating a drop in CO₂ transport with MgO loading that exceeds the anticipated reduction based strictly on the Maxwell expression.

An additional consideration in characterizing the permeability of the PEGDA/MgO composites is the potential influence of toluene diluent present during the sample preparation process. As noted above, the inclusion of toluene in the prepolymerization mixture results in a reduction in the bulk density of the composites as compared to samples prepared under neat conditions. This leads to an increase in the infinite dilution permeability of these samples, as demonstrated for CO₂ in **Figure 7.10**. Those composites prepared in the presence of toluene show markedly higher CO₂ permeability at higher loadings of MgO (*i.e.*, 20 and 40 wt%). However, for all composite samples, permeability remains below the value obtained for the unfilled XLPEGDA network.

Estimates of gas diffusion coefficients from transient flux measurements are given in **Figure 7.11** for CO₂, CH₄ and O₂ (upstream pressure was 4.4 atm). In the case of H₂, the time lag obtained for these samples was too short to establish reliable values. The diffusion coefficients decrease with increasing MgO loading; at 30 wt% (~ 17.5 vol%) MgO, the CO₂ diffusion coefficient is approximately one order of magnitude below that in neat XLPEGDA. This reduction in diffusivity is likely caused by the presence of the impermeable particles (without any significant increase in void volume fraction), which increase the tortuosity of the diffusion path. Another factor is the reduction in chain mobility of the polymer matrix with particle loading, as indicated by increasing glass-rubber transition temperature (*cf.* Figure 7.1). As chain mobility decreases, diffusion coefficients could decrease as well; previous studies have demonstrated the importance of polymer chain mobility in determining the gas diffusion characteristics of crosslinked PEO networks [6,7].

Solubility coefficients can be estimated from the permeability and diffusivity values determined at an upstream pressure of 4.4 atm ($S = P/D$); these results are presented in **Figure 7.12**. A significant increase in CO₂ solubility was observed with increasing MgO loading, in a manner consistent with the rubbery PB/MgO composites described by Matteucci et al [11]. In the latter case, increased CO₂ solubility was attributed to strong gas adsorption by the MgO nanoparticles. However, the marked increase in void volume fraction observed in the PB/MgO system was not apparent in the *in-situ* polymerized PEGDA/MgO composites studied here. Thus, the potential benefits obtained from reversible CO₂ sorption by the nanoparticles are offset by decreasing overall gas diffusivity, which accounts for the lack of any significant enhancement in permeability for the PEGDA/MgO system.

7.4 Conclusions

The glass transition and gas transport characteristics of a series of polymer nanoparticle composites based on crosslinked poly(ethylene oxide) have been investigated. UV photopolymerization of poly(ethylene glycol) diacrylate crosslinker in the presence of MgO or SiO₂ nanoparticles led to the formation of rubbery, amorphous nanocomposite networks. Bulk density values for the nanocomposites were close to volume additivity predictions, with only minimal void volume fraction indicated at higher particle loadings. The introduction of the nanoparticles in the XLPEGDA network led to a modest increase in glass transition temperature for both systems as measured by dynamic mechanical and dielectric methods (T_g increased by as much as 6°C), but glass-rubber relaxation breadth remained essentially unchanged with particle loading. The relationship between rubbery modulus and filler content was described by the Mooney equation, with the resulting

parameters suggesting some degree of particle agglomeration within the matrix. Gas permeability measurements on the PEGDA/MgO series of samples indicated a decrease in infinite dilution permeability with increasing particle loading that stood in contrast to prior results reported for rubbery 1,2-polybutadiene/MgO composites. The decrease in permeability was attributable to reduced penetrant diffusivity in the composites, which offset enhancements in (CO₂) gas solubility resulting from nanoparticle adsorption. PEGDA/MgO nanocomposites prepared in the presence of toluene displayed somewhat higher permeability values as compared to the neat formulations, the data correlating with reduced bulk density and potentially greater void volume in the material.

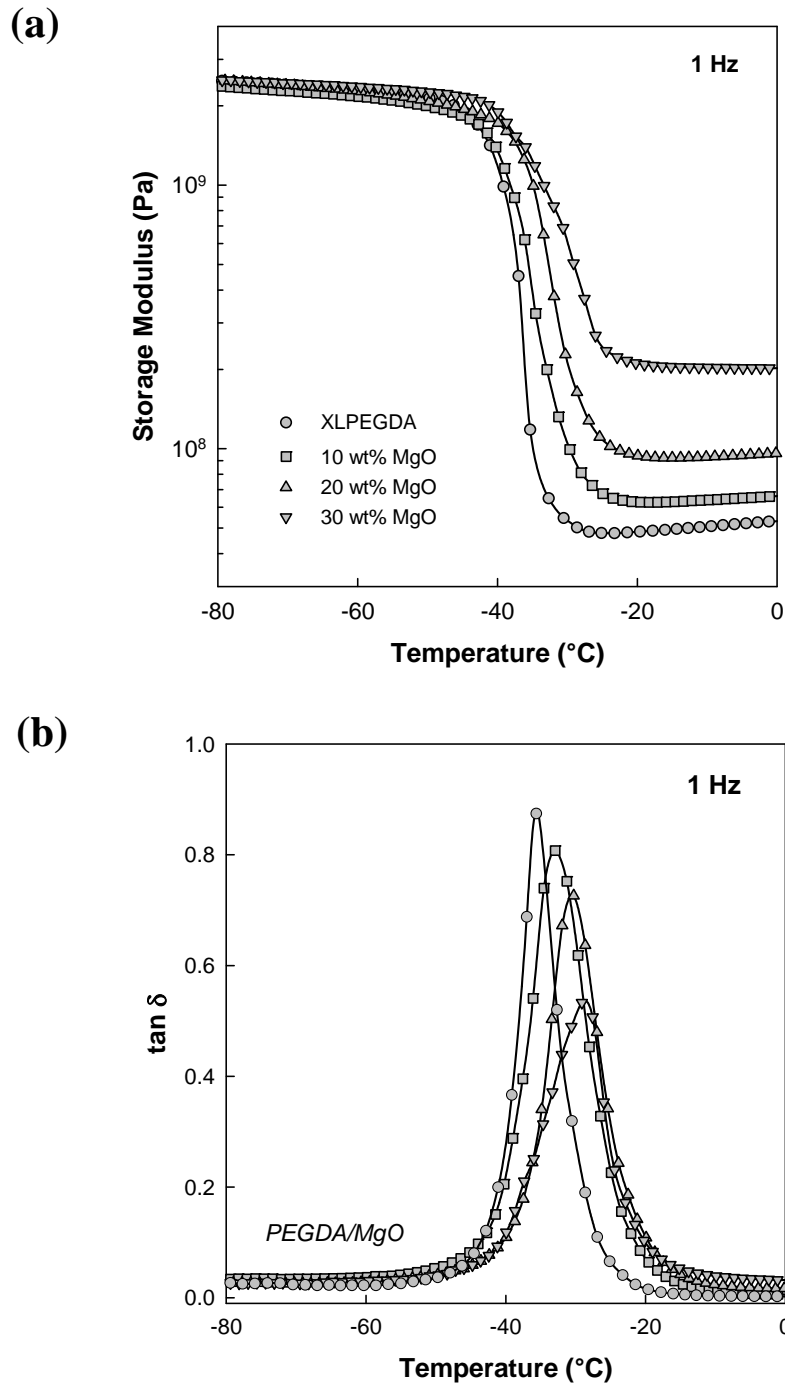


Figure 7.1: Dynamic mechanical properties vs. temperature (°C) for PEGDA/MgO nanocomposites. (a) storage modulus (Pa); (b) $\tan \delta$. Frequency of 1 Hz; heating rate of 1°C/min.

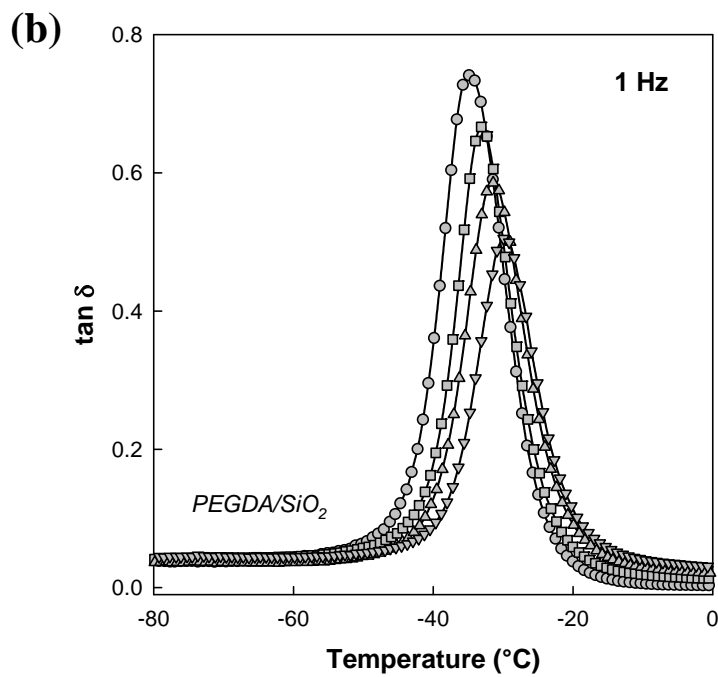
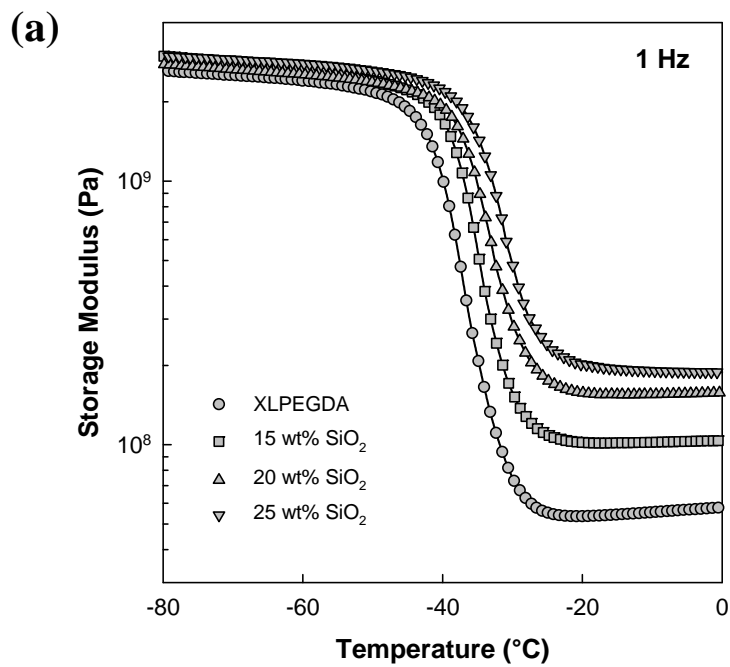


Figure 7.2: Dynamic mechanical properties vs. temperature (°C) for PEGDA/SiO₂ nanocomposites. (a) storage modulus (Pa); (b) tan δ . Frequency of 1 Hz; heating rate of 1°C/min.

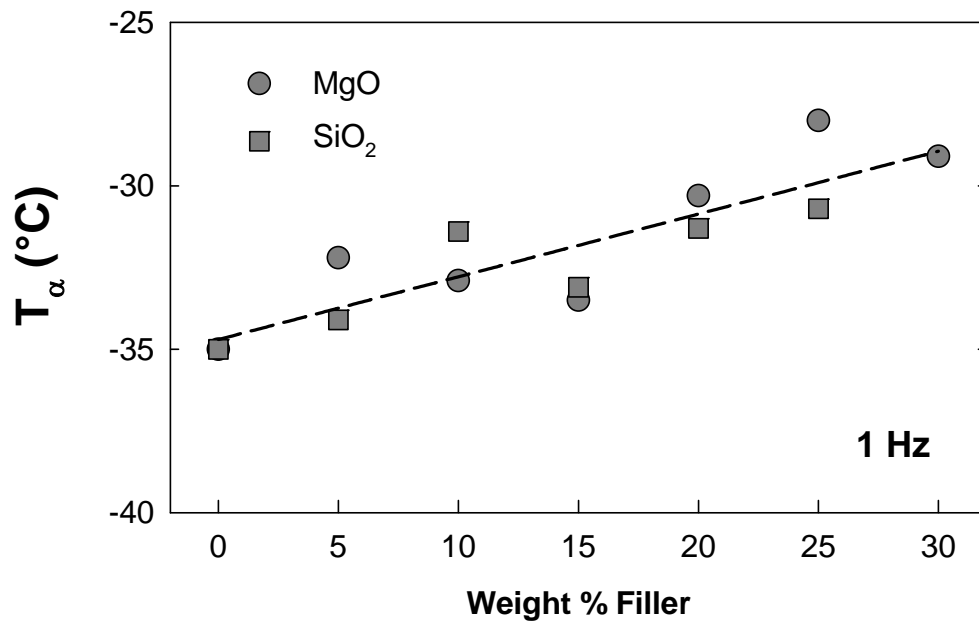


Figure 7.3: Dynamic mechanical peak temperature (°C) vs. weight percent filler for XLPEGDA nanocomposites; glass-rubber transition.

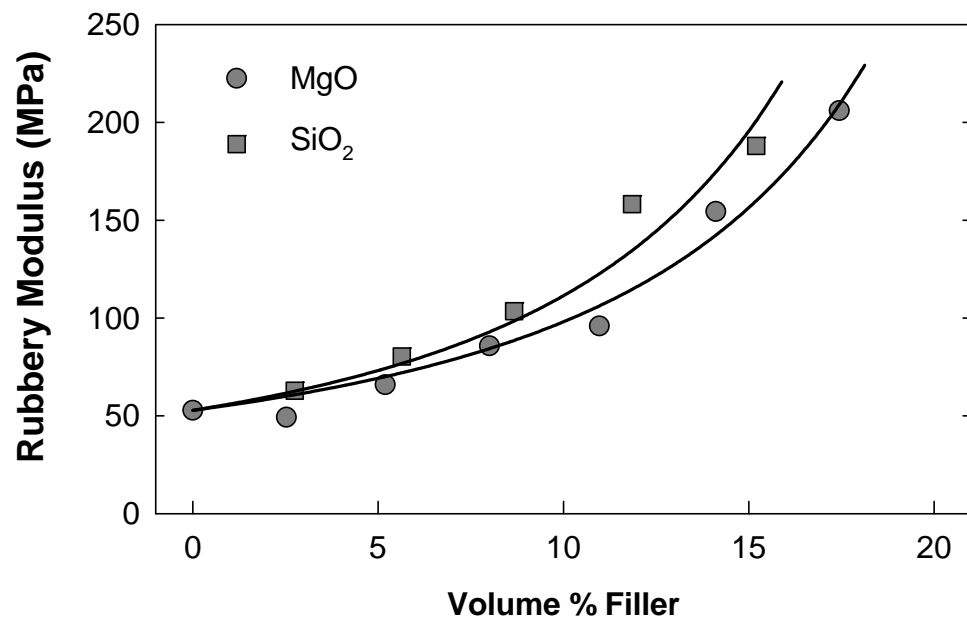


Figure 7.4: Rubbery modulus (0°C; MPa) vs. volume percent filler for XLPEGDA nanocomposites. Curves are best-fits to Eq. (7.2).

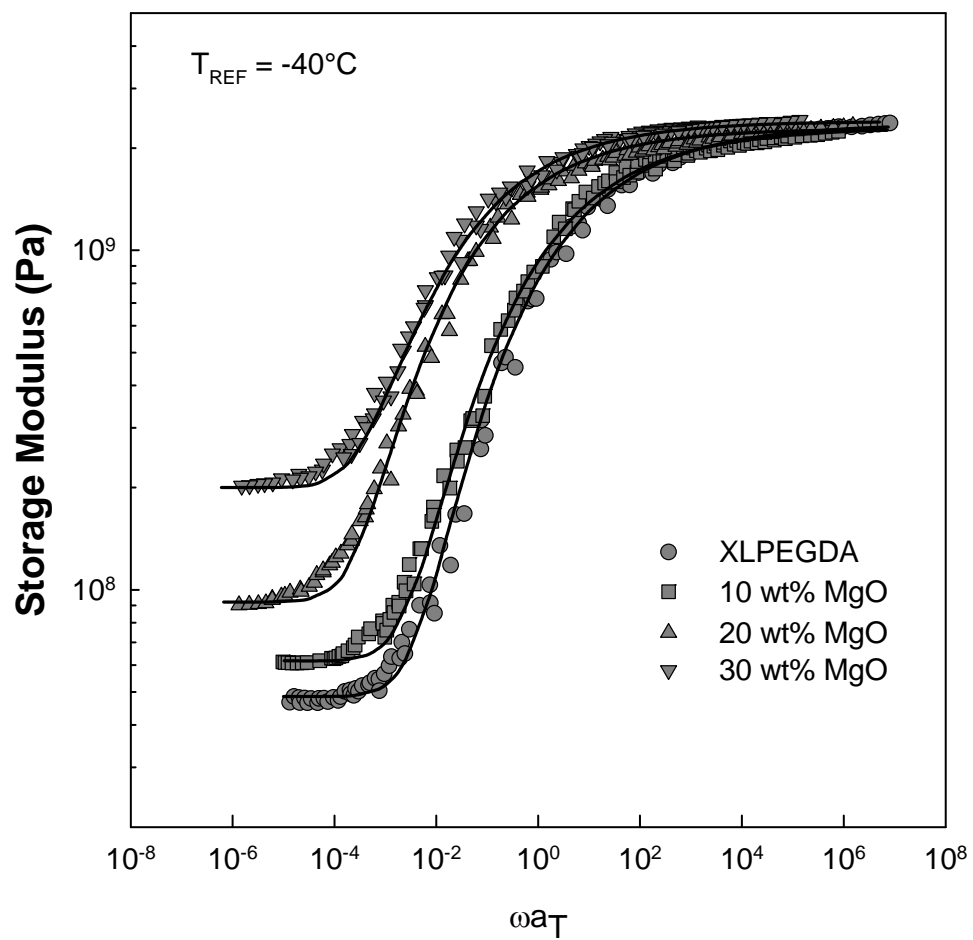


Figure 7.5: Time-temperature master curves (E' vs. ωa_T) for PEGDA/MgO nanocomposites. Reference temperature of -40°C . Solid curves from KWW equation.

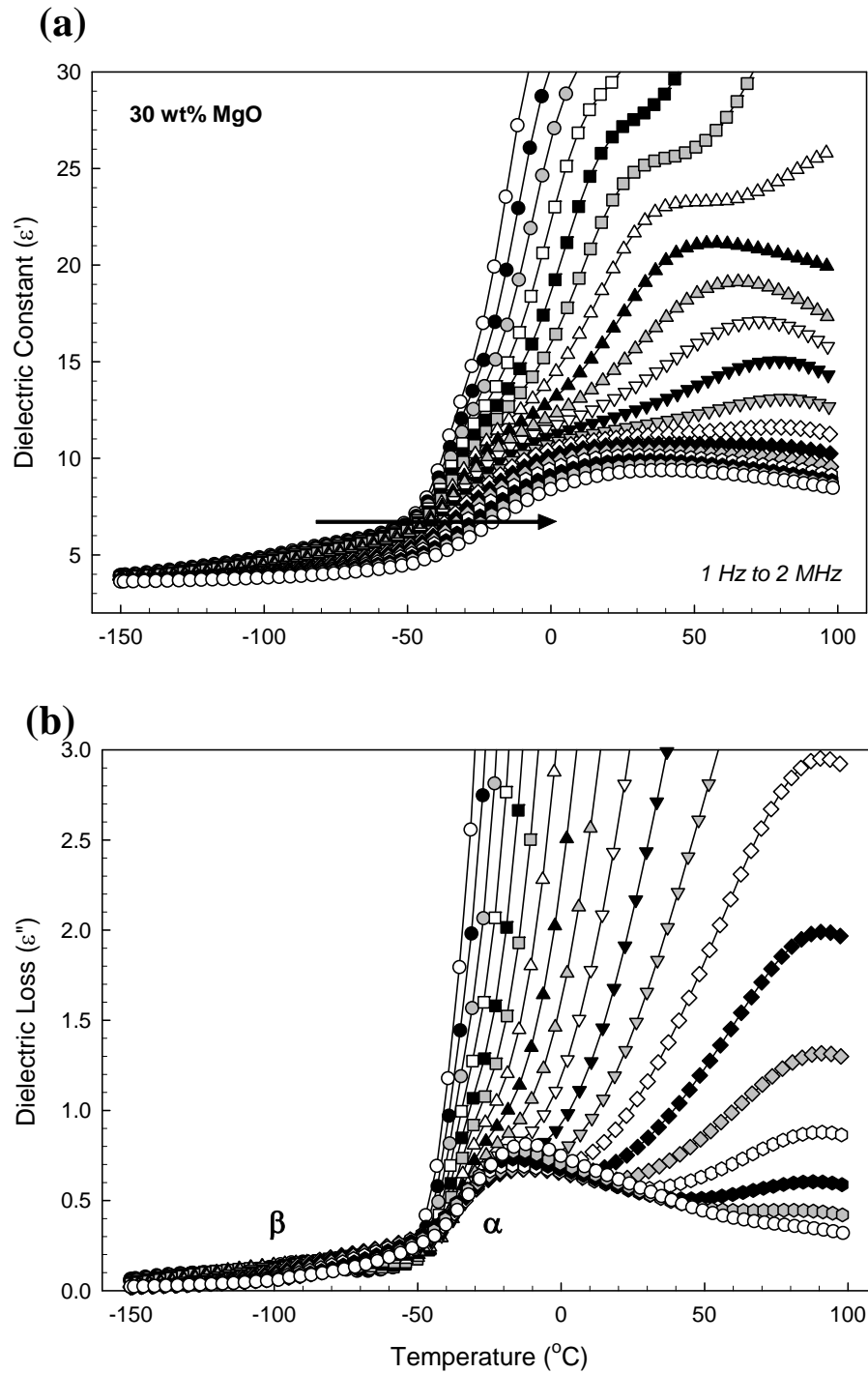


Figure 7.6: Dielectric properties vs. temperature ($^{\circ}\text{C}$) for PEGDA + 30 wt% MgO nanocomposite. (a) dielectric constant; (b) dielectric loss. Heating rate of $2^{\circ}\text{C}/\text{min.}$; frequencies from 1 Hz to 2 MHz. Arrow indicates direction of increasing test frequency.

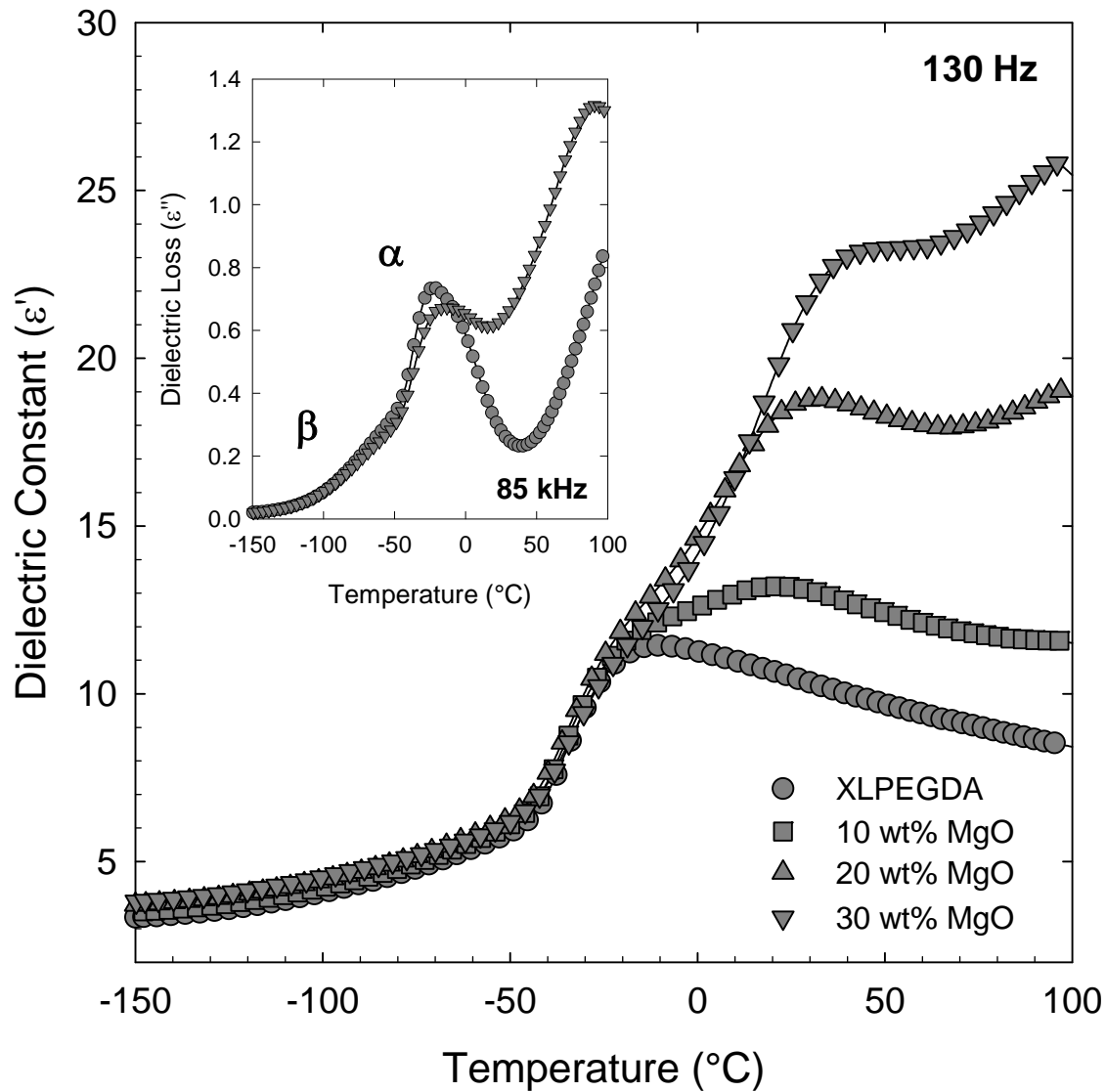


Figure 7.7: Dielectric constant vs. temperature ($^{\circ}\text{C}$) for PEGDA/MgO nanocomposites at 130 Hz. *Inset:* dielectric loss vs. temperature for XLPEGDA and 30 wt% MgO composite at 85 kHz.

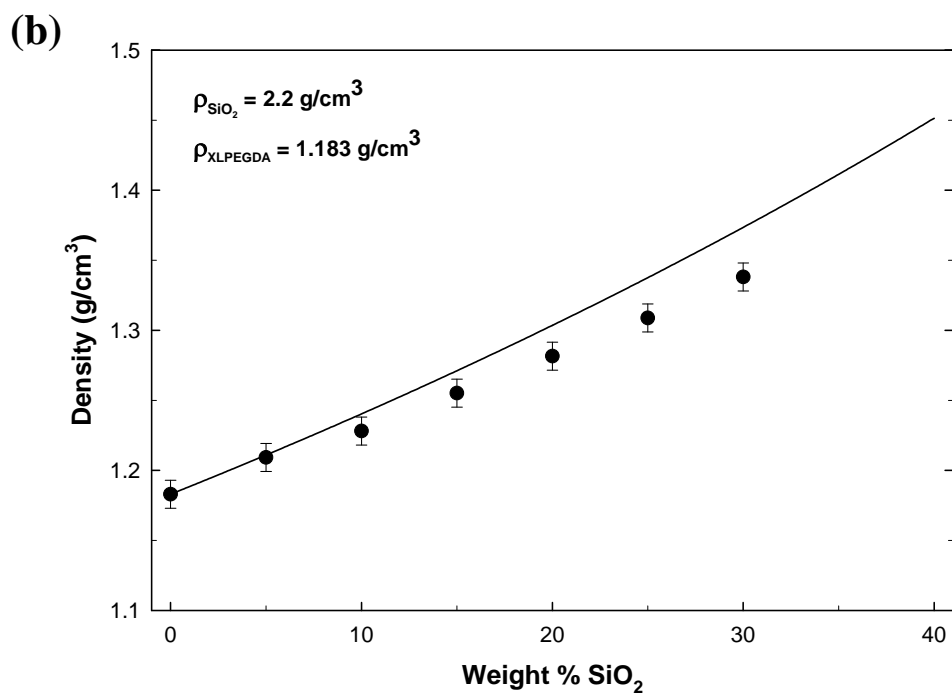
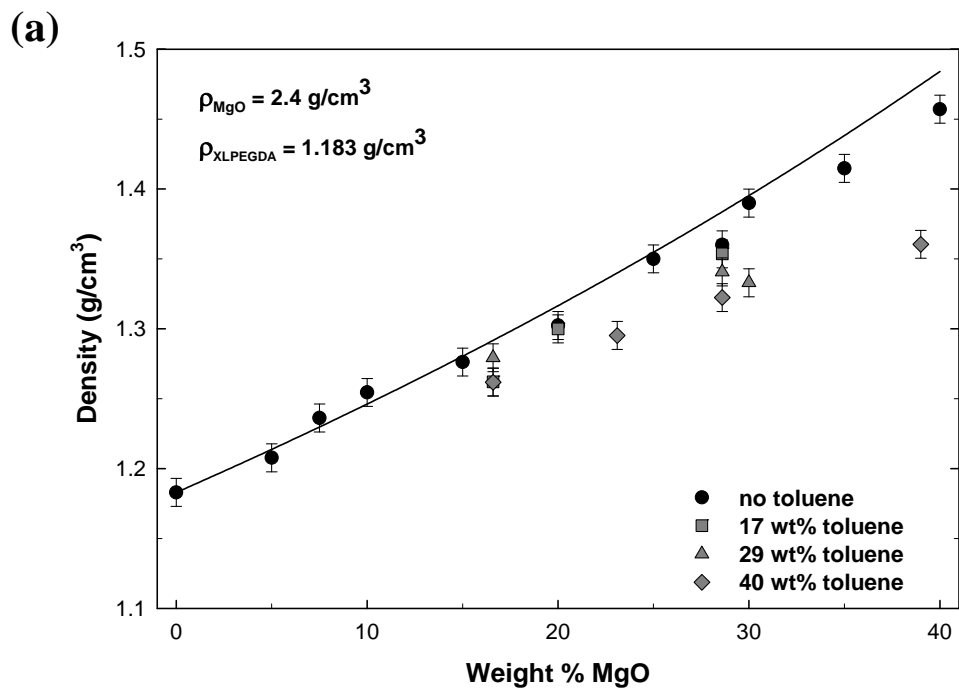


Figure 7.8: Density (g/cm^3) vs. weight percent filler for XLPEGDA nanocomposites: (a) PEGDA/MgO; (b) PEGDA/SiO₂. Solid curve corresponds to volume additivity prediction, per Eq. (7.4).

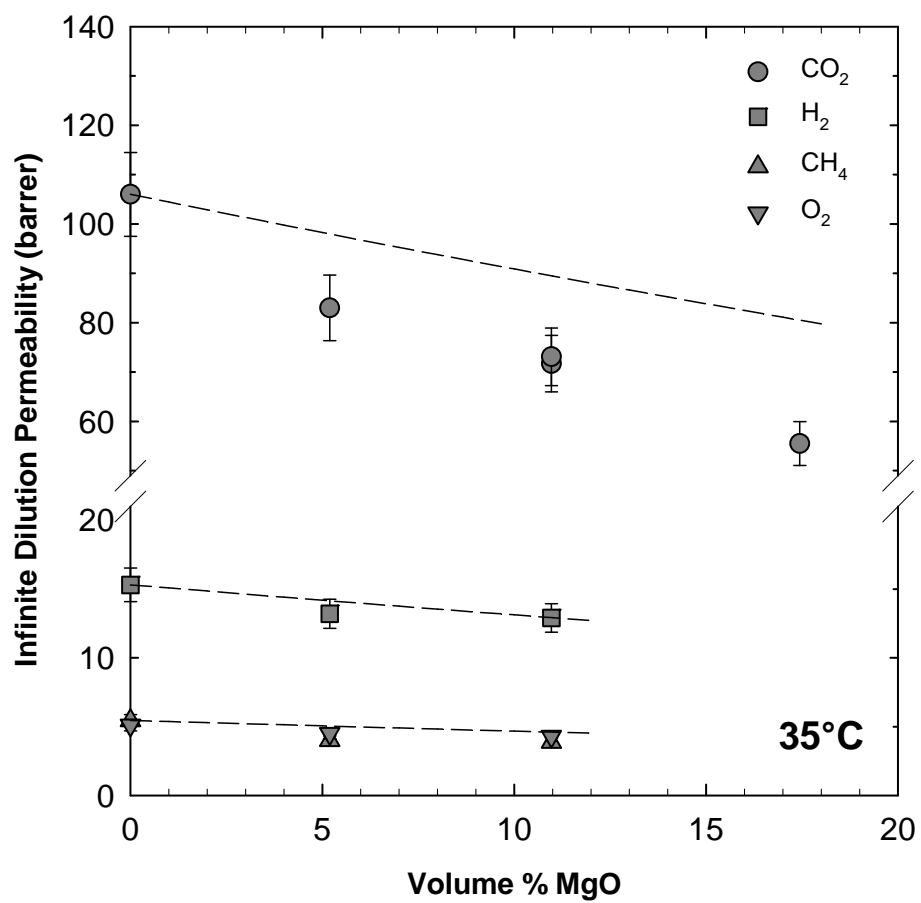


Figure 7.9: Infinite dilution permeability (barrer) vs. volume percent filler for PEGDA/MgO nanocomposites at 35°C. Dashed lines correspond to Maxwell model, Eq. (7.5). 1 barrer = 10^{-10} cm³ (STP) cm/cm²s cmHg = 7.5×10^{-18} m³ (STP) m/m²s Pa.

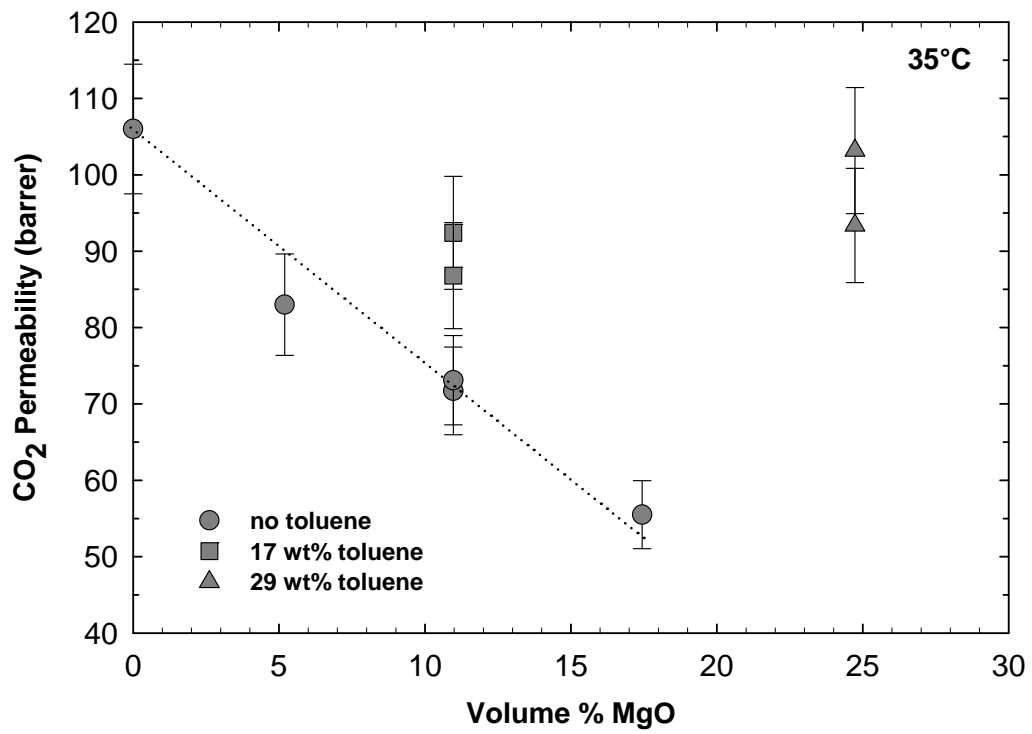


Figure 7.10: CO₂ permeability at infinite dilution (barrer) vs. volume percent filler for PEGDA/MgO nanocomposites at 35°C. Dotted line is a guide for the eye.

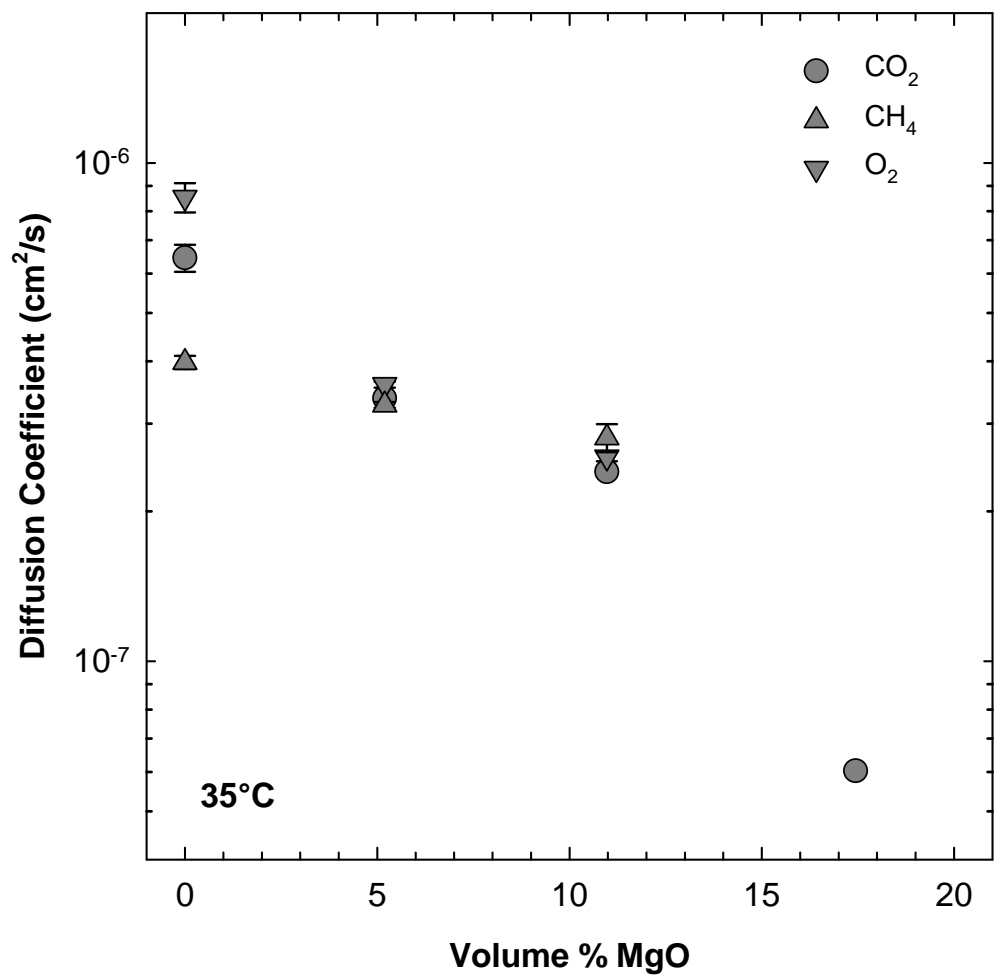


Figure 7.11: Diffusion coefficients at ~ 4.4 atm upstream pressure (cm²/s) vs. volume percent filler for PEGDA/MgO nanocomposites at 35°C, as estimated from transient transport measurements.

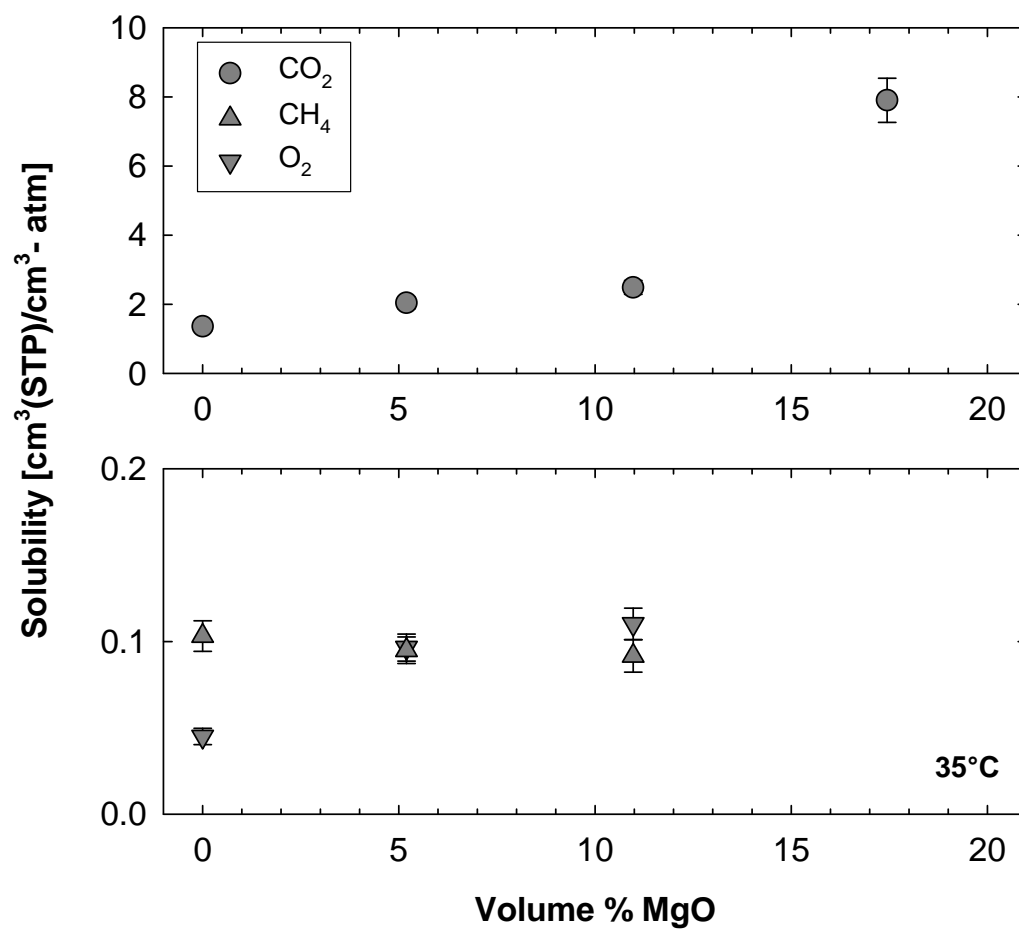


Figure 7.12: Solubility coefficients ($S = P/D$; $\text{cm}^3(\text{STP})/\text{cm}^3\text{-atm}$) at ~ 4.4 atm upstream pressure vs. volume percent filler for PEGDA/MgO nanocomposites at 35°C .

References

- [1] Lin, H.; Van Wagner, E.; Freeman, B.D.; Toy, L.G.; Gupta, R.P. "Plasticization-Enhanced Hydrogen Purification Using Polymeric Membranes", *Science* **2006**, *311*, 639.
- [2] Lin, H.; Van Wagner, E.; Raharjo, R.; Freeman, B.D.; Roman, I. "High-Performance Polymer Membranes for Natural-Gas Sweetening", *Advanced Materials* **2006**, *18*, 39.
- [3] Lin, H.; Freeman, B.D. "Materials Selection Guidelines for Membranes that Remove CO₂ from Gas Mixtures", *Journal of Molecular Structure* **2005**, *739*, 57.
- [4] Lin, H.; Kai, T.; Freeman, B.D.; Kalakkunnath, S.; Kalika, D.S. "The Effect of Crosslinking on Gas Permeability in Cross-linked Poly(ethylene glycol) Diacrylate", *Macromolecules* **2005**, *38*, 8381.
- [5] Lin, H.; Van Wagner, E.; Swinnea, J.S.; Freeman, B.D.; Pas, S.J.; Hill, A.J.; Kalakkunnath, S.; Kalika, D.S. "Transport and Structural Characteristics of Crosslinked Poly(ethylene oxide) Rubbers", *Journal of Membrane Science* **2006**, *276*, 145.
- [6] Kusuma, V.A.; Freeman, B.D.; Borns, M.A.; Kalika, D.S. "Influence of Chemical Structure of Short Chain Pendant Groups on Gas Transport Properties of Cross-linked Poly(ethylene oxide) Copolymers", *Journal of Membrane Science* **2009**, *327*, 195.
- [7] Kusuma, V.A.; Matteucci, S.; Freeman, B.D.; Danquah, M.K.; Kalika, D.S. "Influence of Phenoxy-Terminated Short Chain Pendant Groups on Gas Transport Properties of Crosslinked Poly(ethylene oxide) Copolymers", *Journal of Membrane Science* **2009**, *341*, 84.
- [8] Richards, J.J.; Danquah, M.K.; Kalakkunnath, S.; Kalika, D.S.; Kusuma, V.A.; Matteucci, S.T.; Freeman, B.D. "Relation Between Structure and Gas Transport Properties of Polyethylene Oxide Networks Based on Crosslinked Bisphenol A Ethoxylate Diacrylate", *Chemical Engineering Science* **2009**, *64*, 4707.
- [9] Merkel, T.C.; Freeman, B.D.; Spontak, R.J.; He, Z.; Pinnau, I.; Meakin, P.; Hill, A.J. "Ultraporous, Reverse-Selective Nanocomposite Membranes", *Science* **2002**, *296*, 519.
- [10] Merkel, T.C.; Freeman, B.D.; Spontak, R.J.; He, Z.; Pinnau, I.; Meakin, P.; Hill, A.J. "Sorption, Transport, and Structural Evidence for Enhanced Free Volume in Poly (4-methyl-2-pentyne)/Fumed Silica Nanocomposite Membranes", *Chemistry of Materials* **2003**, *15*, 109.

- [11] Matteucci, S.; Raharjo, R.D.; Kusuma, V.A.; Swinnea, S.; Freeman, B.D. "Gas Permeability, Solubility, and Diffusion Coefficients in 1,2-Polybutadiene Containing Magnesium Oxide", *Macromolecules* **2008**, *41*, 2144.
- [12] Matteucci, S.; Kusuma, V.A.; Swinnea, S.; Freeman, B.D. "Gas Permeability, Solubility and Diffusivity in 1,2-Polybutadiene Containing Brookite Nanoparticles", *Polymer* **2008**, *49*, 757.
- [13] Matteucci, S.; Yampolskii, Y.; Freeman, B.D.; Pinnau, I., "Transport of gases and vapors in glassy and rubbery polymers", In *Materials Science of Membranes for Gas and Vapor Separation*; Yampolskii, Y.; Pinnau, I.; Freeman, B.D., eds.; John Wiley and Sons: New York, **2006**; pp 1-47.
- [14] Nielsen, L.E.; Landel, R.F. *Mechanical Properties of Polymers and Composites*, 2nd edition; Marcel Dekker: New York, **1994**.
- [15] Yim, A.; Chahal, R.S.; St. Pierre, L.E. "Effect of Polymer-Filler Interaction Energy on the T_g (glass transition temperature) of Filled Polymers", *Journal of Colloid and Interface Science* **1973**, *43*, 583.
- [16] Reid, C.G.; Greenberg, A.R. "Influence of Silica Reinforcement Upon the Glass-Transition Behavior of Acrylic Polymers", *Journal of Applied Polymer Science* **1990**, *39*, 995.
- [17] Tsagaropoulos, G.; Eisenberg, A. "Direct Observation of Two Glass Transitions in Silica-Filled Polymers. Implications for the Morphology of Random Ionomers", *Macromolecules* **1995**, *28*, 396.
- [18] Tsagaropoulos, G.; Eisenberg, A. "Dynamic Mechanical Study of the Factors Affecting the Two Glass Transition Behavior of Filled Polymers. Similarities and Differences with Random Ionomers", *Macromolecules* **1995**, *28*, 6067.
- [19] Arrighi, V.; McEwen, I.J.; Qian, H.; Prieto, M.B.S. "The Glass Transition and Interfacial Layer in Styrene-Butadiene Rubber Containing Silica Nanofiller", *Polymer* **2003**, *44*, 6259.
- [20] Ash, B.J.; Siegel, R.W.; Schadler, L.S. "Glass-Transition Temperature Behavior of Alumina/PMMA Nanocomposites", *Journal of Polymer Science, Part B: Polymer Physics* **2004**, *42*, 4371.
- [21] Bansal, A.; Yang, H.; Li, C.; Benicewicz, B.C.; Kumar, S.K.; Schadler, L.S. "Controlling the Thermomechanical Properties of Polymer Nanocomposites by Tailoring the Polymer-Particle Interface", *Journal of Polymer Science, Part B: Polymer Physics* **2006**, *44*, 2944.

- [22] Bansal, A.; Yang, H.; Li, C.; Cho, K.; Benicewicz, B.C.; Kumar, S.K.; Schadler, L.S. "Quantitative Equivalence Between Polymer Nanocomposites and Thin Polymer Films", *Nature Materials* **2005**, *4*, 693.
- [23] Rittigstein, P.; Torkelson, J.M. "Polymer-Nanoparticle Interfacial Interactions in Polymer Nanocomposites: Confinement Effects on Glass Transition Temperature and Suppression of Physical Aging", *Journal of Polymer Science, Part B: Polymer Physics* **2006**, *44*, 2935.
- [24] Rittigstein, P.; Priestley, R.D.; Broadbelt, L.J.; Torkelson, J.M. "Model Polymer Nanocomposites Provide an Understanding of Confinement Effects in Real Nanocomposites", *Nature Materials* **2007**, *6*, 278.
- [25] Lin, H. "*Solubility Selective Membrane Materials for Carbon Dioxide Removal from Mixtures with Light Gases*"; Ph.D. Dissertation University of Texas at Austin: Austin, TX, **2005**.
- [26] Bondar, V.I.; Freeman, B.D.; Pinnau, I. "Gas Transport Properties of Poly(ether-b-amide) Segmented Block Copolymers", *Journal of Polymer Science, Part B: Polymer Physics* **2000**, *38*, 2051.
- [27] Lin, H.; Freeman, B.D., "Permeation and Diffusion", In *Springer Handbook of Materials Measurement Methods*; Czichos, H.; Saito, T.; Smith, L.E., eds.; Springer: Berlin, **2006**; pp 371-387.
- [28] Daynes, H.A. "The Process of Diffusion Through a Rubber Membrane", *Proceedings of the Royal Society of London, Series A: Mathematical, Physical and Engineering Sciences* **1920**, *97*, 286.
- [29] Wijmans, J.G.; Baker, R.W. "The Solution-Diffusion Model: A Review", *Journal of Membrane Science* **1995**, *107*, 1.
- [30] Schwarzl, F.R.; Bree, H.W.; Nederveen, C.J.; Schwippert, G.A.; Struik, L.C.E.; Van der Wal, C.W. "Behavior of Unfilled and Filled Rubbers in Shear in the Glass-Rubber Transition Region", *Rheologica Acta* **1966**, *5*, 270.
- [31] Mooney, M. "The Viscosity of a Concentrated Suspension of Spherical Particles", *Journal of Colloid Science* **1951**, *6*, 162.
- [32] Ferry, J.D. *Viscoelastic Properties of Polymers*, 3rd edition; John Wiley and Sons: New York, **1980**.
- [33] Williams, G.; Watts, D.C.; Dev, S.B.; North, A.M. "Further Considerations of Non Symmetrical Dielectric Relaxation Behaviour Arising From a Simple Empirical Decay Function", *Transactions of the Faraday Society* **1971**, *67*, 1323.

- [34] Steeman, P.A.M.; van Turnhout, J., "Dielectric Properties of Inhomogeneous Media", In *Broadband Dielectric Spectroscopy*; Kremer, F.; Schönhals, A., eds.; Springer-Verlag: Berlin, **2003**; pp 495-522.
- [35] Kalakkunnath, S.; Kalika, D.S.; Lin, H.; Raharjo, R.D.; Freeman, B.D. "Molecular Relaxation in Cross-linked Poly(Ethylene Glycol) and Poly(Propylene Glycol) Diacrylate Networks by Dielectric Spectroscopy", *Polymer* **2007**, *48*, 579.
- [36] Kalakkunnath, S.; Kalika, D.S.; Lin, H.; Raharjo, R.D.; Freeman, B.D. "Molecular Dynamics of Poly(Ethylene Glycol) and Poly(Propylene Glycol) Copolymer Networks by Broadband Dielectric Spectroscopy", *Macromolecules* **2007**, *40*, 2773.
- [37] Borns, M.A.; Kalakkunnath, S.; Kalika, D.S.; Kusuma, V.A.; Freeman, B.D. "Dynamic Relaxation Characteristics of Crosslinked Poly(ethylene oxide) Copolymer Networks: Influence of Short Chain Pendant Groups", *Polymer* **2007**, *48*, 7316.
- [38] Takahashi, S.; Paul, D.R. "Gas Permeation in Poly(Ether Imide) Nanocomposite Membranes Based on Surface-Treated Silica. Part 1: Without Chemical Coupling to Matrix", *Polymer* **2006**, *47*, 7519.
- [39] Okay, O.; Kurz, M.; Lutz, K.; Funke, W. "Cyclization and Reduced Pendant Vinyl Group Reactivity During the Free-Radical Cross-Linking Polymerization of 1,4-Divinylbenzene", *Macromolecules* **1995**, *28*, 2728.
- [40] Kizilay, M.; Okay, O. "Effect of Initial Monomer Concentration on Spatial Homogeneity in Poly(acrylamide) Gels", *Macromolecules* **2003**, *36*, 6856.
- [41] Kusuma, V.A.; Freeman, B.D.; Smith, S.L.; Heilman, A.L.; Kalika, D.S. "Influence of TRIS-based Co-monomer on Structure and Gas Transport Properties of Cross-linked Poly(ethylene oxide)", *Journal of Membrane Science* **2010**, *359*, 25.
- [42] Barrer, R.M., In *Diffusion in Polymers*; Crank, J.; Park, G.S., eds.; Academic Press: New York, **1968**; pp 165-217.
- [43] Maxwell, C. *Treatise on Electricity and Magnetism*; Oxford University Press: London, **1873**; Vol. 1.
- [44] Patel, N.P.; Miller, A.C.; Spontak, R.J. "Highly CO₂-Permeable and Selective Polymer Nanocomposite Membranes", *Advanced Materials* **2003**, *15*, 729.

- [45] Patel, N.P.; Miller, A.C.; Spontak, R.J. "Highly CO₂-Permeable and Selective Membranes Derived from Crosslinked Poly(Ethylene Glycol) and its Nanocomposites", *Advanced Functional Materials* **2004**, *14*, 699.

Chapter 8

Conclusions

The dynamic relaxation properties of aromatic polyimides and polymer nanocomposites were investigated using dynamic mechanical and dielectric methods. Aromatic polyimides included commercially available BTDA-DAPI (Matrimid[®]) and custom-synthesized functionalized polymers (HAB-6FDA, APAF-ODPA, and APAF-6FDA) capable of undergoing thermal rearrangement to PBOs. Polymer nanocomposites consisted of poly (ether imide) [PEI] and poly (methyl methacrylate) [PMMA] based materials loaded with native and modified silica filler, and poly (ethylene glycol diacrylate) [PEGDA] networks crosslinked in the presence of MgO and native silica. For the nanocomposite systems, investigations focused on the effect of filler loading and surface chemistry on the glass-rubber and sub-glass relaxations.

Key findings of this work are summarized as follows:

- Investigation of the viscoelastic properties of BTDA-DAPI (Matrimid[®]) revealed two sub-glass relaxations at -112°C (T_{γ}) and 80°C (T_{β}) and the glass-rubber relaxation ($T_{\alpha} = 313^{\circ}\text{C}$) based on the measured maxima in mechanical loss modulus at 1 Hz. The γ transition activation energy ($E_{A,\gamma}$) of 43 kJ/mol was consistent across both the dynamic mechanical and dielectric results. The β transition was more cooperative in character, with a dynamic mechanical $E_{A,\beta}$ of 156 kJ/mol and dielectric $E_{A,\beta}$ of 99 kJ/mol. Time-temperature superposition was employed to establish mechanical master curves across the glass-rubber (α) relaxation and these data could be described using the Kohlrausch-Williams-

Watts function with a corresponding exponent value, $\beta_{\text{KWW}} = 0.34$. A cooperativity plot was used to establish the dynamic fragility of the polymer. The value of the fragility index ($m = 115$) reflected the relatively rigid character of the polyimide backbone, and the observed relation between fragility and β_{KWW} was consistent with the correlation reported in the literature for a wide variety of polymers.

- Dynamic mechanical and dielectric analysis of the HAB-6FDA, APAF-ODPA, and APAF-6FDA polyimides provided essential insight regarding their stability and thermal rearrangement characteristics as a function of both prior thermal history and *in situ* exposure during thermal analysis testing. The sub-glass relaxations in particular reflected distinct local molecular motions that differed based on polymer synthesis method (*i.e.*, chemically or thermally imidized), the extent of thermal conversion, and the influence of moisture. Further studies are required to fully correlate backbone structure and degree of thermal rearrangement to membrane separation performance.
- The dynamic relaxation characteristics of PEI- and PMMA-based polymer nanocomposites were investigated as a function of nanoparticle loading and surface chemistry. Nanoparticles consisted of native SiO₂ and hydrophobic surface-modified silicas. The nanocomposites displayed a “dual-T_g” relaxation behavior: a lower-temperature transition (T_{g1}) corresponding to the relaxation of bulk polymer, and a higher-temperature transition (T_{g2}) reflecting the relaxation of polymer segments constrained owing to their proximity to the polymer-particle

interface. However, dielectric studies on the PEI and PMMA nanocomposites showed no perturbation of the time-temperature characteristics of the local sub-glass relaxations with the presence of nanoscale filler. For the bulk glass-rubber transition (T_{gl}), both dynamic mechanical and dielectric results indicated time-temperature characteristics that were independent of filler content and that followed a single, cooperative Williams-Landel-Ferry (WLF) expression at all composite loadings.

- The glass transition and gas transport characteristics of UV photopolymerized poly(ethylene glycol) diacrylate (PEGDA) networks crosslinked in the presence of MgO and SiO₂ nanoparticles was investigated. Incorporation of the nanoparticles in the crosslinked PEGDA network produced a small increase in glass transition temperature for both systems as measured via dynamic mechanical and dielectric methods, with T_g increasing by up to 6°C. Gas permeability measurements on the PEGDA/MgO series of samples indicated a decrease in permeability with increasing particle loading that was attributed to reduced penetrant diffusivity in the composites, which offset enhancements in (CO₂) gas solubility. PEGDA/MgO nanocomposites prepared in the presence of toluene showed a slight enhancement in permeability.

BIBLIOGRAPHY

- Arnold, F.E., Jr.; Bruno, K.R.; Shen, D.; Eashoo, M.; Lee, C.J.; Harris, F.W.; Cheng, S.Z.D. "The Origin of β Relaxations in Segmented Rigid-Rod Polyimide and Copolyimide Films", *Polymer Engineering and Science* **1993**, *33*, 1373.
- Arrighi, V.; McEwen, I.; Qian, H.; Prieto, M. "The Glass Transition and Interfacial Layer in Styrene-Butadiene Rubber Containing Silica Nanofiller", *Polymer* **2003**, *44*, 6259.
- Ash, B.J.; Rogers, D.F.; Wiegand, C.J.; Schadler, L.S.; Siegel, R.W.; Benicewicz, B.C.; Apple, T. "Mechanical Properties of Al₂O₃/Polymethylmethacrylate Nanocomposites", *Polymer Composites* **2002**, *23*, 1014.
- Ash, B.J.; Siegel, R.W.; Schadler, L.S. "Glass-Transition Temperature Behavior of Alumina/PMMA Nanocomposites", *Journal of Polymer Science, Part B: Polymer Physics* **2004**, *42*, 4371.
- Balazs, A.C.; Emrick, T.; Russell, T.P. "Nanoparticle Polymer Composites: Where Two Small Worlds Meet", *Science* **2006**, *314*, 1107.
- Bansal, A.; Yang, H.; Li, C.; Benicewicz, B.C.; Kumar, S.K.; Schadler, L.S. "Controlling the Thermomechanical Properties of Polymer Nanocomposites by Tailoring the Polymer-Particle Interface", *Journal of Polymer Science, Part B: Polymer Physics* **2006**, *44*, 2944.
- Bansal, A.; Yang, H.; Li, C.; Cho, K.; Benicewicz, B.C.; Kumar, S.K.; Schadler, L.S. "Quantitative Equivalence Between Polymer Nanocomposites and Thin Polymer Films", *Nature Materials* **2005**, *4*, 693.
- Barrer, R.M., In *Diffusion in Polymers*; Crank, J.; Park, G.S., eds.; Academic Press: New York, **1968**; pp 165-217.
- Bas, C.; Tamagna, C.; Pascal, T.; Alberola, N.D. "On the Dynamic Mechanical Behavior of Polyimides Based on Aromatic and Alicyclic Dianhydrides", *Polymer Engineering & Science* **2003**, *43*, 344.
- Bateman, J.; Gordon, D.A. "Soluble Polyimides Derived from Phenylindane Diamines and Dianhydrides", *US Patent 3,856,752* **1974**.
- Bohmer, R.; Ngai, K.L.; Angell, C.A.; Plazek, D.J. "Nonexponential Relaxations in Strong and Fragile Glass Formers", *Journal of Chemical Physics* **1993**, *99*, 4201.

- Bondar, V.I.; Freeman, B.D.; Pinnau, I. "Gas Transport Properties of Poly(ether-b-amide) Segmented Block Copolymers", *Journal of Polymer Science, Part B: Polymer Physics* **2000**, *38*, 2051.
- Borns, M.A.; Kalakkunnath, S.; Kalika, D.S.; Kusuma, V.A.; Freeman, B.D. "Dynamic Relaxation Characteristics of Crosslinked Poly(ethylene oxide) Copolymer Networks: Influence of Short Chain Pendant Groups", *Polymer* **2007**, *48*, 7316.
- Bos, A.; Punt, I.G.M.; Wessling, M.; Strathmann, H. "Plasticization-Resistant Glassy Polyimide Membranes for CO₂/CH₄ Separations", *Separation and Purification Technology* **1998**, *14*, 27.
- Bos, A.; Punt, I.; Strathmann, H.; Wessling, M. "Suppression of Gas Separation Membrane Plasticization by Homogeneous Polymer Blending", *AIChE Journal* **2001**, *47*, 1088.
- Bristow, J.F.; Kalika, D.S. "Investigation of Semicrystalline Morphology in Poly(ether ether ketone)/Poly(ether imide) Blends by Dielectric Relaxation Spectroscopy", *Polymer* **1997**, *38*, 287.
- Bryant, R.G. *Polyimides*; John Wiley & Sons: New York, **2002**.
- Calleja, R.D.; Friederichs, S.; Jaimes, C.; Sanchis, M.J.; Belana, J.; Canadas, J.C.; Diego, J.A.; Mudarra, M. "Comparative Study of Mechanical and Electrical Relaxations in Poly(etherimide). Part 2", *Polymer International* **1998**, *46*, 20.
- Chen, L.; Zheng, K.; Tian, X.; Hu, K.; Wang, R.; Liu, C.; Li, Y.; Cui, P. "Double Glass Transitions and Interfacial Immobilized Layer in in-Situ-Synthesized Poly(vinyl alcohol)/Silica Nanocomposites", *Macromolecules* **2010**, *43*, 1076.
- Cheng, S.Z.D.; Chalmers, T.M.; Gu, Y.; Yoon, Y.; Harris, F.W.; Cheng, J.; Fone, M.; Koenig, J.L. "Relaxation Processes and Molecular Motion in a New Semicrystalline Polyimide", *Macromolecular Chemistry and Physics* **1995**, *196*, 1439.
- Coburn, J.C.; Soper, P.D.; Auman, B.C. "Relaxation Behavior of Polyimides Based on 2,2'-Disubstituted Benzidines", *Macromolecules* **1995**, *28*, 3253.
- Cole, K.S.; Cole, R.H. "Dispersion and Absorption in Dielectrics. I. Alternating-Current Characteristics", *Journal of Chemical Physics* **1941**, *9*, 341.
- Coleman, J.N.; Khan, U.; Gun'ko, Y.K. "Mechanical Reinforcement of Polymers Using Carbon Nanotubes", *Advanced Materials* **2006**, *18*, 689.
- Crosby Alfred J.; Jong-Young, L. "Polymer Nanocomposites: The "Nano" Effect of Mechanical Properties", *Polymer Reviews* **2007**, *47*, 217.

- Dalnoki-Veress, K.; Forrest, J.A.; Murray, C.; Gigault, C.; Dutcher, J.R. "Molecular Weight Dependence of Reductions in the Glass Transition Temperature of Thin, Freely Standing Polymer Films", *Physical Review E* **2001**, *63*, 031801/1.
- Daynes, H.A. "The Process of Diffusion Through a Rubber Membrane", *Proceedings of the Royal Society of London, Series A: Mathematical, Physical and Engineering Sciences* **1920**, *97*, 286.
- Drozдов, A.D. "The Effect of Temperature on Physical Aging of Glassy Polymers", *Journal of Applied Polymer Science* **2001**, *81*, 3309.
- Eichstadt, A.E.; Ward, T.C.; Bagwell, M.D.; Farr, I.V.; Dunson, D.L.; McGrath, J.E. "Synthesis and Characterization of Amorphous Partially Aliphatic Polyimide Copolymers Based on Bisphenol-A Dianhydride", *Macromolecules* **2002**, *35*, 7561.
- Eichstadt, A.E.; Andreev, S.; Ward, T.C. "The Effect of Water on the Viscoelastic Properties of Polyimides", *Proceedings of the Annual Meeting of the Adhesion Society* **2000**, *23*, 484.
- Ekiner, O.M. "Phenylindane Group-Containing Polyimide Gas-Separation Membranes", *US Patent 5,015,270* **1991**.
- Ellison, C.J.; Mundra, M.K.; Torkelson, J.M. "Impacts of Polystyrene Molecular Weight and Modification to the Repeat Unit Structure on the Glass Transition-Nanoconfinement Effect and the Cooperativity Length Scale", *Macromolecules* **2005**, *38*, 1767.
- Esfandiari, A.; Nazokdast, H.; Rashidi, A.-S.; Yazdanshenas, M.-E. "Review of Polymer-Organoclay Nanocomposites", *Journal of Applied Sciences* **2008**, *8*, 545.
- Ferry, J.D. *Viscoelastic Properties of Polymers*, 3rd edition; John Wiley and Sons: New York, **1980**.
- Forrest, J.A.; Dalnoki-Veress, K.; Stevens, J.R.; Dutcher, J.R. "Effect of Free Surfaces on the Glass Transition Temperature of Thin Polymer Films", *Physical Review Letters* **1996**, *77*, 2002.
- Forrest, J.A.; Dalnoki-Veress, K.; Dutcher, J.R. "Interface and Chain Confinement Effects on the Glass Transition Temperature of Thin Polymer Films", *Physical Review E* **1997**, *56*, 5705.
- Forrest, J.A. "A Decade of Dynamics in Thin Films of Polystyrene: Where Are We Now?", *European Physical Journal E* **2002**, *8*, 261.

- Fragiadakis, D.; Pissis, P.; Bokobza, L. "Glass Transition and Molecular Dynamics in Poly(dimethylsiloxane)/Silica Nanocomposites", *Polymer* **2005**, *46*, 6001.
- Fragiadakis, D.; Pissis, P. "Glass Transition and Segmental Dynamics in Poly(dimethylsiloxane)/Silica Nanocomposites Studied by Various Techniques", *Journal of Non-Crystalline Solids* **2007**, *353*, 4344.
- Fu, Y.-J.; Hsiao, S.-W.; Hu, C.-C.; Qui, H.-z.; Lee, K.-R.; Lai, J.-Y. "Effect of Physical Aging on Sorption and Permeation of Small Molecules in Polyimide Membranes", *Desalination* **2008**, *234*, 58.
- "G.E. Plastics: Technical Data Sheet for Ultem Resin 1000", *G.E. Plastics: Technical Data Sheet for Ultem Resin 1000*; **2003**.
- Goodwin, A.A.; Simon, G.P. "Glass Transition Behavior of Poly(ether ether ketone)/Poly(ether imide) Blends", *Polymer* **1996**, *37*, 991.
- Goodwin, A.; Marsh, R. "Dielectric and Dynamic Mechanical Relaxation of Poly(ether ether ketone)/Poly(ether imide) Blends Below the Glass Transition", *Macromolecular Rapid Communications* **1996**, *17*, 475.
- Habas, J.P.; Peyrelasse, J.; Grenier-Loustalot, M.F. "Rheological Study of a High-Performance Polyimide. Interpretation of the Secondary Mechanical Relaxations of a Nadimide Crosslinked System", *High Performance Polymers* **1996**, *8*, 515.
- Havriliak, S.; Negami, S. "Complex Plane Analysis of α -Dispersions in Some Polymer Systems", *Journal of Polymer Science, Polymer Symposia* **1966**, *14*, 99.
- Havriliak, S.; Havriliak, S.J. *Dielectric and Mechanical Relaxation in Materials*; Hanser: Cincinnati, **1997**.
- Hedvig, P. *Dielectric Spectroscopy of Polymers*; John Wiley and Sons: New York, **1977**.
- Hodge, I.M. "Physical Aging in Polymer Glasses", *Science* **1995**, *267*, 1945.
- Huang, Y.; Paul, D.R. "Physical Aging of Thin Glassy Polymer Films Monitored by Gas Permeability", *Polymer* **2004**, *45*, 8377.
- Huang, Y.; Paul, D.R. "Experimental Methods for Tracking Physical Aging of Thin Glassy Polymer Films by Gas Permeation", *Journal of Membrane Science* **2004**, *244*, 167.
- Huang, X.; Shao, L.; Meng, L.; Huang, Y. "Advances in Modification Methods of Polyimide Membranes for Gas Separation", *Mo Kexue Yu Jishu* **2009**, *29*, 101.

- Huang, Y.; Paul, D.R. "Physical Aging of Thin Glassy Polymer Films Monitored by Optical Properties", *Macromolecules* **2006**, *39*, 1554.
- Huang, D.; McKenna, G.B. "New Insights into the Fragility Dilemma in Liquids", *Journal of Chemical Physics* **2001**, *114*, 5621.
- Hub, C.; Harton, S.E.; Hunt, M.A.; Fink, R.; Ade, H. "Influence of Sample Preparation and Processing on Observed Glass Transition Temperatures of Polymer Nanocomposites", *Journal of Polymer Science, Part B: Polymer Physics* **2007**, *45*, 2270.
- Hutchinson, J.M. "Physical Aging of Polymers", *Progress Polymer Science* **1995**, *20*, 703.
- Jancar, J.; Douglas, J.F.; Starr, F.W.; Kumar, S.K.; Cassagnau, P.; Lesser, A.J.; Sternstein, S.S.; Buehler, M.J. "Current Issues in Research on Structure-Property Relationships in Polymer Nanocomposites", *Polymer* **2010**, *51*, 3321.
- Jenkins, M.J. "Relaxation Behaviour in Blends of PEEK and PEI", *Polymer* **2000**, *41*, 6803.
- Jordan, J.; Jacob, K.I.; Tannenbaum, R.; Sharaf, M.A.; Jasiuk, I. "Experimental Trends in Polymer Nanocomposites: A Review", *Materials Science and Engineering, A: Structural Materials: Properties, Microstructure and Processing* **2005**, *393*, 1.
- Kalakkunnath, S.; Kalika, D.S.; Lin, H.; Freeman, B.D. "Segmental Relaxation Characteristics of Cross-Linked Poly(Ethylene Oxide) Copolymer Networks", *Macromolecules* **2005**, *38*, 9679.
- Kalakkunnath, S.; Kalika, D.S.; Lin, H.; Raharjo, R.D.; Freeman, B.D. "Molecular Relaxation in Cross-linked Poly(Ethylene Glycol) and Poly(Propylene Glycol) Diacrylate Networks by Dielectric Spectroscopy", *Polymer* **2007**, *48*, 579.
- Kalakkunnath, S.; Kalika, D.S.; Lin, H.; Raharjo, R.D.; Freeman, B.D. "Molecular Dynamics of Poly(Ethylene Glycol) and Poly(Propylene Glycol) Copolymer Networks by Broadband Dielectric Spectroscopy", *Macromolecules* **2007**, *40*, 2773.
- Kalakkunnath, S. "*Viscoelastic Relaxation Characteristics of Rubbery Polymer Networks and Engineering Polyesters*"; Ph.D. Dissertation University of Kentucky: Lexington, KY, 2007.
- Kase, Y., "Gas Separation by Polyimide Membranes", In *Advanced Membrane Technology Applications*; Li, N.; Fane, A.G.; Ho, W.S.W.; Matsuura, T., eds.; John Wiley & Sons: New York, **2008**; pp 581-598.

- Kawana, S.; Jones, R.A.L. "Character of the Glass Transition in Thin Supported Polymer Films", *Physical Review E* **2001**, *63*, 021501.
- Keddie, J.L.; Jones, R.A.L.; Cory, R.A. "Size-Dependent Depression of the Glass Transition Temperature in Polymer Films", *Europhysics Letters* **1994**, *27*, 59.
- Kim, Y.H.; Moon, B.S.; Harris, F.W.; Cheng, S.Z.D. "Polymerization, Structure and Thermal Properties of ODP-DMB Polyimide Films", *Journal of Thermal Analysis and Calorimetry* **1996**, *46*, 921.
- Kizilay, M.; Okay, O. "Effect of Initial Monomer Concentration on Spatial Homogeneity in Poly(acrylamide) Gels", *Macromolecules* **2003**, *36*, 6856.
- Krishnamoorti, R. "Strategies for Dispersing Nanoparticles in Polymers", *MRS Bulletin* **2007**, *32*, 341.
- Krishnamoorti, R.; Vaia, R.A. "Polymer Nanocomposites", *Journal of Polymer Science, Part B: Polymer Physics* **2007**, *45*, 3252.
- Kusuma, V.A.; Freeman, B.D.; Borna, M.A.; Kalika, D.S. "Influence of Chemical Structure of Short Chain Pendant Groups on Gas Transport Properties of Cross-linked Poly(ethylene oxide) Copolymers", *Journal of Membrane Science* **2009**, *327*, 195.
- Kusuma, V.A.; Matteucci, S.; Freeman, B.D.; Danquah, M.K.; Kalika, D.S. "Influence of Phenoxy-Terminated Short Chain Pendant Groups on Gas Transport Properties of Crosslinked Poly(ethylene oxide) Copolymers", *Journal of Membrane Science* **2009**, *341*, 84.
- Kusuma, V.A.; Freeman, B.D.; Smith, S.L.; Heilman, A.L.; Kalika, D.S. "Influence of TRIS-based Co-monomer on Structure and Gas Transport Properties of Cross-linked Poly(ethylene oxide)", *Journal of Membrane Science* **2010**, *359*, 25.
- Lee, H.H.D.; McGarry, F.J. "The Origin of the Beta Transition and its Influence on Physical Aging", *Polymer* **1993**, *34*, 4267.
- Li, S.; Hsu, B.L.; Li, F.; Li, C.Y.; Harris, F.W.; Cheng, S.Z.D. "A Study of Polyimide Thermoplastics Used as Tougheners in Epoxy Resins - Structure, Property and Solubility Relationships", *Thermochimica Acta* **1999**, *340-341*, 221.
- Li, F.; Fang, S.; Ge, J.J.; Honigfort, P.S.; Chen, J.C.; Harris, F.W.; Cheng, S.Z.D. "Diamine Architecture Effects on Glass Transitions, Relaxation Processes and Other Material Properties in Organo-Soluble Aromatic Polyimide Films", *Polymer* **1999**, *40*, 4571.

- Li, F.; Ge, J.J.; Honigfort, P.S.; Fang, S.; Chen, J.-C.; Harris, F.W.; Cheng, S.Z.D. "Dianhydride Architectural Effects on the Relaxation Behaviors and Thermal and Optical Properties of Organo-Soluble Aromatic Polyimide Films", *Polymer* **1999**, *40*, 4987.
- Lin, H.; Van Wagner, E.; Freeman, B.D.; Toy, L.G.; Gupta, R.P. "Plasticization-Enhanced Hydrogen Purification Using Polymeric Membranes", *Science* **2006**, *311*, 639.
- Lin, H.; Van Wagner, E.; Raharjo, R.; Freeman, B.D.; Roman, I. "High-Performance Polymer Membranes for Natural-Gas Sweetening", *Advanced Materials* **2006**, *18*, 39.
- Lin, H.; Kai, T.; Freeman, B.D.; Kalakkunnath, S.; Kalika, D.S. "The Effect of Crosslinking on Gas Permeability in Crosslinked Poly(ethylene glycol diacrylate)", *Macromolecules* **2005**, *38*, 8381.
- Lin, H.; Freeman, B.D. "Materials Selection Guidelines for Membranes that Remove CO₂ from Gas Mixtures", *Journal of Molecular Structure* **2005**, *739*, 57.
- Lin, H.; Freeman, B.D. "Gas and Vapor Solubility in Cross-Linked Poly(ethylene glycol diacrylate)", *Macromolecules* **2005**, *38*, 8394.
- Lin, H.; Freeman, B.D. "Gas Permeation and Diffusion in Cross-Linked Poly(ethylene glycol diacrylate)", *Macromolecules* **2006**, *39*, 3568.
- Lin, H.; Van Wagner, E.; Swinnea, J.S.; Freeman, B.D.; Pas, S.J.; Hill, A.J.; Kalakkunnath, S.; Kalika, D.S. "Transport and Structural Characteristics of Crosslinked Poly(ethylene oxide) Rubbers", *Journal of Membrane Science* **2006**, *276*, 145.
- Lin, H. "Solubility Selective Membrane Materials for Carbon Dioxide Removal from Mixtures with Light Gases"; Ph.D. Dissertation University of Texas at Austin: Austin, TX, **2005**.
- Lin, H.; Freeman, B.D., "Permeation and Diffusion", In *Springer Handbook of Materials Measurement Methods*; Czichos, H.; Saito, T.; Smith, L.E., eds.; Springer: Berlin, **2006**; pp 371-387.
- Lim, T.; Frosini, V.; Zaleckas, V.; Morrow, D.; Sauer, J.A. "Mechanical Relaxation Phenomena in Polyimide and Poly(2,6-dimethyl-p-phenylene oxide) from 100K to 700K", *Polymer Engineering and Science* **1973**, *13*, 51.
- Madden, W.C.; Punsalan, D.; Koros, W.J. "Age Dependent CO₂ Sorption in Matrimid Asymmetric Hollow Fiber Membranes", *Polymer* **2005**, *46*, 5433.

- Matteucci, S.; Kusuma, V.A.; Kelman, S.D.; Freeman, B.D. "Gas Transport Properties of MgO Filled Poly(1-trimethylsilyl-1-propyne) Nanocomposites", *Polymer* **2008**, *49*, 1659.
- Matteucci, S.; Kusuma, V.A.; Sanders, D.; Swinnea, S.; Freeman, B.D. "Gas Transport in TiO₂ Nanoparticle-Filled Poly(1-trimethylsilyl-1-propyne)", *Journal of Membrane Science* **2008**, *307*, 196.
- Matteucci, S.; Kusuma, V.A.; Swinnea, S.; Freeman, B.D. "Gas Permeability, Solubility and Diffusivity in 1,2-Polybutadiene Containing Brookite Nanoparticles", *Polymer* **2008**, *49*, 757.
- Matteucci, S.; Raharjo, R.D.; Kusuma, V.A.; Swinnea, S.; Freeman, B.D. "Gas Permeability, Solubility, and Diffusion Coefficients in 1,2-Polybutadiene Containing Magnesium Oxide", *Macromolecules* **2008**, *41*, 2144.
- Matteucci, S.; Yampolskii, Y.; Freeman, B.D.; Pinnau, I., "Transport of gases and vapors in glassy and rubbery polymers", In *Materials Science of Membranes for Gas and Vapor Separation*; Yampolskii, Y.; Pinnau, I.; Freeman, B.D., eds.; John Wiley and Sons: New York, **2006**; pp 1-47.
- Mattsson, J.; Forrest, J.A.; Borjesson, L. "Quantifying Glass Transition Behavior in Ultrathin Free-Standing Polymer Films", *Physical Review E* **2000**, *62*, 5187.
- Maxwell, C. *Treatise on Electricity and Magnetism*; Oxford University Press: London, **1873**; Vol. 1.
- Mayes, A.M. "Nanocomposites Softer at the Boundary", *Nature Materials* **2005**, *4*, 651.
- McCrum, N.G.; Read, B.E.; Williams, G. *Anelastic and Dielectric Effects in Polymer Solids*; John Wiley and Sons, 1967, reprinted by Dover Publications: London, **1991**.
- Menczel, J.D.; Prime, R.B.; Editors. *Thermal analysis of polymers: Fundamentals and applications*; John Wiley & Sons, Inc., 2009.
- Merkel, T.C.; Freeman, B.D.; Spontak, R.J.; He, Z.; Pinnau, I.; Meakin, P.; Hill, A.J. "Ultraparable, Reverse-Selective Nanocomposite Membranes", *Science* **2002**, *296*, 519.
- Merkel, T.C.; He, Z.; Pinnau, I.; Freeman, B.D.; Meakin, P.; Hill, A.J. "Effect of Nanoparticles on Gas Sorption and Transport in Poly(1-trimethylsilyl-1-propyne)", *Macromolecules* **2003**, *36*, 6844.

- Merkel, T.C.; Freeman, B.D.; Spontak, R.J.; He, Z.; Pinnau, I.; Meakin, P.; Hill, A.J. "Sorption, Transport, and Structural Evidence for Enhanced Free Volume in Poly (4-methyl-2-pentyne)/Fumed Silica Nanocomposite Membranes", *Chemistry of Materials* **2003**, *15*, 109.
- Merkel, T.C.; He, Z.; Pinnau, I.; Freeman, B.D.; Meakin, P.; Hill, A.J. "Sorption and Transport in Poly (2,2-bis(trifluoromethyl)-4,5-difluoro-1,3-dioxole-co-tetrafluoroethylene) Containing Nanoscale Fumed Silica", *Macromolecules* **2003**, *36*, 8406.
- Mijovic, J., "Dielectric Spectroscopy of Reactive Network-Forming Polymers", In *Broadband Dielectric Spectroscopy*; Kremer, F.; Schönhals, A., eds.; Springer-Verlag: Berlin, 2003; pp 349-384.
- Moniruzzaman, M.; Winey, K.I. "Polymer Nanocomposites Containing Carbon Nanotubes", *Macromolecules* **2006**, *39*, 5194.
- Mooney, M. "The Viscosity of a Concentrated Suspension of Spherical Particles", *Journal of Colloid Science* **1951**, *6*, 162.
- Moy, T.M.; McGrath, J.E. "Synthesis of Hydroxyl-Containing Polyimides Derived from 4,6-Diaminoresorcinol Dihydrochloride and Aromatic Tetracarboxylic Dianhydrides", *Journal of Polymer Science, Part A: Polymer Chemistry* **1994**, *32*, 1903.
- Mundra, M.K.; Donthu, S.K.; Dravid, V.P.; Torkelson, J.M. "Effect of Spatial Confinement on the Glass-Transition Temperature of Patterned Polymer Nanostructures", *Nano Letters* **2007**, *7*, 713.
- Ngai, K.L.; Roland, C.M. "Chemical Structure and Intermolecular Cooperativity: Dielectric Relaxation Results", *Macromolecules* **1993**, *26*, 6824.
- Ngai, K.L.; Paluch, M. "Classification of Secondary Relaxation in Glass-Formers Based on Dynamic Properties", *Journal of Chemical Physics* **2004**, *120*, 857.
- Nielsen, L.E.; Landel, R.F. *Mechanical Properties of Polymers and Composites, 2nd edition*; Marcel Dekker: New York, **1994**.
- Okay, O.; Kurz, M.; Lutz, K.; Funke, W. "Cyclization and Reduced Pendant Vinyl Group Reactivity During the Free-Radical Cross-Linking Polymerization of 1,4-Divinylbenzene", *Macromolecules* **1995**, *28*, 2728.
- Park, H.B.; Jung, C.H.; Lee, Y.M.; Hill, A.J.; Pas, S.J.; Mudie, S.T.; Van Wagner, E.; Freeman, B.D.; Cookson, D.J. "Polymers with Cavities Tuned for Fast Selective Transport of Small Molecules and Ions", *Science* **2007**, *318*, 254.

- Patel, N.P.; Miller, A.C.; Spontak, R.J. "Highly CO₂-Permeable and Selective Polymer Nanocomposite Membranes", *Advanced Materials* **2003**, *15*, 729.
- Patel, N.P.; Miller, A.C.; Spontak, R.J. "Highly CO₂-Permeable and Selective Membranes Derived from Crosslinked Poly(Ethylene Glycol) and its Nanocomposites", *Advanced Functional Materials* **2004**, *14*, 699.
- Patel, N.P.; Aberg, C.M.; Sanchez, A.M.; Capracotta, M.D.; Martin, J.D.; Spontak, R.J. "Morphological, Mechanical and Gas-Transport Characteristics of Crosslinked Poly(Propylene Glycol): Homopolymers, Nanocomposites, and Blends", *Polymer* **2004**, *45*, 5941.
- Paul, D.R.; Robeson, L.M. "Polymer Nanotechnology: Nanocomposites", *Polymer* **2008**, *49*, 3187.
- Perena, J.M. "Dynamic Mechanical Relaxations in Polyimide and Polyamideimide", *Angewandte Makromolekulare Chemie* **1982**, *106*, 61.
- Priestley, R.D.; Mundra, M.K.; Barnett, N.J.; Broadbelt, L.J.; Torkelson, J.M. "Effects of Nanoscale Confinement and Interfaces on the Glass Transition Temperatures of a Series of Poly(n-methacrylate) Films", *Australian Journal of Chemistry* **2007**, *60*, 765.
- Priestley, R.D.; Rittigstein, P.; Broadbelt, L.J.; Fukao, K.; Torkelson, J.M. "Evidence for the Molecular-Scale Origin of the Suppression of Physical Ageing in Confined Polymer: Fluorescence and Dielectric Spectroscopy Studies of Polymer-Silica Nanocomposites", *Journal of Physics: Condensed Matter* **2007**, *19*, 205120/1.
- Qu, W.; Ko, T.M.; Vora, R.H.; Chung, T.S. "Effect of Polyimides with Different Ratios of Para- to Meta- Analogous Fluorinated Diamines on Relaxation Process", *Polymer* **2001**, *42*, 6393.
- Raharjo, R.D.; Lin, H.; Sanders, D.F.; Freeman, B.D.; Kalakkunnath, S.; Kalika, D.S. "Relation Between Network Structure and Gas Transport in Crosslinked Poly(propylene glycol diacrylate)", *Journal of Membrane Science* **2006**, *283*, 253.
- Reid, C.G.; Greenberg, A.R. "Influence of Silica Reinforcement Upon the Glass-Transition Behavior of Acrylic Polymers", *Journal of Applied Polymer Science* **1990**, *39*, 995.
- Richards, J.J.; Danquah, M.K.; Kalakkunnath, S.; Kalika, D.S.; Kusuma, V.A.; Matteucci, S.T.; Freeman, B.D. "Relation Between Structure and Gas Transport Properties of Polyethylene Oxide Networks Based on Crosslinked Bisphenol A Ethoxylate Diacrylate", *Chemical Engineering Science* **2009**, *64*, 4707.

- Rittigstein, P.; Priestley, R.D.; Broadbelt, L.J.; Torkelson, J.M. "Model Polymer Nanocomposites Provide an Understanding of Confinement Effects in Real Nanocomposites", *Nature Materials* **2007**, *6*, 278.
- Rittigstein, P.; Torkelson, J.M. "Polymer-Nanoparticle Interfacial Interactions in Polymer Nanocomposites: Confinement Effects on Glass Transition Temperature and Suppression of Physical Aging", *Journal of Polymer Science, Part B: Polymer Physics* **2006**, *44*, 2935.
- Robertson, C.G.; Roland, C.M. "Glass Transition and Interfacial Segmental Dynamics in Polymer-Particle Composites", *Rubber Chemistry and Technology* **2008**, *81*, 506.
- Robeson, L.M. "The Upper Bound Revisited", *Journal of Membrane Science* **2008**, *320*, 390.
- Roland, C.M.; Santangelo, P.G.; Ngai, K.L. "The Application of the Energy Landscape Model to Polymers", *Journal of Chemical Physics* **1999**, *111*, 5593.
- Rowe, B.W.; Freeman, B.D.; Paul, D.R. "Physical Aging of Ultrathin Glassy Polymer Films Tracked by Gas Permeability", *Polymer* **2009**, *50*, 5565.
- Rowe, B.W.; Freeman, B.D.; Paul, D.R. "Influence of Previous History on Physical Aging in Thin Glassy Polymer Films as Gas Separation Membranes", *Polymer* **2010**, *51*, 3784.
- Rowe, B.W. "*Physical Aging of Thin and Ultrathin Glassy Polymer Films*"; Ph.D. Dissertation University of Texas at Austin: Austin, TX, **2010**.
- Rowe, B.W.; Freeman, B.D.; Paul, D.R. "Effect of Sorbed Water and Temperature on the Optical Properties and Density of Thin Glassy Polymer Films on a Silicon Substrate", *Macromolecules* **2007**, *40*, 2806.
- Schaefer, D.W.; Justice, R.S. "How Nano are Nanocomposites?", *Macromolecules* **2007**, *40*, 8501.
- Schönhals, A.; Kremer, F., "Analysis of Dielectric Spectra", In *Broadband Dielectric Spectroscopy*; Kremer, F.; Schönhals, A., eds.; Springer-Verlag: New York, **2003**; pp 59-98.
- Schwarzl, F.R.; Bree, H.W.; Nederveen, C.J.; Schwippert, G.A.; Struik, L.C.E.; Van der Wal, C.W. "Behavior of Unfilled and Filled Rubbers in Shear in the Glass-Rubber Transition Region", *Rheologica Acta* **1966**, *5*, 270.
- Simmons, J.W.; Ekiner, O.M. "Preparation and Uses of Polyimide and Polyamide-Polyimide Gas Separation Membranes", *US Patent 5,232,472* **1993**.

- Simons, K.; Nijmeijer, K.; Sala, J.G.; Van Der Werf, H.; Benes, N.E.; Dingemans, T.J.; Wessling, M. "CO₂ Sorption and Transport Behavior of ODPA-Based Polyetherimide Polymer Films", *Polymer* **2010**, *51*, 3907.
- Sroog, C.E., "Polyimides", In *Encyclopedia of Polymer Science and Technology*, 1st edition; John Wiley & Sons, Inc., **1969**; Vol. 11, pp 247-272.
- Sroog, C.E. "Polyimides", *Progress in Polymer Science* **1991**, *16*, 561.
- Starkweather, H.W. "Simple and Complex Relaxations", *Macromolecules* **1981**, *14*, 1277.
- Starkweather, H.W. "Aspects of Simple, Noncooperative Relaxations", *Polymer* **1991**, *32*, 2443.
- Starr, F.W.; Schroder, T.B.; Glotzer, S.C. "Effects of a Nanoscopic Filler on the Structure and Dynamics of a Simulated Polymer Melt and the Relationship to Ultrathin Films", *Physical Review E* **2001**, *64*, 021802/1.
- Steeman, P.A.M.; van Turnhout, J., "Dielectric Properties of Inhomogeneous Media", In *Broadband Dielectric Spectroscopy*; Kremer, F.; Schönhals, A., eds.; Springer-Verlag: Berlin, **2003**; pp 495-522.
- Struik, L.C.E. *Physical Aging in Amorphous Polymers and Other Materials*; Elsevier: Amsterdam, **1978**.
- Sun, Z.; Dong, L.; Zhuang, Y.; Cao, L.; Ding, M.; Feng, Z. "Beta Relaxation in Polyimides", *Polymer* **1992**, *33*, 4728.
- Takahashi, S.; Paul, D.R. "Gas Permeation in Poly(Ether Imide) Nanocomposite Membranes Based on Surface-Treated Silica. Part 1: Without Chemical Coupling to Matrix", *Polymer* **2006**, *47*, 7519.
- Takahashi, S.; Paul, D.R. "Gas Permeation in Poly(Ether Imide) Nanocomposite Membranes Based on Surface-Treated Silica. Part 2: With Chemical Coupling to Matrix", *Polymer* **2006**, *47*, 7535.
- Tanaka, K.; Okamoto, K.-I., "Structure and Transport Properties of Polyimides as Materials for Gas and Vapor Membrane Separation", In *Materials Science of Membranes for Gas and Vapor Separation*; Yampolskii, Y.; Pinnau, I.; Freeman, B.D., eds.; John Wiley & Sons: New York, **2006**; pp 271-291.
- Termonia, Y. "Structure-Property Relationships in Nanocomposites", *Polymer* **2007**, *48*, 6948.

- Tjong, S.C. "Structural and Mechanical Properties of Polymer Nanocomposites", *Materials Science & Engineering, R: Reports* **2006**, R53, 73.
- Tsagaropoulos, G.; Eisenberg, A. "Direct Observation of Two Glass Transitions in Silica-Filled Polymers. Implications for the Morphology of Random Ionomers", *Macromolecules* **1995**, 28, 396.
- Tsagaropoulos, G.; Eisenberg, A. "Dynamic Mechanical Study of the Factors Affecting the Two Glass Transition Behavior of Filled Polymers. Similarities and Differences with Random Ionomers", *Macromolecules* **1995**, 28, 6067.
- Vaia, R.A.; Giannelis, E.P. "Polymer Nanocomposites: Status and Opportunities", *MRS Bulletin* **2001**, 26, 394.
- Venditti, R.A.; Gillham, J.K. "Physical Aging Deep in the Glassy State of a Fully Cured Polyimide", *Journal of Applied Polymer Science* **1992**, 45, 1501.
- Wijmans, J.G.; Baker, R.W. "The Solution-Diffusion Model: A Review", *Journal of Membrane Science* **1995**, 107, 1.
- Williams, G.; Watts, D.C.; Dev, S.B.; North, A.M. "Further Considerations of Non Symmetrical Dielectric Relaxation Behaviour Arising From a Simple Empirical Decay Function", *Transactions of the Faraday Society* **1971**, 67, 1323.
- Wind, J.D.; Paul, D.R.; Koros, W.J. "Natural Gas Permeation in Polyimide Membranes", *Journal of Membrane Science* **2004**, 228, 227.
- Winey, K.I., Vaia, R. A., "Polymer Nanocomposites", *MRS Bulletin* **2007**, 32, 314
- Xie, X.-L.; Mai, Y.-W.; Zhou, X.-P. "Dispersion and Alignment of Carbon Nanotubes in Polymer Matrix: A Review", *Materials Science & Engineering, R: Reports* **2005**, R49, 89.
- Xu, G.; Gryte, C.C.; Nowick, A.S.; Li, S.Z.; Pak, Y.S.; Greenbaum, S.G. "Dielectric Relaxation and Deuteron NMR of Water in Polyimide Films", *Journal of Applied Physics* **1989**, 66, 5290.
- Yim, A.; Chahal, R.S.; St. Pierre, L.E. "Effect of Polymer-Filler Interaction Energy on the T_g (glass transition temperature) of Filled Polymers", *Journal of Colloid and Interface Science* **1973**, 43, 583.
- Young, R.J.; Lovell, P.A. *Introduction to Polymers*, 3rd edition; CRC Press, 2009.
- Zanten, J.H.; Wallace, W.E.; Wu, W. "Effect of Strongly Favorable Substrate Interactions on the Thermal Properties of Ultrathin Polymer Films", *Physical Review E* **1996**, 53, 2053.

NOMENCLATURE

C	Capacitance (Farads)
C_o	Capacitance under vacuum (Farads)
C_1	Constant of the Williams-Landel-Ferry equation
C_2	Constant of the Williams-Landel-Ferry equation (K)
D	Diffusivity (cm^2/s)
D	Dielectric displacement (V/m)
$D(t)$	Time-dependent dielectric displacement (V/m)
E	Electric field strength (V/m)
$E(t)$	Time-dependent electric field strength (V/m)
E_A	Apparent activation energy (kJ/mol)
$E_A (\gamma)$	Apparent activation energy for the γ relaxation (kJ/mol)
$E_A (\beta)$	Apparent activation energy for the β relaxation (kJ/mol)
E_P	Modulus of polymer matrix (MPa)
E_1	Storage modulus (in-phase elastic component) (Pa)
E_2	Loss modulus (out-of-phase viscous component) (Pa)
E'	Storage modulus (Pa)
E''	Loss modulus (Pa)
P	Polarization (Coulombs/ m^2)
P	Permeability (Barrer; 1 barrer = $10^{-10} \text{cm}^3(\text{STP}) \text{cm}/(\text{cm}^2 \text{s cmHg})$)
P_C	Permeability of the composite (Barrer)
P_P	Permeability of the pure polymer (Barrer)

Q	Charge magnitude (Coulombs)
R	Gas constant (J/mol K)
S	Solubility (cm ³ (STP)/cm ³ -atm)
ΔS^{\ddagger}	Activation entropy (kJ/mol-K)
T	Absolute temperature (K)
T_g	Glass transition temperature (°C)
T_{REF}	Reference temperature (K)
T_{α}	Alpha transition temperature (°C)
T_{β}	Beta transition temperature (°C)
T_{γ}	Gamma transition temperature (°C)
T'	Relaxation temperature (K)
V	Potential difference (Volts)
a_T	Shift factor
a_{HN}	Broadening parameter
b_{HN}	Skewing parameter
d	Distance between parallel plates of a capacitor (m)
e	Strain
e_o	Strain amplitude
f	Frequency (Hz)
f_{MAX}	Frequency corresponding to the position of the maximum in the dynamic mechanical or dielectric loss peak (Hz)
h	Planck's constant
k	Boltzmann's constant
k_E	Einstein coefficient

m	Fragility index
p	Upstream pressure (atm)
w_F	Particle weight fraction
t	Time (s)
β_{KWW}	Kohlrausch-Williams-Watts distribution or breadth parameter
δ	Phase angle (radians)
$\Delta\epsilon$	Dielectric relaxation intensity
ϵ^*	Dielectric constant in complex notation
ϵ_s	Relative static permittivity
ϵ_R	Relaxed dielectric constant
ϵ_U	Unrelaxed dielectric constant
ϵ'	Dielectric constant
ϵ''	Dielectric loss
ϕ_F	Volume fraction of filler
ϕ_M	Maximum volume fraction of filler
ϕ_P	Polymer volume fraction
$\emptyset(t)$	Kohlrausch-Williams-Watts (KWW) “stretched exponential” relaxation time distribution function
ρ_{ADD}	Composite density based on volume additivity (g/cm^3)
ρ_F	Density of filler (g/cm^3)
ρ_{FILL}	Density of filler (g/cm^3)
ρ_P	Polymer density (g/cm^3)
σ	Charge density ($\text{Coulombs}/\text{m}^2$)

σ	Stress (Pa)
σ_o	Stress amplitude (Pa)
τ	Characteristic relaxation time (s)
$\langle \tau \rangle$	Central relaxation time (s)
τ_{ave}	Average relaxation time (s)
τ_{HN}	Havriliak-Negami (HN) relaxation time (s)
τ_{MAX}	Relaxation time associated with the maximum in dielectric loss peak (s)
τ_o	Relaxation time (s)
$\tau_{o,ave}$	Average relaxation time at reference temperature T_0 (s)
τ_α	Characteristic relaxation time corresponding to the glass transition temperature, T_α (s)
ω	Frequency (radians/sec)

ABBREVIATIONS

^1H NMR	Proton nuclear magnetic resonance
APAF-6FDA	2,2'-bis(3-amino-4-hydroxyphenyl) hexafluoropropane and 4,4'-(hexafluoroisopropylidene)-diphthalic anhydride
APAF-ODPA	2,2'-bis(3-amino-4-hydroxyphenyl) hexafluoropropane and 4,4'-oxydiphthalic anhydride
APIs	Aromatic polyimides
BDS	Broadband dielectric spectroscopy
BTDA-DAPI	3,3'-4,4'-benzophenone tetracarboxylic dianhydride and diaminophenylindane (Matrimid [®])
CI	Chemical imidization
DMA	Dynamic mechanical analysis
DMF	Dimethylformamide
DMTA	Dynamic mechanical thermal analyzer
FTIR-ATR	Attenuated total reflectance fourier-transform infrared spectroscopy
HAB-6FDA	3,3'-dihydroxy-4,4'-diaminobiphenyl and 4,4'-(hexafluoroisopropylidene)-diphthalic anhydride
HCPK	1 hydroxyl-cyclohexyl phenyl ketone
HN	Havriliak-Negami
KWW	Kohlrausch-Williams-Watts
P2VP	Poly (2-vinyl pyridine)
PALS	Positron annihilation lifetime spectroscopy
PB	Polybutadiene
PBOs	Polybenzoxazoles

PEGDA	Poly (ethylene glycol) diacrylate
PEI	Poly (ether imide)
PMMA	Poly (methyl methacrylate)
PMP	Poly (4-methyl-2-pentyne)
PPGDA	Poly (propylene glycol diacrylate)
PTMSP	Poly (1-trimethylsilyl-1-propyne)
SEM	Scanning electron microscopy
TEM	Transition electron microscopy
TGA	Thermogravimetric analysis
THF	Tetrahydrofuran
TI	Thermal imidization
TR	Thermal rearrangement or thermally rearranged
TTS	Time-temperature superposition
WLF	Williams-Landel-Ferry
XLPEGDA	Crosslinked poly (ethylene glycol) diacrylate
XLPEO	Crosslinked poly(ethylene oxide)

VITA

Date of birth:
March 10, 1958
Gary, IN

EDUCATION

Master of Science December 1982

Department of Chemical and Materials Engineering
University of Kentucky, Lexington, KY

- Thesis title: *Surface Areas and Pore Properties of Eastern U.S. Oil Shales*
- Advisor: Professor J. T. Schrodt

Bachelor of Science May 1980

Department of Chemical Engineering
Purdue University, West Lafayette, IN

PUBLICATIONS

A.C. Comer, A.L. Heilman and D.S. Kalika, “*Dynamic Relaxation Characteristics of Polymer Nanocomposites Based on Poly(ether imide) and Poly(methyl methacrylate)*”. *Polymer*, 51, 5245-5254 (2010).

A.C. Comer, D.S. Kalika, V.A. Kusuma and B.D. Freeman, “*Glass Transition and Gas Transport Characteristics of Polymer Nanocomposites Based on Crosslinked Poly(ethylene oxide)*”. *J. Applied Polymer Science*, 117, 2395-2405 (2010).

A.C. Comer, D.S. Kalika, B.W. Rowe, B.D. Freeman and D.R. Paul, “*Dynamic Relaxation Characteristics of Matrimid Polyimide*”. *Polymer*, 50, 891-897 (2009).

MEETINGS: ORAL PRESENTATIONS

A.C. Comer, C.P. Ribeiro, B.D. Freeman, S. Kalakkunnath and D.S. Kalika, “*Structure and Relaxation Characteristics of Thermally-Modified Aromatic Polyimides for Selective Separations*”. AICHE Annual Meeting, Salt Lake City, 2010.

A.C. Comer, A.L. Heilman and D.S. Kalika, “*Dynamic Relaxation Properties of Polymer Nanocomposites*”. AICHE Annual Meeting, Nashville, 2009.

MEETINGS: ORAL PRESENTATIONS (cont.)

A.C. Comer, V.A. Kusuma, B.D. Freeman and **D.S. Kalika**, “*Influence of Nanoparticle Filler on the Dynamic Relaxation Characteristics of Polymer Nanocomposites*”. AIChE Annual Meeting, Philadelphia, 2008.

MEETINGS: POSTER PRESENTATIONS

A.C. Comer and D.S. Kalika, “*Investigation of Glass-Rubber Relaxation Characteristics in Polymer Nanoparticle Composites*”. AIChE Annual Meeting, Nashville, 2009.

A.C. Comer, V.A. Kusuma, B.D. Freeman and **D.S. Kalika**, “*Dynamic Relaxation Properties of Polymer Nanocomposites: Effect of Nanoparticles on the Glass-Rubber and Sub-Glass Transitions*”. AIChE Annual Meeting, Philadelphia, 2008.